

1-1-2013

Design, Synthesis, Biological Evaluation And Molecular Modeling Studies Of Novel Multifunctional Neuroprotective Drugs For The Treatment Of Parkinson's Disease: An Effort Towards The Improvement Of In Vivo Efficacy And Modulation Of Alpha Synuclein Aggregation Property Of The Neuroprotective Parent

Gyan Prakash Modi
Wayne State University,

Follow this and additional works at: http://digitalcommons.wayne.edu/oa_dissertations

 Part of the [Medicinal Chemistry and Pharmaceutics Commons](#)

Recommended Citation

Modi, Gyan Prakash, "Design, Synthesis, Biological Evaluation And Molecular Modeling Studies Of Novel Multifunctional Neuroprotective Drugs For The Treatment Of Parkinson's Disease: An Effort Towards The Improvement Of In Vivo Efficacy And Modulation Of Alpha Synuclein Aggregation Property Of The Neuroprotective Parent" (2013). *Wayne State University Dissertations*. Paper 905.

**DESIGN, SYNTHESIS, BIOLOGICAL EVALUATION AND MOLECULAR
MODELING STUDIES OF NOVEL MULTIFUNCTIONAL NEUROPROTECTIVE
DRUGS FOR THE TREATMENT OF PARKINSON'S DISEASE: AN EFFORT
TOWARDS THE IMPROVEMENT OF *IN VIVO* EFFICACY AND MODULATION OF
ALPHA SYNUCLEIN AGGREGATION PROPERTY OF THE NEUROPROTECTIVE
PARENT MOLECULE (D-264)**

by

GYAN PRAKASH MODI

DISSERTATION

Submitted to the Graduate School

of Wayne State University,

Detroit, Michigan

in partial fulfillment of the requirements

for the degree of

DOCTOR OF PHILOSOPHY

2014

MAJOR: PHARMACEUTICAL SCIENCES

Approved by:

Advisor

Date

DEDICATION

This work is dedicated to people who are suffering from Parkinson's disease.

ACKNOWLEDGMENT

It is a matter of great honor and privilege for me to have the opportunity to convey my gratitude to a great number of people whose contribution in assorted ways helped me throughout my journey towards completion of the graduate study.

In the first place I would like to record my gratitude to Dr. Alope Dutta for his supervision, advice, and guidance from the very early stage of my research as well as giving me extraordinary experiences through out the work. Above all and the most needed, he provided me unflinching encouragement and support in various ways. His mentorship was paramount in providing a well rounded experience consistent my long-term career goals. He encouraged me to not only grow as an experimentalist and a chemist but also as an instructor and an independent thinker. I am indebted to him more than he knows. Writing of this dissertation would have never been successful without his constant guidance and careful review.

I am also benefited by outstanding works from our collaborator Dr. Maarten E. A. Reith, New York School of medicine, with his particular skill in many biological assays.

I gratefully acknowledge my committee members Dr. Commissaris, Dr. Andreana and Dr. Moszczynska for their supervision and crucial contribution which made them a vital part of this dissertation. I am thankful that in the midst of all their activity, they accepted to be members of my dissertation committee.

Thanks are due to all past and present members in Dr. Dutta's group who have given me invaluable technical help and comments at various stages of my research work.

I would like to express my gratitude towards the department Pharmaceutical Sciences, Wayne State University for giving me the opportunity to pursue my graduate study over here.

I express my sincere thanks to all faculty, staff and student members of the department of Pharmaceutical Sciences for helping me in carrying out the experiments. I am also thankful to National Institute of Health (**NIH/NS047198**) for providing financial support for this study.

Last but not the least, I like to especially thank to my family. Words alone cannot express my gratitude towards them. Without their inspiration, encouragement and support this dissertation would never have had written.

TABLE OF CONTENTS

Dedication	ii
Acknowledgement	iii
List of Tables	xi
List of Figures	xiii
List of Schemes	xix
CHAPTER 1- Introduction	1
1.1. Parkinson's disease	1
1.2. Statistics of Parkinson's disease	1
1.3. Pathogenetic factors of PD	2
1.3.1. Oxidative stress hypothesis	3
1.3.2. Protein aggregation	6
1.3.2. Mitochondrial dysfunction	13
1.3.4. Role of iron in pathogenesis of PD	14
1.4. Therapy in PD	15
1.4.1. Levodopa therapy	15
1.4.2. Neuroprotective therapy	17
1.5. An Overview of dopamine receptor system	18
1.5.1. human D2 and D3 receptor- A comparison	20

1.5.2. Significance of D3 receptors in PD	21
1.6. Receptor independent neuroprotection	22
1.7. Receptor dependent neuroprotection	23
1.8. Clinical trial of neuroprotection in PD with dopamine	25
receptor agonists	
1.9. Modulation of ASN aggregation as a therapeutics target	26
to treat PD	
1.9.1. Small molecules as a possible modulator of.....	28
ASN aggregation	
1.9.2. Other alternative pathways to combat ASN toxicity	32
1.10. Multi-target-directed ligand (MTDL) therapy	33
CHAPTER 2 – Research Background in the evolution of D3	35
preferring ligands and other approaches to PD therapy	
2.1. Development of D3 preferring ligands	35
2.1.1. Rigidization of Dopamine.....	35
2.1.2. Bioisosteric replacement of catechol moiety.....	37
of dopamine	
2.1.3. Evolution of accessory binding molecular determinant.....	41
2.2. Development of multifunctional ligands for neurodegenerative	47
Diseases	
2.2.1. Currently available treatments.....	47
2.2.2. Emergence of multifunction drugs for the treatment of	48
neurodegeneration	
CHAPTER 3- Hypothesis and specific aims	60

3.1. Hypothesis	60
3.2. General aims	62
3.2.1. Specific aims	62
3.2.2. Ligand design and synthesis	64
3.2.3. Separation of enantiomers of the racemic compounds.....	65
3.2.4. Radioligand binding assay.....	65
3.2.5. [³⁵ S]-GTPγS-binding <i>in vitro</i> functional assay.....	66
3.2.6. Biochemical antioxidant assay	66
3.2.7. Neuroprotection study	66
3.2.8. ASN aggregation study.....	66
3.2.9. In vivo assays with rat model of PD.....	66
3.2.10. Molecular modeling study	67
CHAPTER 4- Result and discussion	68
4.1. Chemistry involved synthesizing first series compounds.....	69
4.2. <i>In vitro</i> characterization with the first series compounds	79
4.3. <i>In vivo</i> experiments with lead molecules from first	87
series of compounds	
4.3.1. Evaluation of In vivo blood brain barrier crossing ability of lead . 87	
compounds by reversal of reserpine-Induced Hypolocomotion in Rats	
4.3.2. Induction of contralateral rotation by (-)- 8b , and (-)- 9b in	89
unilaterally lesioned rats in Ungerstedt rat model for PD	

4.4. Antioxidant assay with lead compounds.....	90
4.5. Neuroprotection studies with MN9D cell line	92
4.5.1. Neuroprotection against MPP+ induced toxicity	94
4.5.2. Neuroprotection against 6-OHDA induced toxicity	95
4.6. <i>In vitro</i> of characterization of dihydroxyl derivatives of D-264	96
4.7. <i>In vivo</i> experiments with lead molecules from second series	102
4.7.1. Reversal of reserpine-Induced hypolocomotion in Rats	102
4.7.2. <i>In vivo</i> pharmacology with 6-OHDA lesioned rat	103
4.8. Evaluation of anti-oligomeric and/or anti-fibrillar activity of.....	105
potential inhibitors of ASN aggregation	
4.8.1. Generation of ASN aggregates using cell-free system.....	105
4.8.2. Assessment of potential lead compounds for their ability.....	107
to modify ASN aggregation in cell-free system	
4.8.3. Generation of α -synuclein aggregates to assess.....	109
extracellular toxicity in cell-culture models	
CHAPTER 5 -Molecular Modeling Studies	124
5.1. CoMFA analysis: D2 and D3 receptor binding affinity	130
5.2. CoMSIA analysis: D2 and D3 receptor binding affinity	132
5.3. CoMFA and CoMSIA analysis: selectivity for D3 over D2 receptors	133
5.4. Graphical interpretation of the CoMFA and CoMSIA models	144
5.4.1. DA D2 receptor binding affinity	144

5.4.2. DA D3 receptor binding affinity	147
5.4.3. Selectivity for D3 over D2 receptor	151
CHAPTER 6- Materials and method	155
6.1. Chemistry	155
6.2. <i>In vitro</i> binding assay.....	194
6.2. <i>In vitro</i> [³⁵ S]-GTPγS-binding functional assay	195
6.3. Reversal of Reserpine-Induced Hypolocomotion	198
in Rats DA.	
6.4. Rotational experiment with 6-Hydroxy dopamine lesioned rats	198
6.5. Evaluation of antioxidant activity: DPPH Assay	200
6.6. Neuroprotection Studies.....	201
6.7. ASN aggregation studies.....	203
6.8. Molecular modeling studies.....	210
CHAPTER 7 Conclusion	216
References.....	219
Abstract.....	240
Autobiographic Statement	243

LIST OF TABLES

Table 1. Currently available Treatments for Parkinson's Disease	46
Table 2. Inhibition constants for competition with [³ H]spiroperidol binding to cloned rat D _{2L} and D ₃ receptors expressed in HEK-293 cells	83
Table 3. Stimulation of [³⁵ S]GTPγS binding to hD ₂ and hD ₃ receptor expressed in CHO cells	86
Table 4. Affinities for Cloned D _{2L} and D ₃ Receptors Expressed in Human Embryonic Kidney Cells measured by Inhibition of [³ H]-spiroperidol Binding	
Table 5. Stimulation of [³⁵ S] GTPγS Binding to Cloned Human D ₂ receptor and D ₃ Receptor Expressed in CHO Cells	101
Table 6. Summary of ASN experiments in cell free and with PC-12 cells	120
Table 7. Structures and affinity of compounds for the cloned D _{2L} and D ₃ receptors expressed in HEK cells	124
Table 8. Experimental and fitted/predicted activities of D ₂ /D ₃ ligands used as the training and test sets for CoMFA and CoMSIA analyses	134
Table 9. Experimental and fitted/predicted activities of D ₂ /D ₃ ligands used as the training and test sets for selectivity (D ₃ over D ₂) analyses using CoMFA and CoMSIA	137
Table 10. Summary of 3D QSAR CoMFA results	139
Table 11. Summary of 3D QSAR CoMSIA results	140

LIST OF FIGURES

Figure 1. Schematic diagram showing dopamine pathways in the brain.....	3
Figure 2. Structures of different auto-oxidation products of dopamine	4
Figure 3. Dopamine metabolism by enzyme monoamine oxidase	5
Figure 4. Fenton reaction by which H ₂ O ₂ forms hydroxyl radical.....	5
Figure 5. Proposed pathway for the production of quinones from RNS	6
Figure 6. Primary structure of alpha synuclein (ASN).....	8
Figure 7. Model of ASN cell to cell transfer	9
Figure 8. Schematic representation of interaction of ASN with dopamine quinone	12
Figure 9. Mitochondrial pathways of MPP ⁺ induced toxicity	14
Figure 10. Iron and oxidative stress hypothesis of Parkinson's disease	15
Figure 11. Characterization of Dopamine Receptors in CNS	19
Figure 12. Structure of D2/D3 selective agonists with preferential selectivity at D3	26
Figure 13. Possible Therapeutics Pathways to Modulate ASN aggregation.....	27
Figure 14. Scavenging of ROS by flavanoids.....	28
Figure 15. Comparision of ASN aggregation modulaltion property of various flavanoids.....	29
Figure 16. Chemical strucuture know ASN aggregation modulators	30
Figure 17. Chemcial Strucuture of non-hydroxyl ASN	

aggregation modulators.....	31
Figure 18. Heat shock protein (Hsp) modulators.....	32
Figure 19. Evolution of aminotetraline class of molecules by Rigidization of dopamine	36
Figure 20. Structure of 2-Amino-5, 6-dihydroxy tetrahydronaphthalene (ADTN) and its 6, 7-dihydroxyl isomer.....	37
Figure 21. Structure of tricyclic DA agonists (+)-PD 128907	37
Figure 22. Pyrrole derivatives with diversified the position of the nitrogen atom in the aromatic ring	39
Figure 23. Non-aromatic D3 preferring agonist	40
Figure 24. Structure of metabolically stable heterocyclicD3 preferring agonists.....	41
Figure 25. Hybrid Drug Design Model	41
Figure 26. Sulpiride based benzamide analogs having high D3 selectivity	42
Figure 27. Hybrid structures of conformationally flexible benzamide analogs and aryl piperazine with high D3 selectivity	43
Figure 28. Structure of some of the hybrids of 2-aminotetraline or its metabolically stable bioisosteric moiety and flexible benzamide moiety	44
Figure 29. Structure of some of the hybrids metabolically stable bioisosteric of 2-aminotetraline.....	45
Figure 30. 4-Phenyl piperazine analogs with high D3 selectivity.....	46
Figure 31. Design to develop bifunctional compounds.....	51
Figure 31. Design to develop bifunctional compounds.....	52
Figure 33. Design strategy of bifunctional compound having adenosine A2a	

antagonism and MAO-B reversible inhibition.....	53
Figure 34. Chemical Structure of alpha synuclein aggregation modulators.....	56
Figure 35. Design strategy of Co-drug or Prodrug	58
Figure 36. Various possible pathways of proposed D3 selective hybrid dopaminergic agonist for symptomatic and neuroprotective treatment of PD	60
Figure 37. Schematic representation of interaction of novel proposed D3 selective agonist at the pre and postsynaptic nerve terminals ..	62
Figure 38. Schematic representation of interaction of proposed hybrid D3 selective agonist with ASN	64
Figure 39. Effect of different drugs upon reserpine (5.0 mg/Kg, s.c.)- induced hypolocomotion in rats	87
Figure 40. Comparison of the effects of (-)-8b and (-)-9b with a dose of 10 μ Mol/kg and 5 μ Mol/kg and vehicle in unilaterally 6-OH-DA lesioned rats	90
Figure 41. DPPH radical scavenging activity by D-264, (-)-9b, (-)-8b, (-)-11 and ascorbic acid	92
Figure 42. Dose dependent effect of combination of pretreatment followed by co-treatment of D-264 and D-433 with 100 μ M MPP+ on cell viability of MN9D cells from toxicity of MPP+	93
Figure 43. Dose dependent effect of combination of pretreatment followed by co-treatment of D-264 and D-433 with 75 μ M 6-OHDA on cell viability of MN9D cells from toxicity of 6-OHDA.....	94
Figure 44. Effect of different drugs upon reserpine (5.0 mg/Kg, s.c.) induced hypolocomotion in rats	102
Figure 45. Effect on turning behavior of two different doses of 24b and vehicle in lesioned rats studied for maximum 6 h	103
Figure 46. Thioflavin T assay (Monitoring ASN aggregation)	

ASN fibrillization observed under different conditions	111
Figure 47. ASN oligomerization in the presence of DA, DA+ H ₂ O ₂ and DA+Various Drugs.....	114
Figure 48. Electron microscopic images (TEM) of α -SN aggregates.....	116
Figure 49. Electron microscopic images (TEM) of α -SN aggregates.....	117
Figure 50. Time dependent cytotoxic effect of asn alone or asn +DA in PC12 cells.....	118
Figure 51. Cytoprotective effect of the compounds against asn induced toxicity in PC12 cells	119
Figure 52. Flexible and Atom-based alignments of the dataset molecules.....	129
Figure 53. Experimental versus fitted (training set) activity from the CoMFA analyses of the training and test set molecules for D2 and D3 receptors	140
Figure 54. Experimental versus fitted (training set) activity from the CoMSIA analyses of the training and test set molecules for D2 and D3 receptors.....	141
Figure 55. Experimental versus fitted (training set) activity from the CoMFA and CoMSIA analyses of the training and test set molecules for selectivity analysis.....	142
Figure 56. CoMFA contour plots showing steric and electrostatic features for D2 and D3 binding potency	149
Figure 57. CoMSIA contour plots showing HDon and HAcc features for D2 and D3 binding potency	150
Figure 58. CoMFA and CoMSIA contour plots showing steric, electrostatic HDon and HAcc features for D2 and D3 binding potency	153

LIST OF SCHEMES

Scheme 1	69
Scheme 2	70
Scheme 3	72
Scheme 4	73
Scheme 5	74
Scheme 6	75
Scheme 7	76
Scheme 8	77
Scheme 9.....	78

Chapter 1

Introduction

1.1. Parkinson's disease:

Parkinson's disease (PD), first described by Dr. James Parkinson in 1817 as shaking palsy, is a multifactorial progressive neurological disorder that results from the degeneration of dopaminergic neurons in the substantia nigra pars compacta (SNPc) region of the brain¹. The presence of α -synuclein aggregates called Lewy body (LBs) or Lewy neuritis (LN) are pathological hallmark of PD. LBs or LN are responsible the degeneration of dopaminergic neurons in the substantia nigra (SN) region of the brain. It is estimated that PD affects 1-2% of the people older than 65 years of age. Common symptoms associated with PD include rigidity, bradykinesia, resting tremors, postural instability, and cognitive psychiatric complications³. The severity and symptoms of PD varies according to the satge of the disease⁴. PD also has symptoms of depression as well as dementia.

1.2. Statistics about the Parkinson's disease:

PD is the second most-prevalent neurodegenerative disorder in the western world after Alzheimer's disease. According to a statistical analysis published by the PD foundation, approximately 60,000 Americans are diagnosed with PD each year, and an estimated seven to ten million people worldwide are living with PD. PD afffects 1% of the population at age 65 to 5% at age 85 ⁵. Incidence of PD increases with age, but about 15% of people with the condition develop "young-onset" PD before reaching at the age 50. Men are more prone to have Parkinson's than women. Most cases of PD are sporadic, which means, it occurs in people with no apparent history

of the disorder in their family. However, approximately 15 percent of people with PD have a family history of this disorder. The research from the past two decades in PD area has provided more insights into the basic pathogenetic factors of PD such as roles of oxidative stress, aggregation of ASN protein and the presence of iron. The cost of PD treatment, is estimated to be nearly \$25 billion per year in the United States alone.

1.3. Pathogenetic Factors of PD:

The pathological features of PD are the progressive degeneration of the dopaminergic neurons in the substantia nigra which projects into the striatum and the presence of ASN aggregates known as LBs or LN in the DA neurons. Presence of ASN aggregates LBs represents an underlying similarity of PD pathogenesis with other neurodegenerative diseases such as AD. Although the etiology of PD is not known yet, It has been shown that both mitochondrial dysfunction and oxidative stress are interdependent and thus, emphasizing a central role in the pathogenesis of the disease process^{2, 6}. Oxidative stress and excessive amounts of metals especially iron can lead to the formation of reactive oxygen species (ROS). These mitochondria-derived ROS inhibits mitochondrial respiration and promotes the aggregation of alpha synuclein protein (aSN), which ultimately forms LBs and LN². Pathological features of PD appear when about 75 % of the nigral dopaminergic neurons are degenerated⁷. The research from the past two decades in PD area has provided more insights into the basic pathogenetic factors of PD such as roles of oxidative stress, aggregation of ASN proteins in the form soluble toxic aggregates and fibrils, and increased concentration of iron in the PD brain etc⁸.

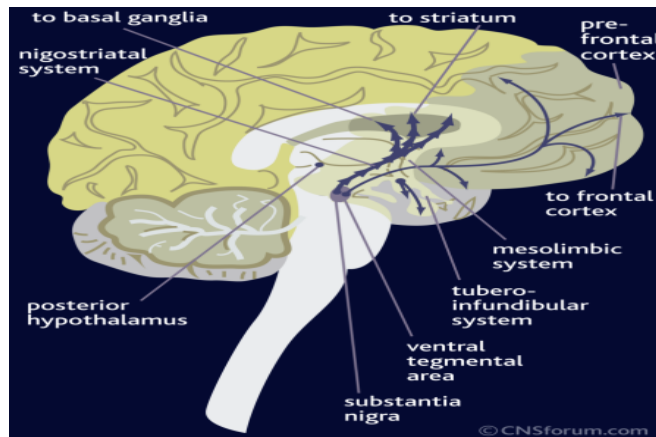


Figure 1. The Dopamine Pathways in the Brain. (Source: CNS Forum.com)

1.3.1. Oxidative Stress Hypothesis:

Cellular oxidation produces superoxide anion (O_2^-), hydrogen peroxide (H_2O_2) and hydroxyl radical ($OH\cdot$) which are collectively known as ROS. Oxidative stress is a redox imbalance with an excess formation of ROS or deficiency in antioxidants mechanism of the body⁹. Oxidative stress has been implicated in the pathogenesis of many neurodegenerative diseases besides Parkinson's disease (PD). The brain is more susceptible to damage by ROS because of the presence of high amount of polyunsaturated fatty acids, low level of antioxidants and elevated amount of iron in the specific regions of the brain.

1.3.1.1. Excessive formation of ROS:

It has been shown in the literature that ROS derived from combined presence of dopamine; low GSH and high iron are major culprits of dopaminergic neuronal loss. Dopamine is chemically unstable and undergoes auto-oxidation to form dopamine quinones, and free radicals (figure 2). Auto-oxidation of dopamine may be increased

in the early stages of the disease because of the increased turnover of DA to compensate for dying dopaminergic neurons.

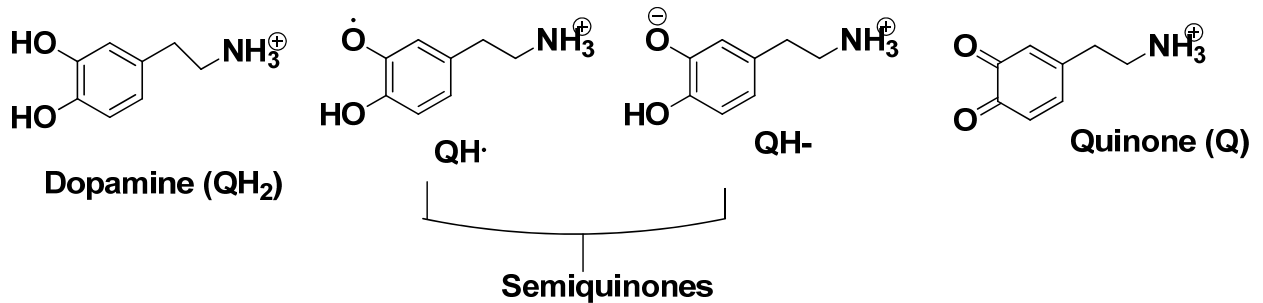


Figure 2. Structures of different auto-oxidation products of dopamine.

Monoamine oxidase, specifically MAO-B catalyzes the oxidative deamination of dopamine in the substantia nigra and striatum and forms hydrogen peroxide as major by-product (Figure 3). The level of MAO-B enzyme increases with age.¹⁰ Moreover, H₂O₂ produced in the glial cells can cross into the nearby dopaminergic cells, where it can potentially react with free iron and produces toxic hydroxyl radical which can damage cellular components.

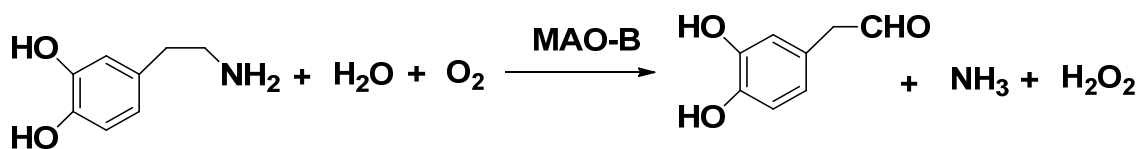


Figure 3. Dopamine metabolism by enzyme monoamine oxidase (MAO).

There is a substantial role of iron in oxidative stress in PD brain. The iron content of the SN is elevated in the PD brain as compared to normal person, which leads to enhance conversion of H₂O₂ to OH radical via the Fenton reaction and favors the Haber Weiss cycle (Figure 4).

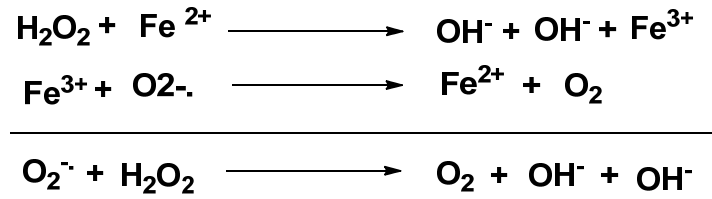


Figure 4. Fenton reaction by which H_2O_2 forms hydroxyl radical in iron rich environment.

Reactive nitrogen species such as NO and its metabolite peroxynitrite (PN) may also play a major role in PD. NO is known to inhibit complexes I and IV of the mitochondrial electron transport chain.

1.3.1.2. Decreased detoxification of free radicals:

Cellular oxidation produces H_2O_2 and free radicals, which are counterbalanced by the body's antioxidant mechanisms, such as by glutathione peroxidase, catalase, and superoxide dismutase. Depletion of GSH has also been reported to result in inhibition of glutathione reductase activity¹¹. The peroxisomes contain catalase enzyme which decomposes hydrogen peroxide and their H_2O_2 neutralizing capacity can be compromised during pathological conditions. This leads to the release of H_2O_2 into the cytosol which can contribute to oxidative stress (Figure 5). GSH loss and alteration of the cellular redox state can lead to decrease of the GSH/GSSG ratio.

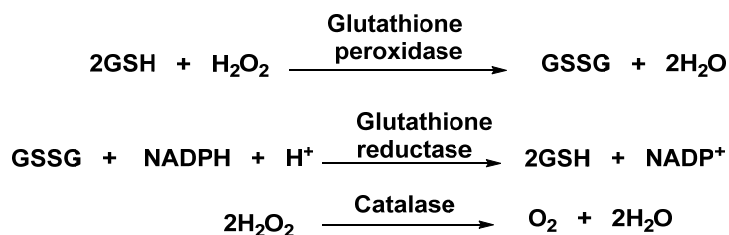


Figure 5. Proposed pathway for the production of quinones from RNS.

1.3.2. Protein aggregation:

The mitochondria-derived ROS inhibits mitochondrial respiration and promotes the aggregation of alpha synuclein protein (ASN), which ultimately forms lewy bodies (LBs) and lewy neuritis (LN)². LBs and LN are neuropathological hallmark of PD and toxic toward dopaminergic neurons. The common observations for the involvement of ASN aggregation in PD are: ASN is a component of Lewy bodies which is the cardinal hallmark of PD pathology². Second, familial early onset of PD is caused by over-expression of ASN due to mutation of SNCA gene^{12, 13}. Third, ASN forms toxic oligomers or fibrils. Currently it is not known how the aggregation of ASN triggers cell death, but it has been postulated that soluble oligomeric form of ASN, known as protofibrils, are the major culprit.

PD is associated with mitochondrial dysfunction, and oxidative stress. Over expression of ASN in hypothalamic tumor cell line (GT1-7) causes mitochondrial dysfunction, which can lead to the formation of reactive oxygen species (ROS), and finally, cell death.¹⁴ Raised level of ASN can also damage Lysosomes and Golgi apparatus. Furthermore, increased human ASN expression in transgenic flies (*Drosophila*) is associated with loss of dopaminergic neurons, formation of intracellular inclusions and locomotor dysfunction.¹⁵

1.3.2.1. Structure and functions of ASN: The name 'synuclein' was coined in 1988 by Maroteaux et al. ASN was originally identified in the electric organ of the Pacific electric eel *Torpedo California*.¹⁶ Antibodies against that protein labeled both synapses and nuclei, which coined the name of synuclein. In human, there are three synuclein family members (α -, β -, γ -) and all the synuclein genes are relatively well conserved both within and between species.. Synuclein has overall 44% identity, β –

synuclein shares 78% identity with ASN and γ -synuclein shares 60% identity with ASN¹⁷. All three members (α -, β -, γ -) of synuclein family are presynaptic neuronal proteins, there are some evidences of involvement of extranigral β - and γ - synuclein in synucleinopathies¹⁸. ASN is expressed at high level in the brain but it is also found, for unknown reasons, in erythrocytes and platelets¹⁹. The SNCA gene encodes ASN, composed of 140 amino acid, which in aqueous solution does not have defined structure, but it can form α - helical structure on binding to the lipids, and β -sheet structure on prolong period of incubation.

Primary structure of ASN can be divided into three regions: the amino terminal region (1-60), which contains 11- amino acid imperfect repeat with a conserved motif (KTKEGV), this region confers the propensity to form α - helical structure on membrane binding, the central region (61-95) which is composed of extremely hydrophobic NAC (non-A β component of Alzheimer's disease amyloid), which provides the β - sheet potential on prolong period of incubation, and the highly conserved C-terminal region (96-140), which is responsible for chaperone property of ASN¹⁷.

The functions of ASN are unclear but due to its association with synaptic vesicles the main function seems to release of neurotransmitter through the effect on SNARE complex²⁰. It has been postulated that ASN can play a role in synaptic plasticity, and it regulates specific pool of synaptic vesicles to modulate synaptic function in brain^{17,21}. ASN may act as a protein chaperon to protect the cell against the stress induced death,²² and it may be associated with the non-motor symptoms of PD²³.

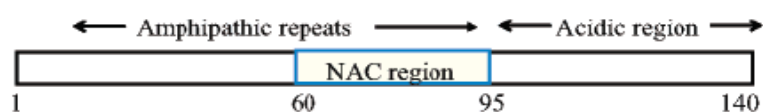


Figure 6. Primary structure of ASN.

1.3.2.2. Theories of ASN propagation: ASN is present not only in intracellular compartment but it could be detected in the extracellular fluids like in plasma and CSF. In PD, ASN aggregates in the central nervous system (CNS) first appear in the lower brain stem nuclei, and spread sequentially into the mid brain, followed by mesocortical and neocortical regions²⁴. This progression can be either due to aggregation in each cell and in each brain region independent of each other. Alternatively, protein aggregates may form in different areas of brain during the earlier stages, then may be transmitted to the other area by a mechanism like to prion propagation. Apart, form that small amount of ASN is released from the cell via exocytosis, and this release increases under the stress condition.

ASN, either monomer or in aggregated form, can leave cells via multiple mechanism like secretion, exocytosis, impairment of autophagy-lysosome pathway, or via exosomes etc²⁵. Once ASN leaves the donor cell, it can reach to the recipient cell either direct cell to cell transfer or through the tunneling nanotubes (TNTs). It can gain access to the recipient cell by directly interacting with lipid and membranes, or by passive diffusion. These aggregates of ASN are packaged into endocytic vesicle, but due to their lipid bilayer disrupting activity they can gain access to the cytosol. Due to the nucleation or seeding activity of the released ASN, it can induce the aggregation of cytoplasmic ASN protein, and it can also lead to the impairment of the proteasome activity in the recipient cell²⁵.

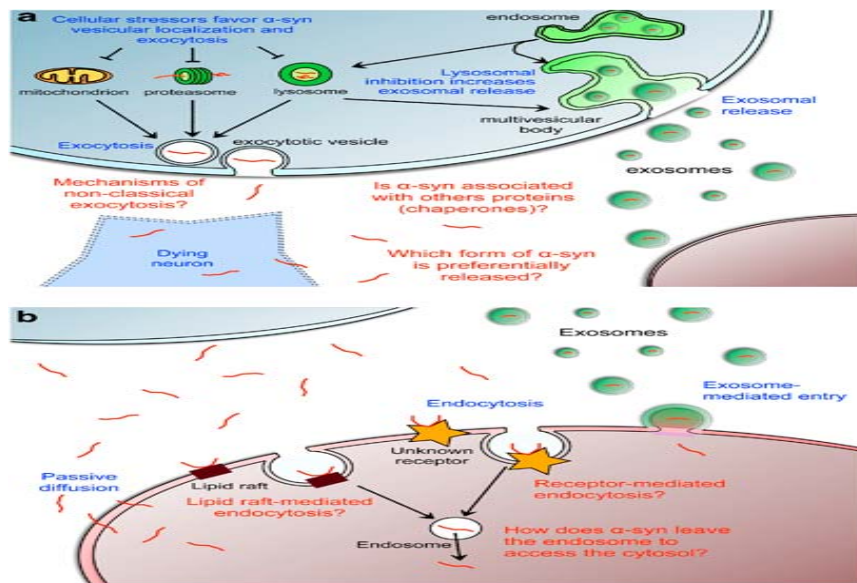


Figure 7. Model of ASN cell to cell transfer. (Source: Reference 25)

1.3.2.3. Pathogenic effects of ASN: Overexpression of ASN can lead to the neurotoxicity in cell culture and *in vivo* animal model, inhibits neurotransmitter release by reducing in the size of synaptic vesicle recycling pool, and remarkable changes in SNARE protein^{20,26,27}. PD can result from high activity of L-type Ca^{2+} channel that increases cytoplasmic Ca^{2+} , which can upregulate DA synthesis, and further interaction of DA with ASN lead to the formation of toxic oligomeric species²⁸. At low concentration, both wild and mutant ASN oligomers but not the monomeric form, can change the permeability of vesicular membrane by forming the pores like structures on the membrane which may cause excessive influx of calcium²⁹. Overexpression of ASN in PC12 cells can change vesicular pH which leads to the release of excessive neurotransmitter like dopamine, which may turn into the oxidative stress induced cell death³⁰.

Double labeling immunofluorescence revealed that tubulin co-localize with ASN in Lewy body, infect, tubulin can accelerate ASN aggregation³¹. ASN can enhance the tau phosphorylation because of its interaction with tubulin protein. ASN can also

affect cellular trafficking and synaptic functions. ASN either WT or mutant can cause proteasomal and lysosomal dysfunction, furthermore WT α -synuclein can reduce autophagy²⁰. ASN interacts with the histone protein in the nucleus, and reduces the histone acetylation.

1.3.2.4. Aggregation potential of ASN: ASN intrinsically may exist as monomeric or in tetrameric form which is not completely known yet^{32, 33}. Wild type and mutants of ASN (A53T and A30P), do not form significant secondary β sheet structure in aqueous solution at low concentration, however, at high concentration they are prone to self aggregates. The mutant form, particularly A53T form, can aggregate at rapid speed because this mutation disrupts the α helical structure. The fibrillation is a nucleation polymerization process, which can be divided into an initial lag phase, followed by the exponential growth phase, and an equilibrium phase. During this process initially soluble oligomeric species (oligomers or protofibrils, 6-8 nm in diameter) of ASN can take various shapes like spherical or ring. Protofibrils become insoluble and associate with each other into fibril (10 nm and above). Some of these intermediate species can be observed on SDS/polyacrylamide gel while other forms can be separated on native gel or by size exclusion chromatography. There is no general consensus that which species, either soluble or insoluble form, is more neurotoxic but a general hypothesis is that early soluble species are more hazardous than the fibril. Fibrillation rate mainly depends on concentration, presence of other metals, pH, and temperature.

Lansbury Jr. et. al.³⁴, demonstrated that fibril generated *in vitro* from both the wild type and mutant (A53T, A30P) ASN, possess very similar features like amyloid fibril. Upon incubation of WT as well as mutant ASN forms fibril in size range of 8-10 nm in height and 10 nm in width as well as some spherical species of 4 nm in height.

While the size of fibril can be same for both WT and mutant protein but the morphology can varies from one type of ASN to another. This fibril can be stained with the antibody preparation that stains LB in PD patient. Upon incubation of α -SN the minimum at 200 nm in CD disappears with simultaneously appearance of β -sheet characteristic minimum at 220 nm. The antiparallel β -sheet structure can be confirmed by amide I band at 1626 cm^{-1} and amide II band at 1693 cm^{-1} in IR spectroscopy. The fibrillar structure of ASN can further confirmed by it's binding to the dye Congo red and ThT. The absorption spectrum of Congo red shifts from 490 nm to 540 nm in presence of fibril α -SN while fibril of ASN can detected by strong increase in ThT signal at 490 nm upon excitation at 450 nm.)

Several mechanisms have been proposed for α -synuclein aggregation but oxidative stress and ubiquitin proteasome system (UPS) inhibition are most validated till now²². Metabolism of Dopamine (DA) in the nigral neurons produces reactive oxygen species (ROS) and other highly reactive species like DA-quinone (DAQ). Both DA and DAQ can interact with specific amino acid of ASN, probably with lysine, and inhibit further conversion of protofibrils to mature fibril both *in vitro* and *in vivo*. Overexpression of ASN, especially its mutant form may enhance the vulnerability of neurons to DA induced cell death due to excessive generation of intracellular ROS. This dopaminergic specificity of ASN neurotoxicity can be inhibited by the specific TH inhibitor, α -methyl-p-tyrosine, in the cultured dopaminergic neurons³⁵. It has been shown in literature that wild type α -synuclein over expression in cells may regulate the dopamine synthesis by acting on several enzymes like tyrosine hydroxylase (TH) or DOPA decarboxylase.

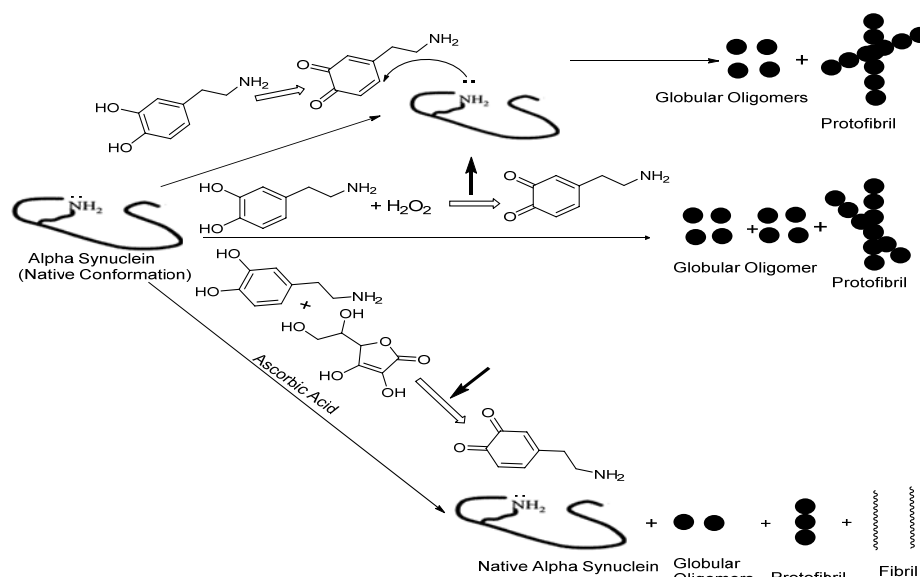


Figure 8. Schematic representation of interaction of ASN with dopamine quinone

UPS is the one of the major biochemical pathway responsible for degradation of normal and abnormal intracellular protein. It has been shown in literature that ubiquitin-dependent protein degradation may be impaired in many neurodegenerative disease like PD and diffuse LB Lewy body disease (DLBD), which leads to the accumulation of polyubiquitinated chains of LB- ubiquitin in the *substantia nigra pars compacta* region of brain²².

There are literatures evidences that altered metal homeostasis can lead to the loss of dopaminergic neurons in the SN region of brain. In this regards iron is the central point of attention because it is the most abundant metal of the body and it has been found that total nigral iron level is increased in PD brain compared to the controls. Metals especially iron can lead to the fibrilization of ASN either via the release of long-range interaction between N- and C- terminus region of ASN or metals like iron can lead to generate hydroxyl radicals by Fenton reaction which can further cause oxidation of α -synuclein known as metal catalyzed oxidation (MCO)³⁶. Interestingly,

phosphorylation at Tyr125 or at Ser129 can increase trivalent metal binding to the C-terminus of α -synuclein.

ASN can bind to Cu^{2+} via several binding sites, the Cu^{2+} complex with ASN promotes formation of ASN oligomers, which are cytotoxic in nature towards the SHSY-5Y neuroblastoma cell. Due to the low redox potential of ASN - Cu^{2+} complex, it can oxidize certain cellular reductants like ascorbic acid, GSH etc., which leads to generate H_2O_2 ³⁷. DA cannot be oxidized by ASN - Cu^{2+} complex but the H_2O_2 can oxidize DA into the corresponding quinone form.

1.3.3. Mitochondrial dysfunction:

Normally during oxidative phosphorylation, electrons are transferred to molecular oxygen and H_2O is produced by complex IV. However, 1-2 % of oxygen that is not reduced at complex IV is reduced nonenzymatically to superoxide ($\text{O}_2^{\cdot-}$) and H_2O_2 by electrons that leak from the sites in ETC. In PD brain, there is a site of electron leak in complex I of the ETC. It has been found that several neurotoxic agents, such as rotenone, paraquat and MPP^+ inhibit complex I and enhance ROS production. Local ROS can further damage complex I of the electron transport chain which further cause degeneration of neurons in the substantia nigra³.

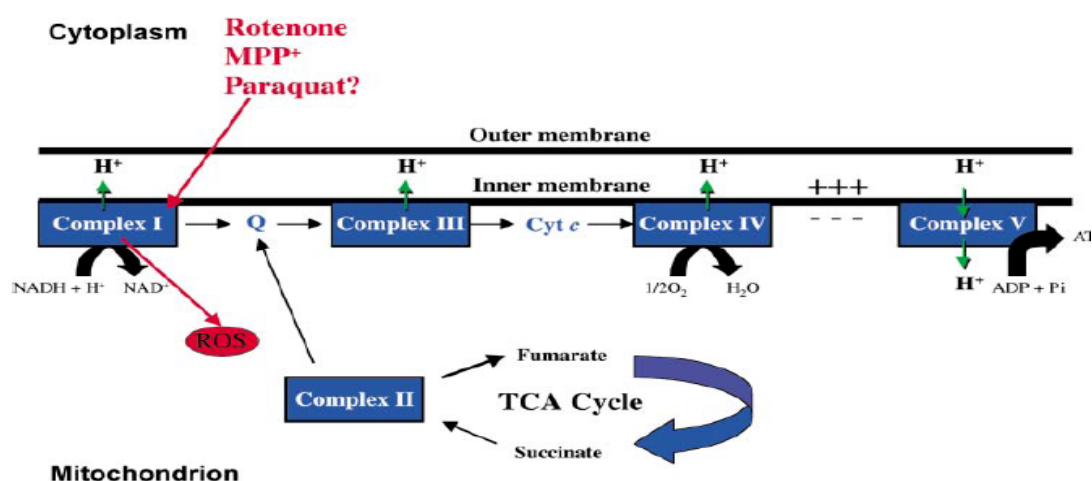


Figure 9: Mitochondrial pathway of MPP+ induced toxicity

1.3.4. Role of iron in PD pathogenesis:

There is pivotal role of iron in production of oxidative stress in PD brain. It has been reported that iron concentration in PD brain is 10 to 20 times more than its need for the normal physiological functions³⁸. Iron along with H_2O_2 can undergo nonenzymatic fenton reaction to produce hydroxyl radical. The autoxidation of dopamine can lead to formation of neuromelanin in the SN region of brain^{39, 40}. Iron in the form of Fe^{3+} can bind to melanine. Further, melanine can augment hydroxy radical radical formation. Overall, increased concentration of iron along with increased concentration of H_2O_2 from dopamine metabolism leads to enhance the vulnerability of SN neurons towards oxidative stress. The level of non heme iron concentration increases with age in SN region of the brain^{41, 42}. It has been shown in the literature that amount of iron content is directly correlated with motor dysfunction^{43, 44, 45}. Further, treatment with MPTP and 6-hydroxy dopamine raises iron level in the specific region of brain^{46, 47}.

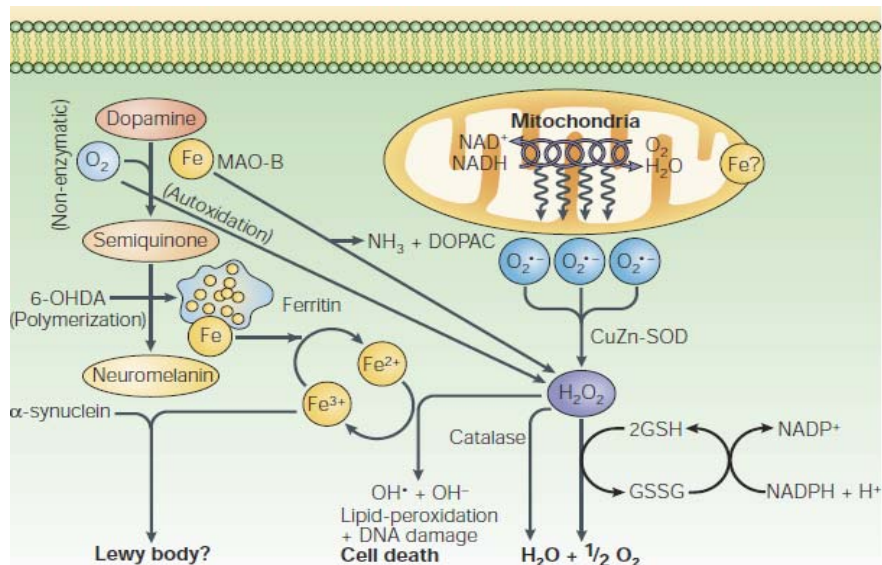


Figure 10. Iron and oxidative stress hypothesis of Parkinson's disease. (Source: Reference 41)

1.4. Therapy in PD:

1.4.1. Levodopa Therapy:

Levodopa (L-DOPA) became available in 1960s for the treatment of PD and is still being considered as one of the main stream therapies ⁴⁸. L-dopa administration causes a dramatic improvement in the symptoms of PD. However, in long L-dopa administration is associated with major side effects abnormal involuntary movements, dyskinesia, freezing, dementia, etc⁴⁹. L-dopa can provide the prominent symptomatic effect but cannot stop the progression of underlying disease progress. ⁵⁰ The L-dopa derived dopamine accelerates dopaminergic neuronal degeneration. ⁷. Over the years, several strategies have been developed to combat this problem. Dopamine agonists have been used as an adjunct to L-dopa therapy to reduce oxidative stress as well as L-dopa related motor complications. Dopamine agonists control DA synthesis by interacting with DA autoreceptors. Further, clinical studies has shown the promising results with DA agonist monotherapy alone ⁵¹. However, dopamine agonist monotherapy in early stage of PD patients reduces the motor symptoms but eventually patient need L-dopa treatment. The advantage of treatment with dopamine receptor agonists in early PD is that it delays the initiation of L-dopa therapy. The advantage of using combination therapy of dopamine agonists and L-dopa is that it slows down the increase of L-dopa dose. Therefore, the motor complications associated with the use of L-dopa are much less in combination therapy. So, the current strategy of PD therapy is to delay the initiation of L-dopa therapy, slow down the increase of L-dopa requirement or extend the

period of L-dopa treatment. Clinical studies showed initial therapy with MAO-B inhibitors delays initiation of L-dopa therapy. Catechol-O-methyl transferase (COMT) inhibitors inhibit the peripheral metabolism of L-dopa, thereby increasing the half life of L-dopa in the brain. However, none of these strategies address the limitations of L-dopa. Therefore, the need of therapeutic agent which will have disease modifying effect, is of paramount importance⁴⁹.

1.4.2. Neuroprotective therapy:

The development of a neuroprotective therapy that slows, stops, or reverses neurodegeneration in PD is the paramount choice of treatment. Current therapies of PD provide only symptomatic treatment without addressing the basic pathogenetic factors of the disease. Critical pathogenetic factors like oxidative stress, ASN aggregation, mitochondrial dysfunction, and excessive amount of iron are majorly responsible for PD. Therefore, multifunctional drug therapy, a drug while providing symptomatic relief also act as ASN aggregation modulator, antioxidants, iron chelator and neuroprotective can be evaluated as possible drug candidates for the treatment of PD.

1.4.2.1. The use of dopamine agonists as neuroprotective therapy in PD:

1.4.2.1.1. L-dopa sparring strategy:

Dopamine agonists can delay the introduction of L-dopa for months to years. Therefore, dopamine agonists can be used to decrease the cumulative L-dopa dose taken by PD patients over the course of the illness. The administration of lesser amounts of L-dopa gives rise to a lower level of ROS formation, resulting in less oxidative stress that ultimately cause neuronal degeneration. Studies in PD animal

models have demonstrated that the levels of striatal dopamine and their metabolites are significantly higher in animals treated with L-dopa compared to the level of dopamine agonists, despite comparable behavioral effects⁵².

1.4.2.1.2. Stimulation of dopamine autoreceptor:

Dopamine D2/D3 receptors are located both pre and post synaptically. Dopamine D2/D3 receptor agonists have the potential to stimulate presynaptically located autoreceptors on dopaminergic neurons and thereby inhibit dopamine synthesis, release and metabolism to form ROS⁵³. *In vitro* studies demonstrated that the addition of the dopamine receptor agonist pramipexole to cultured dopaminergic neurons induces a dose dependant decrease in dopamine concentration in the medium⁵⁴. *In vivo* studies have similarly shown that a variety of dopamine agonists, including apomorphine, quinpirole, and pramipexole, can decrease *in vivo* dopamine turnover, as determined by (DOPAC+ HVA)/Dopamine ratio as well as dopaminergic neuronal firing⁵⁴.

1.5. An Overview of dopamine receptor system:

DA neurons and their associated receptors have long been known to be implicated in the pathogenesis of PD. The DA receptors, phylogenetically classified as members of the biogenic amine receptors and part of the “rhodopsin-like” sub-family, belong to the super-family of membrane-bound proteins, termed G-protein coupled receptors. Until 1990, the DA receptor population of the brain and periphery was believed to consist solely of two subtypes, D1 and D2⁵⁵. Cloning of these two receptors led to the discovery of several additional low-abundance DA receptors, including the D3, D4 and D5 subtypes. Extensive studies on these two receptor systems by various *in vitro* and *in vivo* techniques including behavioral,

physiological, neurochemical, pharmacological and molecular approaches revealed some of the basic properties of these two receptor systems.

The D₁-like receptors, including D₁ and D₅, were found to be related by their stimulatory nature, thereby activating the second messenger enzyme, adenylyl cyclase, to produce cAMP. In contrast, D₂-like receptors, including D₂, D₃ and D₄, are negatively coupled to adenylyl cyclase and the production of cAMP⁵⁶. Both D₁ and D₂ receptors exist in high affinity states for dopamine agonists. The cloning of the D₃ receptor, initially undertaken by Sokoloff and colleagues, using cDNA from rat and probes derived from the D₂ receptor sequence, became of particular interest due to new hypotheses that proposed the D₃ receptor as a therapeutic target for neuropsychiatric disorders and PD.

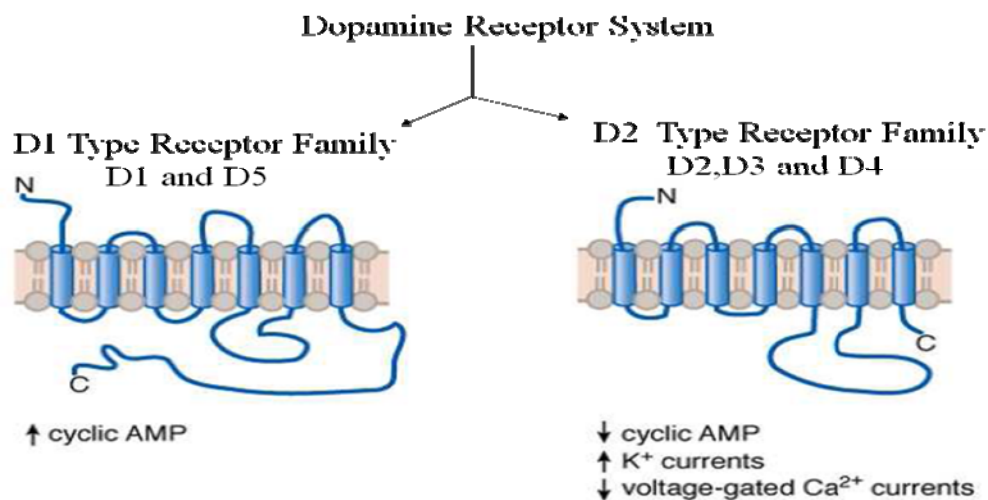


Figure 11. Characterization of Dopamine Receptors in CNS.

(Goodman & Gilman's, The Pharmacological Basis of Therapeutics, 12ed, 13.7)

1.5.1. human D2 and D3 receptor- A Comparison:

Human dopamine D₂ (hD₂) and D₃ (hD₃) receptors display considerable amino acid sequence similarity/identity. In the case of D₂ receptor, three different splice variants

have been revealed the D2 short, long and longer form contain 414, 443 amino acids, and 445 amino acids, respectively^{57, 58}. The difference in the length of the splice variants causes a difference in the length of the huge intracellular (IL3) loop. However, the wild type D3 receptor in humans does not have any splice variants that are functional⁵⁷. Interestingly, the difference in the length of IL3 in D3 receptor in mice causes two splice variants^{59, 60}. The overall amino acid sequence similarity is 50 % between D2 and D3 receptor, which represents a very high number in terms of similarity. That number increases to 90% in ligand recognition sites between two receptors⁶¹. Some important residues are located in the binding site crevice. These include Ser (192) and Ser (196), which are located in transmembrane domain V and forms bifurcated hydrogen bonds with the two hydroxyl groups of catechol. Asp (110) may participate in salt linking with the amine groups of monoamines. In addition, the location and orientation of Ser (192/196) and Asp (110) appear to allow for optimal bonds with oxygenated 2-aminotetralins, such as 7-hydroxy-dipropylaminotetralin (7-OH-DPAT). This may explain why these compounds show higher D3 affinity over D2.

Both hD2 and hD3 receptors possess a large third intracytoplasmic loop and a short carboxyl-terminal tail, a characteristic of receptors that couple to the Gai/o subfamily of G proteins. Activation of D2 and D3 receptors inhibit dopamine synthesis in a dopamine producing cell line, while D2 receptor mediates robust inhibition of cAMP accumulation, whereas inhibition of cAMP accumulation by the D3 receptor is modest or absent. This indicates a weak coupling of the D3 receptor with inhibitory G-proteins.⁶²⁻⁶⁵

In general, dopamine and several dopaminergic agonists have a higher affinity for hD3 than for hD2 receptors, whereas the affinity of antagonists is usually slightly

higher for hD2 receptors (Sokoloff et al., 1992). The distribution of hD3 receptors in the brain seems to be confined to the mesolimbic areas, whereas hD2 receptors are found in all dopaminergic brain areas⁶⁶. In situ hybridization studies in rat brain demonstrate that mRNA for the D3 receptor appears to be expressed preferentially in limbic brain regions. High levels of D3 mRNA are observed in the islands of Calleja, nucleus accumbens and olfactory tubercle. Distribution of D3 mRNA and localization of the encoded receptors was found to be similar in the rat and human brain, although D3 receptor localization in human brain is somewhat less restricted with moderate amounts of D3 receptor found in the basal ganglia and cortical regions.

1.5.2. Significance of D3 receptors in PD:

Although it has been assumed that D2 receptor stimulation is necessary for antiparkinsonian activity, DA agonists used in the treatment of PD have higher affinity for the D3 receptor. It is thought that mesolimbic D3 receptors could play a role in antiparkinsonian relief, as the limbic striatum is known to be involved in aspects of movement, such as goal-directed behaviors and locomotor activity. Locomotor stimulatory activity is observed in 6-OHDA-lesioned rats at the same doses of D3-preferring agonists that are inhibitory in normosensitive rats, suggesting that D3-preferring agonists may be a viable option for antiparkinsonian treatment of DA-depleted animals.

Most neuroprotection studies are conducted using the well known D3 receptor selective agonist pramipexole, which indicates a possible connection of neuroprotection with D3 preferring agonism.⁶⁷ In two separate clinical trials, D3-preferring agonists, pramipexole have proved to be the most potent neuroprotective

agents identified to date against MPTP and 6-OHDA-induced toxicity in mice and primates. Recent studies showed that pramipexole and talipexole can prevent neurotoxicity produced by L-dopa in mesencephalic cultures⁶⁸ and by MPP⁺ in neuroblastoma cell line SH-SY5Y⁶⁹. In terminally differentiated SH-SY5Y cells, in which D2 and D3 receptors are expressed, pretreatment with pramipexole demonstrated that: (1) pramipexole is neuroprotective with pretreatment; (2) the neuroprotection is not due to antioxidant properties; (3) neuroprotection is not mediated through DAT and (4) neuroprotection occurs via D2/D3 receptor-mediated mechanisms. It has been suggested that D3 receptor-mediated induction of neuroprotective factors, such as BDNF and Bcl-2, may be responsible for the protective actions of D3-preferring agonists.

1.6. Receptor independent neuroprotection:

Chronic, L-dopa therapy is thought to be neurotoxic due to oxidative species that are produced as a by-product of DA metabolism. Increased DA metabolism may overwhelm natural antioxidant defenses, such as glutathione, catalase and superoxide dismutase, thereby destroys DA cell. Assuming that oxidant stress hypothesis is correct; DA agonists that bypass oxidative DA metabolism should be neuroprotective. Interestingly, many studies with D-3 preferring agonists have concluded that the antioxidant capacity, rather than the agonist activity, is responsible for the neuroprotective actions of these drugs. D3-preferring agonists can decrease DA synthesis and release by D3 autoreceptor activation, which would decrease DA metabolism and overall ROS load. In rostral, mesencephalic tissue culture, pramipexole and other D3-preferring agonists have shown the ability to not only reverse the progressive loss of cells in culture over time, but also to increase cell proliferation. The inactive, *R*(+) enantiomer of pramipexole was found to be as

potent as the active, *S*-(-) enantiomer in inhibiting mitochondrial permeability transition, along with reducing caspase activity and apoptosis⁷⁰.

In addition, there are reports that indicate the ability of ropinirole to increase the concentrations of glutathione, catalase and superoxide dismutase⁷¹. The heterocyclic rings in pramipexole, ropinirole, quinpirole might be responsible for their free radical scavenging effects. But, the amount of drug needed to impart antioxidant effect is quite high, often in micromolar range, which is not achievable during routine use of these drugs in PD patients to alleviate symptoms. Therefore, it is ambiguous whether the direct antioxidant properties of dopamine receptor agonists can cause neuroprotection or not⁷².

1.7. Receptor dependent neuroprotection:

Pramipexole was shown to significantly attenuate L-dopa-induced, tyrosine hydroxylase immunoreactive (THir, a marker for dopamine neurons) cell loss in a dose-dependent fashion ($ED_{50} = 500$ pM). Due to the fact that pramipexole displays antioxidant activity in the micromolar range, a receptor-mediated mechanism for this neuroprotection has been postulated. D3-preferring antagonists were shown to dose-dependently inhibit the neuroprotective action of pramipexole. Taken together, these data suggest that D3 receptor activation is, at least, partially responsible for the neuroprotective effects of pramipexole. Interestingly, treatment of primary mesencephalic cultures with pramipexole was found to increase the expression of Bcl-X₁ and reduce the neurotoxicity of L-dopa. Literature evidences suggest that pramipexole, by increasing Bcl-X₁ expression, is able to stabilize the mitochondrial transition pore⁷³. Pramipexole was found to attenuate TNF α -induced THir cell loss in mesencephalic cultures. Pramipexole may be able to block neurodegenerative

actions of inflammatory cytokines, in addition to its functions as a D3 receptor-preferring agonist and antioxidant. Therefore, D3 receptor-preferring agonists may exert their neuroprotective properties through a number of mechanisms, including receptor-dependent and receptor-independent pathways.

A growing area of neuroprotection research is that of the endogenous production of neurotrophic factors. GDNF, BDNF and fibroblast growth factor (FGF) have proved in preclinical studies to promote the survival and growth of DA neurons. Neurotrophic factors are able to protect DA neurons exposed to neurotoxins, 6-OHDA and MPP⁺. The mechanism by which neurotrophic factors exert their effects has not yet been clearly identified. Dutta et al.⁷⁴, have recently developed D-264, a D3 receptor-preferring agonist, which has shown promise as a neuroprotective therapy in two *in vivo* PD animal models. In MPTP- and lactacystin-treated mice, pretreatment with D-264 has been shown to: 1) increase BDNF and GDNF levels 2) dose-dependently increase the number of TH-positive neurons; 3) significantly attenuate lactacystin-induced inhibition of proteasome activity; 4) inhibit pro-inflammatory, microglia activation; and 5) dose-dependently reduce the activation of astrocytes. Importantly, D3-selective antagonist, U99194, significantly altered the neuroprotective effects of D-264, indicating a significant role for D3 receptors in its neuroprotection. D3-preferring agonists have also been explored for their ability to induce neurogenesis.

1.8. Clinical trial of neuroprotection in PD with dopamine receptor agonists:

The first major neuroprotective clinical trial was the DATATOP study, this was designed to assess the neuroprotective effects of a combination therapy of selegiline and vitamin E⁷⁵. The time period until patients required L-dopa treatment was

compared in each group. It was found that combination therapy delayed the initiation of L-dopa treatment significantly. Another study was carried out to assess the potential neuroprotective effects of seligiline where untreated PD patients were given seligiline along with a symptomatic dopaminergic agent. The outcome of this study proved seligiline to be neuroprotective. As there is a reduction in mitochondrial complex I level in PD, coenzyme Q10 was also used in clinical studies to see if it has neuroprotective effects. The outcome of this study showed neuroprotective effect of this drug. Clinical trial has also been undertaken on Pramipexole and Ropinirole, dopamine D3 receptor selective agonist. In this study, patients were treated with either dopamine agonist or L-dopa. The end point determination of this study was challenging because of the intervention of the symptomatic effect of the drugs. After careful interpretation of the results using various techniques including single photon emission tomography etc, it has been found that dopamine agonists are neuroprotective, though some limitations in this study apply⁷⁶.

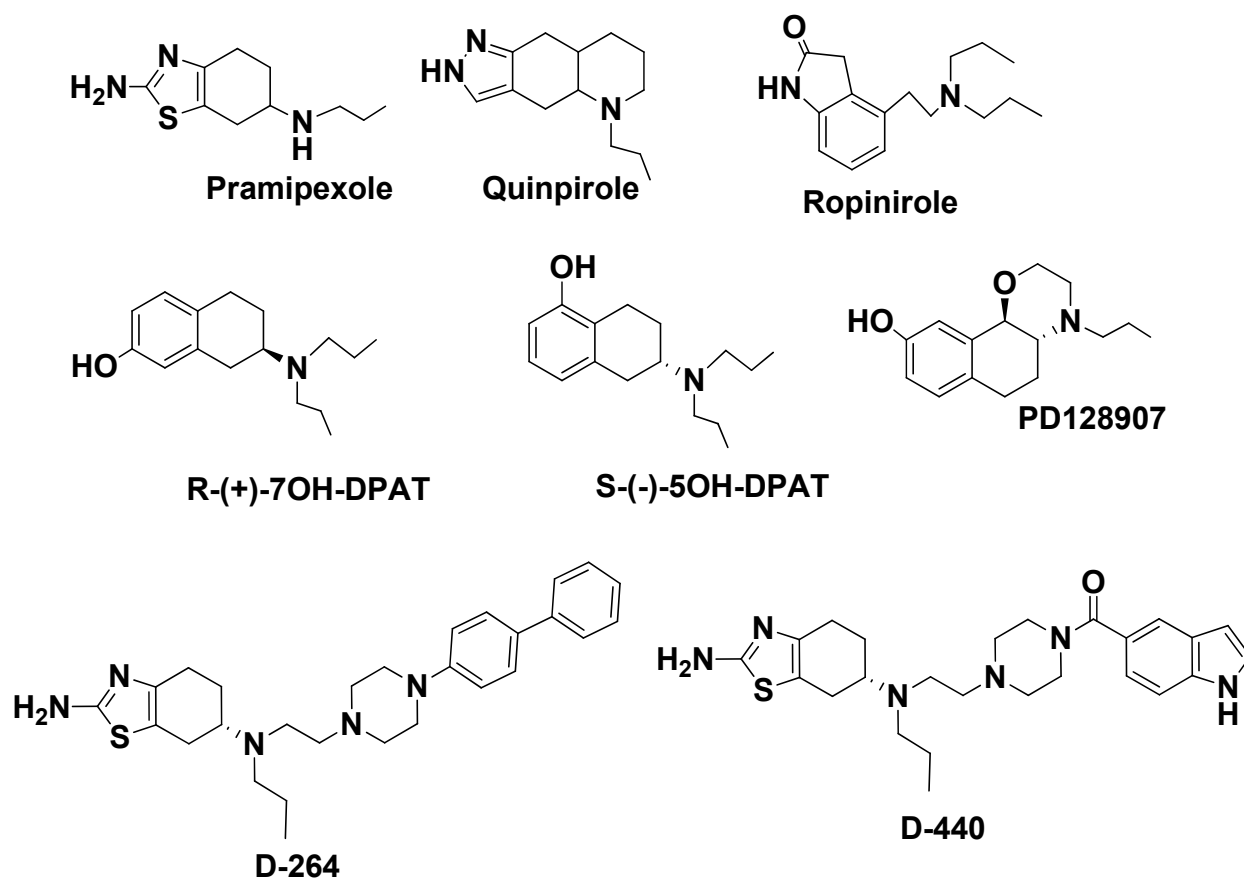


Figure 12. Structure of D2/D3 selective agonists with preferential selectivity at D3.

In summary, there is no therapy available that can either stop the disease progression or restore the dopaminergic neuronal system back to normal condition. Therapy for PD includes symptomatic treatment which is necessary to give relief to the patients. Besides that neuroprotective therapy can also be provided to delay disease progression. The symptomatic therapy can be combined with neuroprotective therapy in a MTDL by designing drug candidate that has agonist property (to alleviate symptoms) as well as antioxidant property (one of the most powerful ways to provide neuroprotection). It will be an added significant advantage if iron chelating property can also be incorporated in the MTDL treatment strategy.

1.9. Modulation of ASN aggregation as a therapeutics target to treat PD:

ASN aggregation is one of the leading causes of neuronal dysfunction and death in PD. The modulation of its aggregation is emerging as a novel therapeutic target to treat PD. Assuming toxicity arises from aggregated form of ASN, possible therapeutic strategies are depicted in figure 13. There are two major aspects that might be targeted therapeutically first, protein is prone to aggregate so anti-aggregative or compounds that can break the preexisting aggregates may be helpful. Second, there are number of molecular events like aggregation propagation or accumulation of aggregates may contribute to toxicity, so these may be targeted therapeutically as well.

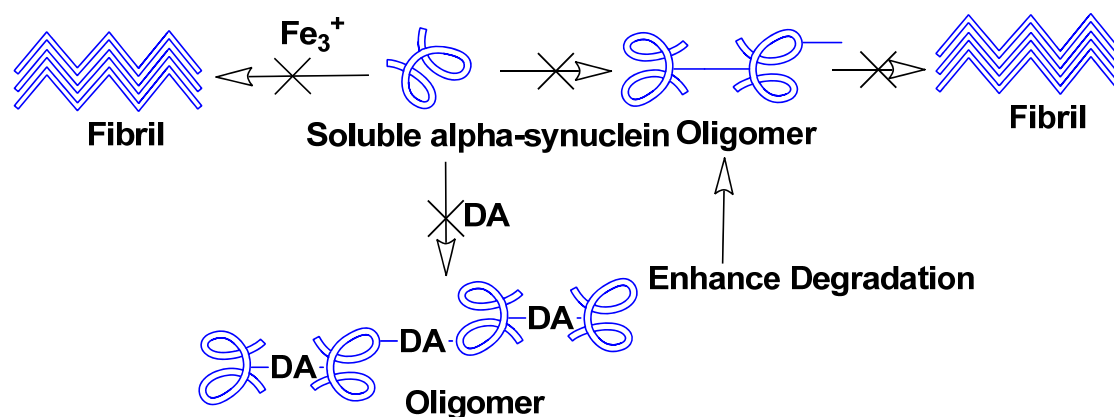


Figure 13. Possible Therapeutics Pathways to Modulate ASN aggregates

1.9.1. Small molecules as a possible modulator of ASN aggregation:

1.9.1.1. Effect of various polyphenolic compounds on ASN aggregation: In last decade small organic molecules, specifically polyphenols have been extensively tested for their ability to inhibit ASN aggregation. It has been clearly shown that certain polyphenols can dramatically inhibit cell death induced by ASN aggregates. Fruits like black tea, red wine, berries etc., are rich source of polyphenols. The daily

average polyphenols intake is difficult to estimate, but it is supposed to be 200-500 mg per day. Most of the polyphenols due to their potent antioxidant nature are salubrious. They are able to reduce highly oxidizing free radicals by hydrogen atom donation.

Where POH indicate polyphenols and $R \cdot$ represents free radicals. The $PO\cdot$ can further react with second radical which lead to the formations of stable quinone structure as shown in figure 14.

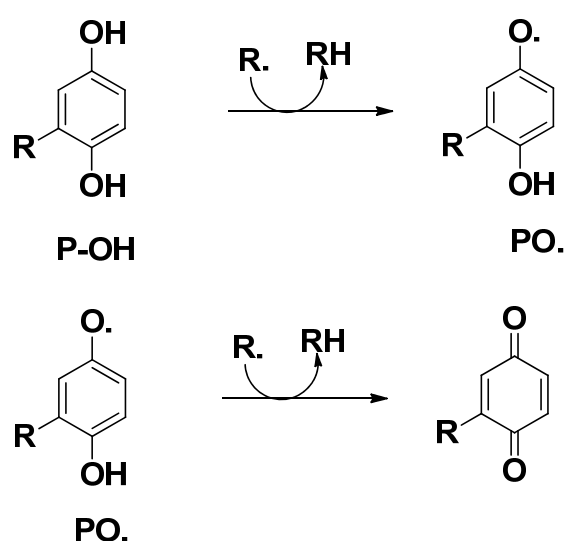


Figure 14. Scavenging of ROS by flavanoids

In general, the radical-scavenging ability depends on the molecular structure and the substitution pattern of hydroxyl group. Besides the radical scavenging ability of the polyphenols, they can also bind to the metal ion which may further enhance their antioxidant activity. Dietary intake of berries can reverse cognitive and motor deficit in rats, and that can lead to lower incidence of dementia. EGCG, (-) epigallocatechin-3-gallate, an antioxidant and metal chelating polyphenol from green tea, has been shown to be neuroprotective in an MPTP induced animal model of PD⁷⁷. Different flavonoids affected the α -synuclein fibrillation to a different extent

which was confirmed by lower ThT fluorescence intensity for the samples containing these flavonoids⁷⁸. It seems vicinal dihydroxylphenyl group is responsible to provide a flavonoids to inhibit ASN fibrillation. Moreover, the difference in the number of the vicinal dihydroxyl group and the number of individual hydroxyl group also lead to difference in the inhibitory activities of the flavonoids. Generally larger the number of hydroxyl group, the stronger the ASN fibril inhibitor as illustrated in figure 15.

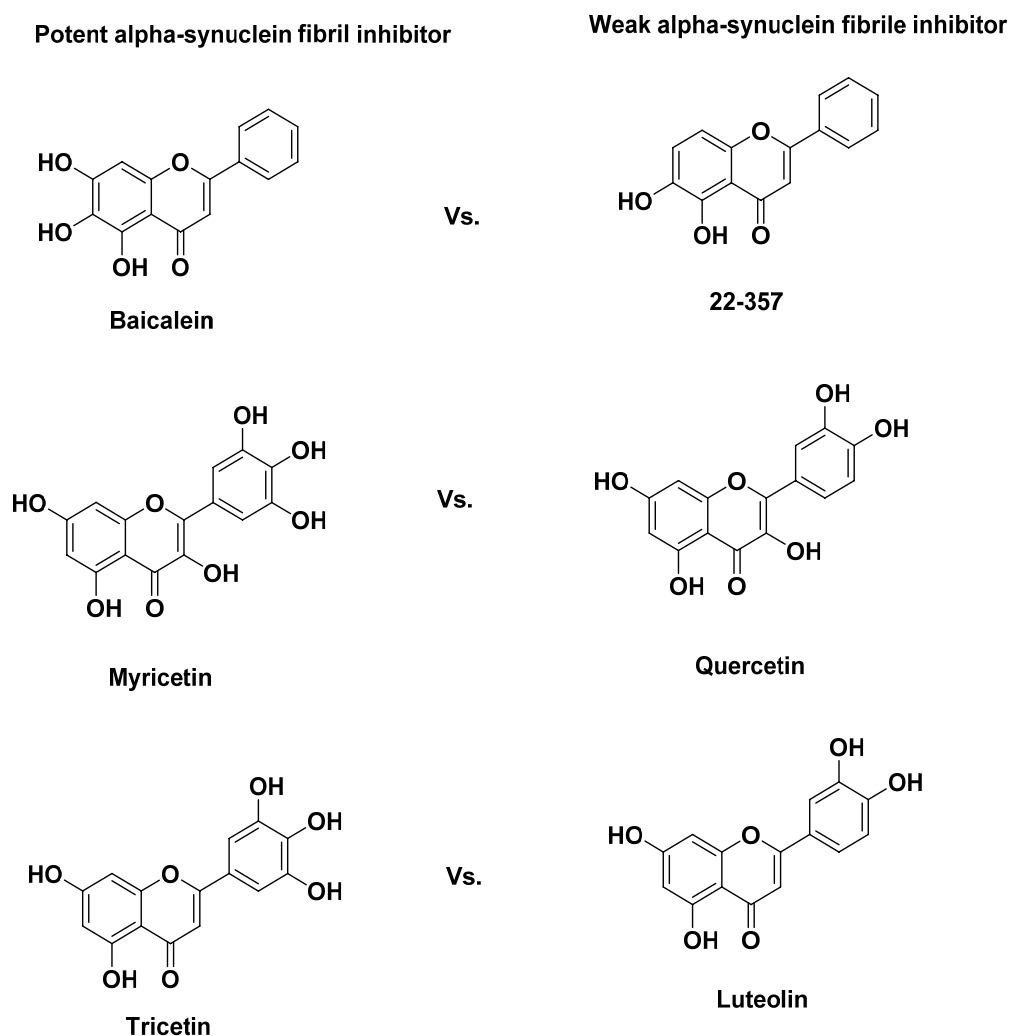


Figure 15. Comparison of ASN aggregation modulation property of various flavanoids

The molecular mechanism underlying the flavonoids-induced inhibition of ASN fibrillation may be combination of noncovalent binding of inhibitory flavonoids to ASN, and the covalent modification by the flavonoids lead to the restriction of the conformational changes in this natively unfolded protein, or the stabilization of soluble flavonoid-modified species of ASN.

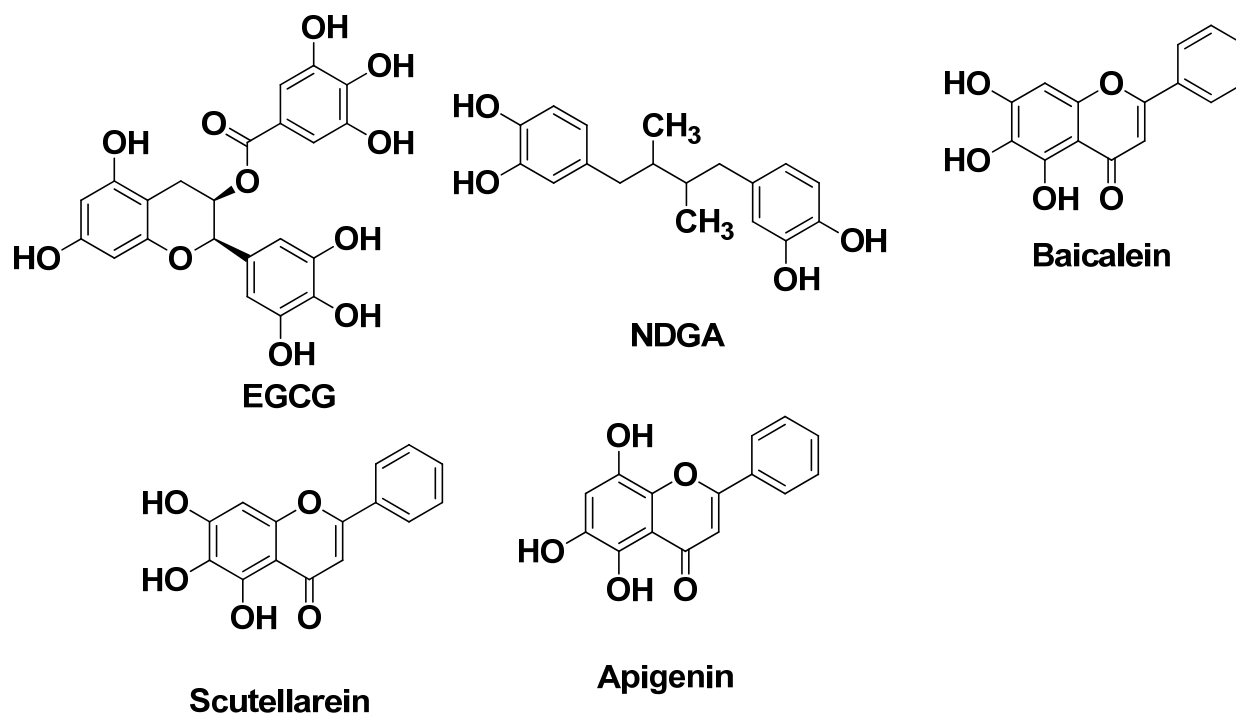


Figure 16. Chemical structure know ASN aggregation modulators

1.9.1.2. Other small molecules as a possible modulator of ASN aggregation:

Molecular Tweezers (MT), recently Prabhudesai et al., discovered the water soluble “molecular tweezers (MT)”, termed CLR01 specific for lysine as a general inhibitor of aggregation and toxicity of amyloid proteins including ASN.⁷⁹ CLR01 binds specifically with the lysine residue of ASN via the hydrophobic and electrostatic forces. It inhibits the aggregation of ASN into the fibril and caused disaggregation of preformed fibril. Furthermore, CLR01 can also stabilize ASN in the small, nontoxic

oligomeric species and dose dependent inhibits the toxicity by ASN in the cell culture model. Finally, CLR01, has been assessed in *zebrafish* (ZF) embryo against the ASN induced neurotoxicity. Addition of CLR01, to the water in which *zebrafish* (ZF) embryo developed led to dramatic improvement in viability and it maintains ASN in soluble form by restoring ubiquitin proteasomal (UPS) activity.

Effect of B2 on ASN aggregation, It is also possible that compounds that might not inhibit the ASN inclusion formation, yet can block downstream pathways responsible for the toxicity of ASN aggregates.⁸⁰ One of the lead molecule, B2, was tested for its effect on ASN inclusion formation in the CHO-K1 cells transiently transfected with SynT, a tagged α -SN. After B2 treatment a significant enhancement in the ASN aggregates was observed. But when it was tested on ASN transfected H4 neuroglioma, a significant reduction in ASN mediated adenylate kinase release was observed and it protected against toxicity from overexpression of ASN.

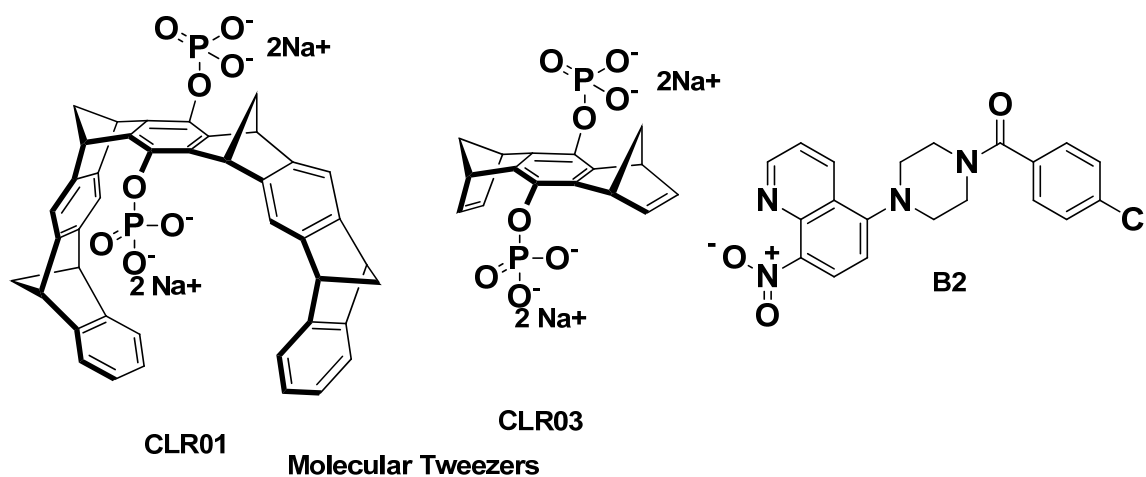


Figure 17. Chemical Structure of non-hydroxyl ASN aggregation modulators

Heat shock protein (Hsp) modulators, Lewy body contains ASN as well as several Hsp, which are molecular chaperones. Hsp modulator are protective against α -SN induced toxicity, and can prevent its aggregation. SNX-2112 and its derivatives are

novel orally available, potent Hsp90 inhibitors which can rescue ASN induced toxicity and oligomerization in *in vitro* in a dose dependent manner.⁸¹

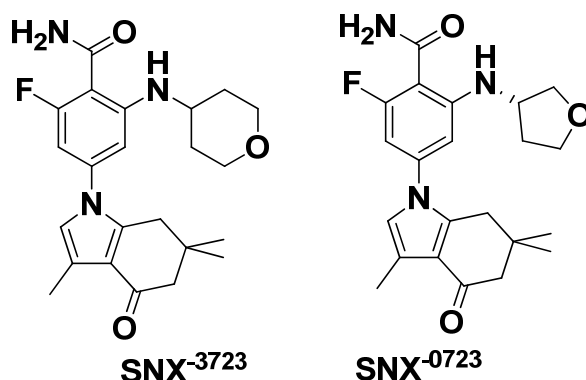


Figure 18. Heat shock protein (Hsp) modulators

Novel Synthetic Peptides, these based on the native sequence of protein can prevent the conversion into the toxic species. El-Agnaf et al, identified the critical binding region in the ASN molecule responsible for its self aggregation.⁸² Then the library of small peptides homologous to this region was synthesized, and the binding of these peptides was studied using ELISA assay.

The shortest peptide responsible for inhibition of ASN aggregation has the sequence AVVT, corresponding the central NAC region of ASN. Furthermore these peptides were able to inhibit the aggregation of alone NAC region. The potential use of these peptides as drug for PD depend upon their ability to cross the blood brain barrier and inhibit the formation of toxic oligomeric species of ASN in the brain.

1.9.2. Other alternative pathways to combat ASN toxicity:

The total amount of ASN is very critical factor for its aggregation which can increase due to the enhance transcription or due to reduced degradation of ASN. Regulator factor for ASN transcription are not clearly known but Intron 1 of SNCA was found to

be responsible element for its transcription. Using the siRNA approach Vekrellis et al, found Zip1 (zinc finger proliferation 1) as one of the elements at the 5' end of intron 1 responsible for ASN transcription in PC12 cells.⁸³ Apart from this, ERK (extracellular-signal-regulated kinase) and PI3K are also important for the regulation of ASN levels. MicroRNAs are also emerging as novel regulators for the ASN gene expression. Degradation of ASN occurs via lysosomal pathways of chaperone-mediated autophagy (CMA), macroautophagy, or by proteasome. Targeting these ASN degradation pathways are also emerging as novel approaches to treat PD. Active and passive immunization is emerging as a novel strategy to treat the synucleinopathies. Masliah et al.,⁸⁴ vaccinated human ASN transgenic mice with human ASN that produced relative high affinity antibodies, and observed a decrease in accumulation of aggregated ASN in neuronal cell bodies and synapses along with improvement in behavioral deficit.

1.10. Multi-target-directed ligand (MTDL) therapy:

Because of the fact that there are multiple interrelated pathogenic factors that are associated with PD, drugs hitting a single target may be inadequate for its treatment. When a single medicine is not sufficient to effectively treat a disease, a multiple-medication therapy (MMT) (combination of drugs) might be used⁸⁵. Usually, an MMT is composed of two or three different drugs that target different therapeutic mechanisms. But this approach might be disadvantageous for patients with compliance problems. A second approach might be the use of a multiple-compound medication (MCM) (also referred to as a "single-pill drug combination"), which implies the incorporation of different drugs into the same formulation in order to simplify dosing regimens and improve patient compliance. Finally, a third strategy is now emerging on the basis of the assumption that a single compound may be able

to hit multiple targets that is multiple target directed ligands (MTDL). Clearly, MTDL have inherent advantages over MMT or MCM. It would obviate the challenge of administering multiple single-drug entities, which could have different bioavailability, pharmacokinetics, and metabolism. Furthermore, in terms of pharmacokinetic and ADMET optimization, the clinical development of a drug able to hit multiple targets should not, in principle, be different from the development of any other single lead molecule. It thus offers a much simpler approach than MMT/MCM. In addition, the risk of possible drug-drug interactions and associated side effects would be avoided and the therapeutic regimen greatly simplified in relation to MMT. There is a strong indication that the development of compounds able to hit multiple targets might disclose new avenues for the treatment of, for example, major neurodegenerative diseases, for which an effective cure is an urgent need and an unmet goal. MTDLs more completely describes those compounds that are effective in treating complex diseases because of their ability to interact with the multiple targets thought to be responsible for the disease pathogenesis.

Chapter 2

Research Background in the evolution of D3 preferring ligands and other approaches to PD therapy

2.1. Development of D3 preferring ligands

2.1.1. Rigid analogs of Dopamine:

Following discovery of the DA D3 receptor in 1990, several well-known DA receptor agonists were evaluated for their D3 receptor binding affinity and selectivity. In order to introduce higher affinity and selectivity for D2/D3, structural evolution has been made from the endogenous agonist dopamine to metabolically more stable, bioisosterically modified moieties. It is important to mention that D2 and D3 receptor subtypes exhibit 50% homology in their amino acid sequence and it extends to 75-80% in the helical transmembrane spanning domains, where agonist binding sites are believed to be located.^{86, 87} This makes the task of developing D3-selective ligands challenging. An enormous amount of work has been done to develop D3 selective agonist and to identify key pharmacophoric features responsible for selectivity for D3 receptor over D2.^{61, 88-96} The endogenous ligand, DA, binds both high and low affinity state (3.9 nM and 73 nM, respectively) of the human D3 receptor. DA has also displayed low selectivity ($D2/D3 = 0.4-46$) for D3 over D2 receptors. Rigidization of the aminoethyl side chain of DA has yielded the 2-aminotetralins, (*S*)-5-OH- and (*R*)-7-OH-DPAT. These conformationally restricted analogs correspond to the α - and β -rotomers of DA and were designed based on SAR studies that determined only the *m*-hydroxyl group of DA to be crucial for DA receptor agonist activity. SAR studies have indicated moderate D3 selectivity for both (*S*)-5-OH- and (*R*)-7-OH-DPAT ($D2/D3 = 26$ and 60 , respectively).

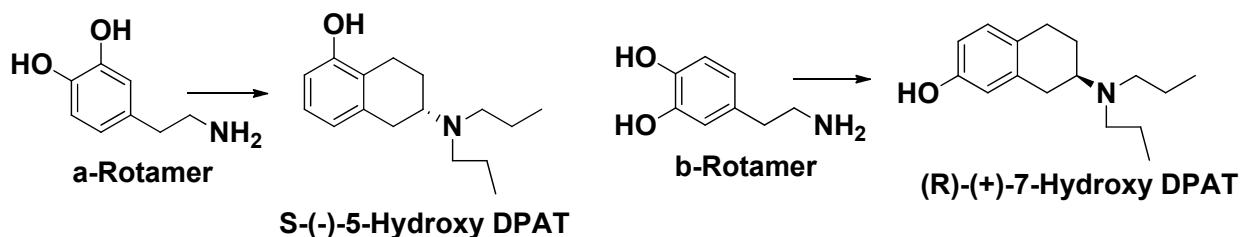


Figure 19. Evolution of aminotetraline class of molecules by Rigidization of dopamine

Extensive SAR study has been done on these two classes of molecules, some of which suggest hydroxyl group at 7 position of the aromatic ring is more preferable for the affinity toward D3 receptor over D2 receptor⁹⁷. Resolution of racemic (\pm)-7-OH-DPAT⁹⁸ causes increase in affinity in R-(+)-7-OH-DPAT. In contrast to this finding, the S-(-) enantiomer of 5-OH-DPAT is more potent. It is important to mention again that the selectivity ratio largely depends on the assay conditions.

The substitutions of primary amine with two propyl groups in both 7-OH- DPAT and 5-OH- DPAT series make them less potent for D2 receptor without much change in the affinity towards D3 receptor, thereby, increasing the selectivity for D3 receptor. It indicates change in basicity of the nitrogen is not very important to increase the affinity of those molecules toward D3 receptor and the basicity of the tertiary amine at that position is strong enough to establish hydrogen bonding with ASP110 residue in the transmembrane domain of the receptor. However, propyl group is optimal for receptor interaction which suggests that one of its N substituent must fit into a receptor cavity known as propyl cleft. A great deal of work has been done to establish structure activity relationships of amino tetralines before the discovery of different receptor subtypes. The importance of both hydroxyl groups as 5, 6 dihydroxy or 6, 7 dihydroxy in aminotetraline structure (Figure 20) have also been

studied⁹⁹. The result showed 6,7 Dihydroxy compound (20b in figure 20) is more potent agonist for dopamine receptor than its 5, 6 Dihydroxy isomer in stimulating the release of radioactive dopamine in rat brain slices⁹⁹.

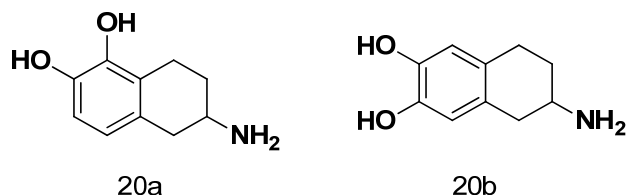


Figure 20. 2-Amino-5, 6-dihydroxy tetrahydronaphthalene (ADTN) analogs.

Further Rigidization of the 2-aminotetralins, specifically 7-OH-DPAT, led to tricyclic DA agonists, such as (+)-PD 128907¹⁰⁰. (+)-PD 128907 binds to the D3 receptor with high affinity (1-2 nM) and selectivity (D2/D3 = 220-1270). It has been hypothesized that incorporation of an oxygen atom at position 6 of PD 128907 enhances D3-selectivity versus D2 receptor due to a decrease in hydrophobicity.

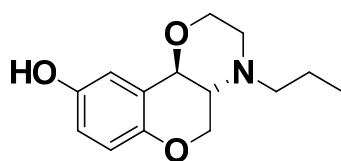


Figure 21. Structure of tricyclic DA agonists (+)-PD 128907.

2.1.2. Bioisosteric Replacement of Catechol Moiety of Dopamine:

After this initial strategy of rigidization of dopamine molecule to come up with potent dopamine D3 receptor preferring agonists, the catechol moiety of dopamine was replaced with metabolically more stable bioisosteric heterocyclic moieties. In this regard, introduction of 2-aminothazole (Pramipexole) as a bioisosteric replacement of catechol moiety increases oral bioavailability of the compound⁹⁷. Generally, many D3 preferring agonists were developed that incorporates heterocyclic moiety in their

agonist binding site. Examples of such compounds are pramipexole, pergolide, quinpirole, quinlorane, ropinirole, etc (Figure 24). Pramipexole, which replaces the catechol moiety of DA with an aminothiazole substructure, maintains high D3 affinity ($K_i = 0.5-8.5$ nM), while D3 selectivity ranges from moderate to high, depending on experimental conditions. Another example of bioisosteric replacement of the catechol moiety is pergolide, a semi-synthetic ergot alkaloid, which was developed as a selective, D3 autoreceptor agonist ¹⁰¹. Pergolide was found to decrease DA turnover at low doses (0.01 mg/kg, i.p), sparking interest into exploring additional bioisosteric replacements within the pergolide skeleton. Quinpirole, containing elements of the ergoline template, along with a pyrrole ring system acting as a bioisostere, binds with relatively high affinity (K_i D3 = 0.96-43? nM) to D3 receptors and with low to high selectivity (D2/D3 = 0.8-133) ¹⁰². Quinpirole also displayed an 8-fold functional selectivity for D3 receptor (D2 EC50 = 2.4 nM, D3 EC50 = 0.29 nM) versus D2 receptor. The pyrrole moiety was further investigated in a series of molecules that diversified the position of the nitrogen atom in the aromatic ring ^{89, 103}. In this series of analogues, the 1-aza derivative, (S)-20 (22a in figure 22) displayed moderate potency (K_i D3 = 38 nM) and high selectivity (D2/D3 = 316) for D3 over other DA receptor subtypes. Likewise, other 1-aza derivatives, containing N-methyl (S)-22 (22b in figure 22) or N-formyl (S)-23 (22c in figure 22), indicate similar D3 affinity with moderate selectivity. Introduction of formyl in the 7a-aza derivative lead to development of FAUC 54 (22d in figure 22)), which exhibited enhanced D3 affinity ($K_i = 5.3$ nM), along with maintaining some selectivity. FAUC 54 was found to be a full agonist at D3 receptor (EC50 = 1.1 nM, 89% efficacy relative to quinpirole). Interestingly, aminotetrahydropyrazolo derivative was designed, in which the hydrogen-bond accepting formyl (FACU) or cyano functions are truncated to the lone

pair of the sp^2 nitrogen. Similar to (S)-24a, (S)-25 displayed high D3 affinity (K_i D3 = 4.0 nM, D2 = 180 nM) and weak binding to D2 receptor. (S)-25 exhibits high potency (EC_{50} = 3.4 nM) and intrinsic activity (82%) in stimulation of mitogenesis at D3 receptors.

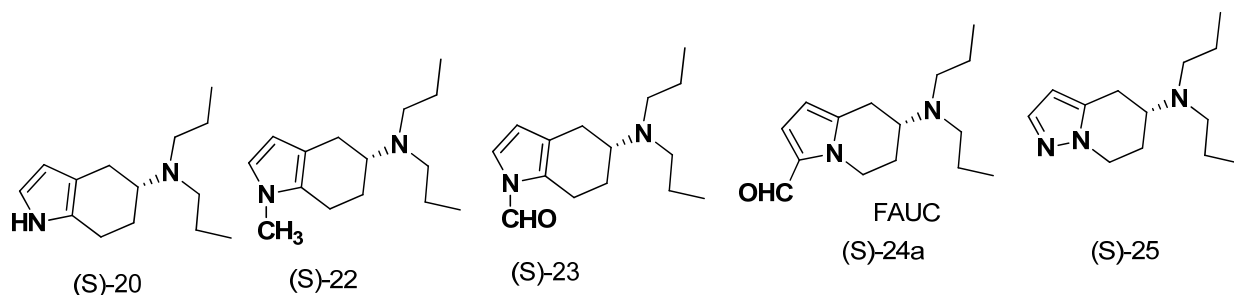


Figure 22. Pyrrole derivatives with diversified the position of the nitrogen atom in the aromatic ring.

2.1.2.1. Non-aromatic D3 preferring agonist:

Interestingly, several types of non-aromatic, but conjugated π -systems have been discovered to mimic the catechol nucleus of DA. Increasing evidence suggests that optimized hydrophobic effects can compensate for the attractive forces resulting from hydrogen bonding. The conformationally restricted enyne, FAUC 73, was found to have high affinity for D3 receptor (5.2 nM) and a 52-fold preference for D3 over D2 receptor. Replacement of the acetylene function in FAUC 73 by a vinyl group yielded FAUC 206. FAUC 206 maintained D3 affinity (5.6 nM) and preference over D2 (41-fold), while gaining a 64-fold preference over D4 receptors. Insertion of an adjacent acetylene unit in FAUC 73 produced FAUC 88, which showed a significant increase in D3 affinity (3.2 nM) and a 29-fold preference over D2 receptor, making it the most potent non-aromatic DA agonist known to date. FAUC 73 and FAUC 88 each show high efficacy at D2 (85% for both) and D3 (72% for FAUC 88 and 74%

for FAUC 73) receptors in mitogenesis assay. The high potency and selectivity of these ligands suggest that aromatic or heteroaromatic systems are not required for ligand recognition or intrinsic activity at D3 receptor.

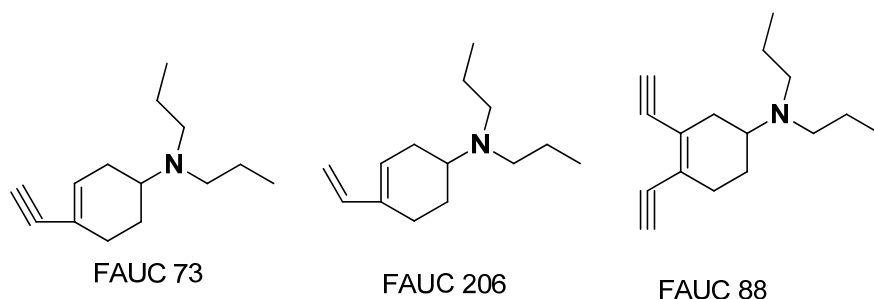


Figure 23. Non-aromatic D3 preferring agonist.

Changing the fragment of the molecule that imparts agonist property from catechol or phenol to bioisosteric heterocycle is challenging, because changes in the receptor interaction as a result of molecular modification can potentially alter a molecule from agonist to partial agonist or to antagonist. However, all of these compounds have moderate to high selectivity for D3 receptor over D2. Pramipexole is proven to be agonist with 100% intrinsic activity at D2 and 80% at D3 in mitogenesis functional assay¹⁰⁴ compared to reference compound quinpirole, which is considered as reference full agonist. Functional potencies were also evaluated for these compounds by [³⁵S]GTPγS binding to the cloned D2, D3 receptors expressed in CHO cells. This assay typically shows more selectivity for D3 over D2 compared to mitogenesis functional assay. All of those above mentioned compounds are either full agonist or partial agonist for D2/D3 receptor¹⁰⁵.

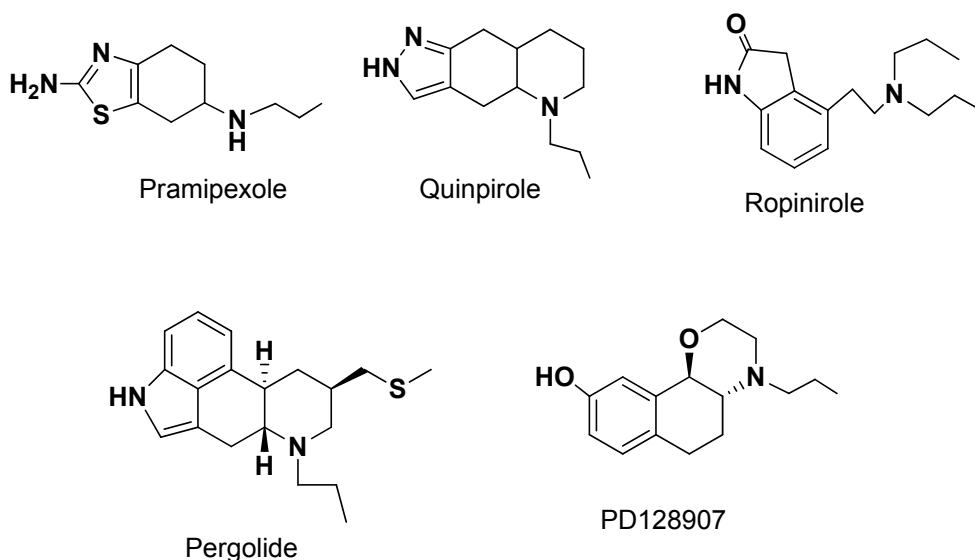


Figure 24. Structure of metabolically stable heterocyclic D3 preferring agonists.

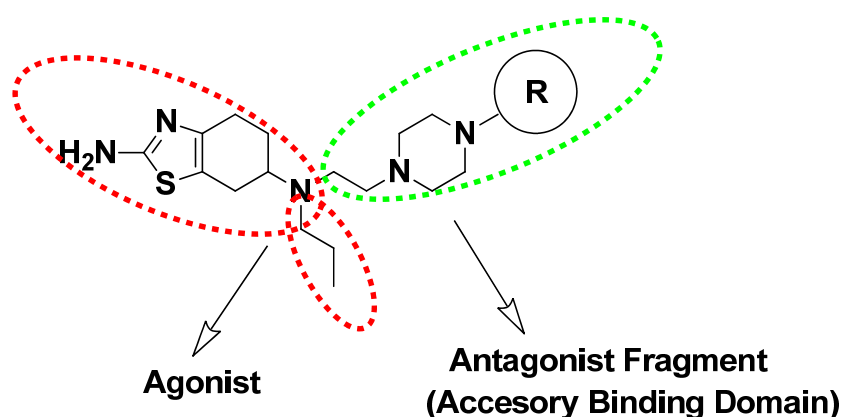


Figure 25. Hybrid Drug Design Model

2.1.3. Evolution of Accessory Binding Molecular Determinant:

So far, our discussion was based on design of the portion of the molecule that imparts agonist property. However, our goal in research is also to increase D3 selectivity of the compounds by incorporating molecular determinants that should interact with accessory binding sites in the receptor binding cavity while retaining its functional activity. As we discussed, N-propyl substitution is an optimum and a requirement for potent agonist¹⁰⁶ activity and various N, N-di alkyl substitution in the

secondary amine is also tolerated by the receptor. A great deal of research has already been done for side chain modification in aminotetralines and heterocyclic analogous structures. It has been found that slight modification in second N-alkyl side chain leads to D3 selective compounds.

Several studies showed benzamide class of molecules as potent D3 selective antagonists. The position of benzamide varies in the structures. Benzamide analogs such as sulpiride, raclopride, which are atypical antipsychotics, display a high affinity for both D2/D3 receptors. Other sulpiride based benzamide analogs (Figure 26) had been developed which function as antagonist for D2/D3 receptors¹⁰⁷.

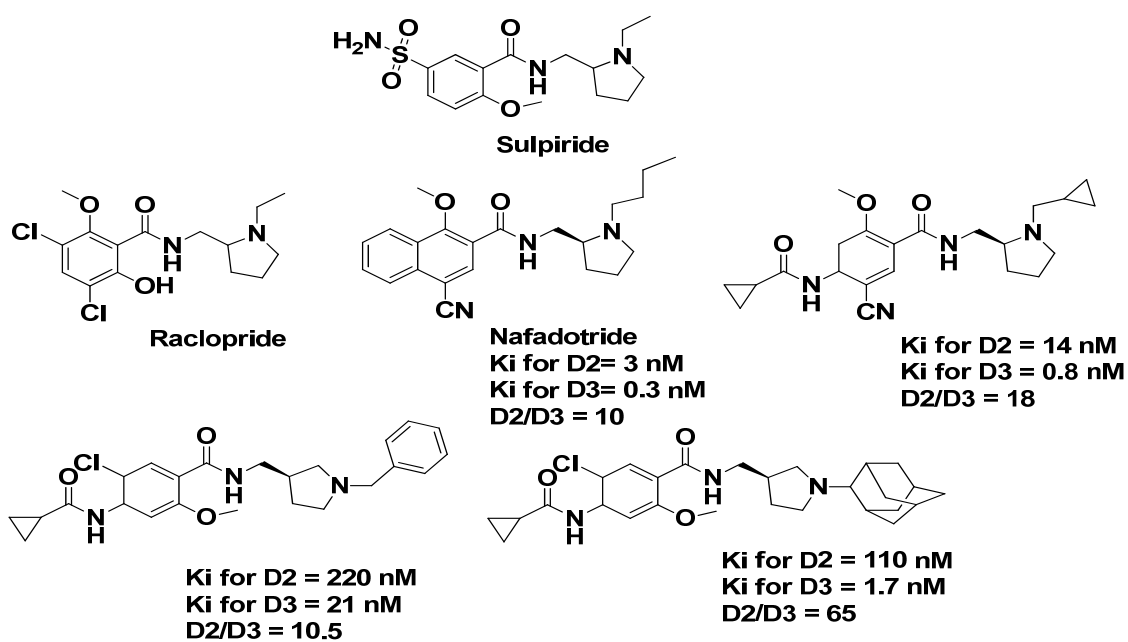


Figure 26. Sulpiride based benzamide analogs having high D3 selectivity.

The sulpiride based benzamide series was followed by conformationally flexible benzamide analogs¹⁰⁸ that incorporated aryl piperazine fragment. In fact, the basic nitrogen in sulpiride based nitrogen was replaced by one piperazine nitrogen. This class of molecules also lacked methoxy substitution in aromatic ring of the benzamide. Another characteristic of this class of molecules was separation of the

basic amine from the benzamide by a conformationally flexible tetramethylene linker (Figure 27). GR103691, an atypical antipsychotic agent is a prototypical example of this class¹⁰⁸ which showed high affinity and selectivity for D3 receptor ($D2/D3 = 133$). Murray et al. (1995) reported that the aryl piperazine portion in molecules, which came from accessory binding site of known 5-HT_{1A} receptor agonists molecules. Addition of the 4-biphenyl carboxamide butyl side-chain (taken from known D3 receptor preferring antagonists) was responsible for the high D3 affinity and antagonist property of GR103691 and the other compounds in that series. The molecule containing aryl piperazine fragment GR103691 is 133 fold selective for D3 over D2, but only 10 fold selective over 5-HT_{1A} receptor.

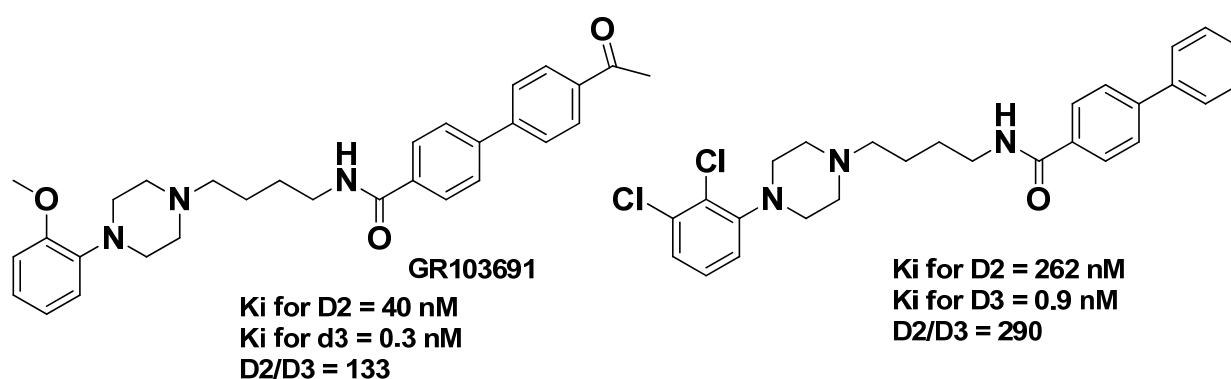


Figure 27. Hybrid structures of conformationally flexible benzamide analogs and aryl piperazine with high D3 selectivity¹⁰⁸.

After the discovery of the series of aryl piperazine and 4-biphenyl carboxamide hybrids¹⁰⁸ (Figure 27), another strategy that was followed to synthesize D3 selective ligands is hybridization of two chemical entities, 2-aminotetraline and conformationally flexible 4-biphenyl carboxamide structure¹⁰⁹ (Figure 28). Boyfield et al. reported combination of 5-hydroxy DPAT and benzamide fragment. The compounds in this series were highly potent (Ki for D3 is 0.2 nM in compound 28a in

figure 28) and selective (D2/D3 ratio as high as 310). Some of these compounds were proven to be agonist in functional assay. Other well known D3 agonists were also used to generate hybrid structures like quinlorane¹¹⁰. Example of that class of molecule is shown in figure 28 (compound 28a, 28b). The quinlorane derived 2-amino analog showed high affinity (K_i for D3 = 0.8 nM) and high D3 selectivity (D2/D3 = 250).

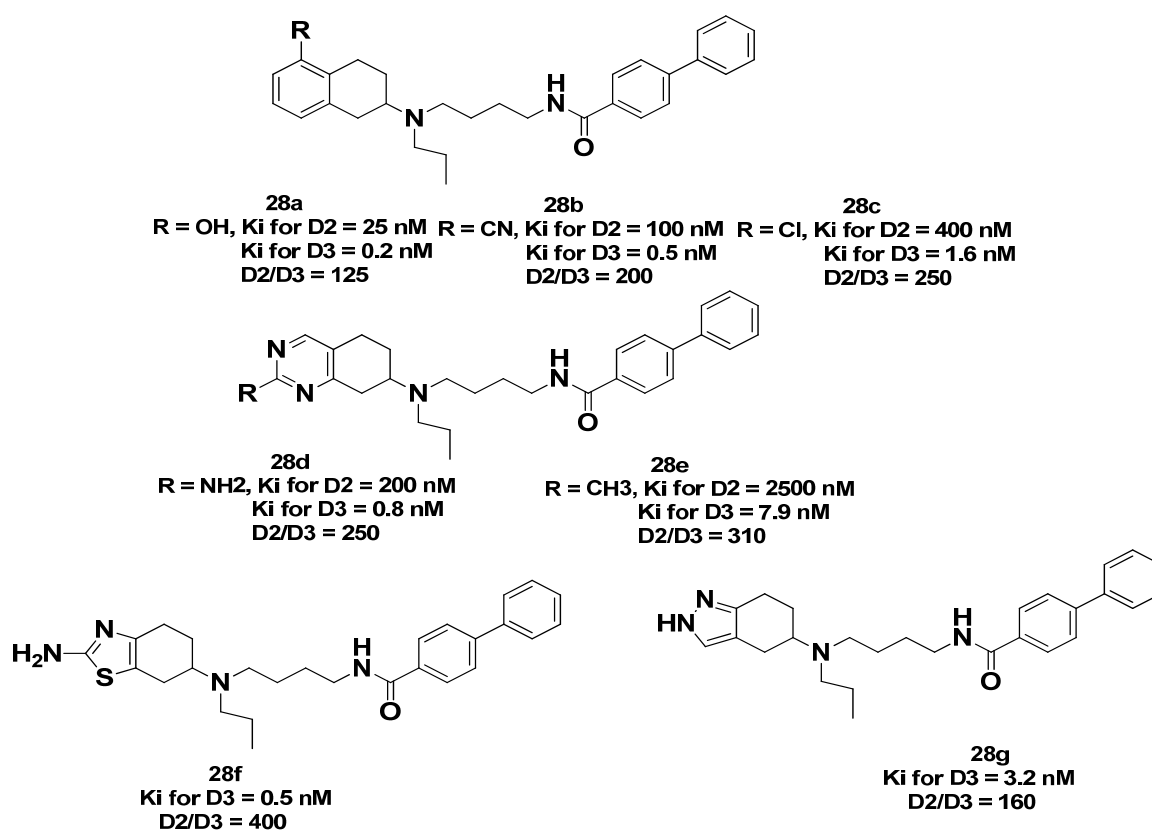


Figure 28. Structure of some of the hybrids of 2-aminotetraline or its metabolically stable bioisosteric moiety and flexible benzamide moiety^{109, 110}.

Rapid metabolism of 2-aminotetraline hybrid molecules via N-depropylation leads to discovery of a series of molecules that replaces the N-propyl side chain with a 5 or 6-membered ring system. The correct stereochemistry of the ring fusion is

apparently important, since racemic isomer is less potent and selective for D3 receptors.

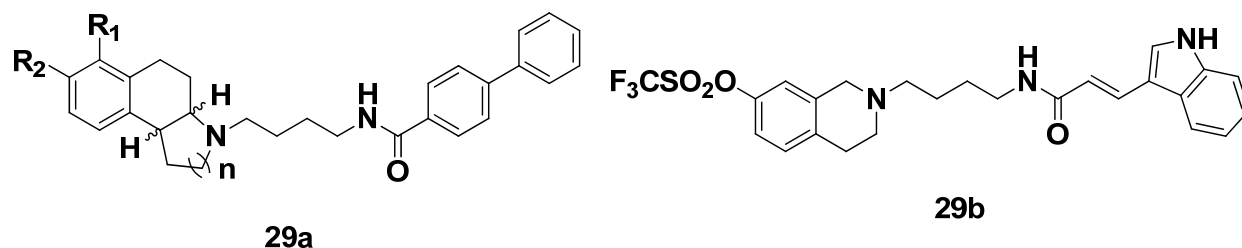


Figure 29. Structure of some of the hybrids metabolically stable bioisosteric of 2-aminotetraline.

Another strategy to avoid the fast metabolism for 2-aminotetraline type molecules is to integrate the basic nitrogen into the cyclohexane ring and the substitution of the biphenyl moiety with indole like functionalities. Compound **29b** is a potent and selective antagonist of D3 receptor with good brain penetration, low blood clearance and a reasonable long plasma half life.

Other agonists such as pramipexole, quinpirole were also combined with benzamide fragment which leads to agonists with high D3 selectivity. 4-Arylpiperazines and its analogs are well known for its affinity towards D3 receptor. 2,3-dichlorophenyl piperazine derivatives **30a** (Figure 30)¹⁰⁸ where piperazine was linked to the naphthamide through ethyl linker exhibited high D3 affinity and selectivity (Figure 30) than for propyl (D2/D3 = 6) or butyl (D2/D3 = 8) linker. Preference for ethyl linker is very unique for this class of molecules, because, all previous D3 receptor ligands possessed tetramethylene linker. Substituents at the phenyl moiety are found to be better tolerated in the ortho than in the *meta* or *para* positions in terms of retaining D3 receptor affinity.

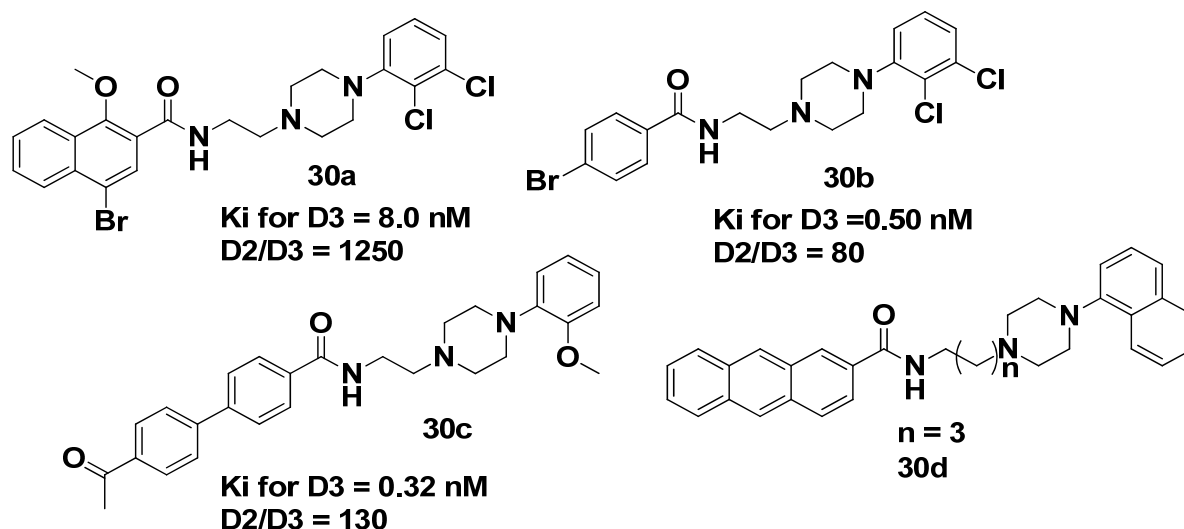


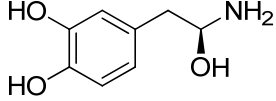
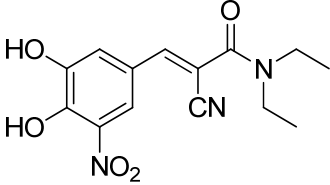
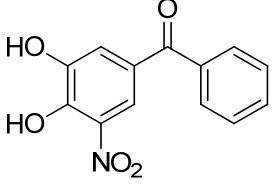
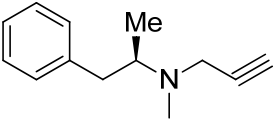
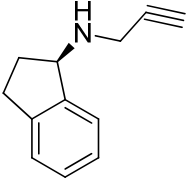
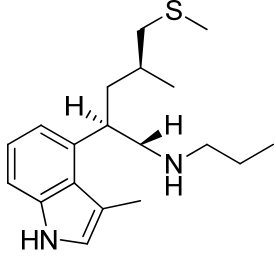
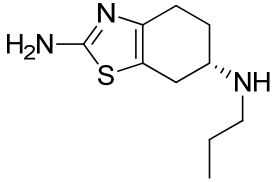
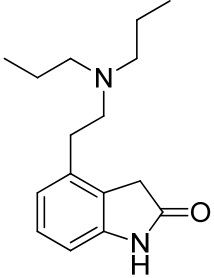
Figure 30. 4-Phenyl piperazine analogs with high D3 selectivity.

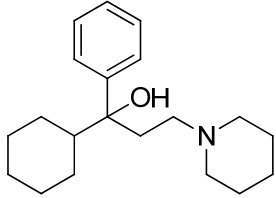
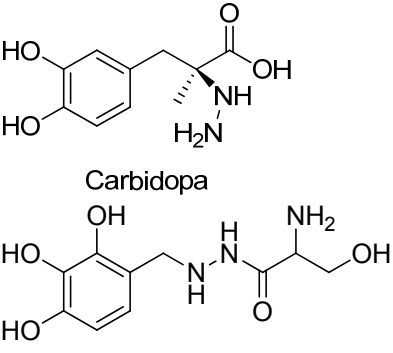
2.2. Development of multifunctional ligands for neurodegenerative diseases:

2.2.1. Currently available Treatments

The current therapies improve the symptoms but without halting the progression of the neurodegenerative disease process or reversing the neuronal degeneration. Furthermore, the treatment of the resulting predominantly nonmotor features like dementia remains a challenge. To compensate for the depleted striatal DA from the loss of nigral projections is the main goal for the currently available drugs (**Table 1**). The classes of compounds that still hold a prominent position in current anti-PD drug discovery are L-dopa and dopaminergic receptor agonists (both used alone or as MMT) and MMT/MCM of L-dopa with DA level modifying drugs, such as (i) peripheral dopa decarboxylase inhibitors,⁷¹ (ii) catechol-Omethyltransferase (COMT)

Mode of Action	Drugs

DA precursor	 <p style="text-align: center;">L-dopa</p>
COMT inhibitor	<div style="display: flex; justify-content: space-around; align-items: center;"> <div style="text-align: center;">  <p>Entacapone</p> </div> <div style="text-align: center;">  <p>Tolcapone</p> </div> </div>
MAO-B inhibitor	<div style="display: flex; justify-content: space-around; align-items: center;"> <div style="text-align: center;">  <p>Selegiline</p> </div> <div style="text-align: center;">  <p>Rasagiline</p> </div> </div>
Dopaminergic receptor agonist (ergot derivatives)	<div style="text-align: center;">  <p>Pergolide</p> </div>
Dopaminergic receptor agonist (non-ergot derivatives)	<div style="display: flex; justify-content: space-around; align-items: center;"> <div style="text-align: center;">  <p>Pramipexole</p> </div> <div style="text-align: center;">  <p>Ropinirole</p> </div> </div>

Muscarinic Receptor Antagonists	 <p style="text-align: center;">Triexphenidyl</p>
Peripheral dopa decarboxylase inhibitor	 <p style="text-align: center;">Carbidopa</p> <p style="text-align: center;">Benserazide</p>

inhibitors, and (iii) selective monoaminooxidase type B (MAO-B) inhibitors.

2.2.2. Emergence of multifunction drugs for the treatment of neurodegeneration

More recently, a new paradigm that addresses disease etiological complexity by a multi-targeted-single-ligand approach has gained increasing acceptance. Morphy & Rankovic have reported the structure and activity of compounds designed as multifunctional drugs ¹¹¹.

2.2.2.1. Combination of MAO-B and COMT inhibitor

MAO-B inhibitors (Selegiline and Rasagiline) ¹¹² and COMT inhibitors (Entacapone and Tolacapone) ¹¹³ are used mainly as MMT to reduce the L-dopa metabolism. It has been described in the chapter 1 that dopaminergic receptor agonists may be used either alone or with L-dopa to increase its effectiveness. More recent

therapeutic approaches to PD are represented by nicotine, anti-inflammatory agents, melatonin, selenium, iron chelators, and vitamins A, C, and E¹¹⁴.

2.2.2.2. Targeting MAO, iron and oxidative stress

A common approach has been the combination, in a single molecule, of the pharmacophoric features responsible for modulating the biological activity of a validated molecular target with the chemical functions able to confer metal-chelating and/or antioxidant properties and/or MAO inhibitory activity. Rasagiline was originally designed as a monoamine oxidase B (MAO-B) inhibitor to increase levels of dopamine in the brain, specifically in the striatum, to restore the motor function in PD. This disease-modifying effect of rasagiline is due to its interaction with an array of targets along the pathological pathways of PD. However, rasagiline specifically activates enzymes playing a key role in cellular events including mitochondria viability, modulation of apoptotic processes, and neuronal plasticity. This pharmacological action is associated with (i) the prevention of both the neurotoxin-induced fall in mitochondrial membrane potential and opening of mitochondria permeability transition pore,⁷¹ (ii) activation of the proteasome-ubiquitin complex, (iii) inhibition of cytochrome-c release, and (iv) prevention of caspase-3 activation¹¹⁵. The molecular mechanism of neuroprotective antiapoptotic activity of rasagiline has been attributed to its ability to modulate Bcl-2 protein family, up-regulating the antiapoptotic Bcl-2 and Bcl-xL while down-regulating Bad and Bax^{116, 117}.

As proof of concept, Zheng et al. developed dual dual iron chelator and MAO-A/B inhibitor for the treatment of PD. The authors have used antioxidant moiety propargylamine with the iron chelator part of an 8-hydroxyquinoline to synthesize the neuroprotective brain-permeable iron chelator VK-28. The resulting product, HLA20,

preferably inhibits MAO-B with an IC₅₀ of 110 nM, acts as a free radical scavenger. Another propargylamine (M30) was found to be a highly potent MAO-A and -B inhibitor in vitro and in vivo, in addition to having iron chelating properties similar to desferoxamine. M30 behaves similarly to other propargylamine MAO inhibitors. In PC12 cells, some of these derivatives [HLA20 and M30] were also found to be potent lipid peroxidation inhibitors. This is possibly as a consequence of two different mechanisms: (i) strong iron-chelating compounds interfere with Fenton's reaction, thus decreasing hydroxyl free radical production;⁷¹ (ii) metal chelators can also directly act as radical scavengers, blocking the formation of free radical species¹¹⁸. Conversely, in vivo, **M-30A** inhibited MAO enzymes at concentrations that were 2-3 orders of magnitude higher than those of **M-30**. This is in line with the profile of N-demethylated derivatives of other MAO-B inhibitors such as Selegiline and Rasagiline ¹¹⁹. Because of its nonselective MAO inhibiting profile, **M-30** was also able to increase 5-HT and adrenaline in the CNS, in addition to DA, providing a probable adjunct profile as an antidepressant. A molecule, able to simultaneously inhibit both MAO-A and MAO-B, without potentiating the tyramine-mediated cardiovascular activity holds a promising profile for the treatment of PD.

The success of rasagiline led to the designed development of unique DML ladostigil, from the same group of researchers. Ladostigil is a dual ACh-butrylcholine (BuCh)-esterase and brain-selective MAO-A and -B inhibitor in vivo. Ladostigil is currently in Phase II studies, and anticipated to be beneficial for the treatment of dementia comorbid with extrapyramidal disorders and depression. The propargylamine moiety was found to be a key pharmacophoric features responsible for neuroprotective activity.

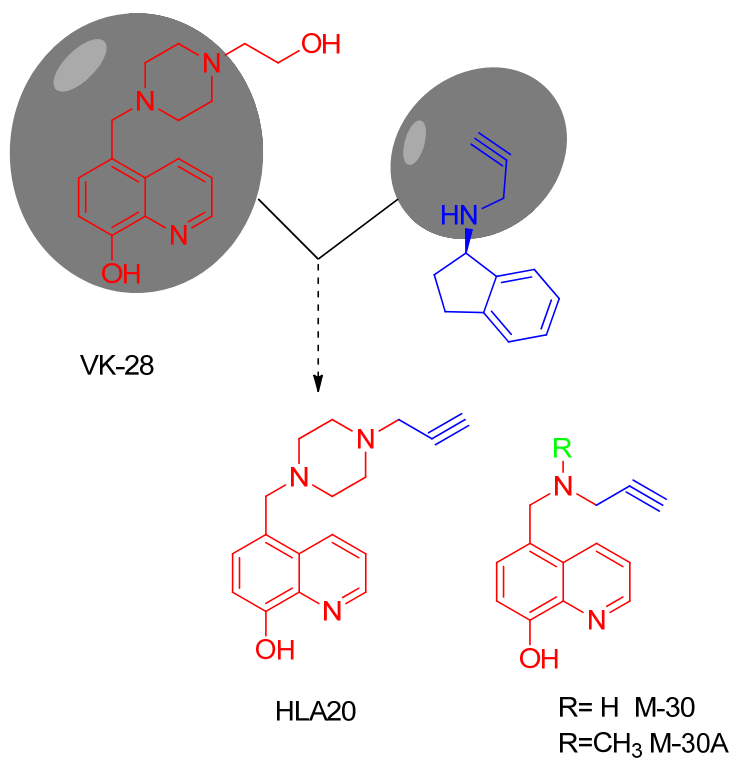


Figure 31. Design to develop bifunctional compounds.

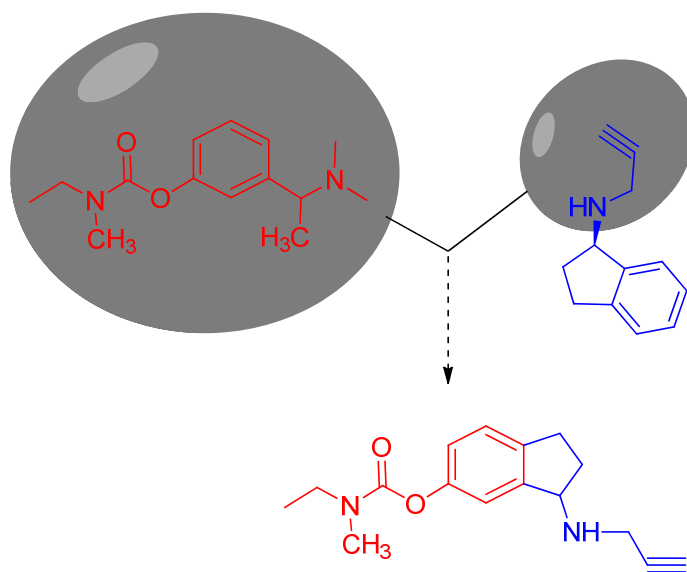


Figure 32. Design to develop bifunctional compounds

2.2.2.3. Targeting MAO and Adenosine A_{2A} receptor

A second class of potential anti-PD MTDLs was developed by combining MAO inhibition and adenosine A_{2A} receptor antagonism. The rationale for the design strategy was based on the observation that caffeine consumption is associated with a reduced risk of developing PD^{120, 121}. Adenosine A_{2A} receptor antagonists are currently being investigated as possible therapeutic agents for the symptomatic treatment of motor deficit in PD¹²². One compound is currently undergoing clinical trials for this purpose¹²³. In addition, it has recently been shown that adenosine A_{2A} receptor antagonists can also protect against neuronal degenerative processes^{124, 125}. A selective and potent adenosine A_{2A} receptor antagonist, 8-(3-chlorostyryl)caffeine (**33**)¹²⁶ (**Figure 33**) with MAO-B inhibitory activity, was tested *in vitro* against MAO-B mitochondrial activity to assess a potential bifunctional profile, showing a K_i of about 100 nM¹²⁴. It was then characterized *in vivo* using the MPTP (1-methyl-4-(1-methylpyrrol-2-yl)-1,2,3,6-tetrahydropyridine) animal model of PD¹²⁷. To cause neurotoxicity, MPTP requires its oxidation to 1-methyl-4-phenylpyridinium (MPP+) by MAO-B. The effects of **33** on the MPTP metabolism were therefore also investigated *in vivo*. The inhibition of MPTP metabolism by **33** suggests that adenosine A_{2A} receptor does not regulate MAO-B activity. It also suggests that the two biological profiles, MAO-B inhibition and adenosine A_{2A} receptor antagonism, are indeed unrelated, acting on two parallel biochemical pathways¹²⁸. Conversely, the metal-chelating MAO-inhibitor MTDLs discussed above, reduced the hydroxyl radical formation synergistically by modulating steps within the same linear biochemical pathway. In the design of MTDLs for complex multifactorial diseases, it is still unclear whether it is more beneficial for an MTDL to act at different points within the same biochemical pathway or to modulate targets belonging to parallel pathways. The observation was that a bifunctional adenosine A_{2A} receptor

antagonist and MAO-B inhibitor might bear enhanced therapeutic potential for the treatment of PD¹²⁸. As discussed, current MTDLs for PD have been based on MAO inhibition combined with a second activity, such as iron chelation and antioxidation and adenosine A_{2A} receptor antagonism.

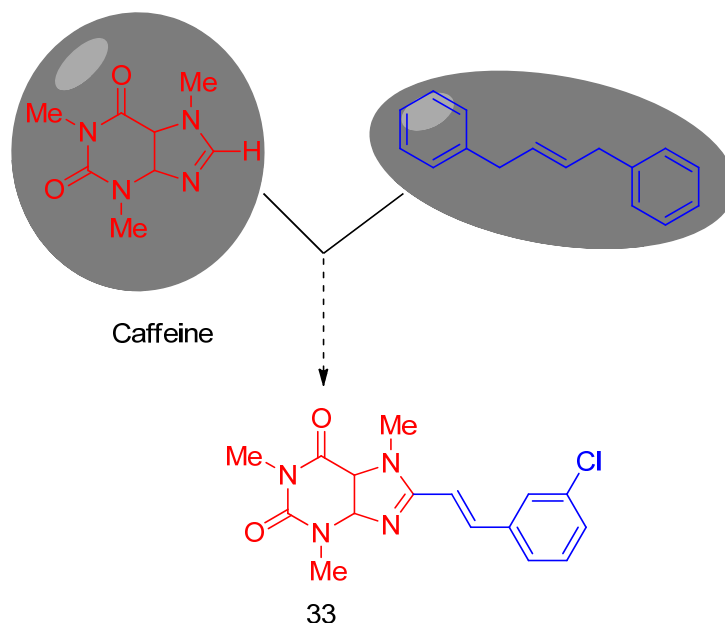


Figure 33. Design strategy of bifunctional compound having adenosine A_{2a} receptor antagonism and MAO-B reversible inhibition.

2.2.2.4. Targeting the Protein Aggregation:

The groups of Bolognesi and Melchiorre have conducted extensive studies on the polyamine-quinone compound memoqui and a series of related compounds. These compounds address several mechanisms relevant to AD, including the processing and aggregation of A β peptides, the formation of reactive oxygen species (ROS), and acetylcholinesterase (AChE) inhibitory activity. Recently, a novel series of memoquin derivatives was created by linking the 2,5-diamino-benzoquinone core of this compounds with motifs seen in known amyloid binding agents, including the naturally occurring polyphenol curcumin¹²⁹.

Curcumin a polyphenolic compound has antioxidant and anti-inflammatory property. Wang et al., tested curcumin against ASN induced cytotoxicity in SH-SY5Y neuroblastoma cell line.¹³⁰ Extracellular incubation of SH-SY5Y cells with oligomeric but not the monomeric or fibril form of ASN can induce significant cytotoxicity. Curcumin can significantly reduce the cytotoxicity of preformed ASN oligomeric species by reducing the ROS and inhibiting caspase-3 activity. It can also protect against intracellular induced ASN toxicity by over expressing ASN in transient transfected SH-SY5Y cells.

Rifampicin (Rif.) a semisynthetic derivate of rifamycins, which is obtained from *Nocardia mediterranei* and commonly used for treatment of leprosy. Patients on the treatment with rifampicin are less prone to develop senile dementia. It has been shown that rifampicin and its analog, p-benzoquinone, inhibited A β -42 aggregation and neurotoxicity *in-vitro*. Based on these observations and naphthoquinone core in the structure of rifampicin, Li et al., investigated it for ASN aggregation inhibitory property.¹³¹ After incubation of ASN (50 μ M) for 42 hr in presence of rifampicin (100 μ M), size exclusion chromatography (SEC) profile indicated large amount of monomer of ASN left over compared with the incubation of ASN (50 μ M) alone. In anaerobic condition as well in presence of antioxidant, the inhibitory effect of rifampicin reduced significantly which indicates the oxidized quinone form is majorly responsible for its activity. Quinones are susceptible to nucleophilic attack via Michael addition to form imine with the lysine side chain of ASN, leading to covalent modification.

Baicalein, a Chinese herbal medicine is a well known potent antioxidant, free radical scavenger, and iron chelator. It can potentially inhibit ASN oligomerization in both cell free and cellular system¹³². In this study Agnaf et al., using ThT, oligomeric

specific ELISA (to monitor oligomers formation in cell free system), and BiFC (to monitor oligomers formation in cellular system) assay, tested 8 different compounds for their antioligomeric and antifibrillar activity. Baicalein effectively inhibited ASN oligomerization at 50 μ M in a dose dependent manner. First time using the oligomeric specific, BiFC assay, authors demonstrated that baicalein inhibit the formation of HMW ASN oligomers in a dose dependent manner in Hela and SH-SY5Y cell lines transfected with GNS and GSC plasmids. **Dopamine analogs** has been studied for their effect on the ASN aggregation^{133, 134}. ASN can readily aggregate into the fibril form upon incubation for sufficient period of time and this process can be monitored using thioflavin T(ThT) fluorescence assay, AFM etc. The quinone form of polyphenols like dopamine, hydroquinone (HQ), catechol (CA), p-nitorphenol (pNP), and ascorbic acid are efficacious inhibitors of ASN fibrillation. Li et al., confirmed this hypothesis by increase in absorbance in the UV spectra at 280 nm and 345 nm in SEC profile, ThT assay and SDS/PAGE¹³⁴. Further mass spectra analysis revealed a large amount of ASN adducts dimers in which one protein dimer was attached with several quinones to give a molecular mass mixture. This quinone interacts with lysine residue of ASN, which lead to the inhibition of ASN fibrilization. The covalent cross linked adduct by dopamine (DA) were majorly HMW oligomers while the most of the catechol formed largely monomers or dimers. Although DA modification inhibit ASN fibrilization process, the MTT assay on PC12 cells revealed that DA-modified HMW oligomers of ASN were significant cytotoxicity compared to low molecular weight (LMW) species of ASN.

Selegiline is a noncompetitive monoaminoxidase B (MAO-B) inhibitor with neuroprotective effect, and widely used alone or in combination with other drugs to treat PD. Being an antioxidant in nature, Selegiline inhibits the conversion of DA into

ROS and reduces oxidative stress which further contributes to its action against PD. Selegiline interfere with earlier nucleation formation, and to a lesser extent with fibril elongation but the mechanism is not completely known yet.

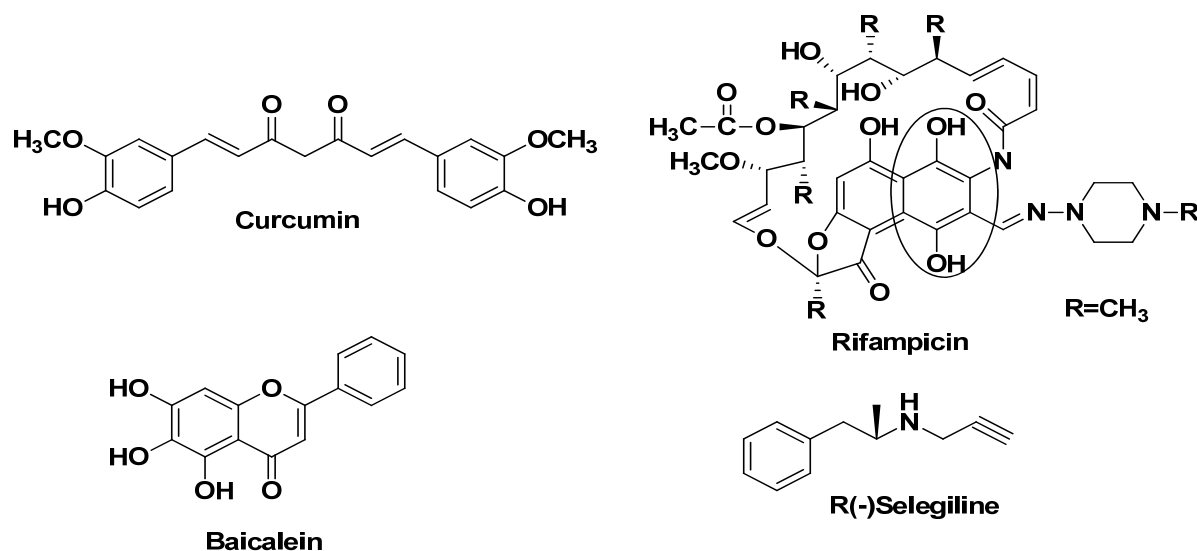


Figure 34. Chemical Structure of alpha synuclein aggregation modulaotrs.

2.2.2.5. Targeting inflammation, MAO and mito-NEET: pioglitazone and rosiglitazone

Peroxisome proliferator activated receptor gamma (PPAR- γ) agonists have been developed to combat diabetics. PPAR- γ agonists containing the thiazolidinedione (TZD) moiety have become a new focus group of compounds in the treatment of ischemic stroke and PD. PPAR- γ belongs to the orphan receptor group of ligand-activated transcription factors. Several studies have now been published which suggest that PPAR-g agonists might be neuroprotective in stroke ¹³⁵.

PPAR- γ agonists appear able to modulate the inflammatory response and reduce the size of the infarcted area. Additionally, they seem to interact with mechanisms of inflammation as well as with pathways that lead to ROS, and inhibition of matrix

metallopeptidase. Pioglitazone also has been shown to reduce cytokine release when cells are treated with lipopolysaccharide (LPS).

The PPAR-g agonists appear to inhibit beta-amyloid-stimulated secretion of inflammatory mediators, as well as deposition of beta-amyloid in the brain¹³⁶. Several groups have shown that pioglitazone and rosiglitazone are protective in the MPTP parkinsonian mouse model may be through inhibition of MAO-B¹³⁷. It has been shown that Pioglitazone stabilizes mito NEET and acts as a neuroprotective drug by altering mitochondrial function.

2.2.2.6. Design of Prodrug

In addition to these compounds, small molecules derived by conjugating L-dopa and DA with LA (lipoic acid) have recently been reported¹³⁸. The rationale for the development of these molecules (**38a-d**) was derived from the well-recognized observation that ROS play a role in the progressive and selective loss of the nigrostriatal dopaminergic neurons in PD. However, it is noted that low molecular weight free radical scavengers, such as glutathione, vitamin E, carnosine, and ascorbic acid, have limited antioxidant properties because of their marginal efficiency in crossing BBB and/or affecting iron accumulation. Conversely, LA readily crosses BBB, accumulates in neuronal cell types¹³⁹, and is reduced by mitochondrial dehydrogenases to dihydrolipoic acid (DHLA), which lowers the redox activities of free iron cations¹⁴⁰. Furthermore, LA is also a good metal chelator and can therefore contribute to the tackling of the neuron damaging effects of iron accumulation in aging brains. The concept of a co-drug is somewhat different from the original meaning of MTDLs. An MTDL is a single chemical entity able to simultaneously modulate different molecular targets responsible for a multifactorial disease. A co-

drug, however, is essentially a prodrug made by two parent compounds linked together by a chemical bond. It has to be stable at the gastrointestinal level, but then it has to be hydrolyzed to provide two (or more) different drugs. The final biological effects of an MTDL and a codrug are essentially the same. Conceptually, they represent different approaches to the discovery of multifunctional compounds.

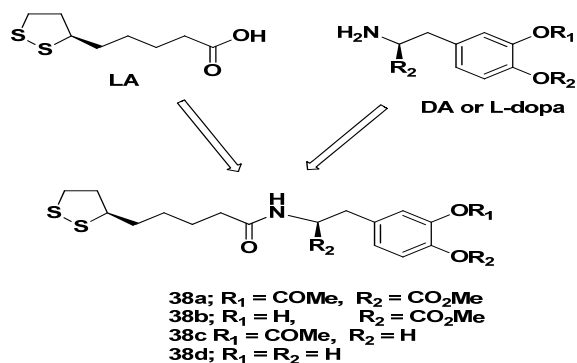


Figure 35. Design strategy of Co-drug or Prodrug.

CHAPTER 3

HYPOTHESIS AND SPECIFIC AIMS

Parkinson's disease (PD) is a progressive age-related neurodegenerative disorder of the central nervous system that is characterized by gradual loss of dopaminergic neurons in the substantia nigra region of the brain. Common symptoms associated with PD include rigidity, bradykinesia, resting tremors, postural instability, and cognitive psychiatric complications. Levodopa (L-DOPA) became available in 1960 for the treatment of PD and is still being considered as one of the main stream therapies of choice. However, prolog use of L-DOPA gives rise to “on” and “off” episode along with motor fluctuations, and eventual oxidation of dopamine (DA) derived from L-DOPA might further facilitates neurodegeneration. One of the current strategies of PD therapy is to delay the initiation of L-DOPA therapy, by using various combinations of other therapeutic agents such as dopamine agonists, inhibitors of dopamine metabolism, etc. However, none of these strategies address the limitations of L-dopa. Therefore, the need of therapeutic agents which will have disease modifying effect, is of paramount importance.

3.1. Hypothesis:

It is increasingly evident that drugs aiming a single target may be inadequate for the treatment of complex diseases such as PD, which is multifactorial in nature. Thus, it is hypothesized that multifunctional drugs exhibiting multiple pharmacological activities addressing underlying pathogenic factors of PD should be effective as a disease modifying agent. With this in mind, we initiated our drug discovery approach aimed at identifying novel multifunctional agents possessing D2/D3 agonist or D3 preferring agonist activity along with antioxidant, iron chelator, and modulation of ASN aggregation activities.

One of the major goals behinds the first phase of study was to enhance brain penetration of D-264 related compounds without compromising its agonist and neuroprotection properties. In order to achieve this we have carried out a structure activity study with different analogues of lead compound D-264.

There are plethora of literature evidences indicating the toxicity of ASN aggregetges towards the dopaminergic neurons². ASN is a component of Lewy bodies, a pathological hall mark of PD. These protein aggregates may be responsible for triggering the degeneration of dopaminergic neurons in the SN region of the brain. ASN forms toxic oligomers or fibrils. Currently, it is not known how the aggregation of ASN triggers cell death. The modulation of its aggregation is emerging as a novel therapeutic target to treat PD. One of the major aspects that might be targeted therapeutically is to inhibit the aggregation of ASN so anti-aggregative compounds or the compounds that can break the preexisting aggregates may be helpful. These ASN modulators have been proven to be neuroprotective in both *in vitro* and *in vivo* animal models of PD^{79, 130, 132}. In our second approach to develop D2/D3 agonist molecules with ASN modulator will give not only symptomatic relief but also provide neuroprotection.

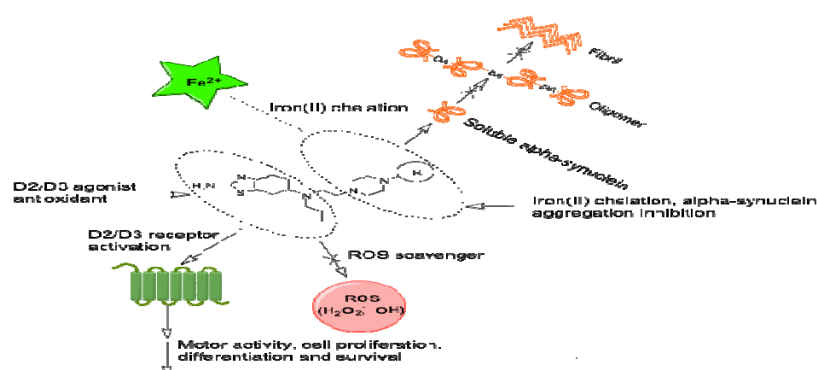


Figure 36. Various possible pathways of proposed D3 selective hybrid dopaminergic agonist for symptomatic and neuroprotective treatment of PD.

3.2. General aims:

In our effort to design and develop novel D3 selective potent ligands with high affinity for both D2, D3 receptors, we have adopted a 'hybrid structure approach'. In our hybrid drug design approach we combine known D2/D3 agonists with D2/D3 antagonist fragments, which lead to the development of a number of potent and *in vivo* active D3 selective ligands^{74, 141-154}. One of our D3 preferring lead compounds, D-264, exhibited potent *in-vivo* activity in PD animal models and also exhibited neuroprotective properties in two different PD animal models^{74, 149, 150}. In spite of interesting neuroprotective property of D-264, it suffers from poor brain penetration. *In vivo* activity of D-264 was enhanced significantly when D-264 was solubilized in 5-10 % β -hydroxy-propyl-cyclodextrin solution presumably by encapsulating the molecule leading to enhanced blood brain barrier penetration of D-264.

Our general aim is to design and synthesize D3 selective agonists with enhance entry into the brain. We have also proposed to develop multifunctional molecules with the property to modulate ASN aggregation in order to reduce toxicity.

3.2.1. Specific Aims:

1. **To enhance blood brain barrier crossing ability of D-264:** In our first phase of study to enhance brain penetration of D-264 related compounds, we plan to carry out a structure activity relationship of our lead compound D-264. The goal behind this SAR study is to enhance the entry of suitable derivatives of D-264 into the brain without compromising its agonist and neuroprotection properties to further enhance multifunctional property.

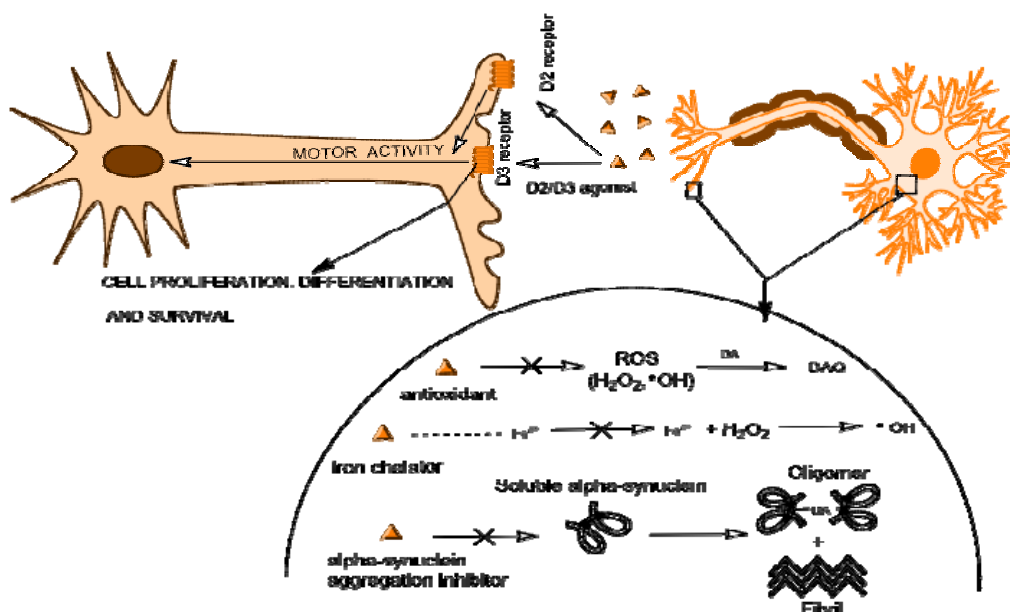


Figure 37. Schematic representation of interaction of novel proposed D3 selective agonist at the pre and postsynaptic nerve terminals.

2. **ASN aggregation modulators:** In the second series of molecules our aim is to further enhance multifunctional property of our molecules. In order to achieve this, we plan to incorporate ASN aggregation modulator functionality e.g. dihydroxyl group, at various positions on the accessory binding biphenyl ring of the hybrid molecule.
3. **To elucidate the basis of potency and selectivity for D3 over D2 (D2/D3):** To gain an insights into the structural requirements for dopamine D2 and D3 agonists in the treatment of Parkinson's disease (PD) and to elucidate the basis of selectivity for D3 over D2 (D2/D3), CoMFA (comparative molecular field analysis) and CoMSIA (comparative molecular simulation analysis) three-dimensional quantitative structure-activity relationship (3-D QSAR) studies will be performed on a series of 45 related D2 and D3 dopaminergic agonists.

3.2.2. Ligand design and synthesis:

Our structure activity relationship study in the first series of molecules is focused on introduction of methoxy and hydroxyl group at various positions on the accessory binding biphenyl ring of this hybrid molecule. The introduction of hydroxyl group or combination of hydroxyl/methoxy group at a suitable position could further potentiate its antioxidant and neuroprotection. Methoxy and hydroxyl substitutions also should help us to examine the possible contribution of any hydrogen-bonding interaction originating from this region of the molecule with D2 and D3 receptors. Apart from these modifications, other molecular alterations involving bioisosteric replacement of thiazolidium moiety by aminotetraline or quanzoline rings, change of ethylene linker length, and incorporation of amide bond at the piperazine nitrogen atom distal to the agonist head group have also been incorporated.

In the next series of molecules, we are developing a SAR study, incorporating known ASN aggregation inhibitor moieties, into our established D2/D3 pharmacophore structure. By means of incorporating ASN aggregation modulator moieties on the accessory binding biphenyl ring of the hybrid template, we will explore their ASN aggregation inhibition property along with its receptor binding, functional and in vivo activity. We have envisioned that dihydroxyl group will not affect the agonist activity of the compounds.

Therefore two classes of molecules and their bioisosters were designed and synthesized to develop lead molecules.

- 4'-(4-(2-((2-amino-4,5,6,7-tetrahydrobenzo[d]thiazol-6-yl)(propyl)amino)ethyl)piperazin-1-yl)-[1,1'-biphenyl]-3-ol.

- 4'-(4-(2-((2-amino-4,5,6,7-tetrahydrobenzo[d]thiazol-6-yl)(propyl)amino)ethyl)piperazin-1-yl)-[1,1'-biphenyl]-3,4-diol.

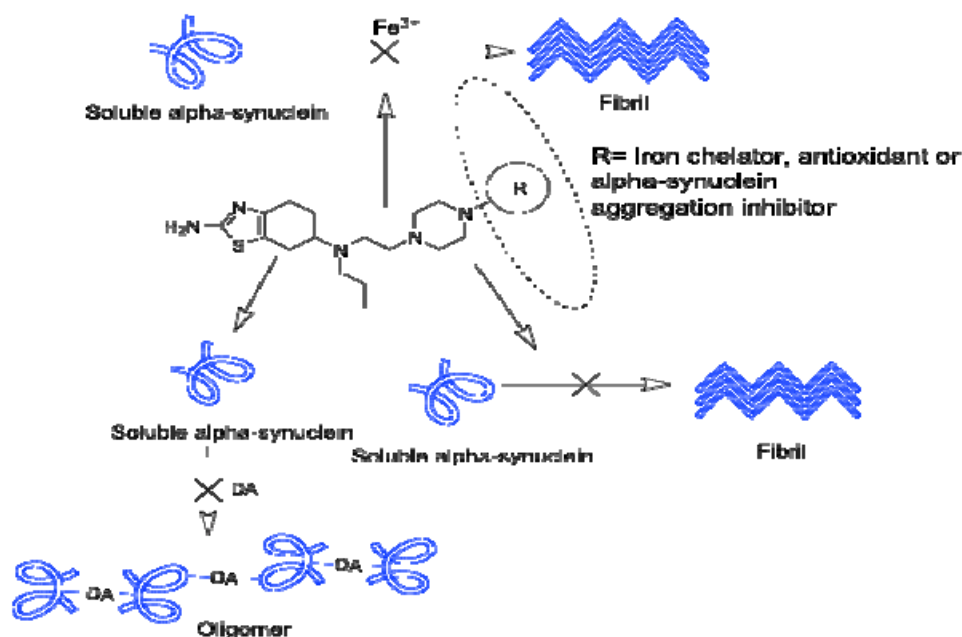


Figure 38. Schematic representation of interaction of proposed hybrid D3 selective agonist with ASN.

3.2.3. Separation of enantiomers of the potent racemic compounds:

We plan to separate the enantiomers of the potent racemic compounds to evaluate the chiral requirement of the receptor for biological activity for those compounds.

3.2.4. Radioligand binding assay using radioligand [³H]-spiperone:

We will perform in vitro competitive binding assay of all our synthesized ligands to evaluate in vitro binding affinity of compounds towards D2 and D3 receptors.

3.2.5. [³⁵S]-GTPγS-binding in vitro functional assay:

We plan to evaluate functional activity of our selected ligands by this in vitro functional assay. Potency of the compounds will be estimated from half maximal

concentration (EC_{50}). Dopamine is considered full agonist to estimate the maximal stimulation (E_{max}).

3.2.6. Biochemical antioxidant assay:

Selected lead compounds will be tested in a biochemical colorimetric antioxidant assay, known as DPPH assay.

3.2.7. Neuroprotection study:

Selected lead compounds will be evaluated in vitro neuroprotection experiment with dopaminergic MN9D cells in reversing the toxicity of MPP+ or 6-OHDA.

3.2.8. ASN aggregation study:

We will assess the ability of our in-vivo active lead compounds to inhibit the aggregation of α -synuclein in both the cell free and cellular system. The time dependent toxicity of pre-fabricated ASN in rat pheochromocytoma cell line PC12 using pre-fabricated α SN aggregate which will be followed by evaluation of effect of selected drugs in modulation of toxicity.

3.2.9. *In vivo* assays with rat model of PD:

Selected lead compounds will be tested in the animal models of Parkinson's disease by using 'reversal of reserpine-induced hypolocomotion in rat' model or '6-hydroxy dopamine treated unilaterally lesioned rat' model to evaluate *in vivo* potency of the test compounds and their blood brain crossing ability.

3.2.10. Molecular modeling study:

Two alignment methods (atom-based and flexible) and two charge calculation methods (Gasteinger-Huckel and MOPAC) will be used in the present study.

CHAPTER 4
RESULTS AND DISCUSSION

Our first objective was to design and develop a series of novel ligands for dopamine receptors that will possess enhanced blood brain barrier crossing ability compared to the first generation hybrid compound **D-264** without compromising its DA receptor binding and neuroprotection properties. The molecules with high affinity and selectivity for binding at the dopamine D3 receptor compared to D2 in *in vitro* binding assay were selected as potential candidate for *in vitro* functional assay to test its agonist potency. The compounds that produced appreciable stimulation of the dopamine receptors in *in vitro* functional assay system compared to **D-264** were tested in *in vivo* assay to evaluate potential antiparkinsonian property. Next, objective was to carry out *in vitro* biochemical assay system to evaluate the antioxidant potency. In line with our multifunctional drug development objective, one of our important goal was to evaluate *in vitro* neuroprotection ability of the lead compounds. Our final goal was to develop potent *in vivo* active dopamine D2/D3 receptor agonists which should modulate ASN aggregation in a way that will inhibit the toxicity of wild type ASN aggregates in the cell culture system. Therefore, in this chapter, we will discuss

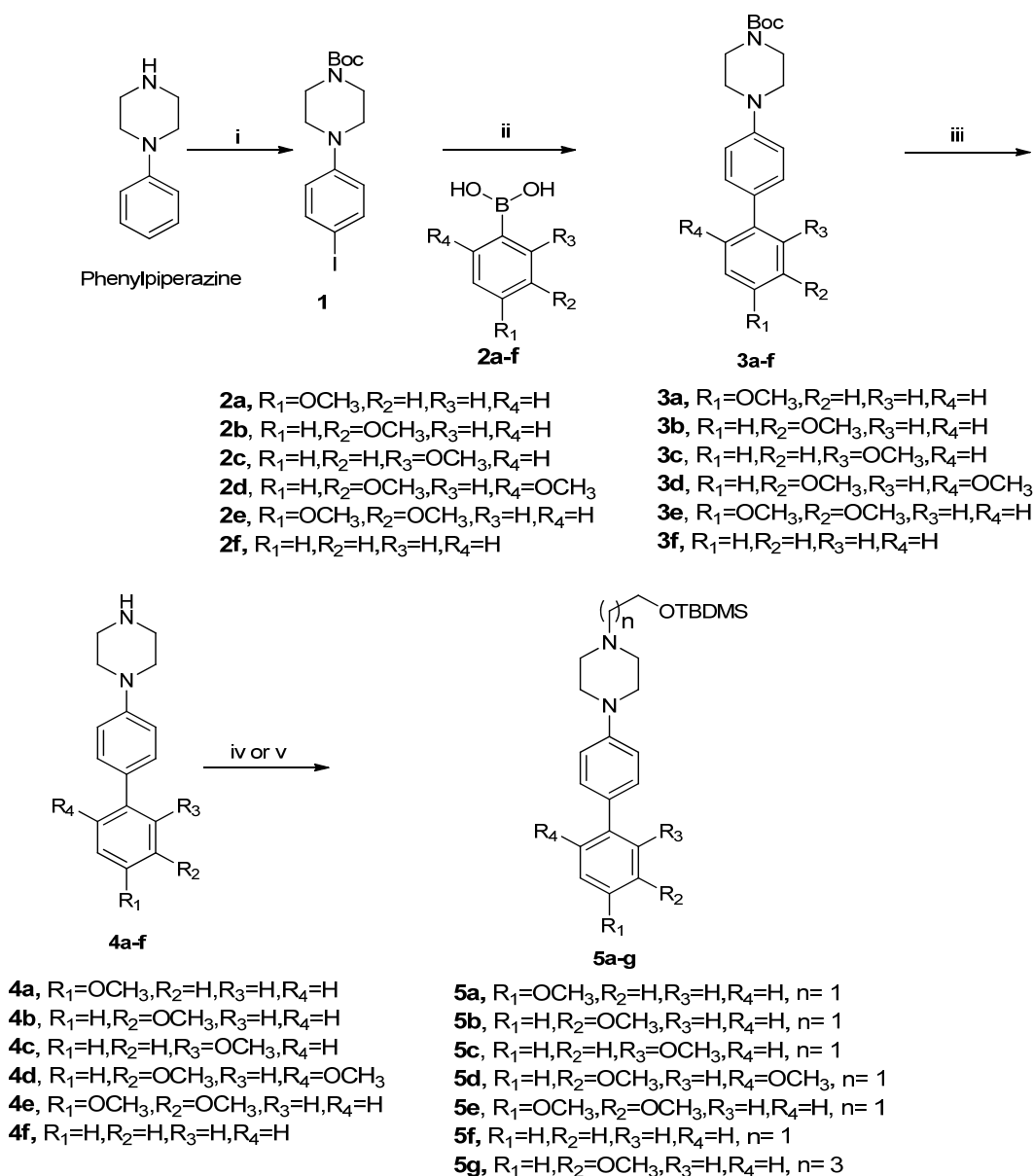
- 1) Chemistry involved in synthesizing library of compounds
- 2) *In vitro* binding data for all synthesized compounds
- 3) *In vitro* functional activity data for selected compounds
- 4) *In vivo* activity data for selected compounds
- 5) *In vitro* antioxidant data for our lead compounds
- 6) *In vitro* neuroprotection experiment
- 7) *In vitro* ASN aggregation experiment

The procedure followed to do all the above mentioned assays will be discussed in detail in the *materials and methods* section.

4.1. Chemistry involved synthesizing the compounds:

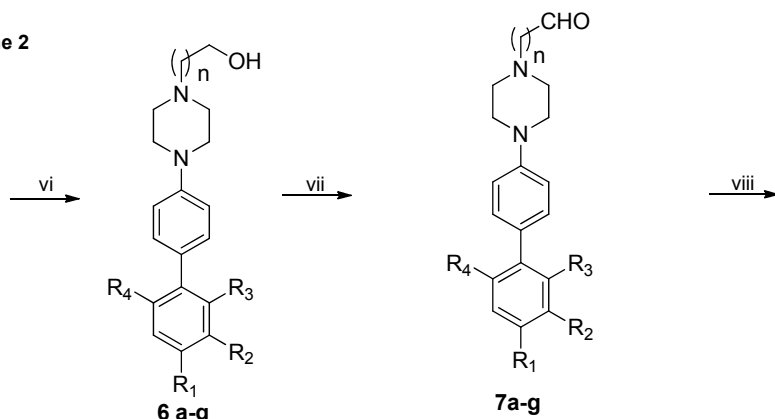
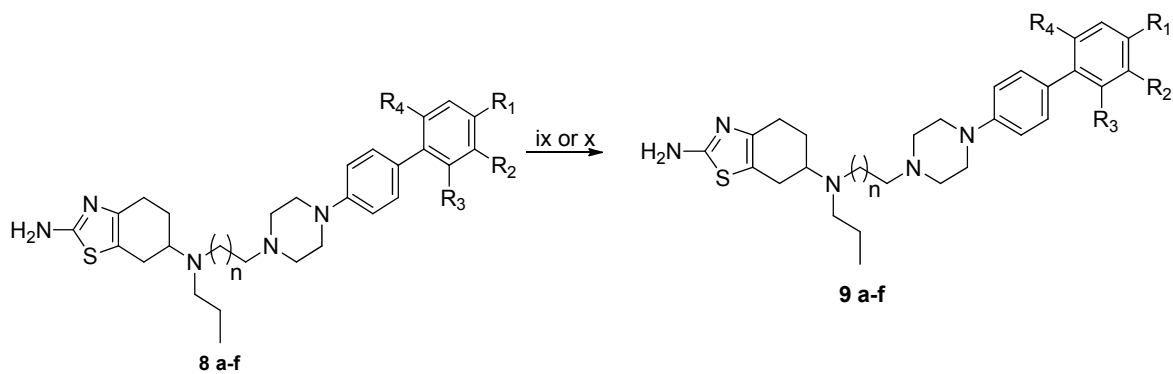
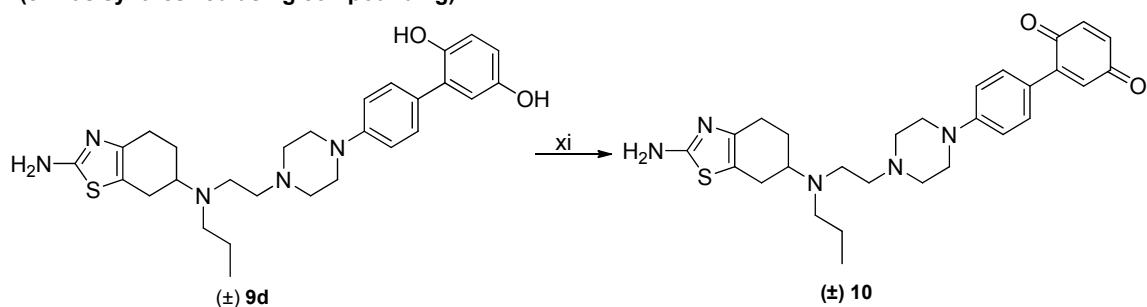
Schemes 1 and 2 describe the synthesis of final compounds **(±)8a**, **(±)8b**, **(±)8c**, **(±)9a**, **(±)9b**, **(±)9c**, **(±)9d**, **(±)9e**, **(±)9f**, **(-) 11** and their enantiomers. Iodination of phenyl piperazine was done following the literature procedure. The 1-(4-iodophenyl) piperazine was treated with Boc-anhydride to synthesize mono Boc protected intermediate **(1)**. Boc protected intermediate was then subjected to Suzuki coupling reaction ^{155, 156} with various commercially available substituted benzene boronic acids. The amine protecting t-Boc group was removed by using trifluoroacetic acid. The free amines **(4a-f)** were subjected to N-alkylation reaction with TBDMS protected bromoalcohol to get intermediates **(5a-g)** which further underwent TBDMS deprotection using tetrabutyl ammonium fluoride solution (TBAF) to get the alcohol intermediate **(6a-g)**. These alcohol intermediates **(6a-g)** were oxidized under Swern oxidation conditions to get the arylpiperazine aldehydes **(7a-g)** which were further condensed with **(±)-**, **S(-)**, or **R(+)**-pramipexole under reductive amination conditions to give four final compounds **(±)8a**, **(±)8b**, **(±)8c**, **(-)8b**, and other intermediates including the four linker intermediate **(±)8d**. The demethylation of these intermediates with either boron tribromide or with freshly distilled aqueous hydrobromic acid (48%) yielded the six more final compounds **(9a-f)** and their enantiomers. One more final quinone compound **10** was generated by oxidation of **(±)9d** in presence of MnO_2 .

Scheme 1



Reagents and conditions: (i)(a) ICl, acetic acid, water, 55 °C, 1h, 70-75%(b) (Boc)₂O, Et₃N, dichloromethane, rt, 12 h,80-85% (ii) ArB(OH)₂, Pd(PPh₃)₄, Na₂CO₃, dimethoxy ethane, ethanol, 95 °C, 2 h, 65-70%;(iii) TFA, dichloromethane, rt, 2h, 90-95% (iv) (2-bromoethoxy)(*tert*-butyl)dimethylsilane, K₂CO₃, acetonitrile, reflux, 14 h (for compound **5a-f**), 80-85% (v) (4-bromobutoxy)(*tert*-butyl)dimethylsilane, K₂CO₃, acetonitrile, reflux, 14 h (for compound **5g**),80-85%

Scheme 2

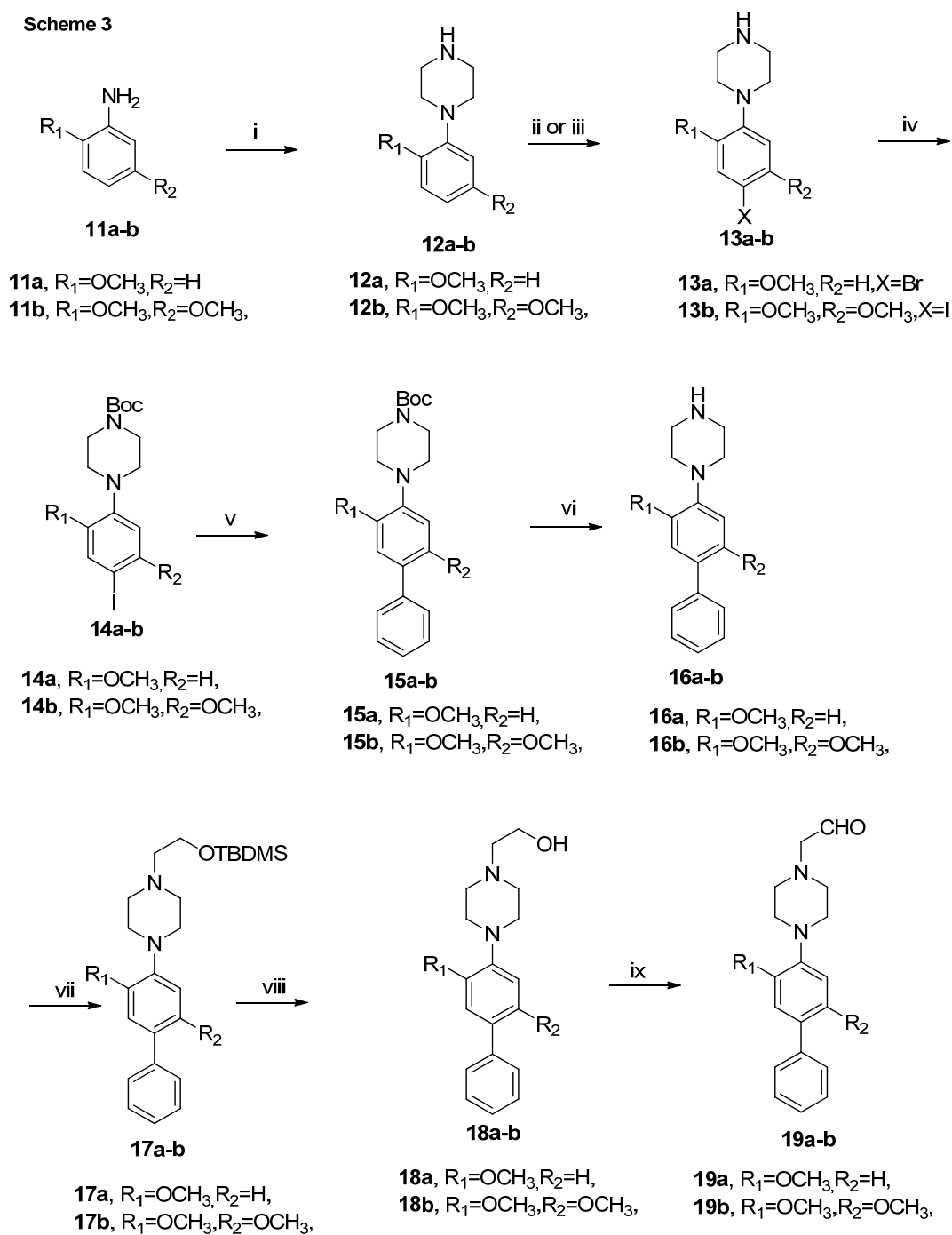
**6a**, R₁=OCH₃, R₂=H, R₃=H, R₄=H, n= 1**6b**, R₁=H, R₂=OCH₃, R₃=H, R₄=H, n= 1**6c**, R₁=H, R₂=H, R₃=OCH₃, R₄=H, n= 1**6d**, R₁=H, R₂=OCH₃, R₃=H, R₄=OCH₃, n= 1**6e**, R₁=OCH₃, R₂=OCH₃, R₃=H, R₄=H, n= 1**6f**, R₁=H, R₂=H, R₃=H, R₄=H, n= 1**6g**, R₁=H, R₂=OCH₃, R₃=H, R₄=H, n= 3**7a**, R₁=OCH₃, R₂=H, R₃=H, R₄=H, n= 1**7b**, R₁=H, R₂=OCH₃, R₃=H, R₄=H, n= 1**7c**, R₁=H, R₂=H, R₃=OCH₃, R₄=H, n= 1**7d**, R₁=H, R₂=OCH₃, R₃=H, R₄=OCH₃, n= 1**7e**, R₁=OCH₃, R₂=OCH₃, R₃=H, R₄=H, n= 1**7f**, R₁=H, R₂=H, R₃=H, R₄=H, n= 1**7g**, R₁=H, R₂=OCH₃, R₃=H, R₄=H, n= 3(±) **8a**, R₁=OCH₃, R₂=H, R₃=H, R₄=H, n= 1(±) **8b**, (-) **8b**, (+) **8b**, R₁=H, R₂=OCH₃, R₃=H, R₄=H, n= 1(±) **8c**, R₁=H, R₂=H, R₃=OCH₃, R₄=H, n= 1(±) **8d**, (-) **8d**, (+) **8d**, R₁=H, R₂=OCH₃, R₃=H, R₄=OCH₃, n= 1(-) **8e**, (+) **8e**, R₁=OCH₃, R₂=OCH₃, R₃=H, R₄=H, n= 1(±) **8f**, R₁=H, R₂=OCH₃, R₃=H, R₄=H, n= 3(±) **9a**, R₁=OH, R₂=H, R₃=H, R₄=H, n= 1(±) **9b**, (-) **9b**, (+) **9b**, R₁=H, R₂=OH, R₃=H, R₄=H, n= 1(±) **9c**, R₁=H, R₂=H, R₃=OH, R₄=H, n= 1(±) **9d**, (-) **9d**, (+) **9d**, R₁=H, R₂=OH, R₃=H, R₄=OH, n= 1(-) **9e**, (+) **9e**, R₁=OH, R₂=OH, R₃=H, R₄=H, n= 1(±) **9f**, R₁=H, R₂=OH, R₃=H, R₄=H, n= 3**(8f was synthesized using compound 7g)**

Reagents and Conditions: (vi) *n*-Bu₄NF, THF, rt, 1.5 h, 80-95%; (vii) oxalyl chloride, DMSO, TEA, CH₂Cl₂, -78 °C, 2 h, 70-80% ; (viii) (±)-pramipexole, (-)-pramipexole, (+)-pramipexole NaBH(OAc)₃, CH₂Cl₂, rt, 48 h, 65-70%; (ix) BBr₃, CH₂Cl₂, -78 °C, (for compound (±) **8a**, (±) **8b** and (±) **8c**), 48 h, 55-60%; (x) 48% aq. HBr, reflux, 6 h, 70-80% (for compound (-) **8b**, (+) **8b** and for **8d** to **8f**); (xi) MnO₂, dichloromethane, r.t., 12 hrs, 50%.

Schemes 3 and 4 depict the synthesis of final target compounds (**±**)-**21a**, (**±**)-**21b**, and (**±**)-**22**. Various substituted Methoxyanilines (**11a-b**) were subjected to cyclization by following the literature procedure¹⁵⁷ to produce intermediate **12a-b**. Further, iodination of the intermediate, **12a-b**, yielded iodo derivatives, **13a-b**. These amine intermediates were converted into t-Boc protected compound, **14a-b**, followed by their Suzuki coupling reaction with commercially available benzene boronic acids, and subsequently t-Boc group was removed by using TFA to yield **16a-b**. The free amine intermediates, **16a-b**, were N-alkylated with (2-bromoethoxy)-tertbutyldimethylsilane to get compounds, **17a-b**, which on TBDMS deprotection yielded alcohols, **18a-b**. Compounds **18a-b** were converted into aldehyde derivatives **19a-b** under Swern oxidation conditions followed by condensation with (**±**)-pramipexole under reductive amination conditions and subsequently treated with aqueous hydrobromic acid (48%) to yield the final compounds (**±**)-**21a**, (**±**)-**21b**. One of the final compounds (**±**)-**21b** was oxidized in presence of MnO₂ to yield final compound (**±**)-**22**.

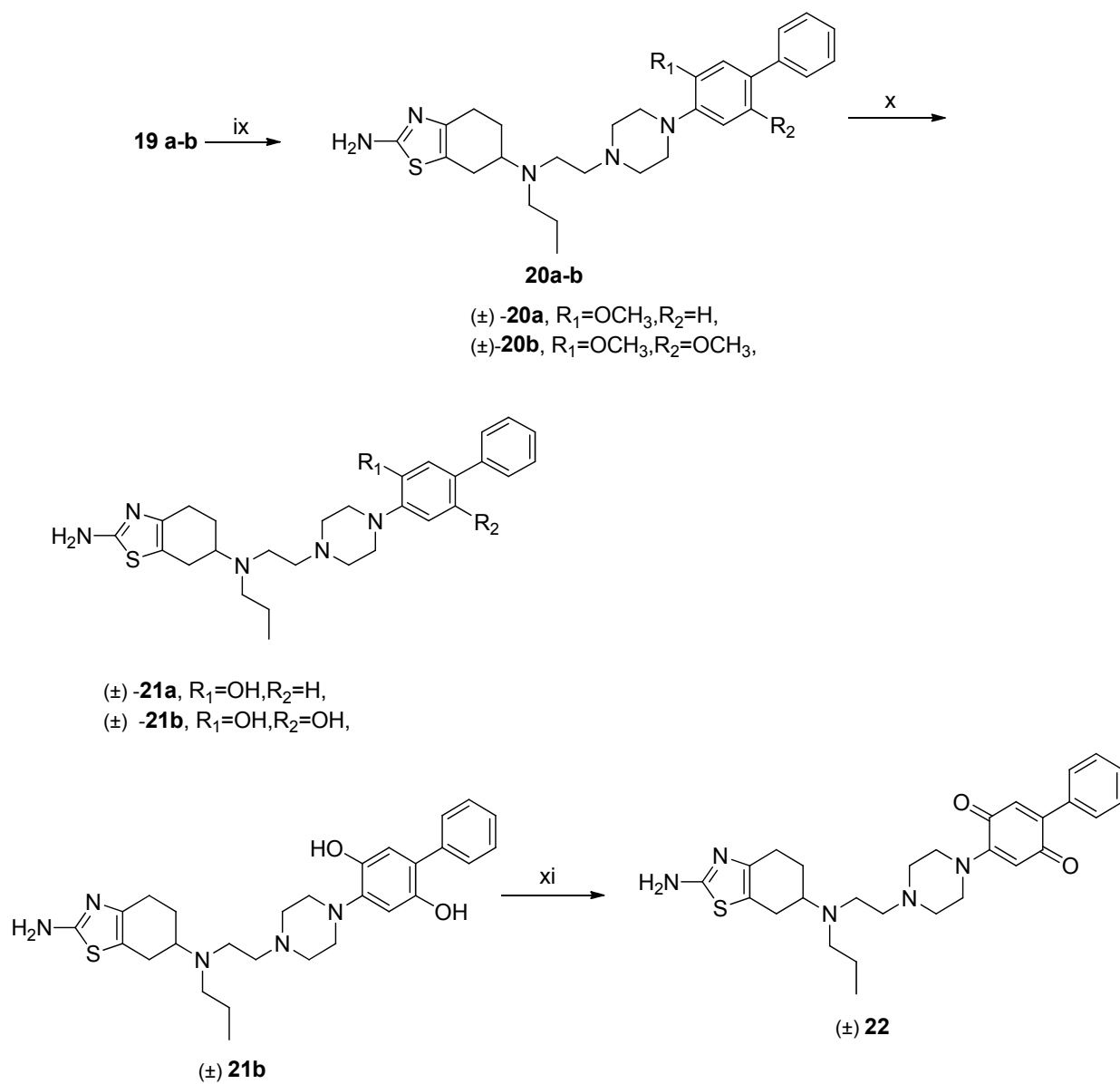
In Schemes **5 and 6**, we describe the synthesis of bioisosteric analogs of 2-aminothiazole agonist pharmacophoric head group using aminotetraline and quanazoline moiety. The intermediates described in **Scheme 1**, the arylpiperazine aldehyde, **7b and 7e**, were subjected under reductive amination conditions to react with (S)-(5-methoxy-1,2,3,4-tetrahydro-naphthalen-2-yl)-propyl-amine to get corresponding methoxy intermediates (**-**)-**23a and (-)**-**23b** and subsequently treated with aqueous hydrobromic acid (48%) to furnish the final compound (**-**)-**24a and (-)**-**24b**. While the quanazoline derivatives were synthesized as reported in our earlier publication, Briefly, 1,4 Cyclohexanedionemonoethyleneketal, on treatment with n-propylamine under reductive

Scheme 3



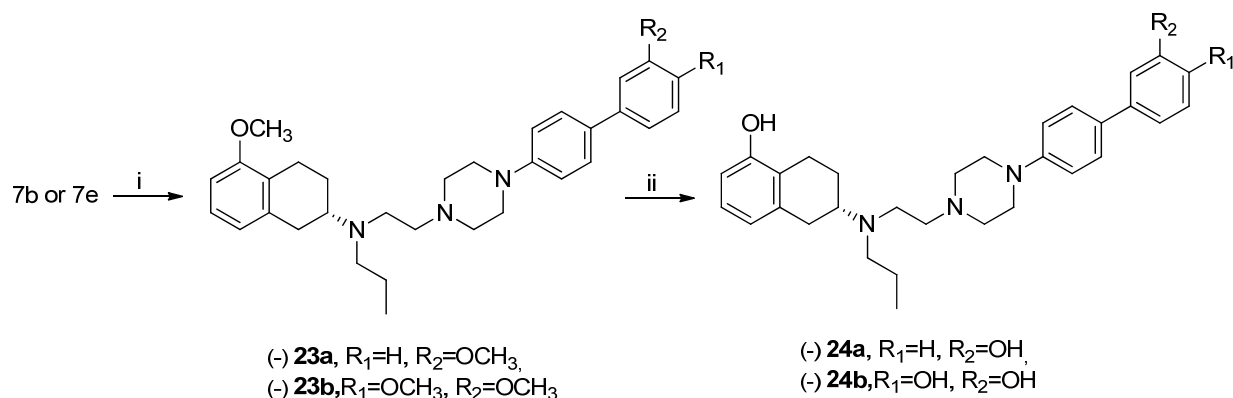
Reagents and conditions: (i) Bis(2-chloroethyl)amine, diethylene glycol monomethyl ether, 150 °C, 7 h; 65-70% (ii) Br₂, CH₂Cl₂, 0 °C, 2h, NaOH, 80% (for compound 13a) (iii) ICl, acetic acid, water, 55 °C, 1h, 85-90% (for compound 13b, 13c) ; (iv) (Boc)₂O, Et₃N, dichloromethane, rt, 12h, 75-80%; (v) phenyl boronic acid, Pd(PPh₃)₄, Na₂CO₃, dimethoxy ethane, ethanol, 95 °C, 2h, 76-80%; (vi) TFA, dichloromethane, rt, 4h, 90-95% ; (vii) (2-bromoethoxy)-*tert*-butyl-dimethyl-silane, K₂CO₃, CH₃CN, reflux, 12h, 80-85%; (viii) Bu₄NF, THF, rt, 2 h, 70-75%; (ix) oxalyl chloride, DMSO, TEA, CH₂Cl₂, -78 °C, 2 h; 65-70%

Scheme 4



Reagents and conditions: (ix) (±)-pramipexole, $\text{NaBH}(\text{OAc})_3$, CH_2Cl_2 , rt, 48 h, 65-70%; (x) 48% aq. HBr, reflux, 6 h, 70-80%; (xi) MnO_2 , dichloromethane, r.t., 12 hrs, 50%.

Scheme 5

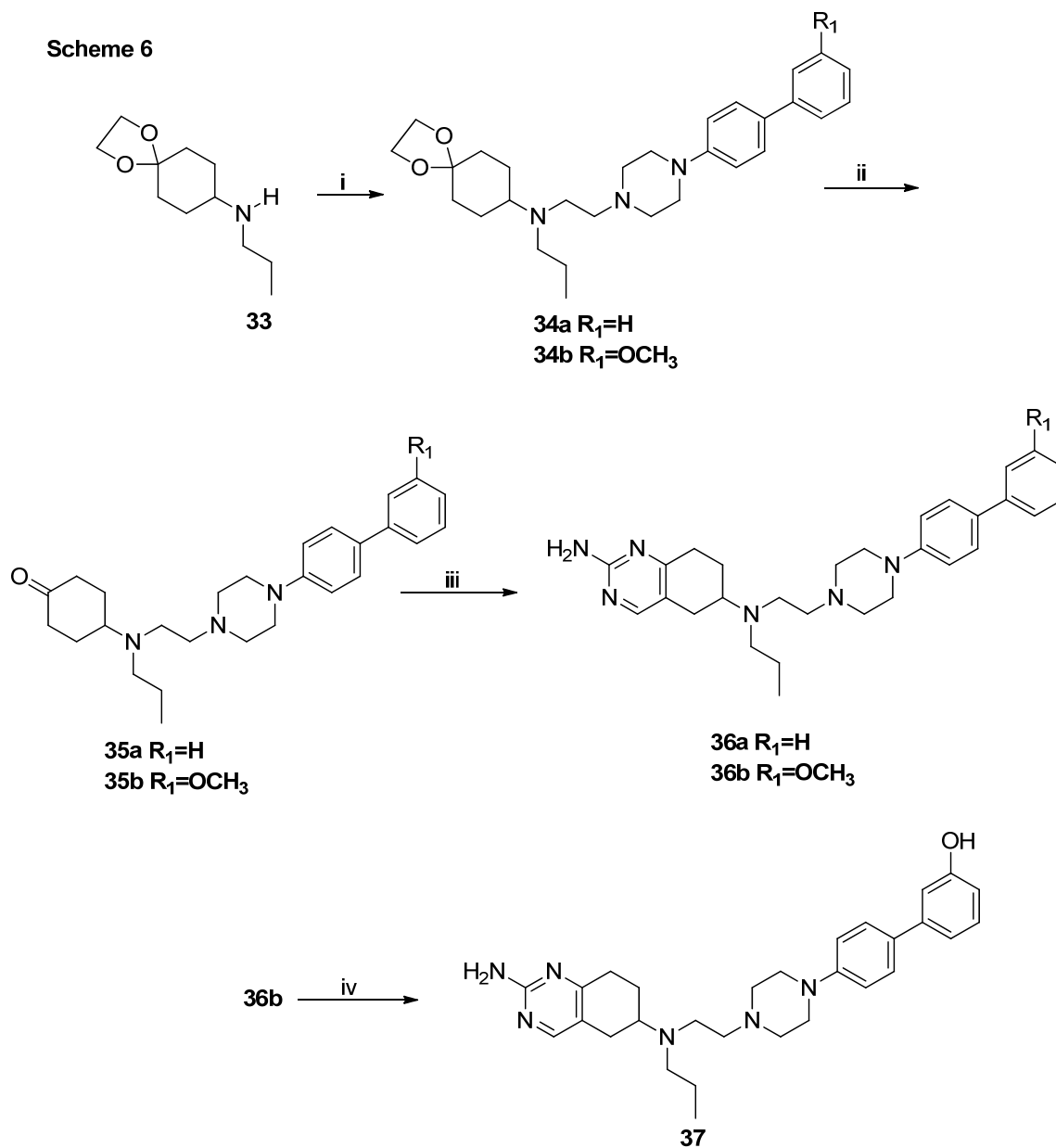


Reagents and conditions: (i) (S)-(5-methoxy-1,2,3,4-tetrahydro-naphthalen-2-yl)-propyl-amine, NaBH(OAc)₃, CH₂Cl₂, rt, 48 h, 70-80%; (ii) 48% aq. HBr, reflux, 6 h, 65-80%.

amination condition yielded intermediate **33**. This intermediate **33** was coupled with aldehyde **7d** and **7b** to afford **34a** and **34b**. Removal of the ketal group by dilute HCl in THF followed by ring formation in two step synthesis afforded the final compound **36a** and the intermediate **36b**. Final target **37** was produced by demethylation of methoxy group of **26b**, using 48% aqueous HBr.

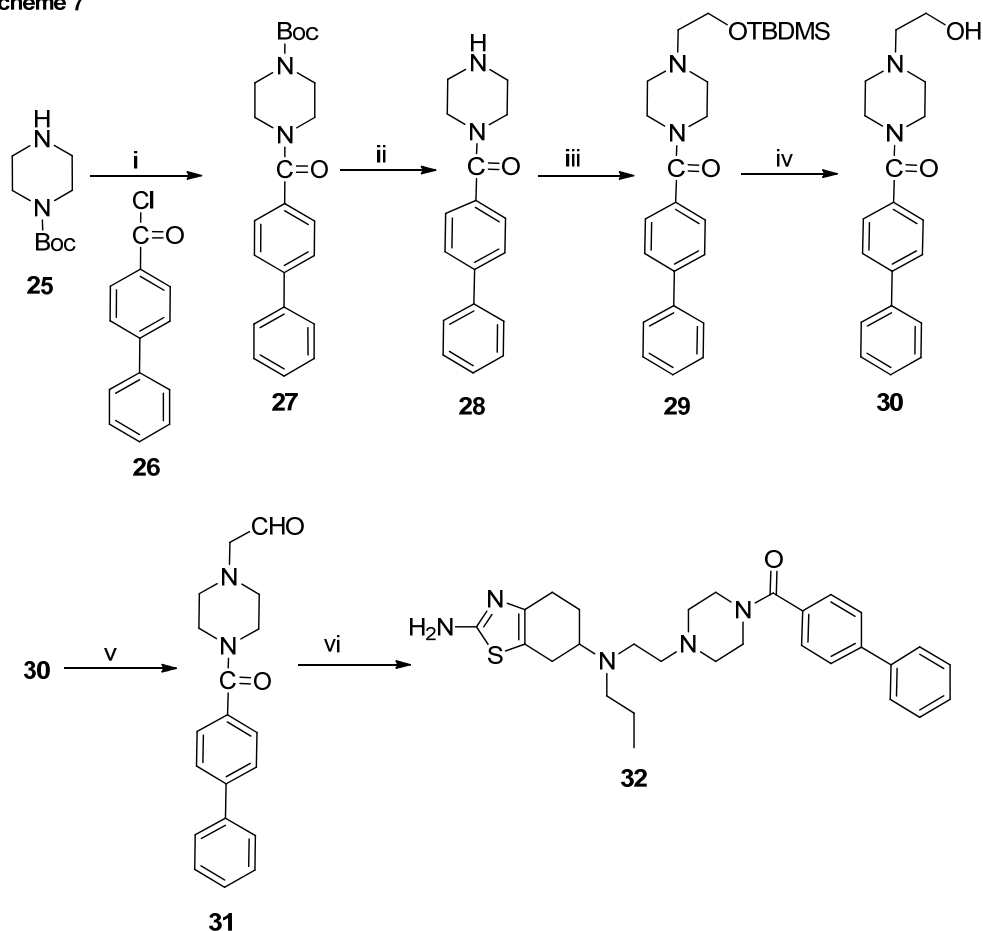
The synthesis of the final compound **32** is shown in Scheme 7. Mono-t-Boc protected amine **25** was reacted with commercially available biphenyl carbonyl chloride **26** at room temperature in THF in presence of diisopropylethylamine as base to provide **27**. The t-Boc group was removed using TFA followed by N-alkylation with TBDMS protected bromoethanol and subsequently TBDMS group was removed using TBAF to yield corresponding alcohol **30**. Alcohol **30** was converted, under swern oxidation condition, into its aldehyde derivative **31** followed by reductive amination with (±)-pramipexole to afford the final compound **32**.

Scheme 6



Reagents and conditions: (i) **7b,7f**, NaBH(OAc)₃, HOAc, ClCH₂CH₂Cl, rt, 48 h, 60-70%; (ii) 2N HCl, THF, reflux, 6 hours, 85-90% (iii) Tris(dimethylamino)methane, toluene, reflux Guanidine carbonate/EtOH, reflux, 4 h, 70-75% (iv) 48% aq. HBr, reflux, 10 h, 65%.

Scheme 7

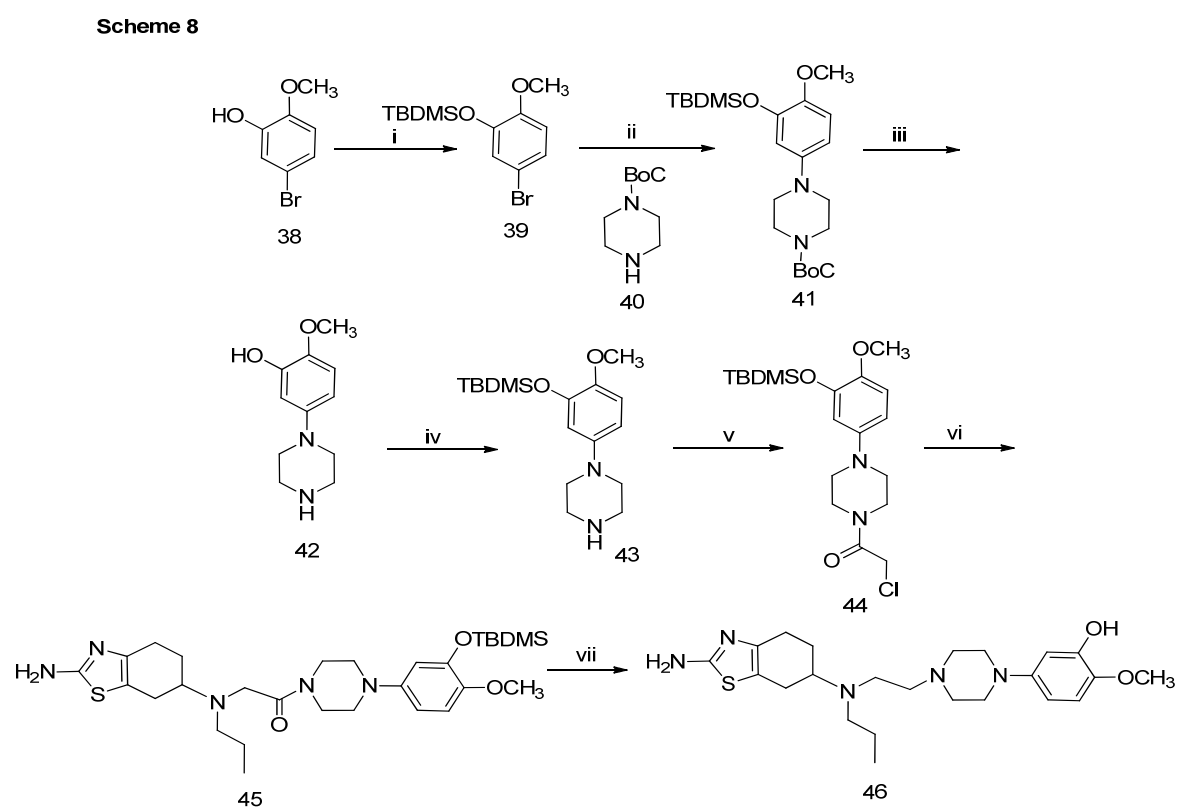


Reagents and conditions: (i) Diisopropylethylamine, THF, room temp., overnight, 80%; (ii) TFA, dichloromethane, rt, 2h, 95%; (iii) (2-bromo-ethyl)-tert-butyldimethylsilane, K₂CO₃, acetonitrile, reflux, 14 h, 70%; (iv) *n*-Bu₄NF, THF, rt, 1.5 h, 90%; (v) oxalyl chloride, DMSO, TEA, CH₂Cl₂, -78 °C, 2 h, 85%; (vi) (±)-pramipexole, NaBH(OAc)₃, CH₂Cl₂, rt, 48 h, 70%.

Scheme 8 and **9** describes the synthesis of two more final compounds (**±**)**46**, (**±**)**53**.

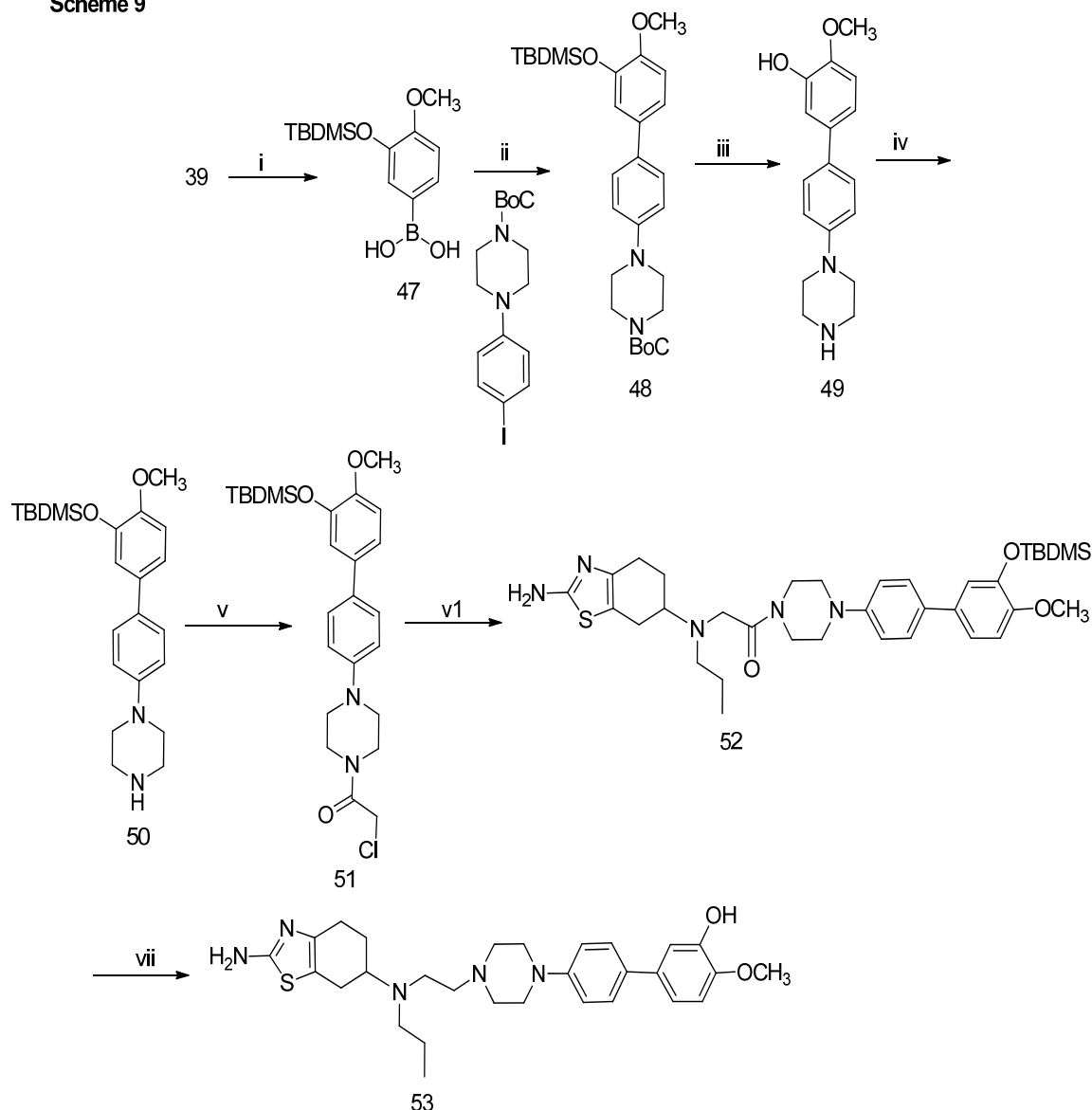
TBDMS protection of starting material bromo alcohol (**38**), was performed following the literature procedure²³, after protection the bromo intermediate, was coupled with mono Boc protected piperazine intermediate **40**, to synthesize the intermediate **41**. The amine protecting group, Boc, was removed using trifluoroacetic acid. The free amine **42** was reacted TBDMS chloride using triethylamine as base to get intermediates **43** which was treated with chloroacetyl chloride to provide substituted piperazine derivative **44**. In presence of a base and potassium iodide yielded

racemic substituted amide, **45**. Reduction of amide with borane produced the final compound **46**. While to synthesize the biphenyl derivate **53**, intermediate **39** from scheme 8 was reacted with n-butyllithium and triisopropylborate to get the corresponding boronic acid intermediate **47**. Substituted benzene boronic acid **47** was then be exposed to Suzuki coupling reaction ^{25,26} with Boc protected intermediate. The amine protecting group, Boc, was removed using trifluoroacetic acid followed by **scheme 8** to yield the final compound **53**.



Reagents and Conditions: i. TBS-Cl, Et₃N, DCM;80% ii. Pd catalyst, sodium t-butoxide, toluene, reflux, 12h, 55%; iii. TFA, DCM, 3h, 85%; iv. TBS-Cl, Et₃N, DCM,75%; v. Chloroacetyl chloride, Et₃N, DCM, -40°C, 0.5 h,50%; vi. (±)-pramipexole, K₂CO₃, KI, acetonitrile, 70°C, 3h,40%; vii. BH₃ in THF, THF, 36 hrs,60%.

Scheme 9



Reagents and Conditions: i. n-BuLi, B(OCH₂CH₃)₃, THF, -78°C to rt, 12h; 75% ii. Pd(PPh₃)₄, Na₂CO₃, DME:EtOH (1:1), 95°C, 1.5 h; 50% iii. TFA, DCM, 3h, 95%; iv. *tert*-butylchlorodimethylsilane, Et₃N, DCM, 85%; v. Chloroacetyl chloride, Et₃N, DCM, -40°C, 0.5 h, 50%; vi. (±)-pramipexole, K₂CO₃, KI, Acetonitrile, 70°C, 3h, 30%; xi. BH₃ in THF, THF, 36 h, 60%.

4.2. *In vitro* characterization with the first series compounds:

In this series, we have developed **16** final target compounds which were tested in *in vitro* binding assay to determine their affinity toward dopamine D2 and D3 receptors. The binding assay is a competition assay that determines the inhibition constants of the compounds for displacing the binding of dopamine receptor antagonist [³H]-

Spiperone at the cloned hD2L and D3 receptors expressed in HEK-293 cells. The detailed procedure is written in the *material and method* section (**Chapter 6**).

We envisioned that our SAR studies on hybrid compounds will produce highly potent and selective compounds for dopamine D3 receptors. The results showed that almost all of our compounds in this series exhibited high binding affinity at nanomolar range as well as different selectivity range for dopamine D3 receptor.

Table 2 shows the binding results of our synthesized compounds.

As mentioned in the introduction section, in order to develop multifunctional agents as potential therapeutic agents for PD, we described development of first generation hybrid compound **D-264** as potent and selective agonist for D3 receptor. One of the major goals behind first series of compounds is to enhance the blood brain crossing ability of D-264 without compromising its agonist potency. The structural modifications are mainly centered around the introduction of methoxy and hydroxyl groups at various positions on the accessory binding biphenyl moiety of this hybrid molecule. Methoxy and hydroxyl substitutions also should help us to examine the possible contribution of any hydrogen-bonding interaction originating from this region of the molecule with D2 and D3 receptors. Apart from these modifications, other molecular alterations involving bioisosteric replacement of thiazolidium moiety by aminotetraline or quanzoline rings, change of ethylene linker length, and incorporation of amide bond at the piperazine nitrogen atom distal to the agonist head group have also been incorporated.

First of all we wanted to observe the influence of introduction of methoxy and hydroxyl substitutions on the biphenyl ring of **D-264** with rat dopamine D2 and D3 (rD2 and rD3) receptors expressed in HEK-293 cells. To this end, a series of

racemic derivatives **8a-c**, **9a-c** and **20a** were synthesized and characterized. It is evident from **Table 2** that most of these compounds displayed high affinity for D3 and moderate affinity for D2 receptors. Among this series of analogs, compound **9b** with monohydroxyl substitution on the meta position of the phenyl ring distal to the piperazine found to be the most potent and selective for D3 (K_i , D2 = 347, D3= 1.20 nM, D2/D3= 289). On the other hand, **20a** with hydroxyl group on the ortho position of phenyl ring proximal to piperazine ring (K_i , D2=70.6, D3= 2.35 nM, D2/D3= 30) proved to be the most potent for D2. While compound **8b**, a methoxy analog of **9b**, exhibited somewhat lower binding affinity at D2 receptor, **while** D3 affinity decreased approximately 2-fold in comparison to **9b** (K_i , D2=464, D3=2.11 nM, D2/D3= 220 for **8b**). These results indicated that introduction of monomethoxy and monohydroxyl groups are well tolerated on the distal phenyl ring of **D-264** and, increased the selectivity for the D3 receptor.

Next, we synthesized two enantiomerically pure forms of racemic **9b**, compound (-)-**9b** (K_i , D2 = 369 nM, D3 = 1.73 nM, D2/D3=213) and compound (+)-**9b** (K_i , D2 = 1507 nM, K_i D3 = 19.7 nM, D2/D3=76) to evaluate the differential potency and selectivity of the enantiomers at the dopamine receptors. In agreement with our earlier results, (-)-**9b** exhibited higher potency at both D2 and D3 receptors compared to (+)-**9b**. Compound (-)-**9b** represents addition of a hydroxyl functionality into the parent compound **D-264**, which resulted in retention of almost similar binding affinity at D3 with slightly lower binding affinity for D2, with overall higher selectivity of (-)-**9b** for D3 compared to **D-264** (K_i ; D2/D3=213 vs. D2/D3 = 86 for (-)-**9b** and **D-264**, respectively). The (-)-isomer of **8b** was made, to evaluate whether free hydroxyl group in (-)-**9b** is critical for activity (**Table 2**). Compound (-)-**8b**, which is a methoxy analog, maintained D2 receptor affinity similar to (-)-**9b** (K_i ; D2=343 nM

vs. $D_2=369$ nM for (-)-**8b** and (-) **9b**, respectively), while the binding affinity toward D_3 dropped approximately 2-fold (K_i ; $D_3=2.33$ nM vs. $D_3=1.73$ nM for (-)-**8b** and (-)-**9b**, respectively) with similar selectivity for D_3 over D_2 receptors compared to (-)-**9b** ($D_2/D_3=220$ vs. $D_2/D_3=213$ for (-)-**8b** and (-)-**9b**, respectively). All compounds in this series showed nanomolar potency for the D_3 receptor in the competitive binding assay.

In our next design of compounds we incorporated aminotetraline, and amino pyrimidine moieties as the bioisosteric replacement of thiazolidium moiety of pramipexole in **9b** or **D-264**, which resulted in the design and development of (-)-**24a**, **36a**, and **37**. It has been hypothesized that in both cases H-bonding interaction of parent amino group with Serine-192 should be maintained. Specifically, (-) isomer of 5-hydroxy aminotetraline was synthesized, as we have shown in our previous reports that the (-)-enantiomer exhibits the highest affinity compared to the (+)-isomer for both D_2 and D_3 receptors. As expected, compound (-)-**24a**, which is a 5-hydroxy aminotetraline analog, exhibited higher affinity for both D_2 and D_3 receptors with over all less selectivity for D_3 receptor compared to (-)-**9b** (K_i , $D_2=27.8$, $D_3=0.77$ nM, $D_2/D_3=36$). In Our pervious report phenolic moiety of 5-hydroxy aminotetraline was replaced by an amino pyrimidine moiety, which is a known bioisostere of a phenolic group. Here we wanted to explore this further with linearly fused biphenyl moiety. Our initial design to incorporate amino pyrimidine and linearly fused biphenyl moiety led to development of compound **36a**. Compound **36a** exhibited less potency for both D_2/D_3 receptors (K_i , $D_2=735$ nM, $D_3=3.65$ nM), with decrease in selectivity ($D_2/D_3=201$) compared to **9b**. Next, we wanted to introduce hydroxyl group on the accessory binding biphenyl ring of **36a** which resulted in the development of compound **37**. Compound **37**, which is a bioisosteric analog of

compound **9b**, exhibited significantly decreased binding affinity at both D2 and D3 receptors compared to **9b** (K_i , D2=13,121 nM, D3= 67 nM, vs. D2=235 nM, D3= 0.70 nM for **37** and **9b**, respectively). This suggests that it is the combination of either 2-aminothiazole or hydroxy-tetralins and linearly fused biphenyl moiety gives rise to potency and selectivity for both D2 and D3 receptors. Next, we increased the length of the two carbon linker in **9b** to four carbons. In agreement to our previous results with compound containing four methylene linker, compound **9f** (K_i , D2=567 nM, D3= 9.43 nM) displayed lower potency at both D2 and D3 receptors compared to **9b**.¹⁵⁰

Finally, in one of our earlier publications, we reported compound **D-440** as one of the most potent and selective agonists for D3 receptor known to date and this compound contains an amide bond, between the piperazine nitrogen atom and 5-position of indole, distal to the agonist head group.¹⁴¹ So, in order to probe the impact of introduction of a carbonyl group on D3 receptor selectivity in our first generation hybrid compound **D-264**, we incorporated an amide bond between the piperazine nitrogen and the accessory binding biphenyl ring of **D-264**. This modification generated compound **32**, scheme 4, which exhibited lower binding affinity for D2/D3 receptors (K_i , D2=1666 nM, D3= 9.58 nM) and its selectivity was reduced (D2L/D3= 174) compared to parent compound **D-264**. This result indicated that introduction of a carbonyl group between the piperazine nitrogen and the biphenyl ring impacted D3 affinity and selectivity unfavorably.

Table 2. Inhibition constants for competition with [³H]spiroperidol binding to cloned rat D2L and D3 receptors expressed in HEK-293 cells.

Compound	K_i (nM), rD2L [³ H]spiroperidol	K_i (nM), rD3 [³ H]spiroperidol	D2L/D3

(-)-5-OH-DPAT	58.8 ± 11.0	1.36 ± 0.28	43.2
D-264	186 ± 34	2.10 ± 0.34	86
8a (D-415)	213 ± 12	1.41 ± 0.12	151
8b (D-417)	464 ± 93	2.11 ± 0.34	220
8c (D-419)	274 ± 45	3.57 ± 0.44	78
(-)-8b (D-533)	343 ± 65	2.33 ± 0.26	147
9a (D-416)	230 ± 50	1.17 ± 0.37	196
9b (D-418)	347 ± 54	1.20 ± 0.14	289
(-)-9b (D-433)	369 ± 39	1.73 ± 0.14	213
(+)-9b (D-434)	1507 ± 312	19.7 ± 2.1	76
9c (D-425)	208 ± 15	1.80 ± 0.38	115
9f (D-492)	567 ± 83	9.43 ± 1.14	60
(-)-11 (D-437)	27.8 ± 1.8	0.77 ± 0.030	36
22 (D-424)	70.6 ± 10.2	2.35 ± 0.13	30
26a (D-468)	735 ± 198	3.65 ± 0.64	201
27 (D-467)	13,121 ± 4539	67 ± 7.8	196
35 (D-517)	1666 ± 282	9.58 ± 1.18	174

On the basis of the binding results, selected compounds **(-)-8b** and **(-)-9b** were subjected to the GTP γ S binding functional assay for D2 and D3 receptors and compared with endogenous ligand dopamine and the parent compound **D-264**. The functional assay measures quantitatively the ability of the compound to stimulate the receptor to initiate downstream events. The maximum stimulation of a particular receptor produced by the compound compared to the reference compound dopamine (which is considered to be full agonist and produce 100% maximum stimulation) is represented by E_{max} . The maximum stimulatory potency (E_{max}) determines if the compound is full agonist, partial agonist or antagonist compared to the reference compound which is considered to be full agonist. The concentration of the compound that produces half maximal response (EC_{50}) determines the affinity of the compound towards the high affinity state of the receptor. In this assay, amount of binding of nonhydrolyzable analog of GTP ($[^{35}S]$ GTP γ S) to the α -subunit of heterotrimeric G-protein was measured and compared with the reference compound dopamine which was considered to be 100 % agonist for both the receptors. This binding event is one of the first steps in signal transduction process in GPCRs after the ligand is bound to the receptor. The assays were carried out with cloned human D2 and D3 receptors expressed in CHO cells.

All three compounds exhibited high affinity for the D3 receptor and their affinity were in the subnanomolar range (**Table 3**). Compound **(-)-9b** displayed higher functional potency for D2/D3 and selectivity for D3 receptor in comparison to **D-264** and dopamine (**Table 3**). **(-)-9b** demonstrated 15-fold increase in functional potency (EC_{50} = **12.3 nM** vs. **33.1nM** for **D2** and **0.1 nM** vs. **1.51 nM** for **D3**, for **(-)-9b** and **D-264**, respectively) and an almost 5-fold increase in functional selectivity (D2/D3 = 123 vs. 22.1 for **(-)-9b** vs. **D-264**) for D3 receptor in comparison to **D-264**.

Compounds **(-)-9b** and **D-264** exhibited full agonist activity at D2 and D3 receptors, while their selectivity for D3 receptor dropped significantly when compared to binding data. On the other hand, compound **(-)-8b** turned out to be functionally two fold less potent at D3 receptor ($EC_{50}=3.42$ nM) in comparison to **D-264**. The functional potency of compound **(-)-8b** for D2 receptor was comparable with **D-264** ($EC_{50}= 36.8$ nM vs. **33.1nM** for **(-)-8b** vs.**D-264**, respectively).

Table 3. Stimulation of [35 S]GTP γ S binding to hD2 and hD3 receptors expressed in CHO cells.

Compd	CHO-D2		CHO-D3		D2/D3
	EC_{50} (nM) ^a [35 S]GTP γ S	%E _{max}	EC_{50} (nM) ^a [35 S]GTP γ S	%E _{max}	
Dopamine	218 ± 12	100	10.6 ± 2.1	100	26.5
Ropinirole	304 ± 11	73.9 ± 0.9	10.3 ± 1.5	66.6 ± 8.1	29.5
(-)-D-264	33.1 ± 6.6	104 ± 5	1.51 ± 0.02	90 ± 4.3	22
(-)-8b(D-533)	36.8 ± 7.2	105 ± 6	3.42 ± 1.01	67.3 ± 5.6	10.8
(-)-9b(D-433)	15.9 ± 1.8	116 ± 10	0.10 ± 0.02	95.8 ± 3.7	159

EC_{50} is the concentration producing half-maximal stimulation; for each compound, maximal stimulation (E_{max}) is expressed as percent of the E_{max} observed with 1

mM (D2) or 100 μ M (D3) of the full agonist DA (%Emax). Results are the means \pm SEM for 3-6 experiments each performed in triplicate.

4.3. *In vivo* experiments with lead molecules from first series of compounds.

Based on the *in vitro* binding and functional activity results, we decided to evaluate (-) **8b** or (**D-533**), (-) **9b** or (**D-433**) in our pharmacological studies. Ropinirole was also evaluated as a reference compound for comparison purpose.

4.3.1. Evaluation of In Vivo Blood Brain Barrier Crossing Ability of **D-264**, (-) **8b**, (-) **9b**, and Ropinirole by Reversal of Reserpine Induced Hypolocomotion in Rats:

Reserpine induces depletion of catecholamine in nerve terminals, resulting in a cataleptic condition in rats, which is a well established animal model for PD.^{158, 159}

Significant inhibition of locomotion of rats was observed 18 h after the administration of reserpine (5 mg/ kg,sc) which indicated the development of akinesia in rats. Compound (-)**8b** and (-)**9b** at a dose of 5 μ Mol/ kg, i.p., DI water, were highly efficacious in reversing akinesia (**Figure 39**) while **D-264** at the same dose (5 μ Mol/kg, i.p., DI water) failed to produce any significant effect in reversing akinesia in the reserpine treated rats. However, the **D-264** was more effective when it was dissolved in 10% beta-hydroxy cyclodextrin solution (**Figure 39**). The locomotor activity of (-)**8b** at the end of 6h remained high compare to (-)**9b**. It is evident from the result that compounds (-)**8b** and (-)**9b** were the most efficacious in producing reversal of akinesia when (-)**8b** seems to exhibit greater potency. Thus, the results indicate that the compounds (-)**8b** and (-)**9b** could efficiently crossed the blood brain barrier, exhibited early onset, demonstrated long duration of action whereas compound **D-264** was able to produce in vivo activity if dissolved in 10% beta-hydroxy propyl cyclodextrin solution.

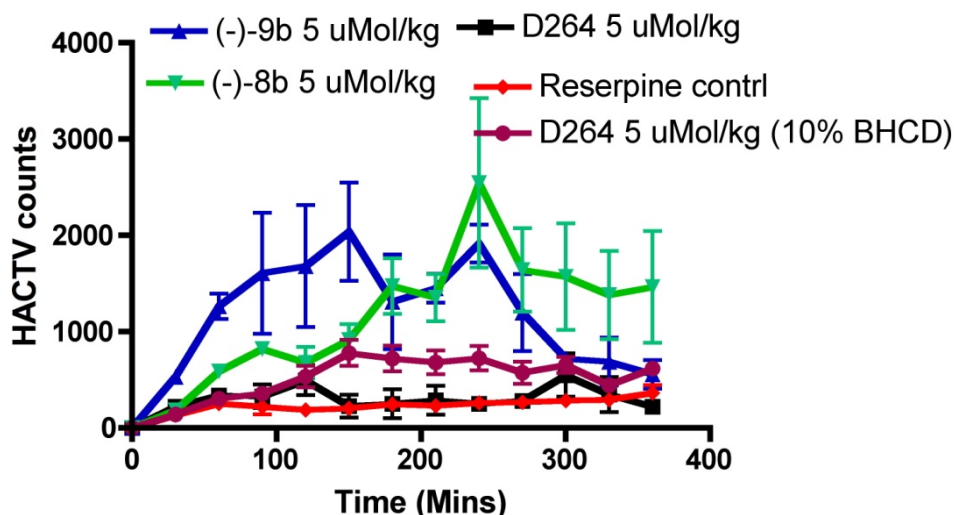


Figure 39. Effect of different drugs upon reserpine (5.0 mg/Kg, s.c.)-induced hypolocomotion in rats. Data are means \pm S.E.M, $n = 4$ per value. Horizontal activity was measured as described under materials and methods. The plots are the representation of horizontal locomotor activity at discrete 30-min intervals after the administration of (-)**9b** (i.p.), (-)**8b** (i.p.) and D-264 (i.p.) at the dose of 5 μ Mol/kg compared to control reserpine treated rats in 18 h post reserpine treatment. One way ANOVA analysis demonstrates significant effect among treatments $F(5,95) = 14.16$ ($P < 0.0001$). Dunnett's analysis following ANOVA showed that the effects of (-)**9b** ($P < 0.01$) and (-)**8b** ($P < 0.01$) were significantly different compared to reserpine control.

Degeneration of the substantia nigral dopaminergic neurons which leads to profound striatal dopamine deficiency syndrome is responsible for its classic motor symptoms akinesia and bradykinesia^{127, 159}. Reserpine administration causes depletion of monoamines including dopamine resulting in marked suppression of locomotor activity which resembles the motor impairment found in PD^{127, 159}. Therefore, reserpine model is one of the PD models used to screen drugs used for alleviation of

the symptoms of motor dysfunction in PD^{127, 158}. Compounds **(-) 8b**, **(-) 9b** with the dose of 5 $\mu\text{mol/kg}$ i.p. not only reversed reserpine induced hypokinesia to the normal level of locomotion found in control animals (vehicle treated rats), but also demonstrated significant enhancement of locomotion. The mechanism of the locomotor stimulation in reserpine model is likely to be mediated by the postsynaptic D2/D3 receptor activation.

4.3.2. Induction of contralateral rotation by (-)-8b and (-)-9b in unilaterally lesioned rats in Ungerstedt rat model for PD:

On the basis of above locomotor experimental results, compound **(-)8b and (-)9b** were selected for *in-vivo* evaluation in in the Ungerstedt rat rotation model for Parkinson's disease. This is an accepted model for studying dopamine agonist efficacy and their potential utility in the treatment of Parkinson's disease¹⁶⁰. In this model, rats received unilateral lesion by administration of neurotoxic 6-Hydroxy dopamine selectively in the medial forebrain bundle (MFB) region of the brain, the area that projects dopaminergic neurons to the striatum. The lesion caused gradual loss of dopaminergic neurons in that area which caused striatal dopamine deficiency on the lesioned side. As a result of the scarcity of dopamine in the synapse, the postsynaptic dopamine receptors became supersensitive in the striatum on the lesioned side. As a result, administration of dopamine agonist causes an imbalanced locomotor activity, the rotational movement away from the lesioned side. The full contralateral rotations were recorded in every 30 minutes and plotted against total time of action.

Both compounds **(-)8b and (-)9b** produced potent rotational activity in a dose dependent manner when administered intraperitoneally (i.p). At 10 $\mu\text{Mol/kg}$ dose,

both **(-)-8b** (6.56 mg/kg) and **(-)-9b** (9.28 mg/kg) produced potent rotations that lasted for more than 10 h (**Figure 40**). Compound **(-)-8b** was more potent in producing maximum rotation numbers compared to **(-)-9b** (5866 vs. 2653 for **(-)-8b** and **(-)-9b**, respectively). Peak effect of both compounds reached at 7.5 h. This is an indication of long duration of action of both compounds in producing contralateral rotation. When tested at a lower doses (5 μ Mol/kg), both compounds, **(-)-8b** (3.28 mg/kg) and **(-)-9b** (4.64 mg/kg), produced lower number of rotations (3333 vs. 1839 for **(-)-8b** and **(-)-9b**, respectively). The rotation in this case lasted for more than 7h (**Figure 40**). Interestingly, both compounds produced initial increase of rotational activity followed by a brief decrease of activity before exhibiting a steady increase of rotational activity. At present, the reason of such biphasic activity is unknown. As indicated in the locomotor activity study with reserpinized rats, the higher efficacy of **(-)-8b** (**Figure 40**) correlates to higher activity of compound **(-)-8b** compared to **(-)-9b** in producing rotational activity in 6-OHDA rats. This more potent nature of **(-)-8b**, mehtoxy analog of **D-264**, in rotational experiment may be due to its high *in-vivo* stability compared to the hydroxyl analog **(-)-9b**.

4.4. Antioxidant assay:

Oxidative stress has been strongly implicated in PD pathogenesis. Therefore, one of our objectives in ligand design was to impart antioxidant activity into our designed drugs. Citrus secondary metabolites such as ascorbic acid posses antioxidant property and have shown several health benefits. Scavenging of DPPH (1,1-diphenyl-2-picrylhydrazyl) radical by **D-264**, **(-)-8b** and **(-)-9b**, **D-437** and **ascorbic acid** was carried out (**Figure 41**). To compare the difference in DPPH free radical scavenging property of the salt versus the free base form of the compounds, the assay was performed with the both forms. The detailed experimental procedure is

discussed in the chapter containing materials and methods. As shown in Figure 41, all compounds inhibited DPPH radical activity dose dependently. However, there is a considerable difference in the kinetics of the reaction with DPPH between the salt form and free base form of the compounds. The reaction rate is much slower with the free base compared to the salt form. The steady state was achieved at 110 minutes and 25 minutes for the free base and salt, respectively. At the end of both assays, the extent of scavenging of the radical was comparable. Overall all the compounds, with the exception of **D-437**, exhibited similar antioxidant potency as ascorbic acid. Interestingly, **D-437** exhibited lesser antioxidant activity in this assay compared to **D-433**, which indicates more potent antioxidant nature of thiazolidum moiety compared to aminotetraline.

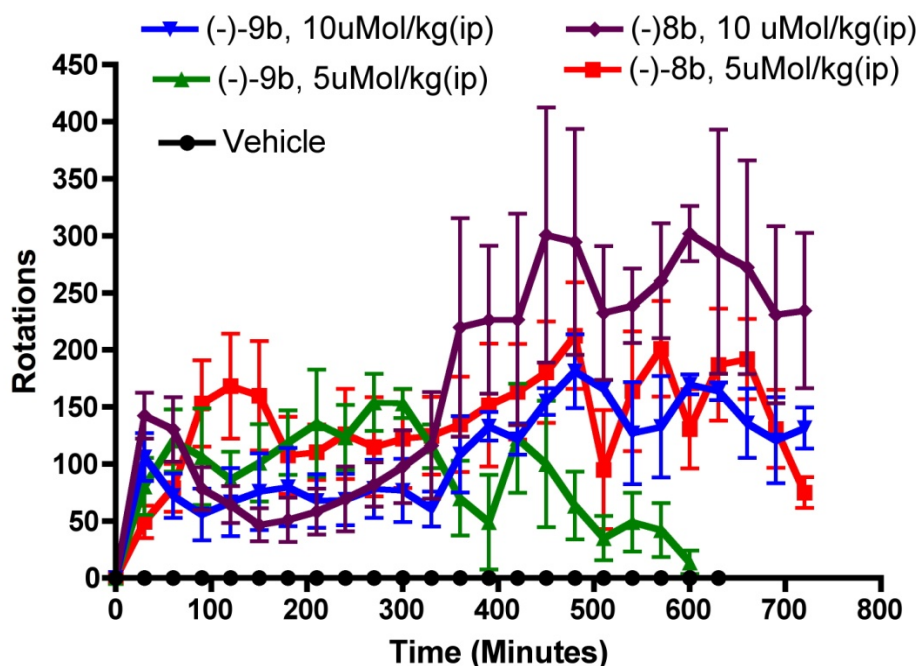


Figure 40. Comparison of the effects of (-)-**8b** and (-)-**9b** with a dose of 10 $\mu\text{Mol/kg}$ and 5 $\mu\text{Mol/kg}$ and vehicle in unilaterally 6-OH-DA lesioned rats studied for maximum 12 h. Each point is the mean \pm SEM of three rats. The drugs were

administered ip. One way ANOVA analysis demonstrates significant effect among treatments: $F(4,95) = 13.87$ ($P < 0.0001$). Dunnett's analysis showed that the effects are significantly different statistically compared to vehicle ($P < 0.01$).

Generally antioxidants will react with DPPH (1,1-Diphenyl-2-picrylhydrazyl), which is a nitrogen-centered radical with a characteristic absorption at 517 nm and converted into 1,1,-diphenyl-2-picryl hydrazine, due to its hydrogen donating ability at a very rapid rate. The degree of discoloration indicates the scavenging potentials of the antioxidants. It is known that free radicals cause auto-oxidation of unsaturated lipids¹⁶¹. On the other hand, antioxidants are believed to intercept the free radical chain of oxidation and to donate hydrogen, thereby forming stable end product, which does not initiate or propagate further oxidation of lipid. The data obtained revealed that the compounds **D-264**, **(-)-8b** and **(-)-9b** are strong free radical scavengers and primary antioxidants that react with DPPH radical. We believe that compounds **D-264**, **(-)-8b** and **(-)-9b** will have potential to reduce the oxidative stress in the parkinsonian brain via quenching free radicals.

4.5. Neuroprotection studies with MN9DCell line:

The MN9D cells are hybridoma cells derived via the somatic infusion of rostral mesencephalic neurons from embryonic C57BL/6J (E14) mice and the N18TG2 neuroblastoma cells. The MN9D cells they represent as one of the most suitable model for *in vitro* study of PD due to high level of expression of tyrosine hydroxylase, have high dopamine content and exhibit other similarities with DA neurons. We carried out experiments to evaluate the effect of treatment of D-264 and **(-)-9b** in the protection of dopaminergic MN9D cells from toxicity of 6-OHDA and MPP+. Both MPP+ and 6-OHDA are known to cause dopamine cell death possibly via different

mechanisms. The MPP⁺ which is a metabolite of MPTP, is a dopaminergic neurotoxin which destroys the nigrostriatal dopaminergic pathway and produces parkinsonian syndrome with massive loss of nigral DA neurons. Inhibition of mitochondrial complex I by MPP⁺, thereby, increasing the oxidative stress is the central mechanism for its toxicity. Oxidation of 6-OHDA is known to produce quinones as well as free radicals such as hydrogen peroxides, superoxides and hydroxyl radicals which induce apoptosis in cells.

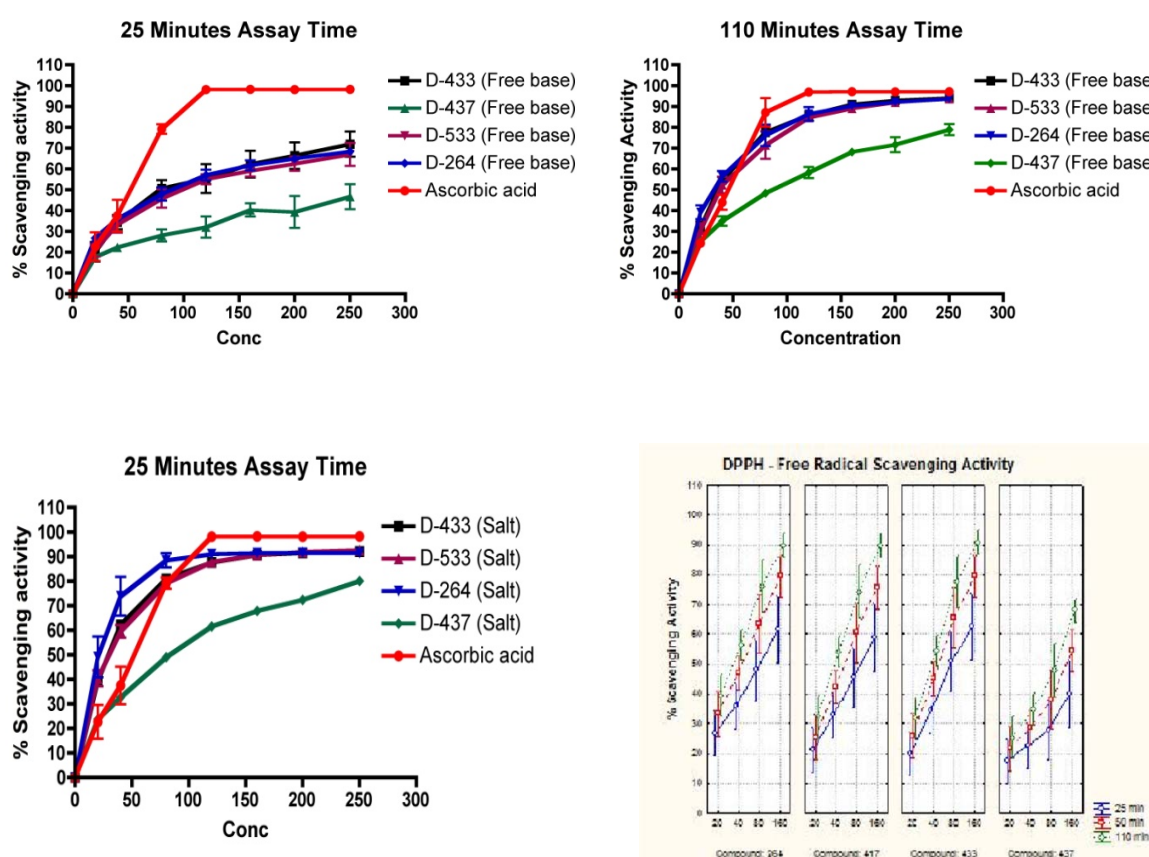


Figure 41. DPPH radical scavenging activity by **D-264**, **(-)-9b**, **(-)-8b**, **(-)-11** and ascorbic acid.

4.5.1. Neuroprotection against MPP⁺ toxicity:

From our previous dose-dependent experiment of MPP⁺, we chose 100 μ M of MPP⁺ which can induce 50-60% cell death, for our study. To test whether D-264 and

(-)-**9b** can protect dopaminergic MN9D cells from MPP⁺ induced toxicity, the cells were pre-treated with various concentrations of (20, 10, 5, 1, 0.1, 0.01 and 0.001 μ M) of either D-264 or (-)-**9b** for 1 h and then co-treated with 100 μ M MPP⁺ for an additional 24 h. The dose dependent effect of treatment of D264 and D-433 in reversing the toxicity of MPP⁺ to dopaminergic MN9D cells is demonstrated in Figure xxx. The data from the MTT assay further indicated that both **D-264** and (-)-**9b** can protect the MN9D cells in a dose-dependent manner. For D-264, significant protection from toxicity of MPP⁺ was conferred by 1, 5, 10 and 20 μ M doses. For D-433, significant neuroprotection was conferred at 5 and 10 μ M doses. It seems D264 is relatively more potent than D433 in this neuroprotection assay.

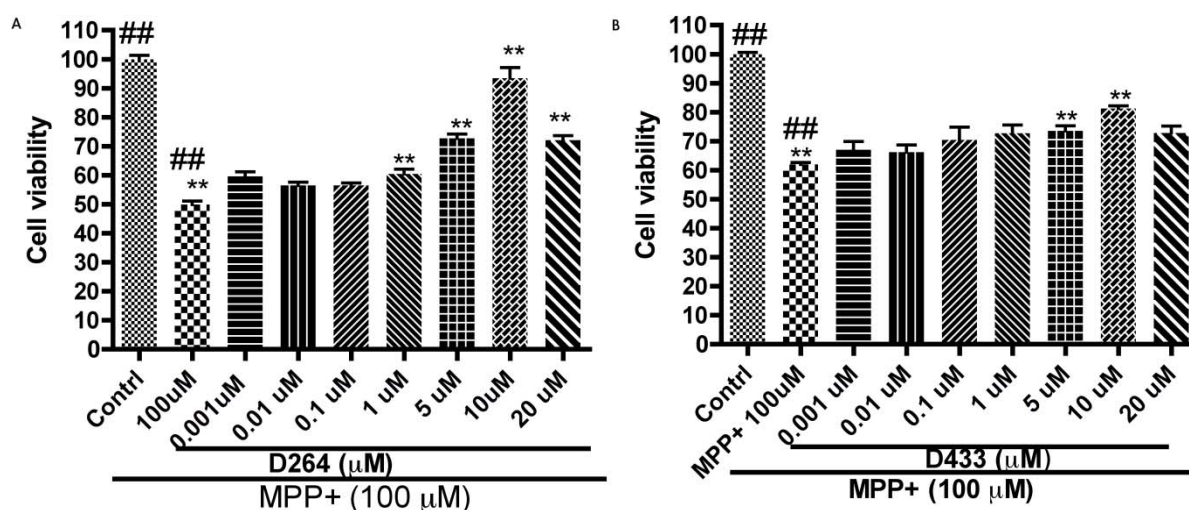


Figure 42. Dose dependent effect of combination of pretreatment followed by co-treatment of D-264 and D-433 with 100 μ M MPP⁺ on cell viability of MN9D cells from toxicity of 100 μ M MPP⁺. A-B: MN9D cells were pretreated with different doses of D-264 and D-433 for 1 h followed by co-treatment with 100 μ M MPP⁺ for 24 h. The values shown are means \pm SDs of three independent experiments performed in 4-6 replicates. One way ANOVA analysis followed by Tukey's Multiple Comparison

post hoc test were performed. (** $p < 0.01$ compared to the MPP+ group. ### $p < 0.001$ compared to the control group).

4.5.2. Neuroprotection against 6-OHDA:

6-OHDA is known to cause cell death in a dose-dependent manner via production of reactive oxygen species. From our previous dose-dependent experiment of 6-OHDA, we chose 75 μM of 6-OHDA which can induce 40-50% cell death for our study. To examine whether **D-264** and **(-)-9b** can protect MN9D cells from the exposure to 75 μM neurotoxin 6-OHDA, the cells were incubated with various concentrations of (20, 10, 5, 1, 0.1, 0.01 and 0.001 μM) of either **D-264** or **(-)-9b** for 1 h and then co-treated with 75 μM 6-OHDA for additional 24 h.

As shown in **Figure 43**, the data from the MTT assay clearly indicated that **D-264** was able to protect significantly the MN9D cells from 6-OHDA toxicity in a dose-dependent manner. The highest protection conferred by **D-264** was exhibited at concentration, 5 and 10 μM , of the drug. At these concentrations, **D-264** conferred almost 25% protection from 6-OHDA toxicity. However, **(-)-9b** was able to protect MN9D almost 12% compared to 6-OHDA treated alone and the highest protection was exhibited at 5 and 10 μM concentrations of the drug. It seems that the extent of protection conferred by **(-)-9b** was slightly less compared to **D-264** (**Figure 43**).

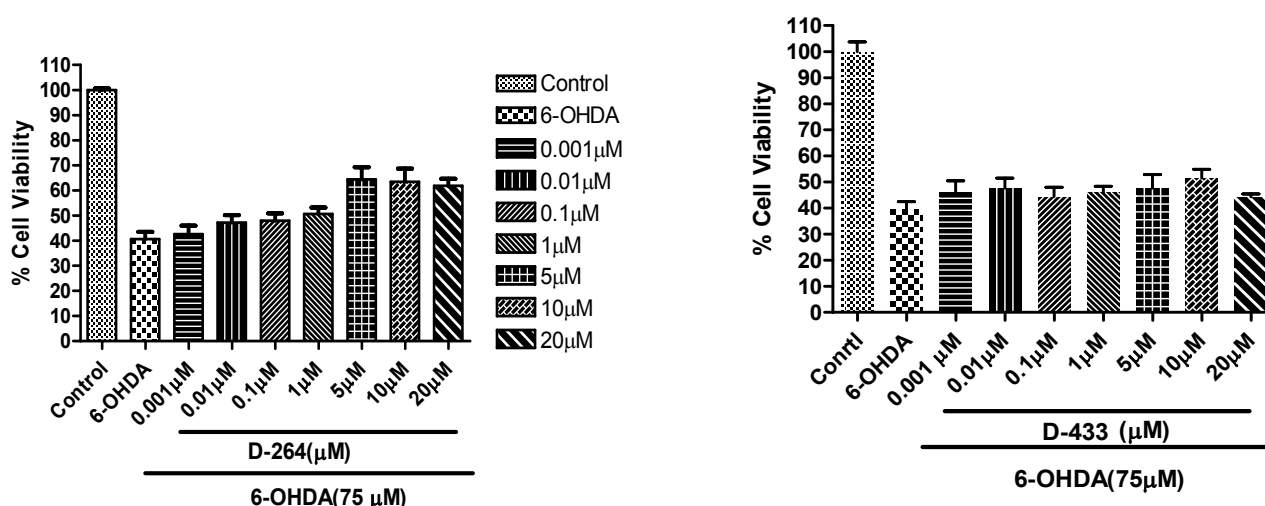


Figure 43. Dose dependent effect of combination of pretreatment followed by co-treatment of D-264 and D-433 with 75 μ M 6-OHDA on cell viability of MN9D cells from toxicity of 100 μ M MPP+. A-B: MN9D cells were pretreated with different doses of D-264 and D-433 for 1 h followed by co-treatment with 75 μ M 6-OHDA for 24 h. The values shown are means \pm SDs of three independent experiments performed in 4-6 replicates. One way ANOVA analysis followed by Tukey's Multiple Comparison post hoc test were performed and it did not show significant effect of D-433.

4.6. *In vitro* characterization of dihydroxyl derivatives of D-264:

In our approach to design multifunctional ligands which should not only act as agonist at dopamine D2/D3 receptor but also be able to modulate ASN aggregation, we decided to introduce two hydroxyl groups in our hybrid template. Numerous studies have shown that compounds with dihydroxy group are able to effectively modulate ASN aggregation. SAR studies on hybrid template have indicated that bulky aromatic substitutions located distally from head group are well tolerated on the piperazine moiety. Our recent SAR studies have demonstrated that monohydroxyl and methoxy moieties are not only well tolerated but also produced highly efficacious *in-vivo* active compounds. Thus, it was hypothesized that introduction of another hydroxyl group on the accessory binding site should not only retain high affinity for the D2/D3 receptor but also should provide potent ASN aggregation modulator. Based on this, preliminary compounds were designed and synthesized. In this series, we have developed **11** final target compounds which were tested in *in-vitro* binding assay to determine their affinity toward dopamine D2 and D3 receptors. The binding assay is a competition based assay that determines the inhibition constants of the compounds for displacing the binding of dopamine receptor antagonist [³H]-Spiperone to the cloned hD2L and D3 receptors expressed

in HEK-293 cells. The detailed procedure is written in the *materials and methods* section (chapter 6).

The two initial compounds that were designed first were **9d** and **21b**. These compounds possess two hydroxyl groups in the para position to each other. Both compounds exhibited low nanomolar potency for D3 receptor (3.50 and 5.29 nM for **9d** and **21b**, respectively). Compound **21b** was twice as potent at D2 receptor compared to **9d** (866 vs. 13,29 nM for **21b** and **9d**, respectively) but it was less potent compared to monohydroxyl derivative, **9b** (235 vs. 866 nM for **9b** and **9d**, respectively). These results indicated that two hydroxyl groups in para position to each other were well tolerated by D3 receptors but exhibited less potency for D2 receptor. It is well established in the literature that conversion of dihydroxyl to quinone is critical to modulate ASN aggregation¹³¹. Therefore, compounds **9d** and **21b**, were converted into corresponding quinone, which led to the generation of compound **10** and **22**, respectively. Surprisingly, there was no significant change in affinity of the **22** towards D3 receptor (7.35 nM) compared to the dihydroxyl compound **21b** (5.29 nM) but affinity towards D2 receptor dropped by four fold compared to **21b** (3210 and 866 nM for **22** and **21b**, respectively). On the other hand, compound **10** showed less affinity towards D3 receptor compared to corresponding parent molecule **9d** (13.4 and 3.50 nM for **10** and **9d**, respectively) while the affinity to D2 receptor did not change significantly compared to **9d** (17,19 and 13,29 nM for **10** and **9d**, respectively). This could be due to the presence of complex interaction of molecule in this region of D2 and D3 receptor but the major factor responsible for this change in affinity is not clear yet.

Next, we synthesized two enantiomerically pure forms of racemic **9d**, using S(-) Pramipexole compound (-)-**9d** (K_i , D2 = 762 nM, D3 = 2.51 nM, D2/D3=303) and the

R(+) pramipexole compound **(+)-9d** (K_i , D2 = 2542 nM, K_i D3 = 34.4 nM, D2/D3=74) to see the change of potency and selectivity at the dopamine receptors. In agreement with our earlier results, **(-)-9d** exhibited higher potency at both D2 and D3 receptors compared to **(+)-9d**. **(-)-9d** showed higher potency for both D2 and D3 receptors compared to the racemic **9d** (K_i , D2=762, D3= 2.51 nM vs. **9d** K_i , D2=13,29, D3= 3.50 nM). All compounds in this series showed nanomolar potency for the D3 receptor in the competitive binding assay.

In our next design of compounds we wanted to evaluate the positional effect of dihydroxyl group on binding affinity and selectivity. The bioisosteric replacement of thiazolidium moiety by aminotetraline was also performed. Specifically, (-) isomer of 5-hydroxy aminotetraline was synthesized, as we have shown in our previous reports on 5-hydroxy series, the (-)-enantiomer exhibited the higher potency for both D2 and D3 receptors with lower selectivity for D3 over D2 compared to 2-aminothiazole head group. This resulted in the design and development of **(-)-9e**, **(+)-9e**, and **(-)-24b**. It has been shown in literature that vicinal dihydroxylphenyl group can provide ASN fibrillation inhibition property to flavonoids. As expected, compound **(-)-24b**, which is a 5-hydroxy aminotetraline analog, exhibited higher affinity for both D2 and D3 receptors (K_i , D2=41.8 nM; D3=0.350 nM,) compared to **(-)-9e** and **(+)-9e** (K_i , D2=556, vs. **(+)-9e** K_i , D2=2852 nM; D3=8.25 nM, vs. **(+)-9e** K_i , D3=18.3 nM). In agreement with our earlier results, **(-)-9e** exhibited higher potency at both D2 and D3 receptors compared to **(+)-9e**.

Curcumin a polyphenolic compound has antioxidant and anti-inflammatory property. Wang et al., tested curcumin against ASN induced cytotoxicity in SH-SY5Y neuroblastoma cell line.¹³⁰ Extracellular incubation of SH-SY5Y cells with oligomeric but not the monomeric or fibril form of ASN can induce significant cytotoxicity.

Curcumin can significantly reduce the cytotoxicity of preformed ASN oligomeric species by reducing the ROS and inhibiting caspase-3 activity. It can also protect against intracellular induced ASN toxicity by over expressing ASN in transient transfected SH-SY5Y cells. However, the Pharmacophoric feature responsible for ASN aggregation modulation property of curcumin is not known yet.

Our SAR studies on hybrid template have indicated that monomethoxy and monohydroxyl groups are well tolerated on the distal phenyl ring. Compounds with mono hydroxyl and methoxy group are potent agonist for both D2 and D3 receptors with high in vivo efficacy. Our SAR also indicated that compounds with dihydroxyl group on the distal phenyl are potent towards D3 receptor, however, binding potency of dihydroxyl substituted compounds for D2 receptors dropped significantly compared to monohydroxyl compounds.

Keeping in mind both the influence of dihydroxyl on the binding potency while probing the key functional groups of curcumin responsible for ASN modulation property, we incorporated combination of critical hydroxyl and methoxy functional group on the accessory binding biphenyl ring of our hybrid molecules. Thus, it was perceived that replacement of dihydroxyl group by hydroxyl methoxy moiety should not only retain high binding affinity for D2/D3 receptors but also provide multifunctional molecules with ASN aggregation modulation property.

Initially, two compounds **46** and **53** were designed, synthesized and evaluated. In these two compounds piperazine moiety was attached to monophenyl and biphenyl ring substituted with hydroxyl and methoxy groups ortho in position to each other. Both compounds displayed nanomolar potency for D3 receptor (K_i ; D3=6.41 nM vs. D3=3.07 nM for **46** and **53**, respectively). Compound **46** was seven times more

potent at D2 receptors compared to 53 (K_i ; D2=356 nM vs. D2=2480 nM for **46** and **53**, respectively). These results indicated that mono phenyl ring with hydroxyl and methoxy substitution is well tolerated at both D2 and D3 receptors. Overall, combination of both the hydrophobicity and electronic nature of the substituent plays a major role towards the binding affinity for D2 and D3 receptors.

Table 4. Affinities for Cloned D_{2L} and D₃ Receptors Expressed in Human Embryonic Kidney Cells Measured by Inhibition of [³H]-spiperidol Binding ^a

S.N.	Compound	K_i , (nM), D _{2L} [³ H]Spiperone	K_i , (nM), D ₃ [³ H]Spiperone	D _{2L} /D ₃
1.	D-264	264 ± 40	0.92 ± 0.23	253
2.	22 (D-489)	3210± 572	7.35 ± 0.56	464
3.	9d (D-490)	13,29± 182	3.50 ± 0.73	380
4.	21c (D-491)	866± 85	5.29 ± 0.91	164
5.	10 (D-493)	1719± 33	13.4 ± 1.33	128
6.	(-) 9d (D-510)	762± 90	2.51± 0.50	303
7.	(+) 9d (D-511)	2542± 462	34.4 ± 6.0	74.0
8.	(-) 9e (D-519)	556±165	8.25 ± 0.98	67
9.	(-) 24b (D-520)	41.8±11.2	0.350 ± 0.101	119
10.	(+) 9e (D-521)	2852±458	18.3 ± 2.5	156

11.	46 (D-546)	356±55	6.41±1.47	55.6
12.	53 (D-553)	2480±602	3.07±0.66	808

^aResults are the means \pm SEM for three to seven experiments, each performed in triplicate.

Following binding analysis, selected compounds **(-)-9d**, **(-)-9e**, and **(-)-24b** were subjected to the [³⁵S]GTPγS functional assay for D2 and D3 receptors and compared with the full agonist dopamine (**Table 5**). The assays were carried out with the cloned human D2 and D3 receptors expressed in CHO cells. In this study, **(-)-9e** as well as **(-)-24b** exhibited high affinity for both D2 (EC₅₀ for **(-)-9e**, 42.4 nM; for **(-)-24b**, 4.73 nM) and D3 (EC₅₀ for **(-)-9e**, 5.92; for **(-)-24b**, 2.18 nM) receptors, compared to the reference compound dopamine (EC₅₀ for dopamine, 227 nM for D2 and 8.53 nM for D3). Compound **(-)-9d** exhibited moderate affinity for D2 (EC₅₀ for D2, 107.2 nM; but demonstrated high affinity for D3 (EC₅₀ for D3 receptor, 2.32). All three compounds were full agonist when compared against reference dopamine.

Table 5. Stimulation of [³⁵S] GTPγS Binding to Cloned Human D2 Receptor and D3 Receptor Expressed in CHO Cells^a

Compd.	hCHO-D2		hCHO-D3		D2/D3
	EC ₅₀	%E _{max}	EC ₅₀	%E _{max}	
DA	227 ± 11	100	8.50	100	26.5
(-) D-264	33.1 ± 6.6	104 ± 5	1.51 ± 0.022	90 ± 4.3	22.1
(-)-D-510	107.2± 19.5	96.0 ± 3.8	2.32 ± 0.22	97.2 ± 4.5	46.2

(-)-D-519	42.4± 13.6	98.2 ± 1.5	5.92 ± 0.74	82.4 ± 0.5	
(-)-D-520	4.73± 0.44	80.9 ± 6.6	2.18 ± 0.30	58.3 ± 9.6	

^aEC₅₀ is the concentration producing half-maximal stimulation; for each compound, maximal stimulation (E_{max}) is expressed as a percent of the E_{max} observed with 1 mM (D2) or 100 μM (D3) of the full agonist DA (% E_{max}). Results are the mean ± SEM for three to six independent experiments, each performed in triplicate.

4.7. *In vivo* experiments with lead molecules from second series of compounds.

4.7.1. Reversal of reserpine-Induced Hypolocomotion in Rats:

Reserpine induces depletion of catecholamines in nerve terminals resulting in a cataleptic condition in rats, which is a well established animal model for PD¹⁵⁸. Significant reduction of locomotion of the rats was observed 18 h after the administration of reserpine (5 mg/kg, s.c.) which indicated the development of akinesia in rats. Compound **(-)-24b (D-520)** was highly efficacious in reversing the locomotor activity of reserpinized rats. The locomotor activity of **(-)-24b** at the end of 5h remained at a high level. The reference drug ropinirole on the other exhibited much shorter action and was much less efficacious compared to **(-)-24b**. Compound **(-)-24b** with the dose of 10 μmol/kg i.p. not only reversed reserpine induced hypokinesia to the normal level of locomotion found in control animals (vehicle treated rats), but also demonstrated significant enhancement of locomotion for the whole time frame of study. The standard drug ropinirole at a dose of 10 μMol/Kg s.c. exhibited much shorter duration of action compare to **(-)-24b**, the peak of action reached within 30 min and the pharmacological action ceased after 90 min. The

mechanism of the locomotor stimulation in reserpine model is likely to be mediated by the postsynaptic D2/D3 receptor activation. The results indicated that compound is a potent agonist which could cross blood brain barrier effectively.

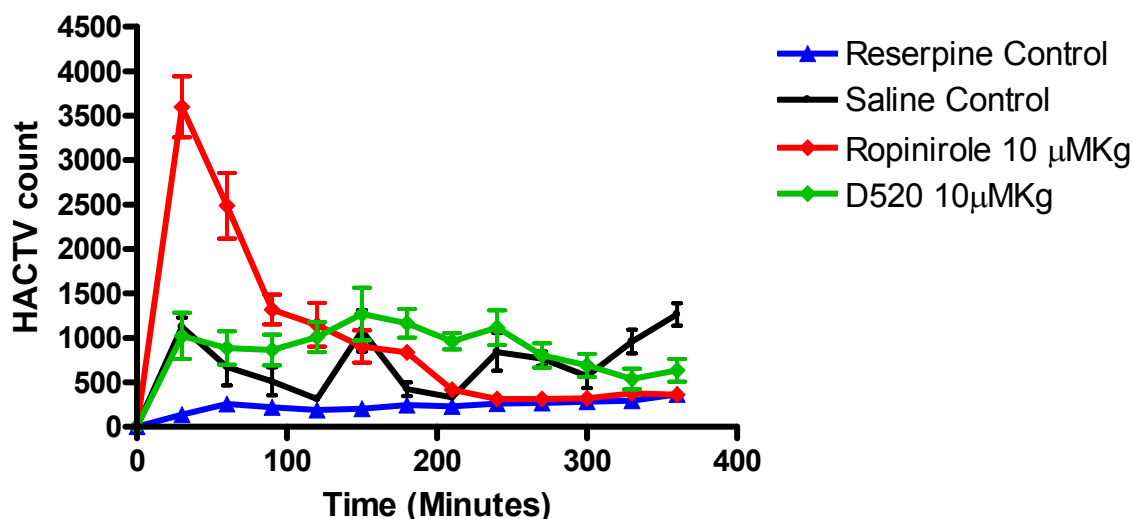


Figure 44. Effect of different drugs upon reserpine (5.0 mg/Kg, s.c.)-induced hypolocomotion in rats. Data are means \pm S.E.M, $n = 3-4$ per value. Horizontal activity was measured as described under materials and methods. It is the representation of horizontal locomotor activity at discrete 30-min intervals after the administration of (-)-**24b** and ropinirole at the dose of 10 μ Mol/kg compare to control rats in 18 h reserpine post treatment. One way ANOVA analysis demonstrates significant effect among treatments: Panel A, $F(3,95) = 31.36$ ($P < 0.05$). Dunnett's analysis following ANOVA showed that the effects of (-)-**24b** ($P < 0.05$) and ropinirole ($P < 0.05$) were significantly different statistically compared to reserpine control.

4.7.2. *In vivo* Pharmacology with 6-OHDA lesioned rats:

Based on the above locomotor activity results, compound (-)-**24b** was selected for *in vivo* evaluation in rats carrying a unilateral lesion in the medial forebrain bundle induced by application of the neurotoxin 6-hydroxydopamine (6-OHDA).

Development of supersensitivity of dopamine receptors takes place resulting from destruction of dopamine neurons in these surgically modified rats. When these rats are challenged with direct acting dopamine agonists, they produce contralateral rotations away from the lesioned side. This rat model is considered to be one of the standard models for preclinical screening of drugs for possible antiparkinsonian property.¹⁶² Compound (-)-**24b** was highly potent in producing large number of rotations at a dose of 2.5 $\mu\text{Mol/kg}$ (Number of rotation = 1180) and the activity lasted more than 5 h. At a higher dose of 5 $\mu\text{Mol/kg}$, the rotational activity was initially higher compared to the lowest dose but the activity remained at high level after 5 h (figure 45). The efficacy of this compound in producing rotations indicated its good bioavailability, excellent brain penetration but rapid metabolism.

4.7.2.1. Effect of **24b** at two different doses (2.5 $\mu\text{M/kg}$, and 0.5 $\mu\text{M/kg}$ i.p) and comparison with standard drug ropinirole:

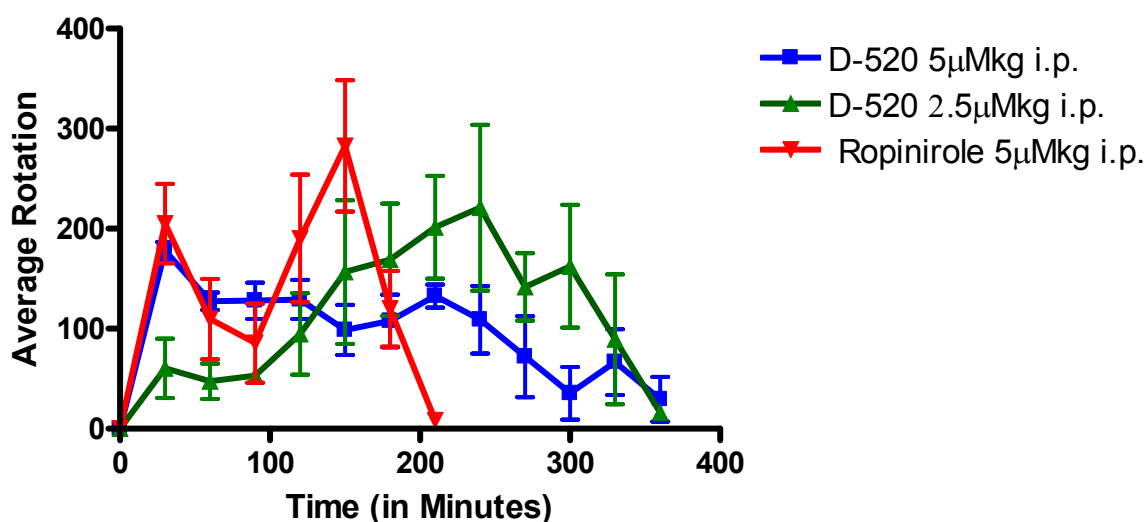


Figure 45. Effect on turning behavior of two different doses of **24b** and vehicle in lesioned rats studied for maximum 8 h. Each point is the mean \pm SEM of 3-4 rats.

The drugs were administered i.p. One way ANOVA analysis didnot demonstrates significant effect among treatments.

4.8. Evaluation of anti-oligomeric and/or anti-fibrillar activity of potential inhibitors of ASN (α -synuclein) aggregation:

The misfolding and aggregation of ASN is proposed to be toxic towards the dopaminergic neurons. ASN oligomers could perforate vesicular membranes of dopaminergic neurons which lead to DA leakage into the cytoplasm. Cytoplasmic DA can quickly form ROS, and DA-quinone, which can form covalent adducts with ASN. It has been shown in the literature that ASN forms soluble, SDS-resistant oligomers in the presence of DA¹³³. In order to assess the ability of our lead molecules to inhibit the aggregation of ASN mediated by dopamine following experiments were carried out.

4.8.1. Generation of ASN aggregates using cell-free system:

Recombinant wild-type human ASN (17.5 μ M) was incubated with 200 μ M of DA for 72 h and the reaction was then analyzed by silver staining and ThT assays (**Figure 46 a**). DA induced increase in ASN oligomerization over the time, whereas in the absence of DA there was no apparent oligomerization of ASN. The sizes of the DA-induced ASN oligomers were consistent with aggregates of ASN into dimers, trimers, and higher molecular weight species. There was a clear reduction in the monomeric band of ASN with concomitant increase in the intensity of the oligomeric species (**Figure 46 a**). To determine if there is a synergistic effect of H₂O₂ and DA on ASN aggregation, a mixtue of H₂O₂ (300 μ M), DA (200 μ M) and ASN (17.5 μ M) was incubated for 72 hrs. There was a clear increase in oligomerization of ASN was

observed, as judged by the intensity of the silver-stained bands (**Figure 47b**) which indicated time dependent, synergistic effect of H₂O₂ with DA on ASN aggregation.

DA and DA+ H₂O₂ -induced ASN oligomers are non sensitive to ThT:

ASN forms amyloid fibrils in vitro, and the kinetics of the fibrillar formation can be monitored using ThT fluorescence. Aggregation of ASN (17.5 μM) in the presence of DA and DA+ H₂O₂, displayed no significant increase in ThT fluorescence even after 72 hrs incubation (**Figure 46b**). This indicated that the DA and DA+ H₂O₂ mediated ASN oligomers are not amyloidogenic and is consistent with the SDS-PAGE profiles (**Figure 47b**).

Generation of iron-induced, SDS-sensitive ASN fibrils:

There are literature evidences that altered metal homeostasis lead to the loss of dopaminergic neurons in the SN region of brain. In this regards iron is the central point of attention because it is the most abundant metal of the body and it has been found that total nigral iron level is increased in PD brain compared to the controls. Metals especially iron can lead to the fibrilization of ASN either via the release of long-range interaction between N- and C- terminus region of ASN or metals like iron can lead to generate hydroxyl radicals by Fenton reaction which can further cause oxidation of α-synuclein known as metal catalyzed oxidation (MCO).³⁶ Interestingly, phosphorylation at Tyr125 or at Ser129 can increase trivalent metal binding to the C-terminus of ASN.

Fe³⁺ can induce the fibrilization of ASN into ThT positive species³⁶. ASN (17.5 μM) was incubated with 17.5 μM of Fe³⁺ for 6 days and the reaction was then analyzed by silver staining and ThT assay (**Figure 46 c**). ASN in presence of iron (Fe³⁺) displayed rapid rate of fibrillaziation, sixteen fold faster compared with ASN alone

while amyloidogenic fibrils were SDS sensitive as shown by the intensity of the silver-stained bands (**Figure 47 c**).

4.8.2. Assessment of potential lead compounds and comparison with reference compounds for their ability to modify ASN aggregation in cell-free system:

In the last decade small organic molecules, specifically polyphenols have been extensively tested for their ability to inhibit ASN aggregation. Overall the potency (inhibition and disaggregation) of compounds could be correlated to the number of hydroxyl groups present on single phenyl group, and it was observed that potency follows this order trihydroxyl > dihydroxyl > monohydroxyl compounds ¹⁶³.

It has been shown that rifampicin (Rif.) and its analog, p-benzoquinone, inhibited A β -42 aggregation and neurotoxicity *in-vitro*. Based on these observations and naphthoquinone core in the structure of rifampicin, Li et al., has shown that rifampicin can inhibit and disaggregate α -SN fibrillation in a dose dependent manner. In anaerobic condition as well in presence of antioxidant, the inhibitory effect of rifampicin reduced significantly which indicates the oxidized quinone form is majorly responsible for its activity.

The first aim of our ASN project was to evaluate the inhibitory potency of *in vivo* active anti-Parkinsonian lead molecules towards the oligomerization of ASN induced in presence of DA and compare with reference compound rifampicin and ascorbic acid in a cell free system. To investigate the influence of D-520, ascorbic acid (AA), rifampicin on ASN aggregation in presence of DA, we incubated either ASN (17.5 μ M) + DA (200 μ M) alone or in the presence of rifampicin /Ascorbic Acid/D-520 each 400 μ M for 10 days. The aggregation process was monitored using SDS-PAGE analysis and ThT assay. As shown in figure **47d-f** after 10 days of incubation, DA

enhanced aggregation of ASN in time dependent manner and similar results were observed with rifampicin, while, ascorbic acid and D-520 abolished ASN oligomer formation as judged by the intensity of the silver-stained bands. Overall, in this assay, D-520 turned out to be the most potent as the intensity of monomeric band of ASN did not change much over the time compared to ASN+DA alone or ASN+DA+Rifampicin/ Ascorbic Acid.

The ThT results were confirmed by TEM, We used samples from 4th day of experiment to evaluate physical characteristics of aggregates. As shown in **figure 48 a**, α -synuclein monomers appeared as a small spherical homogeneous structures, whereas, dopamine incubated α -synuclein appeared as a protofibrillar heterogeneous structure **figure 48 b**. While in the presence of ascorbic acid spherical aggregates were predominantly observed (figure 48 c). Analysis of the sample incubated in presence of DA and rifampicin by TEM revealed somewhat distinct shaped aggregates of α -synuclein, which were morphologically different compared to α -synuclein monomer (figure 48 d), similarly ASN+DA in presence of D-520 showed and gave rise to heterogeneous aggregates of α -synuclein ranging from apparent monomers to aggregates of higher dimensions but smaller than protofibrils (figure 48 e). There are several mechanisms by which these D-520 could inhibit ASN aggregation:

- 1) its ability to stabilize the native monomeric state of protein,
- 2) target different intermediates on the amyloid process and,
- 3) covalently bind with ASN and alter the aggregation potential.

4.8.3. Generation of α -synuclein aggregates to assess extracellular toxicity in cell-culture models:

ASN aggregates were generated with a primary goal to evaluate the effect of various extracellular ASN species on cell viability in PC12 cells. In this experiment, ASN aggregates were formed by two different methods, either to yield β -sheet positive fibrillar structure or to yield β -sheet negative dopamine-induced and co-valently modified oligomeric structure of ASN.

4.8.3.1. Generation of ASN fibrils and ASN oligomers co-valently modified with dopamine:

ASN fibrilization is a concentration-dependent process and it occurs readily under agitation condition with high concentration of protein. We evaluated the fibrilization of ASN under agitation condition in the range of 17.5-120 μ M, and 60 μ M was selected as optimal concentration to assess the ability of compounds to modulate aggregation. Initially, ASN aggregates were generated with primary goal to evaluate the effect of various extracellular ASN species on cellular viability assay in PC12 cells. In this experiment, ASN aggregates were formed by two different methods, either to yield β -sheet positive fibrillar structure or β -sheet negative dopamine-induced and co-valently modified oligomeric structure of ASN. In order to achieve this, we incubated ASN (60 μ M) and ASN (60 μ M) +DA (90 μ M) with mechanical agitation for 10 days and the time course of fibrilization process of ASN alone and ASN+DA were monitored by ThT assay. **Figure 46 d** displays the inhibition of ASN fibrilization by dopamine compared to ASN alone. DA completely destroys ASN fibrilization of ASN at a molar ratio of 1:1.5.

4.8.3.1.1. Evaluation of cytotoxicity of extracellular ASN aggregates (pre-formed) in cell-culture system:

Aliquots obtained from experiments mentioned above were used to evaluate the effect of (pre-formed) various species generated from ASN aggregation experiments on PC12 cell viability (extracellular toxicity). The main objective of this experiment was to optimize the time-point and the aggregation environment that would induce desired cytotoxicity (in ideal conditions, ~50% cell death). For cell-culture experiments, 40 μL aliquots (60 μM ASN) from various time-points were diluted with 200 μL PC12 cell media to make the final concentration of ASN 10 μM in the cell culture experiments. **Figure 50** shows the percentage of MTT reduction in cell culture vs. incubation time. The ASN alone (60 μM) has significant impact on cell viability and was comparable to ASN+DA. However, DA inhibited ASN fibrilization, the MTT experiment suggests that DA-modified has significant cytotoxicity which was comparable to ASN alone (**Figure 50**). It seems that 6 day incubated ASN alone (60 μM) is more toxic to the cells than fresh or samples after incubated for 8-10 days. ASN alone (60 μM) was able to induce around ~ 40% cell death after shaking for 6 days. Therefore, we assessed the ability of some of our lead compound D-520 and a standard drug (rifampicin) to alter cytotoxicity induced by ASN (60 μM) after shaking for 6 days.

4.8.3.1.2. Assessment of lead compounds and standard drug's ability to alter cytotoxicity induced by extracellular α -synuclein:

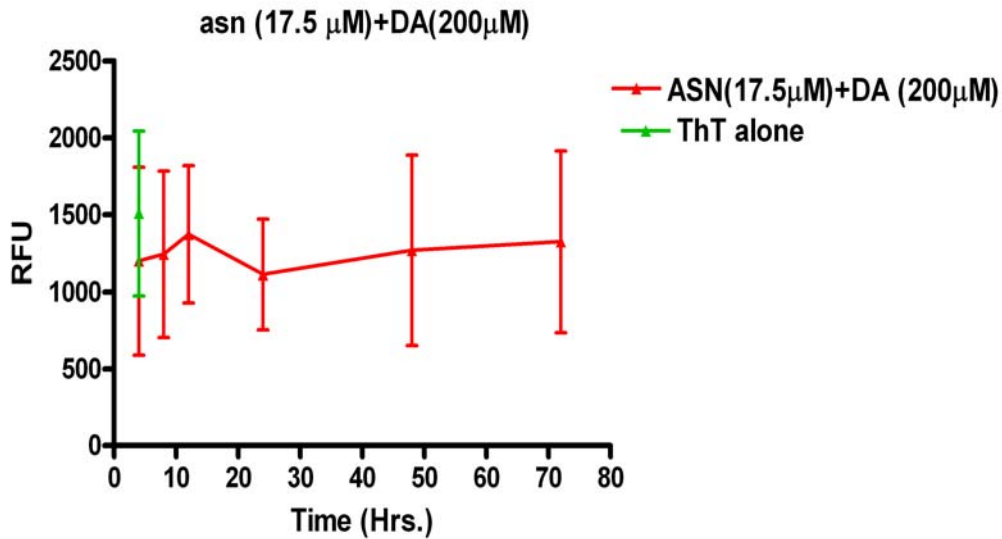
To investigate the influence of our *in vivo* active anti-parkinsonian compound D-520, and the reference drug rifampicin, we monitored the fibrilization of ASN (60 μM) in the absence and presence of D-520 (**120 μM**) using ThT, TEM and MTT assay.

Rifampicin was selected as a reference drug and was tested under the same experimental conditions.

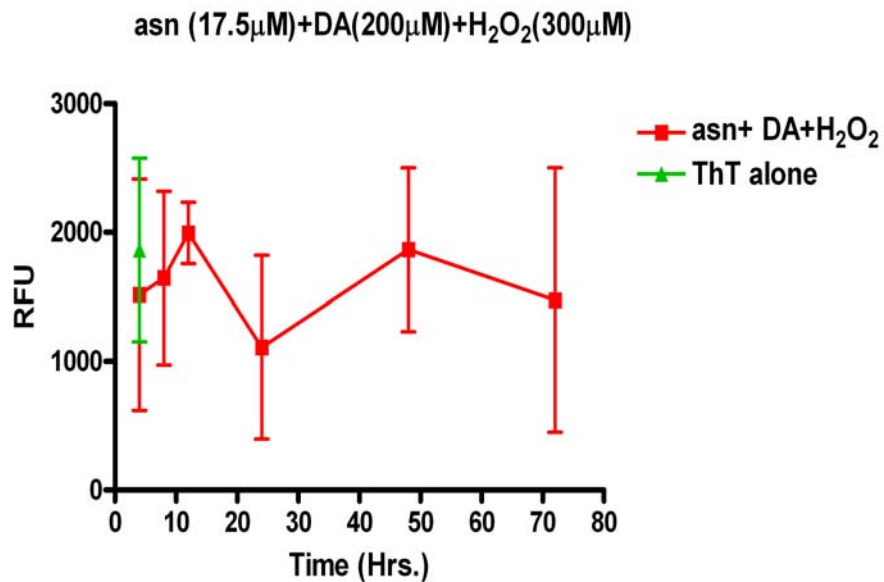
First, the effect of D-520 and rifampicin on ASN fibril formation was analyzed. Solution of ASN monomer was incubated for 6 days at 37°C and samples were collected at 0 day and 6 days. Both D-520 and rifampicin inhibited ThT fluorescence of ASN aggregates to a significant extent (**Figure 46e**). The ThT results were confirmed by TEM, which demonstrated the absence of significant amount of fibril in ASN samples with either D-520/ rifampicin. The control samples (ASN 60 μM) at day 6 showed abundant fibril, helically twisted to each other with varying degree of lateral association and these are complementary to ThT data. ASN in presence of DA showed few fibril structures. In contrast, D-520 showed distinct morphology of small broken fibril (**figure 49D**). The ASN incubated in presence of rifampicin displayed amorphous and annular aggregates with few detectable fibril structures (**figure 49C**).

Next, we quantified the effect of ThT negative spherical aggregates formed in the presence of D-520 and rifampicin on the metabolic activity (?) of PC-12 cells. In order to achieve this we used a mixture of ASN that was incubated in the presence and/or absence of compounds for 0 day and 6 days at 37°C under agitation condition. 40 μL aliquots of ASN/ compound mixture were then diluted with 200μL PC12 cell media to make the final concentration of ASN 10μM for cell culture experiments. The treatment with preaggregated ASN showed a reduction of cell viability by ~ 40% (**figure 51**). Interestingly, earlier time point (0 time) ASN samples which were incubated with D-520 a significant reduction of cell viability, however, later time point (6 day) sample showed a significant increase of cell viability of 40%

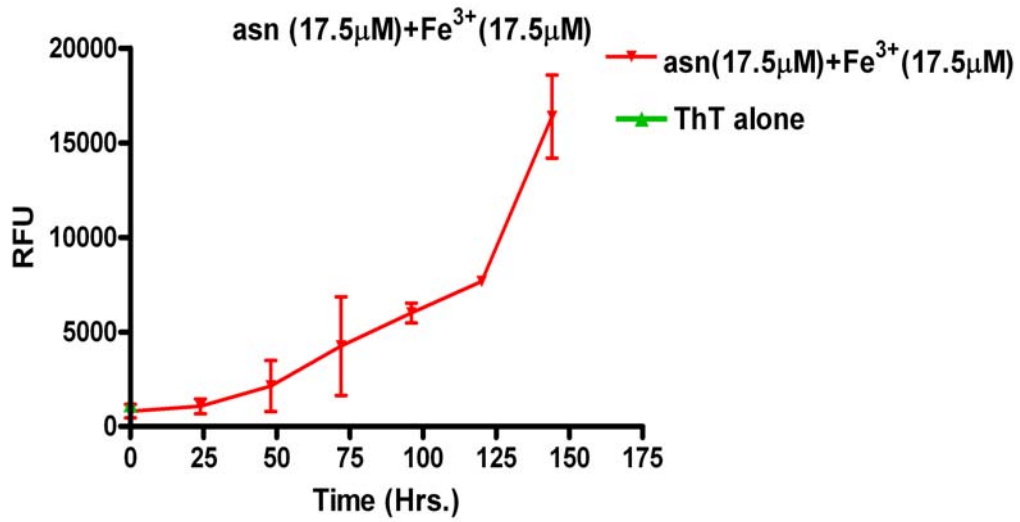
and almost approached to control level. While, the standard drug rifampicin was not able to show significant neurprrotection at higher time point (**figure 51**).



a) ASN (17.5 μ M)+ DA(200 μ M)

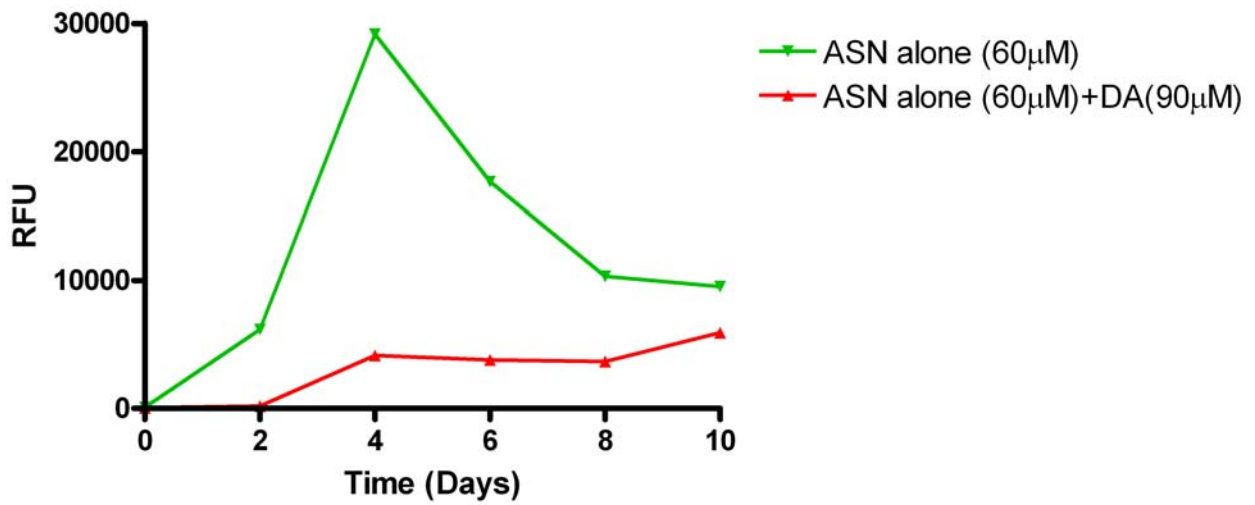


b) ASN (17.5 μ M)+ DA (200 μ M)+H₂O₂((300 μ M)

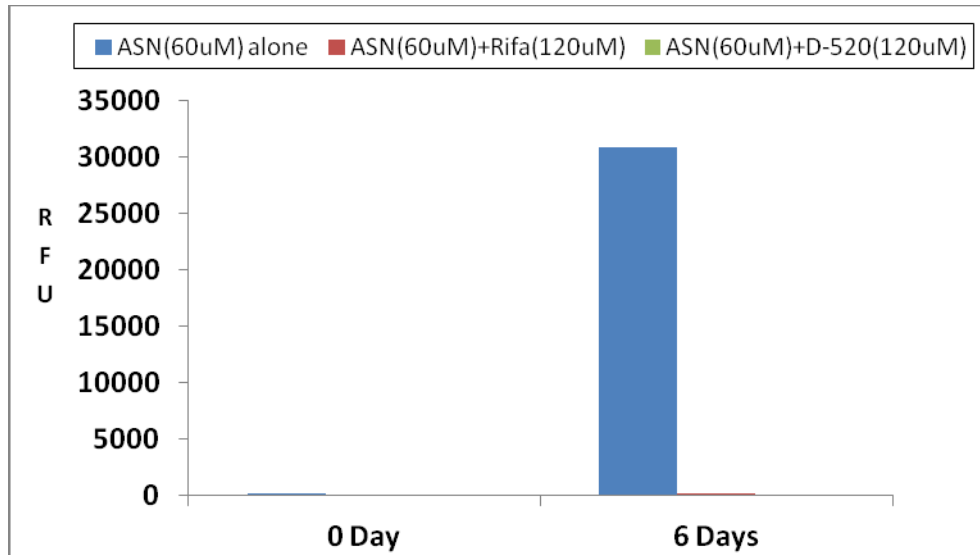


c) ASN (17.5 μ M)+ Fe³⁺(17.5 μ M)

ASN (60 μ M) alone and ASN(60 μ M)+DA(90 μ M)



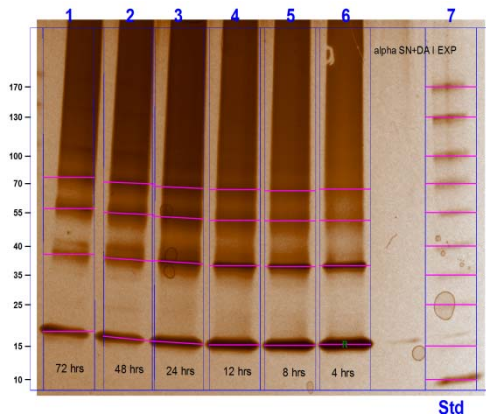
d) ASN (60 μ M) and ASN (60 μ M)+ DA(90 μ M)



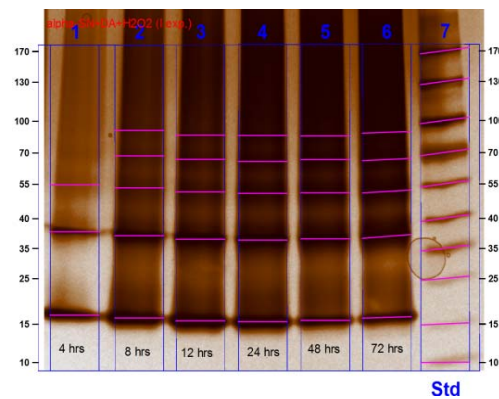
e) ASN (60 μ M) and ASN (60 μ M)+ Drugs(90 μ M)

Figure 46. Thioflavin T assay (Monitoring ASN aggregation) ASN fibrillization observed under different conditions. **a, b)** Over 3 days, ASN (17.5 μ M) was incubated in the presence of 200 μ M DA, and DA (200 μ M)+300 μ M H₂O₂ for 72 h at 37°C, shaking at 1400 rpm. Fibril formation was monitored by an increase in ThT fluorescence at 444 and 485 nm. ASN did not show a significant increase in fluorescence compared with ThT alone, suggesting little or no fibril formation. **c)** ASN (17.5 μ M) was incubated with 17.5 μ M Fe (III) citrate over 6 days at 37°C, shaking at 1400 rpm. Fibril formation was monitored by an increase in ThT fluorescence at 444 and 485 nm, ASN incubated with Fe (III) citrate showed a significant increase in ThT fluorescence, compared ThT alone. **d)** ASN (60 μ M) alone and ASN (60 μ M)+DA (90 μ M) was incubated for 10 days at 37°C, shaking at 1400 rpm. Fibril formation was monitored by an increase in ThT fluorescence at 444 and 485 nm. ASN alone showed a significant increase in ThT fluorescence compared ThT alone while ASN +DA did not show a significant increase in fluorescence compared with ThT alone.

e) ASN (60 μM) alone and ASN (60 μM)+D520/Rifampicin (120 μM) was incubated for 10 days at 37°C, shaking at 1400 rpm. Fibril formation was monitored by an increase in ThT fluorescence at 444 and 485 nm. ASN alone showed a significant increase in ThT fluorescence compared ThT alone while ASN +D-520/Rifampicin did not show a significant increase in fluorescence compared with ThT alone.

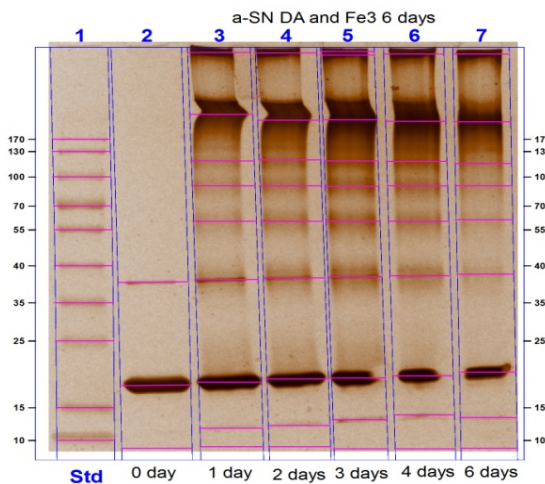


a. ASN (17.5 μM)+ DA(200 μM)

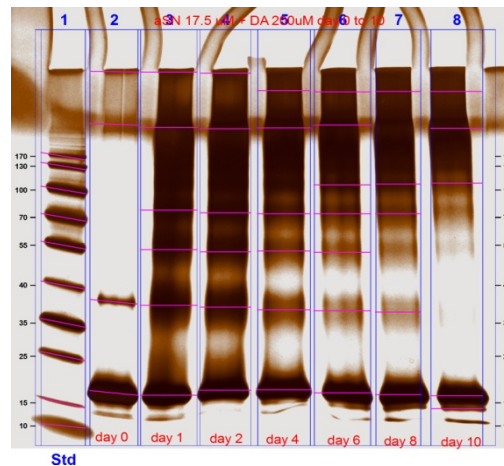


b. ASN (17.5 μM)+ DA

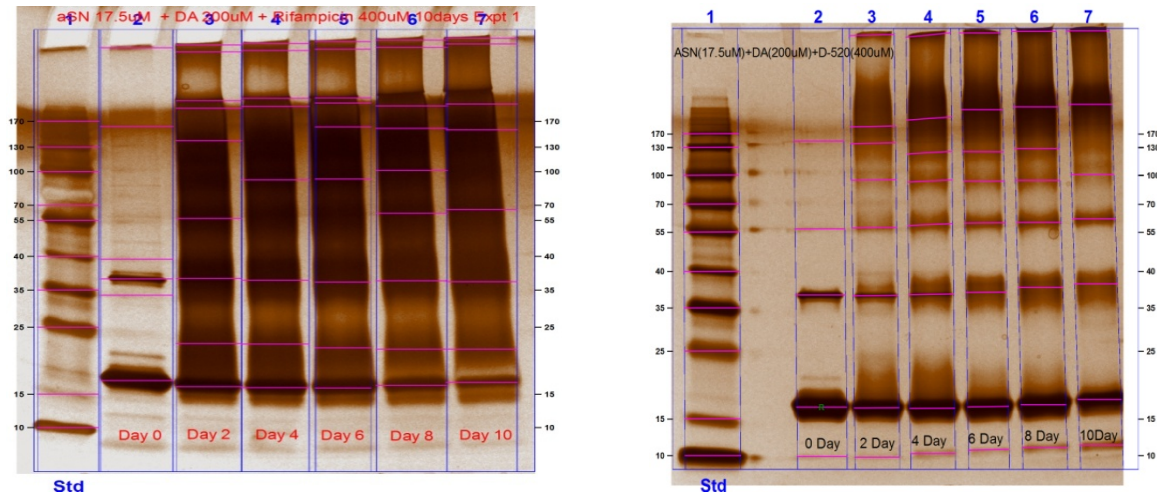
(200 μM)+H₂O₂((300 μM))



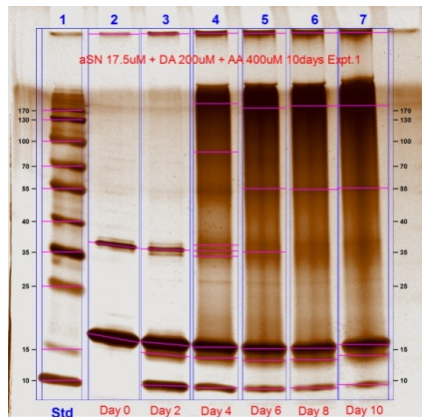
c. ASN (17.5 μM)+ Fe³⁺(17.5 μM)



d. ASN (17.5 μM)+ DA (200 μM)



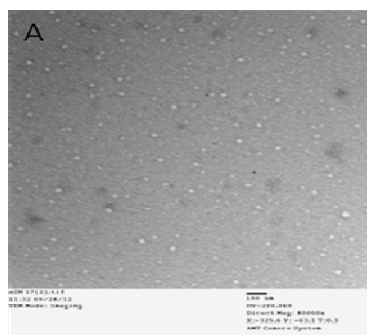
e. ASN(17.5 μ M)+DA(200 μ M)+Rifa.(400 μ M) f. ASN(17.5 μ M)+DA(200 μ M)+D-520(400 μ M)



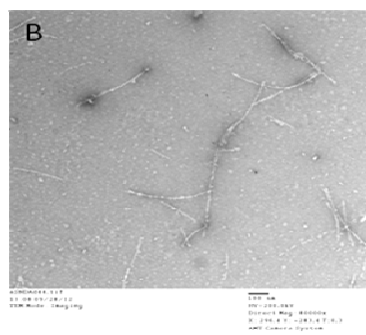
g. ASN(17.5 μ M)+DA(200 μ M)+AA(400 μ M)

Figure 47. ASN oligomerization in the presence of DA, DA+ H₂O₂ and DA+Various Drugs. **a)** Time-dependent ASN oligomerization in presence of DA. ASN (17.5 μ M) was incubated for 72 hrs with 200 μ M of DA concentrations at 37°C, shaking at 1400 rpm. Samples were analyzed on a 12% SDS gel and visualized with silver staining. ASN formed oligomers with 200 μ M DA after a short incubation period. **b)** Time dependent DA + H₂O₂ mediated ASN oligomerization. ASN (17.5 μ M) was incubated with 200 μ M DA+300 μ M H₂O₂ at 37°C, shaking at 1400 rpm. Aliquots were taken at 4, 8, 12, 24, 48, and 72 frozen at -20°C. Samples were analyzed on 12% SDS-

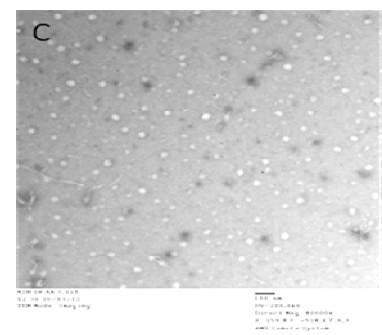
PAGE and visualized with silver staining. ASN with DA + H₂O₂ had the fastest rate of oligomerization. **c)** Time dependent DA + Fe³⁺ mediated ASN oligomerization. ASN (17.5 μM) was incubated with 17.5 μM Fe³⁺ at 37°C, shaking at 1400 rpm. Aliquots were taken at 0, 1, 2, 4, and 6 day 72 frozen at -20°C. Samples were analyzed on 12% SDS-PAGE and visualized with silver staining. **d,e,f,g)** Time dependent DA and DA+Drugs (Rifampicin, D-520, Ascorbic Acid) mediated ASN oligomerization. ASN (17.5 μM) was incubated with 200 μM DA and DA (200 μM)+ 400 μM Drugs (Rifampicin, D-520, Ascorbic Acid) at 37°C, shaking at 1400 rpm. Aliquots were taken at 0, 2, 4, 6, 8, 10 days and frozen at -20°C. Samples were analyzed on 12% SDS-PAGE and visualized with silver staining. ASN with DA and ASN+DA+Rifampicin had the fastest rate of oligomerization. The rate of α-SN oligomerization was intermediate when 400 μM AA was used and it reduced significantly in case of ASN+DA+D-520.



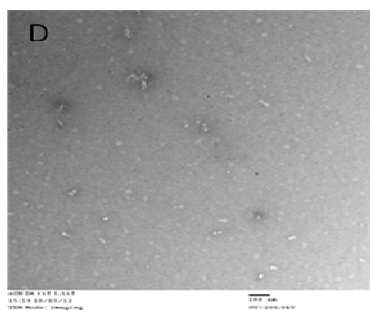
aSN Day0



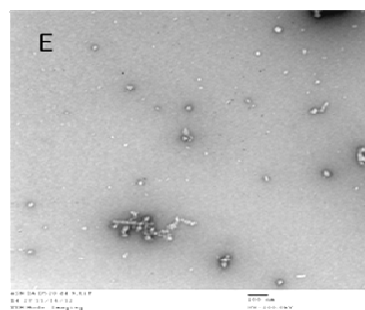
aSN DA Day4



aSN DA AA Day4

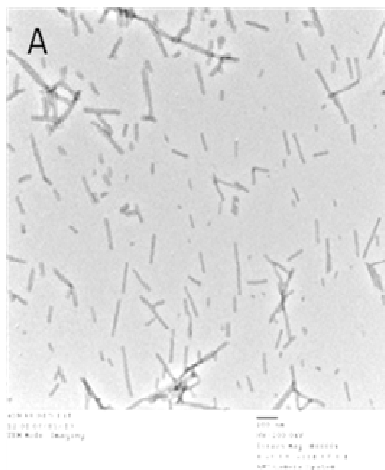


aSN DA Rif Day4

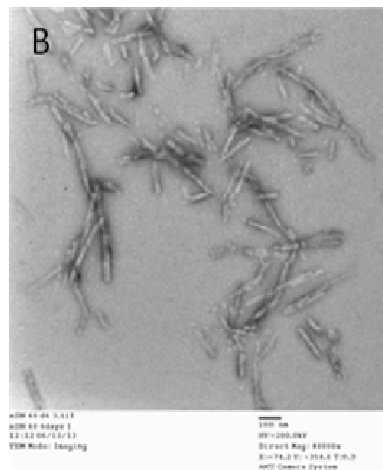


aSN DA D520 Day4

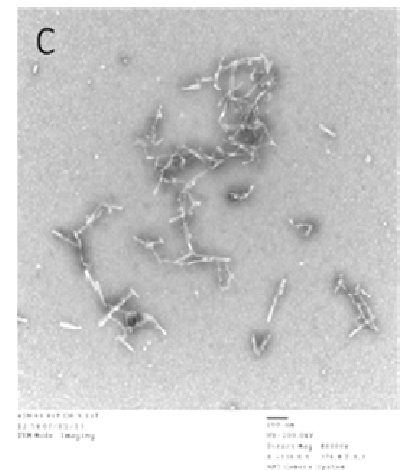
Figure 48: Electron microscopic images (TEM) of α -SN aggregates. α -SN (17.5 μ M) was incubated either alone (**A**) or with 200 μ M DA (**B**) or with 200 μ M DA and 400 μ M AA (**C**) or with 200 μ M DA and 400 μ M Rifampicin (Rif.) (**D**), or with 200 μ M DA and 400 μ M D-520 (**E**), at 37°C, with shaking at 1400 rpm over 10 days.



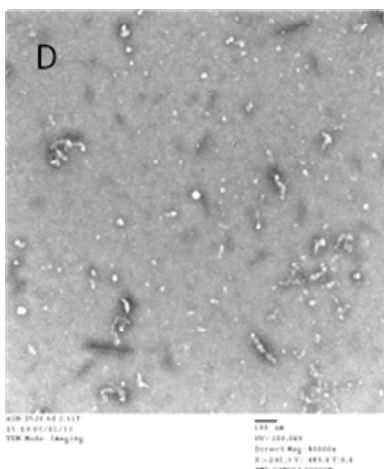
aSN 60uM Day0



aSN 60uM Day6



aSN 60uM Rifampicin 120uM Day6



aSN 60uM D520 120uM Day6

Figure 49: Electron microscopic images (TEM) of α -SN aggregates. α -SN (60 μ M) 0 day (**A**) was incubated either alone (**B**) or with 120 μ M Rifampicin (**C**) or 120 μ M D-520 (**D**), at 37°C, with shaking at 1400 rpm over 10 days.

Effect of aSN 60 μ M or aSN 60 μ M and DA 90 μ M on cell-viability (MTT assay)

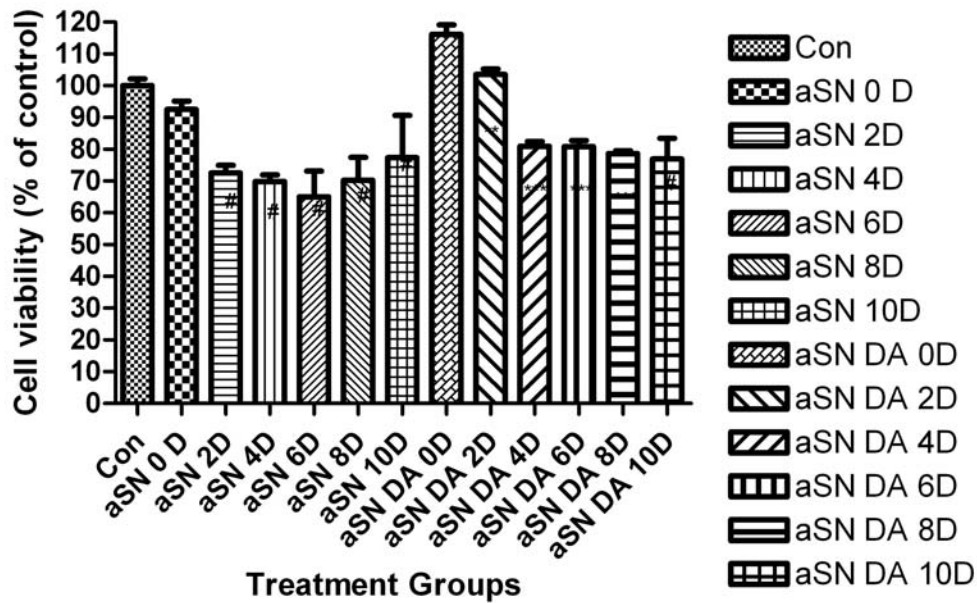


Figure 50. Time dependent cytotoxic effect of asn alone or asn +DA in PC12 cells. PC12 cells were treated with pre-incubated asn (60 μ M) alone or co-incubated with 120 μ M dopamine (DA). The cellular viability was evaluated by MTT assay, and the data were expressed as percentage of the control (non treated cells). The control treatment is set to 100%.

Effect of drugs on extracellular asn-induced cell death in PC12 cells

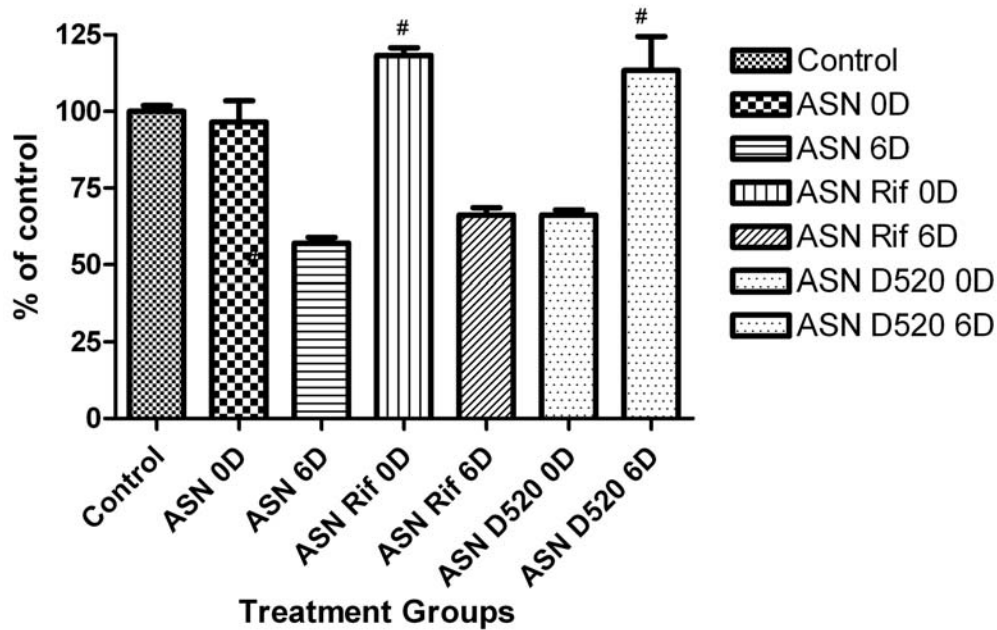


Figure 51. Cytoprotective effect of the compounds against asn induced toxicity in PC12 cells. PC12 cells were treated with pre-incubated asn (60 μ M) alone or co-incubated with 120 μ M rifampicin (Rif) or D-520. The cellular viability was evaluated by MTT assay, and the data were expressed as percentage of the control (non treated cells). The control treatment is set to 100%.

Table 6. Summary of ASN experiments in cell free and with PC-12 cells

Exp. No.	Type of Experiment	Experimental Condition (Conc. of ASN, Days, Sample collection time points)	Silver Staining	ThT Data
1.	ASN+ DA	17.5 μ MASN+200 μ MDA; 3days;	Over the time	No ThT

		4, 8, 12, 24, 48 and 72 hrs.	monomer decreases and oligomeric species increase	signal compared to ThT alone
2.	ASN+ DA+ H ₂ O ₂	17.5μM ASN+200 μMDA+300 μM H ₂ O ₂ ; 3days; 4, 8, 12, 24, 48 and 72 hrs.	Over the time increased oligomer species observed compared to ASN+ DA alone.	No ThT signal compared to ThT alone
3.	ASN+ Fe ³⁺	17.5μM ASN+17.5 μM Ferric Chloride; 6days; 0, 24, 48, 72, 96, and 144 hrs.	Iron induced aggregates fall apart in SDS gel.	From Third day ThT Signal enhanced compared to ThT

				alone
4.	ASN+DA and ASN+DA+ Drug (D-520, AA, Rifa.)	17.5μM ASN+200 μMDA and 17.5μM ASN+200 μMDA+400 μM Drugs (D-520, AA, Rifa.); 10 days; 0, 2, 4, 6, 8, and 10 day.	In ASN+ DA Over the time increased in oligomer species while oligomer species decreased with ASN+ DA +Drugs treatment	No ThT signal compared to ThT alone
5.	ASN alone (Cell Culture Exp.)	60μM ASN; 10 days; 0, 2, 4, 6, 8 and 10 day.	For Cell culture. No gel was run.	From Second day ThT Signal enhanced compared to ThT alone
6.	ASN+DA (Cell Culture Exp.)	60μM ASN+120 μM DA; 10 days; 0, 2, 4, 6, 8 and 10 day.	For Cell culture. No gel was run.	No ThT signal compared

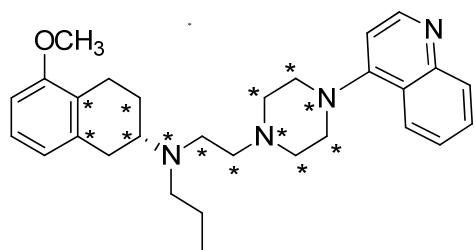
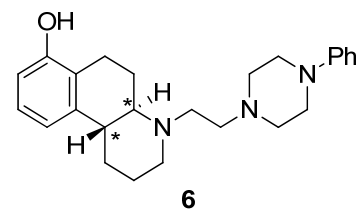
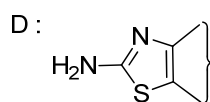
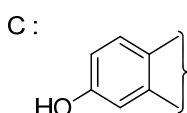
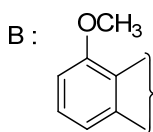
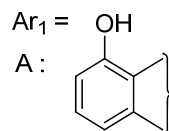
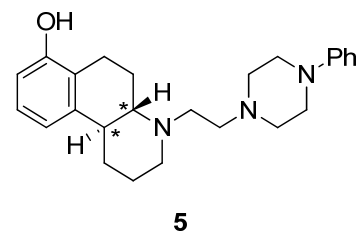
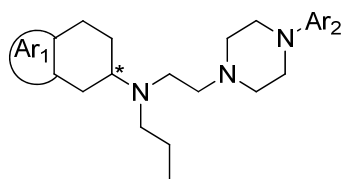
				to ThT alone
7.	ASN+Drugs (Rifa. or D-520), (Cell Culture Exp.)	60µM ASN+ 120 µM Rifa. or D-520; 10 days; 0, 2, 4, 6 ,8 and 10 day.	For Cell culture. No gel was run.	No ThT signal compared to ThT alone

CHAPTER 5

Molecular Modeling Studies

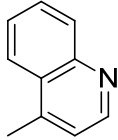
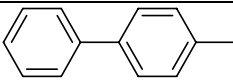
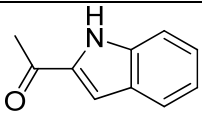
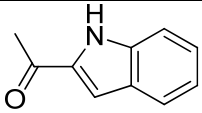
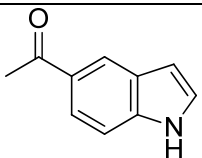
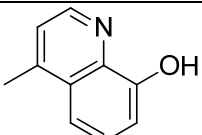
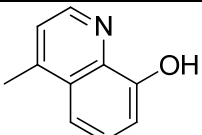
The design and development of the DA D2/D3 agonists using the hybrid approach involved combination of an agonist moiety (e. g., aminothiazole, aminotetraline or bioisosteric equivalent) with (un)substituted arylpiperazine substructure via a suitable linker. Initial SAR studies around the early lead structures focused mainly on the optimization of the linker length and the arylpiperazine moiety. Several conformationally flexible and rigid molecules were synthesized and tested. Once the linker length and possible arylpiperazine moieties were identified, the agonist part of the molecule was varied. These extensive efforts led to structurally diverse, novel molecules. In the present study, a data set of 45 such structurally diverse molecules (**Table 7**) was used to derive the 3D QSAR models. The position of the –OH group on the aminotetraline head group, presence of –C=O group and the absolute configuration (*R* or *S*) of these molecules posed obvious problems for the alignment. Two different alignment methods, atom-based and flexible were tried. Thus, D2 and D3 potency models were built using both alignments rules and compound **4**, the most active analog for both the D2 and D3 receptors, as a template for alignment. Similarly, D2/D3 selectivity models were constructed using the two alignment types but with compound **42**, the most selective analog, as the template. As expected, the flexible alignment provided better superimposition of the data set onto the templates. The representative alignments obtained from the atom-based and flexible modes are shown in **Figure 52**.

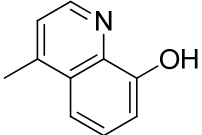
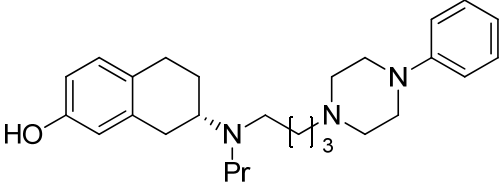
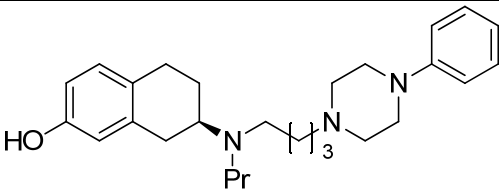
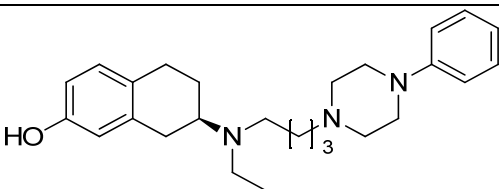
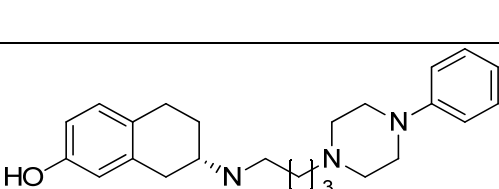
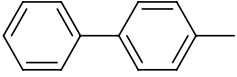
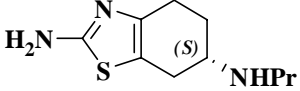
Table 7. Molecular structures, binding potencies (D2 and D3) and the selectivity (D2/D3) of the ligands used in 3D QSAR studies

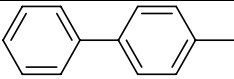
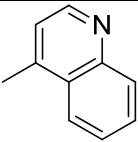
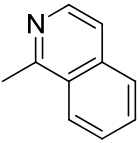
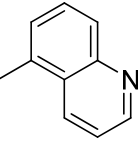
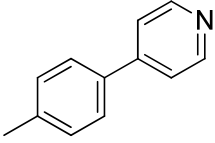
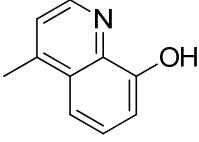
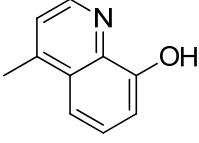
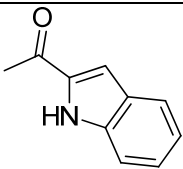
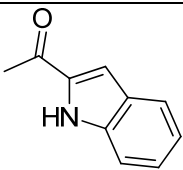


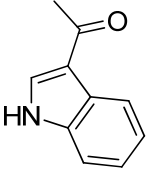
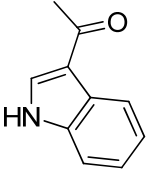
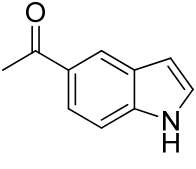
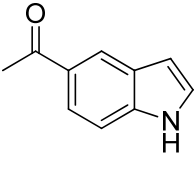
The points indicated by asterisk (*) were used for atom based alignment.

Compound No.	Ar ₁	Ar ₂	Stereoc hemistry	K _i (nM)		D2L/D3
				D2L [³ H]spiperone	D3 [³ H]spiperone	
1^a				220 ± 37.7	4.73 ± 0.64	46.5
2^e	A	Ph	R	238 ± 14	18.4 ± 1.0	12.93
3^e	A	Ph	S	26.0 ± 7.5	0.82 ± 0.13	31.5

4^c	B		S	3.74 ± 0.70	0.19 ± 0.03	19.68
5^a				23.6 ± 1.1	4.95 ± 1.1	4.8
6^a				835 ± 182	89.3 ± 19.4	9.4
7^d	A		S	53.6 ± 12.3	2.36 ± 0.87	22.7
8^e	A	2'-OMePh	R	88.7 ± 3.1	18.8 ± 4.2	4.7
9^e	A	2'-OMePh	S	9.56 ± 2.29	0.46 ± 0.12	20.9
10^d	A	1'-(4'-(4''-pyridyl)phenyl)	S	13.2 ± 1.3	1.53 ± 0.18	8.6
11^d	C	1'-(4'-(4''-pyridyl)phenyl)	S	399 ± 16	16.2 ± 1.8	24.6
12^b	A		R	113 ± 21	3.73 ± 0.56	30.2
13^b	A		S	47.5 ± 6.2	0.57 ± 0.094	83
14^b	A		S	157 ± 35	2.27 ± 0.52	69.2
15^f	A		S	3.75 ± 0.63	1.28 ± 0.08	2.9
16^f	A		R	20.7 ± 1.5	7.73 ± 0.64	2.67
17^a	C	Ph	S	809 ± 65	38.6 ± 0.7	20.9
18^b	C	Ph	R	40.6 ± 3.6	1.77 ± 0.42	22.93

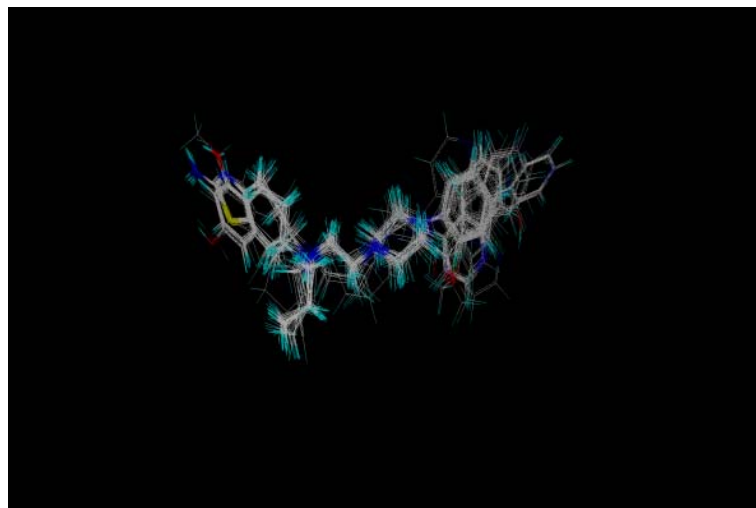
19^f	C		R	4.55 ± 0.59	1.27 ± 0.15	3.58
20^e			S	19.4 ± 1.3	1.22 ± 0.37	15.9
21^e			R	19.3 ± 1.5	0.74 ± 0.069	25.8
22^e			R	32.9 ± 8.6	0.76 ± 0.079	43.2
23^e			S	25.2 ± 7.3	0.35 ± 0.03	71.0
24^d	C		R	58.0 ± 14.7	2.79 ± 0.73	20.8
25^d	C	1'-(4'-(4''-pyridyl)phenyl)	R	24.7 ± 5.8	0.78 ± 0.22	32.0
26^j				6740 ± 510	11.7 ± 2.5	576.1
27^g	D	Ph	S	243 ± 65	4.15 ± 0.76	58.6
28^g	D	Ph	R	1979 ± 567	44.0 ± 10.6	45.0
29^g	D	2'-OMePh	S	288 ± 86	7.01 ± 1.16	41.1

30^g	D	2'-OMePh	R	243 ± 47	101 ± 41	2.40
31^g	D	2',3'-Cl ₂ Ph	S	56.8 ± 15.4	1.80 ± 0.32	31.6
32^g	D	2',3'-Cl ₂ Ph	R	44.2 ± 6.9	12 ± 2.9	3.68
33^g	D		S	264 ± 40	0.92 ± 0.23	253
34^c	D		S	109 ± 14	2.61 ± 0.18	41.8
35^c	D		S	269 ± 16	2.23 ± 0.60	121
36^c	D		S	57.7 ± 3.3	1.21 ± 0.16	47.7
37^c	D		S	270 ± 28	4.78 ± 0.89	56.5
38^h	D		S	27.1 ± 5.0	4.98 ± 0.78	5.4
39^h	D		R	190 ± 29	13.2 ± 2.3	14.5
40ⁱ	D		R	2558 ± 112	54.1 ± 4.2	47.3
41ⁱ	D		S	1073 ± 92	1.84 ± 0.51	583

42ⁱ	D		S	902 ± 130	1.09 ± 0.14	828
43ⁱ	D		R	1316 ± 244	48.2 ± 8.6	27.3
44ⁱ	D		R	2626 ± 229	52.8 ± 8.3	49.7
45ⁱ	D		S	1031 ± 182	1.40 ± 0.29	736

^a Please see Ref. 151 (Dennis Brown, et al.); ^b Please see Ref. 148 (Dennis Brown, et al. 2009); ^c Please see ref. 146 (Ghosh, et al. 2010); ^d Please see ref. 147 (Ghosh, et al. 2010) ; ^e Please see ref. 150 (Biswas, et al. 2008)); ^f Please see ref. 145 (Ghosh, et al. 2010)); ^g Please see ref. 149 (Biswas, et al. 2008) ; ^h Please see ref. 143 (Gogoi, et al. 2011) ; ⁱ Please see ref. 141 (Johnson, et al. 2011)

a)



b)

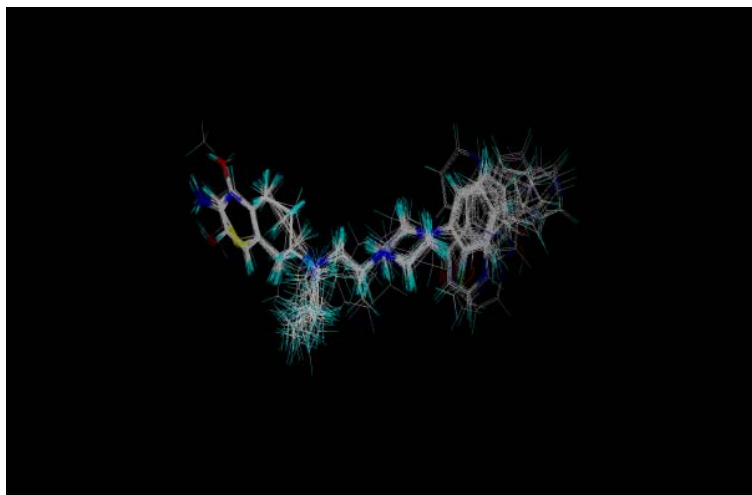


Figure 52. a) Flexible and b) Atom-based alignments of the dataset molecules onto compound **4** (template)

5.1. CoMFA analysis: D2 and D3 receptor binding affinity:

With the help of carefully selected training sets of 37 molecules comprising of enantiomers, statistically significant CoMFA models were obtained. The results of CoMFA analyses are summarized in **Table 10**. Since the experimental activity varied significantly for D2, D3 and selectivity (D2/D3), different training and test set were used for all three cases. The resulting models showed poor internal predictive ability ($r_{cv}^2 < 0.3$) (data not shown). Careful examination of the residuals from the non-cross-validated PLS analysis of the models using all compounds as training set led to identification of the compounds **6**, **11** and **17** as common outliers for both D2 and D3 models. Systematic removal of these outliers from the data set resulted in improved statistics. The 3D QSAR model is considered statistically significant if r_{cv}^2 is greater than 0.3, although a value greater than 0.4 is normally desirable¹⁶⁴. For DA D2 binding affinity, both alignments resulted in models comparable in terms of relevant statistical parameters.

For D2, the best CoMFA model was based on flexible alignment with AM1 charges (Model d) with r^2_{cv} of 0.713 (4 components), conventional r^2 of 0.920 and standard error of estimate (SEE) of 0.234. This model also showed excellent predictive capability with r^2_{pred} of 0.926. Interestingly, for DA D3 receptor binding affinity, the best CoMFA model was based on flexible alignment with Gasteiger –Hückel charges (Model e) with the r^2_{cv} of 0.453 (5 components), r^2_{conv} of 0.941, SEE of 0.169 and r^2_{pred} of 0.710. In comparison, the CoMFA models generated using the atom-based alignment exhibited poor external predictions (Model b, **Table 10**). The experimental and fitted/predicted pK_i values for the training and test sets of the best D2 and D3 CoMFA models (Models d and e, respectively) are given in **Table 8**. The plots of fitted versus experimental activity values for the training set molecules and predicted versus experimental values for the test set molecules for the D2 CoMFA model d are shown in **Figures 53a** and **53c**, respectively. The corresponding CoMFA predicted plots for D3 model e are shown in **Figure 53b** and **53d**, respectively. The steric field describes 41.5% and 63.6% of variance for DA D2 and D3 binding affinities, respectively (refer **Table 10**, Model d and e), while the corresponding contributions from the electrostatic field were found to be 58.5% and 36.4%, respectively.

The LOO cross-validation method might lead to high r^2_{cv} values which do not necessarily reflect a general predictability of the models. Therefore, cross-validation using 10 groups was performed for 10 times. In this method, a model based on about 80% of the variable data predicts each target property. The mean r^2_{cv} values of 0.731 and 0.472 for D2 and D3 binding affinities, respectively, reveal that the models have good internal predictivity and the results were not by chance. To further assess the robustness of the model, boot-strapping analysis (10 groups) was

performed and r_{bs}^2 of 0.950 and 0.963 (SD_{bs} = 0.016 and 0.014) was obtained for D2 and D3, respectively, which further establishes the robustness of the models.

5.2. CoMSIA analysis: D2 and D3 receptor binding affinity:

A total of five fields, steric, electrostatics, hydrophobic, hydrogen bond donor (HDon) and acceptor (HAcc), as implemented in CoMSIA, were used for the generation of the 3D QSAR models. Initial analyses were performed using individual fields as well as various combinations of different fields. The models developed using all the fields gave statistically robust results. It emphasized the importance of hydrophobic, HDon, and HAcc fields in addition to steric and electrostatic fields for D2/D3 binding affinity of the ligands. The summary of the CoMSIA analyses is given in **Table 11**. For D2 binding affinity, CoMSIA model generated using atom-based alignment and AM1 charges performed better (Model a, **Table 11**) with r_{cv}^2 of 0.719 (4 components), r_{conv}^2 of 0.912, SEE of 0.245 with r_{pred}^2 of 0.911 than the corresponding model using flexible alignment and Gasteiger-Hückel charges (Model d, **Table 11**). Similarly, for D3 binding affinity, the best model generated using flexible alignment and Gasteiger-Hückel charges (Model e, **Table 11**) gave r_{cv}^2 of 0.493 (6 components), r_{conv}^2 of 0.898, SEE of 0.227 with r_{pred}^2 of 0.465. Removal of compound **33** (outlier as seen from high residual) improved the value of r_{pred}^2 from 0.465 to 0.640. The outlier behavior of **33** in D3 CoMSIA models could not be reasoned. The experimental and fitted/predicted pK_i values for the training and test sets are given in **Table 8**. The plots of fitted versus experimental activity values for the training set molecules and predicted versus experimental values for the test set molecules for the D2 CoMSIA model a are shown in **Figures 54a** and **54c**, respectively. The corresponding CoMSIA predicted plots for D3 model e are shown in **Figure 54b** and **54d**, respectively.

The field contributions for 3D QSAR CoMSIA models are given in **Table 11**. For cross-validation using 10 groups, the mean r_{cv}^2 values of 0.726 and 0.456 were found for D2 and D3, respectively, while r_{bs}^2 of 0.951 ($SD_{bs}=0.013$) and 0.936 ($SD_{bs}=0.020$) were obtained for D2 and D3, respectively.

Compounds **6**, **11**, and **17** were found to be outliers in CoMFA and CoMSIA models for both D2 and D3 potency, therefore, not included in the analyses. The outlier behavior could be due to several factors. One of the possible reasons could be the structural properties, including stereochemistry, of these compounds. The outlier behavior of compound **6** could be due to its constrained structure along with *R* stereochemistry. For this series of hybrid molecules, it was observed that the compounds with 5-OH DPAT as agonist head group with *R* stereochemistry were less potent than their corresponding *S* isomers. However, it has been observed that compound containing 7-OH-DPAT as agonist head group with *S* stereochemistry due to reorientation loses the favorable interaction with the receptor.

5.3. CoMFA and CoMSIA analysis: selectivity for D3 over D2 receptors

In order to understand the structural features responsible for D3 selectivity, 3D QSAR models were generated using both, the atom-based and flexible alignments. The resulting models showed poor internal predictivity ($r_{cv}^2 < 0.3$) (data not shown). Various combinations of the training and test sets did not improve the statistics. As described previously, compounds showing high residuals were identified. Systemic removal of these outliers from the data set resulted in improvement of the statistics. The summary of the 3D QSAR models is shown in **Tables 10** (CoMFA) and **11** (CoMSIA). The best CoMFA model was obtained using flexible alignment and AM1 charges (model f, **Table 10**) while the best CoMSIA model was based on atom-based alignment and AM1 charges (model c, **Table 11**). The best CoMFA model for

selectivity (n=40) exhibited r^2_{cv} of 0.634 (5 components), r^2_{conv} of 0.958, and SEE of 0.145. This model also showed good external predictivity with r^2_{pred} of 0.864. In case of cross-validation using 10 groups, the mean r^2_{cv} value of 0.640 was found for selectivity model while r^2_{bs} of 0.984 ($SD_{bs}=0.009$) was obtained.

The best CoMSIA model for selectivity (n=39) showed r^2_{cv} of 0.797 (3 components), r^2_{conv} of 0.940, SEE of 0.161, and r^2_{pred} of 0.781. The mean r^2_{cv} value of 0.795 was found for cross-validation using 10 groups for the selectivity model while r^2_{bs} value of 0.955 ($SD_{bs}=0.016$) further confirmed the robustness of the model. The experimental and fitted/predicted pK_i values for the training and test sets are given in **Table 9**. The plots of fitted versus experimental activity values for the training set molecules and predicted versus experimental values for the test set molecules are given in Figures 55a, 55b and 55c, 55d, respectively.

Compounds **30**, **32**, **38**, **40**, **43** and **44** were found to be outliers and therefore, not included in the analyses. The reasons for this observation could be many-fold. Since the selectivity values represent affinity differences, the experimental uncertainty due to error propagation is likely to be higher. Other possible reason could be the structural properties, including stereochemistry, of these compounds. For these series of hybrid molecules, it was observed that the compounds with *R* stereochemistry were less potent than their corresponding *S* isomers. No suitable explanation could be provided for the higher residuals values for compound **38**.

Table 8. Experimental and fitted/predicted activities of D2/D3 ligands used as the training and test sets for CoMFA and CoMSIA analyses

Sr. No.	pK_i^a		
	Experimental	Fitted/Predicted	
		CoMFA	CoMSIA

	D2L	D3	D2L	Rsd ¹	D3	Rsd ²	D2L	Rsd ³	D3	Rsd ⁴
1 ^a	6.657	8.325	6.687	-0.037	8.261	0.064	6.470	0.180	8.49	-0.165
2 ^e	6.623	7.735	7.157	-0.534	7.987	-0.251	7.243	-0.625	7.742	-0.006
3 ^e	7.585	9.086	7.413	0.172	8.834	0.252	7.463	0.122	8.659	0.426
4 ^c	8.427	9.721	8.371	0.058	9.607	0.113	8.208	0.218	9.953	-0.231
5 ^a	7.627	8.305	7.492	0.134	8.205	0.100	7.705	-0.077	7.987	0.318
6 ^a	6.078	7.049	7.423	-1.344	9.167	-2.118	7.724	-1.645	9.430	-2.380
7 ^d	7.270	8.627	7.447	-0.176	8.809	-0.181	7.361	-0.090	8.703	-0.075
8 ^e	7.052	7.725	7.363	-0.311	8.093	-0.368	7.198	-0.145	8.113	-0.387
9 ^e	8.019	9.337	7.796	0.214	8.911	0.425	7.594	0.416	8.822	0.514
10 ^d	7.879	8.815	7.998	-0.119	8.935	-0.119	7.851	0.028	8.770	0.044
11 ^d	6.399	7.790	9.942	-3.542	9.134	-1.343	7.675	-1.276	9.494	-1.704
12 ^b	6.946	8.428	7.054	-0.108	8.304	0.124	6.923	0.022	8.361	0.066
13 ^b	7.323	9.244	7.109	0.214	9.174	0.069	7.089	0.233	9.194	0.050
14 ^b	6.804	8.643	6.936	-0.131	8.648	-0.005	6.685	0.118	8.769	-0.125
15 ^f	8.425	8.892	8.562	-0.136	9.07	-0.178	8.212	0.212	9.063	-0.170
16 ^f	7.684	8.111	8.204	-0.520	8.189	0.077	8.241	-0.558	8.092	0.091
17 ^a	6.092	7.413	7.432	-1.339	9.134	-1.721	7.679	-1.586	9.553	-2.139
18 ^b	7.391	8.752	7.188	0.202	8.504	0.248	7.391	0.000	8.73	0.022
19 ^f	8.341	8.896	8.061	0.280	8.899	-0.003	8.313	0.027	9.008	-0.112
20 ^e	7.712	8.913	7.834	-0.121	9.114	-0.183	7.593	0.119	9.146	-0.215
21 ^e	7.714	9.130	7.546	0.168	9.345	-0.215	7.576	0.138	8.968	0.162
22 ^e	7.482	9.119	7.302	0.180	9.152	-0.032	7.483	-0.001	9.044	0.075
23 ^e	7.598	9.455	7.698	-0.099	9.061	0.393	7.730	-0.132	9.529	-0.074
24 ^d	7.236	8.554	7.198	0.038	8.700	-0.146	7.417	-0.180	8.770	-0.216
25 ^d	7.607	9.107	7.429	0.177	9.019	0.087	7.565	0.042	9.152	-0.044

26^j	5.171	7.931	5.125	0.045	7.814	0.116	4.967	0.204	8.036	-0.104
27^g	6.614	8.381	6.533	0.081	8.274	0.106	6.779	-0.165	8.05	0.331
28^g	5.703	7.356	6.113	-0.410	7.418	-0.061	6.326	-0.622	7.705	-0.349
29^g	6.540	8.154	6.465	0.074	8.328	-0.174	6.697	-0.157	8.121	0.032
30^g	6.614	6.995	6.367	0.247	7.059	-0.063	6.563	0.050	7.312	-0.317
31^g	7.245	8.744	7.045	0.200	8.795	-0.050	7.039	0.206	8.439	0.305
32^g	7.354	7.920	6.805	0.548	7.897	0.022	6.841	0.513	7.385	0.535
33^g	6.630	9.033	6.480	0.150	8.308	0.725	6.415	0.215	8.096	0.936
34^c	6.962	8.583	7.108	-0.146	8.815	-0.232	7.251	-0.288	8.699	-0.116
35^c	6.570	8.651	6.910	-0.340	8.725	-0.074	6.548	0.022	8.778	-0.126
36^c	7.238	8.917	7.118	0.120	8.802	0.114	7.028	0.209	8.947	-0.029
37^c	6.568	8.320	6.651	-0.082	8.437	-0.116	6.841	-0.273	8.267	0.053
38^h	7.567	8.302	7.226	0.340	8.195	0.107	7.619	-0.052	8.248	0.054
39^h	6.721	7.879	7.020	-0.298	7.661	0.218	6.880	-0.158	7.786	0.093
40ⁱ	5.592	7.266	5.815	-0.223	7.872	-0.606	5.681	-0.088	8.069	-0.802
41ⁱ	5.969	8.735	6.061	-0.091	8.794	-0.059	5.870	0.099	8.856	-0.120
42ⁱ	6.044	8.962	5.911	0.133	9.047	-0.084	5.955	0.089	8.811	0.150
43ⁱ	5.880	7.316	5.972	-0.092	7.361	-0.044	5.792	0.088	7.679	-0.363
44ⁱ	5.580	7.277	5.682	-0.101	7.333	-0.055	5.786	-0.205	7.035	0.242
45ⁱ	5.986	8.853	6.040	-0.054	8.755	0.098	5.926	0.059	8.778	0.075

Rsd¹: Residual between predicted and observed activity for D2 CoMFA model

Rsd²: Residual between predicted and observed activity for D3 CoMFA model

Rsd³: Residual between predicted and observed activity for D2 CoMSIA model

Rsd⁴: Residual between predicted and observed activity for D3 CoMSIA model

Table 9. Experimental and fitted/predicted activities of D2/D3 ligands used as the training and test sets for selectivity (D3 over D2) analyses using CoMFA and CoMSIA

Sr. No.	pK_i^a				
	Experimental	Fitted/Predicted			
		CoMFA	Rsd ⁵	CoMSIA	Rsd ⁶
1 ^a	1.668	1.685	-0.017	1.766	-0.095
2 ^e	1.112	1.210	-0.098	1.191	-0.079
3 ^e	1.501	1.270	0.231	1.214	0.286
4 ^c	1.294	1.195	0.099	1.085	0.208
5 ^a	0.678	0.620	0.058	0.809	-0.130
6 ^a	0.971	0.865	0.106	0.929	0.041
7 ^d	1.357	1.212	0.145	1.296	0.060
8 ^e	0.673	1.021	-0.348	1.304	-0.631
9 ^e	1.318	1.054	0.264	1.032	0.295
10 ^d	0.936	0.804	0.132	0.963	-0.026
11 ^d	1.391	1.449	-0.058	1.497	-0.106
12 ^b	1.482	1.592	-0.11	1.601	-0.119
13 ^b	1.921	1.523	0.398	1.616	0.304
14 ^b	1.839	1.811	0.028	1.945	-0.106
15 ^f	0.467	0.386	0.081	0.622	-0.155
16 ^f	0.427	0.469	-0.042	0.401	0.025
17 ^a	1.321	1.434	-0.113	1.408	-0.087
18 ^b	1.361	1.242	0.119	1.394	-0.033
19 ^f	0.555	0.674	-0.119	0.792	-0.236
20 ^e	1.201	1.382	-0.181	1.353	-0.133

21 ^e	1.416	1.545	-0.129	1.392	0.023
22 ^e	1.637	1.445	0.192	1.431	0.257
23 ^e	1.857	1.912	-0.055	1.563	0.293
24 ^d	1.318	1.345	-0.027	1.495	-0.176
25 ^d	1.500	1.378	0.122	1.413	0.086
26 ^j	2.760	2.636	0.124	2.711	0.049
27 ^g	1.767	1.583	0.184	1.652	0.114
28 ^g	1.653	1.692	-0.039	1.847	-0.193
29 ^g	1.614	1.575	0.039	1.670	-0.055
30 ^g	0.381	0.689	-0.308	1.704	-1.32
31 ^g	1.499	1.349	0.15	1.805	-0.305
32 ^g	0.566	1.637	-1.071	1.681	-1.114
33 ^g	2.403	2.406	-0.003	2.084	0.319
34 ^c	1.621	1.785	-0.164	1.741	-0.120
35 ^c	2.081	1.958	0.123	1.981	0.100
36 ^c	1.679	1.788	-0.109	1.637	0.042
37 ^c	1.752	1.918	-0.166	1.760	-0.007
38 ^h	0.735	1.756	-1.021	1.601	-0.866
39 ^h	1.158	1.133	0.025	1.232	-0.074
40 ⁱ	1.674	2.906	-1.232	3.007	1.332
41 ⁱ	2.766	3.029	-0.263	3.043	-0.277
42 ⁱ	2.918	2.827	0.091	2.958	-0.040
43 ⁱ	1.436	2.711	1.275	2.931	-1.495
44 ⁱ	1.697	2.776	-1.079	2.961	-1.126
45 ⁱ	2.867	2.930	-0.063	3.006	-0.138

^a pK_i is the negative logarithm of equilibrium inhibition constant

$${}^b \Delta pK_i = pK_i \text{ D3} - pK_i \text{ D2L}$$

Table 10. Summary of 3D QSAR CoMFA results

	Atom-based alignment			Flexible alignment		
	pK _i D2 ^a	pK _i D3 ^b	Selectivity (D2/D3) ^c	pK _i D2 ^d	pK _i D3 ^e	Selectivity (D2/D3) ^f
Test set molecules	8, 9, 13, 16, 19, 27, 40, 41	5, 8, 10, 23, 24, 32, 33, 40	6, 8, 13, 18, 22, 24, 31, 41	8, 9, 13, 16, 19, 27, 40, 41	5, 8, 10, 23, 24, 32, 33, 40	6, 8, 13, 18, 22, 24, 31, 41
r ² _{conv}	0.903	0.964	0.976	0.920	0.941	0.958
SEE	0.258	0.143	0.111	0.234	0.169	0.145
Components	4	5	5	4	5	5
F values	67.507	145.94	208.99	83.140	89.538	118.68
Pr ² =0	0.00	0.00	0.00	0.00	0.00	0.00
Fractions						
Steric	0.447	0.424	0.437	0.415	0.636	0.528
Electrostatic	0.553	0.576	0.563	0.585	0.364	0.472
r ² _{pred}	0.852	0.249	0.849	0.926	0.710	0.864
σ _{min}	2.0	2.0	2.0	2.0	2.0	2.0

^a Model based on atom-based alignment and AM1 charges

^b Model based on atom-based alignment and AM1 charges

^c Model based on atom-based alignment and AM1 charges

^d Model based on flexible alignment and AM1 charges

^e Model based on flexible alignment and Gasteiger-Hückel charges

^f Model based on flexible alignment and AM1 charges

Table 11. Summary of 3D QSAR CoMSIA results

	Atom-based alignment			Flexible alignment		
	pK _i D2 ^a	pK _i D3 ^b	Selectivity (D2/D3) ^c	pK _i D2 ^d	pK _i D3 ^e	Selectivity (D2/D3) ^f
Test set molecules	8, 9, 13, 16, 19, 27, 40, 41	5, 8, 10, 23, 24, 32, 33, 40	6, 8, 13, 18, 22, 24, 31, 41	8, 9, 13, 16, 19, 27, 40, 41	5, 8, 10, 23, 24, 32, 33, 40	6, 8, 13, 18, 22, 24, 31, 41
r ² _{conv}	0.912	0.963	0.94	0.912	0.898	0.967
SEE	0.245	0.151	0.161	0.246	0.227	0.122
Comp.	4	7	3	4	6	4
F values	75.51	93.179	141.33	75.018	39.5	190.65
Pr ² =0	0	0	0.00	0	0.00	0
Fractions						
Steric	0.069	0.055	0.059	0.078	0.028	0.068
Electrost.	0.157	0.194	0.18	0.156	0.113	0.143
Hydrophobic	0.205	0.174	0.164	0.227	0.204	0.173
Donor	0.229	0.308	0.283	0.211	0.323	0.277
Acceptor	0.34	0.268	0.314	0.328	0.332	0.339
r ² _{pred}	0.911	0.335	0.781	0.814	0.64	0.719
σ _{min}	2.0	2.0	2.0	2.0	2.0	2.0

^a Model based on atom-based alignment and AM1 charges

^b Model based on atom-based alignment and AM1 charges

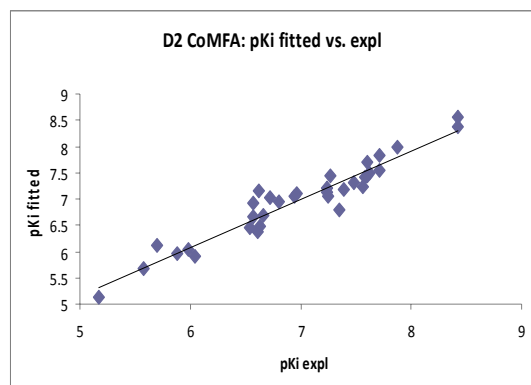
^c Model based on atom-based alignment and AM1 charges

^d Model based flexible alignment and Gasteiger-Hückel charges

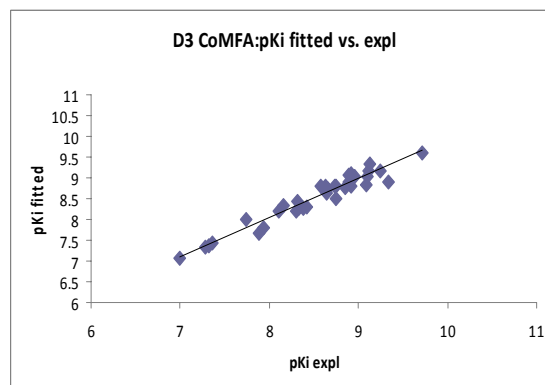
^e Model based on flexible alignment and Gasteiger-Hückel charges

^f Model based on flexible alignment and Gasteiger-Hückel charges

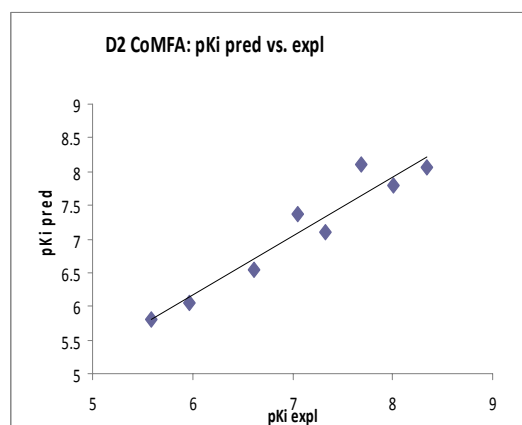
a)



b)



c)



d)

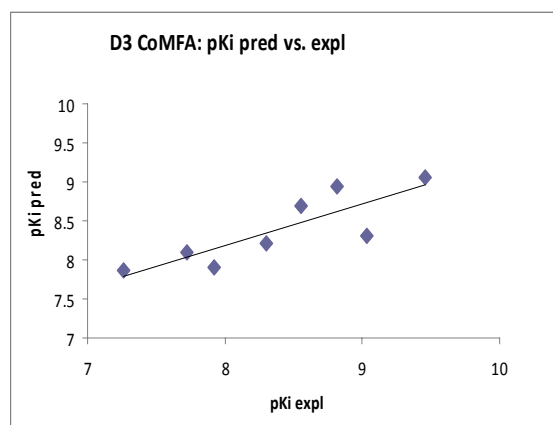
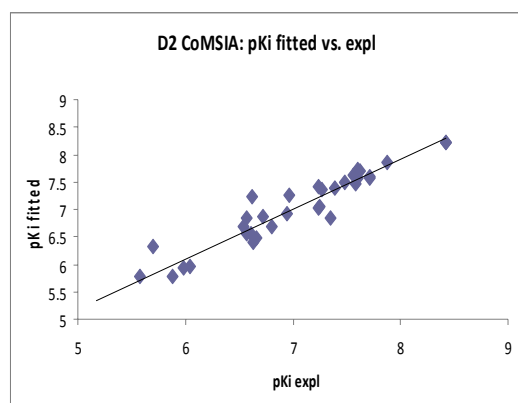
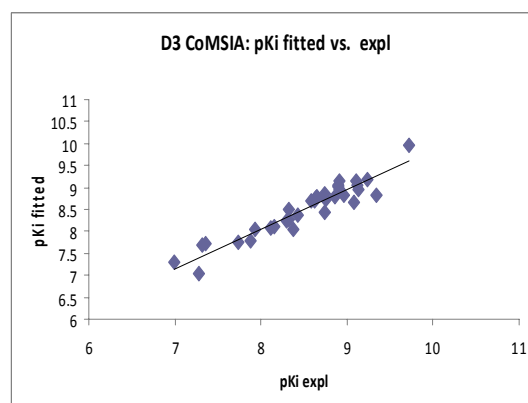


Figure 53. Experimental versus fitted (training set) activity a) DA D2^a and b) DA D3^b from the CoMFA analyses of the training sets and experimental versus predicted (test set) activity c) DA D2^a and d) DA D3^b from the CoMFA analyses. *Note.* ^aThe results are from flexible alignment and AM1 charges. ^bThe results are from flexible alignment and Gasteiger-Hückel charges

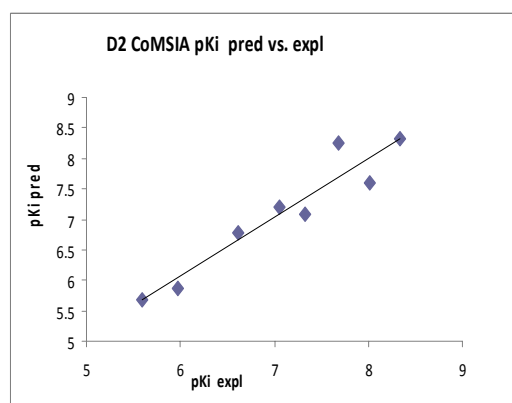
a)



b)



c)



d)

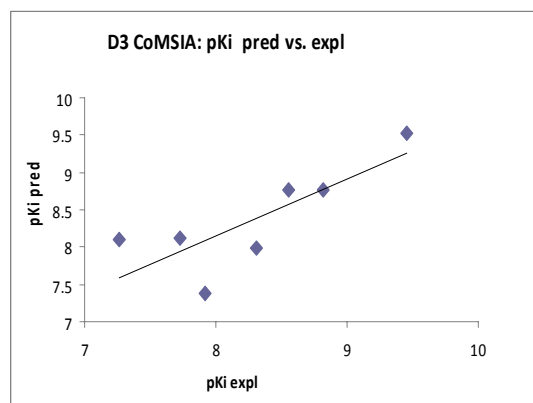
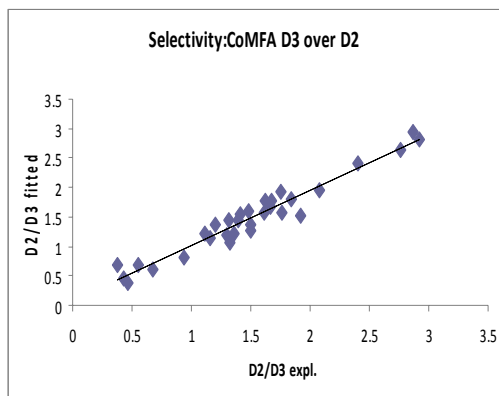
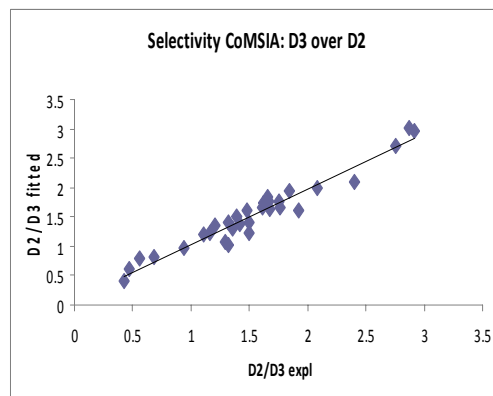


Figure 54. Experimental versus fitted (training set) activity a) DA D2^a and b) DA D3^b from the CoMFA analyses of the training sets and experimental versus predicted (test set) activity c) DA D2^a and d) DA D3^b from the CoMFA analyses. *Note.* ^aThe results are from atom-based alignment and AM1 charges. ^bThe results are from flexible alignment and Gasteiger-Hückel charges

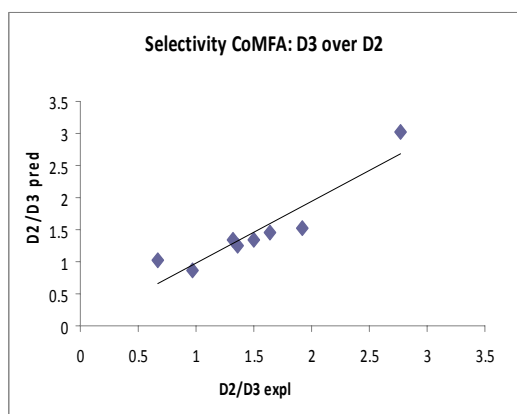
a)



b)



c)



d)

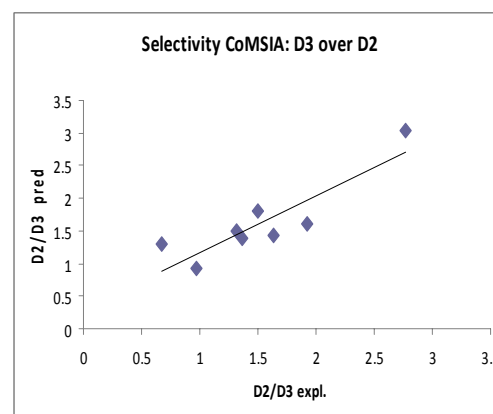


Figure 55. Experimental versus fitted (training set) selectivity (D2/D3) from a) CoMFA analyses^a and b) CoMSIA analyses^b of the training sets and experimental versus predicted (test set) selectivity (D2/D3) from c) CoMFA analyses^a and d) CoMSIA analyses^b. *Note.* ^aThe results are from flexible alignment and AM1 charges. ^bThe results are from atom-based alignment and AM1 charges.

5.4. Graphical Interpretation of the CoMFA and CoMSIA models:

CoMFA and CoMSIA contour maps were generated by interpolating the product between 3D QSAR coefficients and their associated standard deviations. The 3D representation of the field contributions defined as “STDEV*COEFF” contour maps which can provide better insights into the key structural features responsible for the variations in experimental binding affinities. **Figure 56a** shows the steric and electrostatic CoMFA contour maps derived from flexible alignment and AM1 charges for D2 potency while Figure 56b shows the corresponding maps generated using flexible alignment and Gasteiger-Hückel charges for D3 potency with the most active compound **4** shown inside the fields. The green contours (contribution level 80%) suggest that increase in steric bulk would result into an increase in activity, whereas yellow contours (contribution level 20%) suggest the opposite - a sterically bulky group would lead to decreased activity. Similarly, the blue (contribution level 80%) and red (contribution level 20%) contours indicate regions where the addition of electropositive and electronegative substituents, respectively, would result in an increase in activity.

5.4.1. DA D2 receptor binding affinity:

The 3D QSAR contours are divided into two groups – one consisting of contours near the aminotetraline head group (Site 1) and the second group consisting of contours at or near the phenyl ring attached to piperazine (Site 2). Presence of several sterically favored green and disfavored yellow contours (**Figure 56a**) surrounding the head group depicts stricter adherence to the limited steric bulk for both the D2 potency. The head group is likely to be situated in a well-defined cavity in the ligand-binding pockets of the D2 and D3 receptors. A small green contour is

overlapping the 5-methoxy group of aminotetraline moiety of compound **4** suggesting the requirement of steric bulk at this position for high affinity interaction. A sterically unfavorable yellow region around the aminotetraline moiety arises from the third ring of the conformationally rigid analog, **6**, explaining its lower binding affinity for both the receptors compared to its conformationally flexible bicyclic counterpart **2**. Similarly, the presence of a yellow contour near the N-propyl group of aminotetraline moiety suggests the detrimental effect of steric bulk near this position which is in consonance with other findings. In case of electrostatic contour maps, a small red contour is observed near the oxygen of 7 position of aminotetraline head group, indicating the critical importance of hydroxyl group for D2 potency.

As shown in **Figure 56a**, a large sterically unfavorable yellow contour is observed in the vicinity of the quinoline ring of **4**, indicating no steric bulk is allowed in this region and explains the lesser activity of the biphenyl analog **7** compared to **3** (K_i D2= 56.3 nM and 26.0 nM, respectively). Similarly, there are three small green regions located on the 6, 7 and 8 position of quinoline moiety which signifies the importance of limited steric bulk in this region. Lower potency of compounds **2** and **3** compared to **4**, **15**, and **16** could be due to the above interpretation, among others.

The appearance of blue polyhedra pointing away from position 3 position of quinoline moiety (**Figure 56a**) indicates that this region should carry relatively lesser electron density or should be more electropositive in nature for better binding affinity for the D2 receptor. The carbonyl group of the compounds **12**, **13**, **14**, **41**, **42** and **45** is directed towards these blue polyhedra which explain the less potent nature of these molecules. The appearance of red polyhedra in the vicinity of chlorine atom attached to the ortho and meta position of compounds **31** and **32** indicates that substitution with groups, carrying high electron density, is favorable at this position.

This explains the higher potency of **31** and **32** compared to **27** and **28** lacking the halogen substituents (K_i D2 = 56.8 nM and 243 nM for **31** and **27**, respectively; K_i D2 = 44.2 nM and 1979 nM for **32** and **28**, respectively). A blue polyhedron around indole-containing compound **14** indicates that this nitrogen should be more electropositive for better binding affinity at the D2 receptor.

The hydrophobic, HDon and HAcc contour maps of D2 CoMSIA model are displayed in **Figure 57a**. Yellow (the contribution level 80%) and white (the contribution level 20%) contours indicate the region where hydrophobic and hydrophilic groups, respectively, are preferred. There are three hydrophilic regions in this contour map: First, large white contour near the N-propyl group of the aminotetraline head group, which indicates that a hydrophobic group is disfavored at this position. This contour maps onto the tertiary nitrogen of the aminotetraline and aminothiazolidium groups which confer hydrophilicity upon protonation in physiological pH; and is also consistent with the conclusion of the steric field. It is a well-known fact that one of the N substituents of a potent DA receptor agonist fits into a small pocket known as 'propyl cleft'. Another white polyhedron is located around the piperazine ring suggesting that hydrophobic groups will decrease the activity. Third white polyhedron is observed away from the quinoline moiety of the most active compounds which is in consonance with the steric contour map. As seen in Figure 57a, the quinoline group of **4** is surrounded by a yellow contour. These results demonstrate that a hydrophobic function in this region will increase activity which is consistent with CoMFA steric contour map. The HDon-favored and disfavored regions are represented by cyan (contribution level 80%) and purple (contribution level 20%) contours, respectively. The presence of two cyan contours are near the 5- and 7-positions of the aminotetraline head group indicate that HDon functionality

in this region will enhance the binding affinity. The HDon moieties, the hydroxyl and amino groups of the aminotetraline and thiazolidium head groups may be involved in H-bonding with the receptor amino acid residues. These results are in accordance with the similar results obtained by other authors. One cyan contour near the N of the n-propyl group of aminotetraline indicates that a HDon functionality in this region will enhance the binding affinity to D2 receptor. The cyan contour map surrounding the piperazine nitrogen signifies the position of nitrogen atom as donor group present in this class of dopaminergic compounds. It is likely that these nitrogen will exist as protonated species at physiological pH and thus, may serve as HDon and/or cationic center.

CoMSIA HAcc favored and disfavored fields are shown in magenta (contribution level 80%) and red (contribution level 20%) respectively. The large red contour around the **5** position of aminotetraline indicates that any substituent containing an acceptor group will reduce the activity which is in agreement with HDon feature at this region of molecules. On the other hand a red polyhedron is seen around the carbonyl oxygen attached to the piperazine ring in compounds **12, 13, 14, 41, 41** and **45**. This indicates that acceptor group is disfavored at this position and is validated by the presence of carbonyl group in compounds **12, 13, 14, 41, 41** and **45** which resulted in the reduced binding affinity for the D2 receptor. The magenta contours around the nitrogen of quinoline and indole moiety of the compounds **15, 16 and 19** suggest that this nitrogen can act as an acceptor and should be electropositive for better binding affinity.

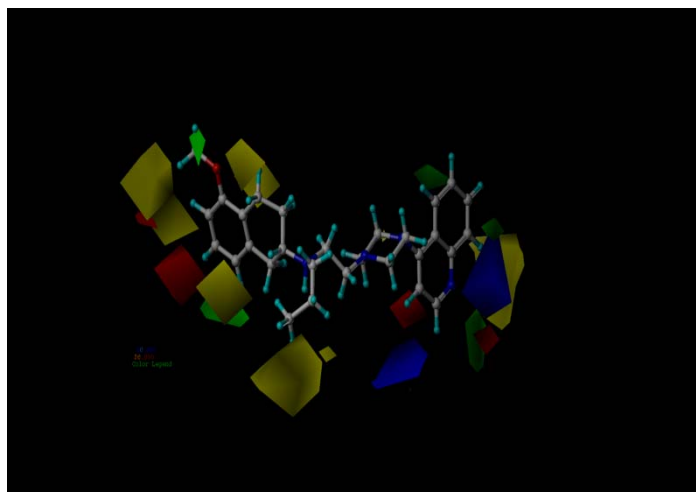
5.4.2. DA D3 receptor binding affinity:

The steric and electrostatic contour plots are shown in **Figure 56b**. Compound **4** is shown for reference. As seen from **Figure 56b**, a large sterically favorable green

contour is observed around the 7- and 8-positions of the aminotetraline head group, suggesting the requirement of bulk near these positions for higher D3 potency. Sterically unfavorable yellow contours are observed near the N-propyl group of aminotetraline and near the pendant ring of the conformationally rigid analogs **5** as observed for D2 potency. Significant number of red contours is observed around the molecules. The red contour seen near the piperazine nitrogen reveals that nitrogen may act as a HAcc to interact with the D3 receptor. A red polyhedron is observed around the nitrogen of the molecules having an indole moiety attached to the piperazine ring in compounds **12**, **13** and **41** which indicates the involvement of indole N in H-bonding with the receptor.

The hydrophobic, HDon and HAcc contour maps of CoMSIA model based on flexible alignment and Gasteiger-Huckel charges are displayed in **Figure 57b** and are generally in accordance with the field distribution pattern seen for D2 potency. In the CoMSIA contour maps for D3 potency, there is a cyan contour map surrounding the piperazine nitrogen implying that donor group is favorable at this location for better activity. However, an acceptor favorable magenta contour on the same nitrogen signifies that the group with the dual donor and acceptor properties are favorable at this position. A magenta polyhedron is seen around the oxygen of the carbonyl group attached to the piperazine ring in molecules **12**, **13**, **14**, **41**, **42** and **45**. This indicates that an acceptor group is favored at this position and the position of carbonyl group in these compounds resulted in the higher binding affinity towards the D3 receptor which is in contrast to the corresponding D2 contour maps. These contour maps may explain the higher D3 selectivity of the carbonyl-containing compounds. The magenta contour map near the oxygen of hydroxyl group containing compounds **15**, **16**, **19** and on **8** position of quinoline moiety signifies that

an acceptor group is favored at this position. The yellow contour on the phenyl and white hydrophobic contour on the cyclohexyl ring of aminotetraline indicate that the hydrophobic and hydrophilic groups, respectively, are favored for higher D3 potency. A white contour near the N-propyl group of the aminotetraline and yellow contours around the quinoline ring of **15**, **16** and **19** is complementary to the D2 CoMSIA contour maps (**Figure 57a**). A large white contour is located around the quinoline moiety suggesting that hydrophobic group will reduce the binding affinity towards D3 receptor.



a)

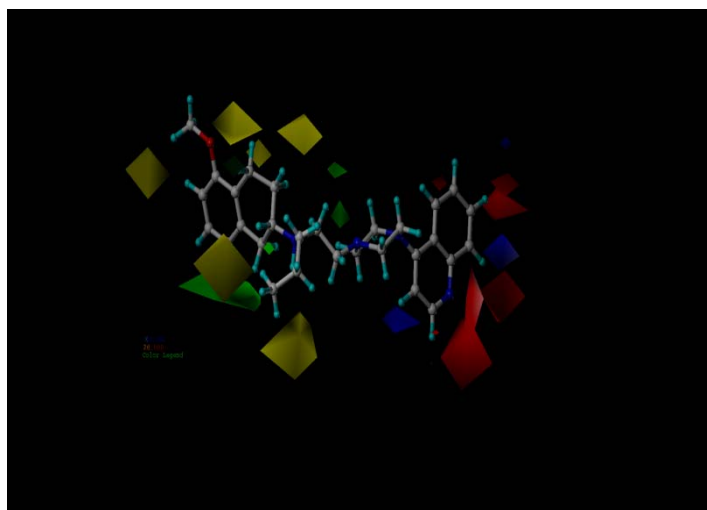
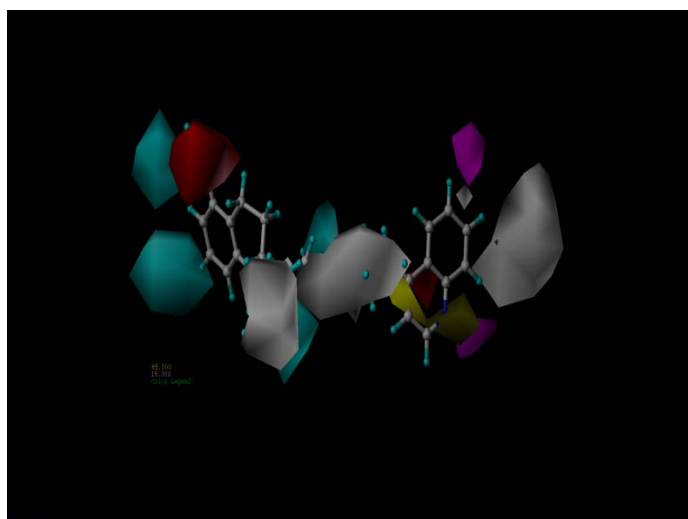


Figure 56. CoMFA STDEV*COEFF contour plots showing steric and electrostatic features from analysis based on a) flexible alignment and AM1 charges for D2 potency and b) flexible alignment and Gasteiger-Hückel charges for D3 potency. Green polyhedra represent sterically favored areas (contribution level of 80%) and yellow polyhedra represent sterically disfavored areas (contribution level of 20%). For electrostatic fields, blue polyhedra (contribution level of 80%) are regions of the molecule where more positive charge and H-bond donors are favored or negative charge or H-bond acceptors are disfavored for high-affinity interactions. Red fields (contribution level of 20%) are regions where negatively charged substituents and H-bond acceptors are favored or more positive charge and H-bond donors are disfavored. Compound **4** is shown inside the fields in both (a) and (b)

a)



b)

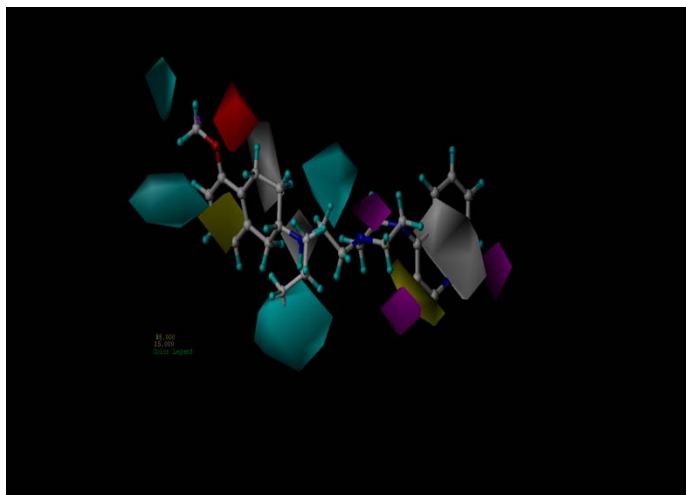


Figure 57. Hydrophobic, HDon and HAcc contour maps from the CoMSIA model using a) atom-based alignment and AM1 charges for D2 potency and b) flexible alignment and Gasteiger-Hückel charges for D3 potency. Compound **42** is shown inside the fields.

Selectivity for D3 over D2

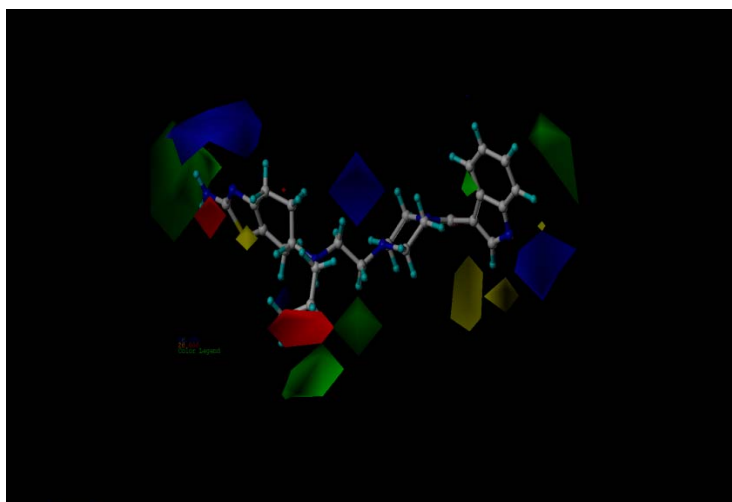
The steric and electrostatic contour plots obtained from the CoMFA analysis based on flexible alignment and AM1 charges are shown in **Figure 58a**, and are generally in accordance with the field distribution pattern seen for D2 CoMFA. Compound **42** has been shown for reference. A large blue and small red contour observed near the nitrogen and the hydroxyl group of the thiazolidium and aminotetraline head groups, respectively, suggests the dominating role of more positive charge and HDon over more negative charge and HAcc in determining D3 selectivity. A blue polyhedron around the piperazine nitrogen suggests that this nitrogen can be protonated at physiological pH and act as donor in this region of receptor. The red polyhedron around the N-propyl group signifies the role of electronegative atom in this area which cannot be explained from the current set of molecules.

A large green contour around the head group in the molecules as shown in Figure 8a substantiates the significance of steric bulk in this region. Selectivity for D3 receptor will increase further with increasing steric bulk in this region of the molecules. Two green polyhedra exist surrounding the n-propyl group indicating that the steric bulk is favored for selectivity in these areas. Compound **5**, which is a rigid analog, lacking N-propyl group, is less selective (D2/D3 4.8) compared to **4** (D2/D3 31.5). A large green contour is observed around the tail region of the molecules which entails the significance of steric bulk for D3 selectivity in the molecules. Compounds with biphenyl ring like compound **33** are more selective (D2/D3 253) compared to compound **27** (D2/D3= 58.6) which is in accordance with other findings. The yellow polyhedron near to the indole moiety of **42** indicates that substitution with bulkier group will decrease selectivity for D3 receptor. This may be the reason why compound **18** is more selective compared to **19**.

The hydrophobic, HDon and HAcc contour maps of the CoMSIA models based on atom based alignment and AM1 charges are displayed in **Figure 58b**, and are generally in accordance with the contour plots observed from D2 CoMSIA with minor modification in contribution level (hydrophobic favored with contribution level 90%, HDon favored and disfavored with the contribution levels 75% and 15%, respectively). The presence of a cyan contour around position 7 of the head group (-OH group) indicates HDon group is favorable at this position for better selectivity. However, development of purple and magenta contour on the 5 position of hydroxyl group around the head group signify that group with HAcc are favorable at this position which is complementary to the CoMFA electrostatic contour maps. This entails the necessity of dual natured group at this position. The magenta polyhedron directed towards the carbonyl group of indole-containing highly D3 selective

compounds **41**, **42** and **45** implies the significance of acceptor group at this location of the molecules. Carbonyl group might be playing a very critical role in the selectivity for D3 receptor which is in agreement with other findings. Red contour is oriented towards the N of quinoline moiety of **15**, **16** and **19** which indicates that the N should be electropositive for better selectivity towards D3 receptor. The cyan contour maps, similar to the D2 and D3 CoMSIA contour maps oriented toward the nitrogen of N-(n-propyl) group indicates that N may be acting as a HDon. A purple contour map located between the N-(n-propyl) and piperazine N indicates that HDon groups are disfavored at this location. Two big yellow contours around the distal part of the molecules imply the significance of hydrophobic features for selectivity towards D3 receptor. The emergence of yellow contours over the linker, between N-(n-propyl) and the piperazine N, suggested that substitution with hydrophobic bulky group at this position is favorable for better selectivity. White contour overlapping one of the N of the piperazine ring suggests that hydrophobic group at this position will reduce the selectivity for D3 receptor.

a)



b)

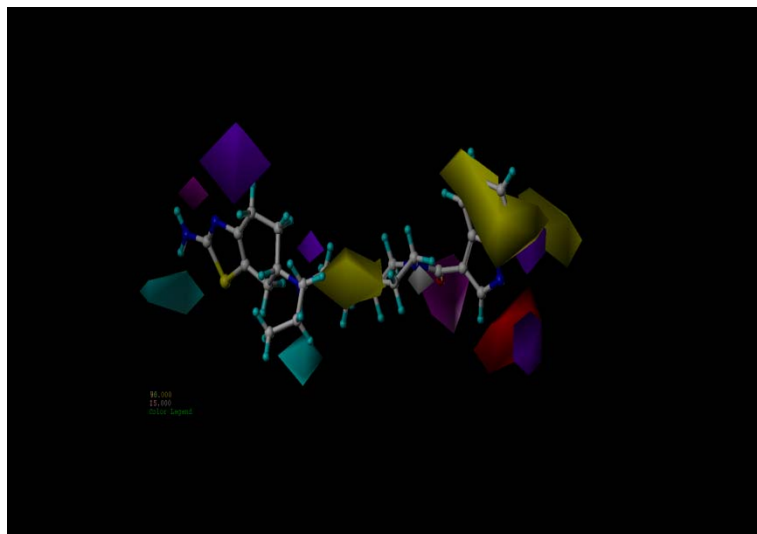


Figure 58. a) Steric and electrostatic CoMFA contour maps using atom-based alignment and AM1 charges and b) hydrophobic, HDon and HAcc CoMSIA contour maps using flexible alignment and Gasteiger-Hückel charges. Compound **4** is shown inside the fields.

CHAPTER 6

Materials and methods

6.1. Chemistry:

Reagents and solvents were obtained from commercial suppliers and used as received unless otherwise indicated. Dry solvents were obtained according to the standard procedure as described in Vogel's book on practical organic chemistry. Analytical silica gel-coated TLC plates (Silica Gel 60 F₂₅₄) were purchased from EM Science and were visualized with UV light or by treatment with phosphomolybdic acid (PMA), ninhydrin and dragondroff solution. Flash chromatography was carried out on Whatman Purasil 60A silicagel 230-400 mesh. ¹H NMR spectra were routinely obtained on Varian 400 MHz FT NMR. The NMR solvent used was either CDCl₃ or CD₃OD as indicated. TMS was used as an internal standard. Elemental analyses were performed by Atlantic Microlab, Inc and were within ± 0.4% of the theoretical value. Optical rotations were recorded on a Perkin Elmer 241 polarimeter and Autopol III, Automatic Polarimeter (Rudolph Research Analytical).

***tert*-Butyl 4-(4-iodophenyl)piperazine-1-carboxylate (1):** Into a stirring solution of 1-phenylpiperazine (21.8 g, 134.0 mmol) in acetic acid/water (3:1, 42 ml), a suspension of iodine monochloride (24.0 g, 148.0 mmol) in acetic acid/water (3:1, 42 ml) was added at 55 °C. The reaction was stirred at 55 °C for 1 h and then at room temperature for another 1 h. The solution was poured into 400 mL of crushed ice and the pH was adjusted to 13 with 4 N NaOH. The product was then extracted with dichloromethane (3 x 100 mL). The combined organic layer was dried over Na₂SO₄, filtered and evaporated in vacuo to provide the free amine of compound **1** as a pale

yellow solid (28.69 g, 74%) which was converted to Boc derivative without further purification.

Into a stirring solution of this amine (28.0 g, 97.17 mmol) in dichloromethane (80 mL), (Boc)₂O (25.44 g, 116.60 mmol) and Et₃N (35.26 mL, 252.64 mmol) were added at room temperature. The reaction mixture was stirred at the same temperature for 12 hours and was extracted with CH₂Cl₂ (3 x 100 mL), washed with water, dried over Na₂SO₄, filtered, and concentrated in vacuo. The crude material was purified by column chromatography over silica gel (Hexane/EtOAc, 9.0:1.0) to give compound **1** (34.70 g, 92%). ¹H (CDCl₃, 400 MHz): δ 1.48 (s, 9 H), 3.10 (t, *J* = 4.8 Hz, 4H), 3.56 (t, *J* = 4.8 Hz, 4H), 6.68 (d, *J* = 8.8 Hz, 2H), 7.53 (d, *J* = 9.2 Hz, 2H).

Procedure A. *tert*-Butyl 4-(4'-methoxybiphenyl-4-yl)piperazine-1-carboxylate

(3a): A suspension of (4-methoxyphenyl)boronic acid **2a** (2.34 g, 15.49 mmol), iodo compound **1** (6.01 g, 15.49 mmol), Na₂CO₃ (3.28 g, 30.98 mmol, 2 M solution in water) and Pd(PPh₃)₄ (875 mg, 0.75 mmol) in dimethoxy ethane/ethanol (1:1) was refluxed for one hour. The solvents were removed in vacuo and the crude product was purified by flash chromatography using solvent system hexane: ethyl acetate (4.0:1.0) to yield compound **3a** (3.82 g, 67%). ¹H NMR (CDCl₃, 400 MHz): δ 1.49 (s, 9H), 3.17 (t, *J* = 4.8 Hz, 4H), 3.61 (t, *J* = 4.8 Hz, 4H), 3.85 (s, 3H), 6.96 (d, *J* = 8.8 Hz, 2H), 6.98(d, *J* = 8.8 Hz, 2H), 7.48 (d, *J* = 8.8 Hz, 2H), 7.49 (d, *J* = 8.8 Hz, 2H).

Synthesis of *tert*-butyl 4-(3'-methoxybiphenyl-4-yl)piperazine-1-carboxylate

(3b): Commercially available, (3-methoxyphenyl)boronic acid, **2b** (4.60 g, 30.44 mmol) was reacted with iodo compound **1** (11.81 g, 30.44 mmol), Na₂CO₃ (6.45 g, 60.88 mmol, 2 M solution in water) and Pd(PPh₃)₄ (1.16 gm, 1.01 mmol) in

dimethoxy ethane/ethanol (46 mL:46 mL) as followed in procedure **A** to yield compound **3b** (6.95 g, 62 % yield). ^1H NMR (CDCl_3 , 400 MHz): δ 1.49 (s, 9H), 3.18 (t, $J = 4.0\text{Hz}$, 4H), 3.59 (t, $J = 4.4\text{Hz}$, 4H), 3.85 (s, 3H), 6.82 (dd, $J = 8.0\text{ Hz}$, 1.6 Hz, 1H), 6.99 (d, $J = 8.0\text{ Hz}$, 2H), 7.09 (bs, 1H), 7.15 (d, $J = 7.2\text{ Hz}$, 1H), 7.32 (t, $J = 7.8\text{Hz}$, 1H), 7.52 (d, $J = 8.0\text{ Hz}$, 2H).

Synthesis of tert-butyl 4-(2'-methoxybiphenyl-4-yl)piperazine-1-carboxylate (3c):

Commercially available, (2-methoxyphenyl)boronic acid, **2c** (2.10 g, 13.90 mmol) was reacted with iodo compound **1** (5.4 g, 13.90 mmol), Na_2CO_3 (2.94 g, 27.80 mmol, 2 M solution in water) and $\text{Pd}(\text{PPh}_3)_4$ (560 mg, 0.484 mmol) in dimethoxy ethane/ethanol (20 mL:20 mL) by following procedure **A** to yield compound **3c** (3.58 g, 70% yield). ^1H NMR (CDCl_3 , 400 MHz): δ 1.50 (s, 9H), 3.19 (t, $J = 4.8\text{ Hz}$, 4H), 3.60 (t, $J = 4.8\text{Hz}$, 4H), 3.81 (s, 3H), 6.96-7.04 (m, 4H), 7.25-7.32 (m, 2H), 7.48 (d, $J = 9.2\text{ Hz}$, 2H).

Synthesis of tert-butyl 4-(2',5'-dimethoxybiphenyl-4-yl)piperazine-1-carboxylate (3d):

Commercially available, (2,5-dimethoxyphenyl)boronic acid, **2d** (4.68 g, 25.70 mmol), was reacted with iodo compound **1** (9.97 g, 25.70 mmol), Na_2CO_3 (5.44 g, 51.40 mmol, 2 M solution in water) and $\text{Pd}(\text{PPh}_3)_4$ (1.47 g, 1.28 mmol) in dimethoxy ethane/ethanol (40 mL:40 mL) followed by procedure **A** to yield compound **3d** (6.64 g, 65%). ^1H NMR (CDCl_3 , 400 MHz): δ 1.49 (s, 9H), 3.18 (bs, 4H), 3.58 (t, $J = 4.4\text{ Hz}$, 4H), 3.74 (s, 3H), 3.84 (s, 3H), 6.83 (dd, $J = 2.8\text{Hz}$, 9.2 Hz, 1H), 6.88-6.90 (m, 2H), 6.96 (d, $J = 8.4\text{ Hz}$, 2H), 7.47 (d, $J = 8.0\text{ Hz}$, 2H).

tert-Butyl 4-(3',4'-dimethoxy-[1,1'-biphenyl]-4-yl)piperazine-1-carboxylate (3e):

A suspension of (3,4-dimethoxyphenyl)boronic acid, **2e**, (2.34 g, 12.88 mmol), iodo compound **1** (5.0 g, 12.88 mmol), Na_2CO_3 (2.73 g, 25.76 mmol, 2 M solution in

water) and Pd(PPh₃)₄ (731 mg, 0.63 mmol) in dimethoxy ethane/ethanol (20 mL:19 mL) followed by procedure **A** to yield compound **3e** (3.43 g, 67%). ¹H NMR (CDCl₃, 400 MHz): δ 1.49 (s, 3H), 3.17 (t, *J* = 4.8 Hz, 4H), 3.60 (t, *J* = 4.8 Hz, 4H), 3.91 (s, 3H), 3.94 (s, 3H), 6.88-7.14 (m, 5H), 7.48 (d, *J* = 8.8 Hz, 2H).

tert-butyl 4-([1,1'-biphenyl]-4-yl)piperazine-1-carboxylate (3f): Commercially available, benzenboronic acid, **2f** (2.5 g, 20.48 mmol), was reacted with iodo compound **1** (7.95 g, 20.48 mmol), Na₂CO₃ (4.34 g, 40.96 mmol, 2 M solution in water) and Pd(PPh₃)₄ (1.18 gm, 1.02 mmol) in dimethoxy ethane/ethanol (25 mL: 25 mL) by following procedure **A** to yield compound **3f** (1.74g, 80%). ¹H NMR (CDCl₃, 400 MHz): δ 1.49 (s, 9H), 3.07 (bs, 4H), 3.61 (t, *J* = 4.8 Hz, 4H), 6.96 (d, *J* = 8.0 Hz, 2H), 7.23 (d, *J* = 7.2 Hz, 1H), 7.41 (t, *J* = 8.0 Hz, 2H), 7.49 (d, *J* = 8.0 Hz, 2H), 7.52 (d, *J* = 7.2 Hz, 2H).

Procedure B. 1-(4'-methoxy-biphenyl-4-yl)piperazine (4a): Into a stirring solution of compound **3a** (3.4 g, 9.23 mmol) in CH₂Cl₂ (30 mL), TFA (20 mL) was added slowly at room temperature and the reaction mixture was stirred for four hours. Unreacted TFA and solvent CH₂Cl₂ were removed in vacuo and the salt formed was washed with diethyl ether. Saturated solution of sodium bicarbonate was added to the salt and it was extracted with dichloromethane (50 x 3 mL). The combined organic layer was dried over Na₂SO₄, filtered and evaporated in vacuo to provide the compound **4a** (2.22 g, 90%). ¹H NMR (CDCl₃, 400 MHz): δ 1.63 (bs, 1H); 3.06 (t, *J* = 4.4Hz, 4H); 3.19 (t, *J* = 4.6Hz, 4H), 3.84 (s, 3H); 6.95 (d, *J* = 8.4 Hz, 2H), 6.98(d, *J* = 8.8 Hz, 2H), 7.47 (d, *J* = 8.0 Hz, 2H), 7.49 (d, *J* = 8.0 Hz, 2H).

1-(3'-methoxy-biphenyl-4-yl)piperazine (4b): Compound **3b** (4.6 g, 12.5 mmol) was reacted with TFA (30 mL) in CH₂Cl₂ (20 mL) by following procedure **B** to give

compound **4b** (3.34 g, 99%). ^1H NMR (CDCl_3 , 400 MHz): δ 3.07 (t, $J = 4.8$ Hz, 4H), 3.21 (t, $J = 7.2$ Hz, 4H), 3.85 (s, 3H), 6.83 (dd, $J = 2.4$ Hz, 8.0 Hz 1H), 6.98 (d, $J = 8.8$ Hz, 2H), 7.09 (t, $J = 2.8$ Hz, 1H), 7.15 (d, $J = 7.2$ Hz, 1H), 7.32 (t, $J = 8.2$ Hz, 1H), 7.52 (d, $J = 8.8$ Hz, 2H).

1-(2'-methoxy-biphenyl-4-yl)piperazine (4c): Compound **3c** (3.4 g, 9.23 mmol) was reacted with TFA (15 mL) in CH_2Cl_2 (20 mL) by following procedure **B** to give compound **4c** (2.47 g, 99%). ^1H NMR (CDCl_3 , 400 MHz): δ 3.08 (bs, 4H); 3.23 (bs, 4H), 3.81 (s, 3H); 6.93-7.06 (m, 4H), 7.25-7.35 (m, 2H), 7.40-7.49 (m, 2H).

1-(2',5'-dimethoxybiphenyl-4-yl)piperazine (4d): Compound **3d** (5.4 g, 14.65 mmol) was reacted with TFA (30 mL) in CHCl_3 (40 mL) using procedure **B** to give compound **4d** (3.41 g, 87%). ^1H NMR (CDCl_3 , 400 MHz): 3.20 (bs, 8H); 3.75 (s, 3H); 3.85 (s, 3H); 6.62 (s, 1H); 6.85 (s, 1H), 7.31 (t, $J = 7.2$ Hz, 1H), 7.40 (t, $J = 7.2$ Hz, 2H), 7.52 (d, $J = 8.0$ Hz, 2H).

1-(3',4'-dimethoxy-[1,1'-biphenyl]-4-yl)piperazine (4e): To a stirring solution of compound **3e** (3.2 g, 8.03 mmol) in CHCl_3 (20 mL), TFA (20 mL) was added slowly at room temperature using procedure **B** to give compound **4e** (2.37 g, 99%). ^1H NMR (CDCl_3 , 400 MHz): δ 1.70 (bs, 1H); 3.06 (t, $J = 4.4$ Hz, 4H); 3.19 (t, $J = 4.4$ Hz, 4H), 3.92 (s, 3H); 3.94 (s, 3H); 6.92 (d, $J = 7.2$ Hz, 1H); 6.99 (d, $J = 7.2$ Hz, 2H), 7.04-7.14 (m, 2H), 7.48 (d, $J = 7.2$ Hz, 2H).

1-(1,1'-biphenyl)-4-yl)piperazine (4f): Compound **3f** (1.7 g, 5.02 mmol) was reacted with TFA (10 mL) in CH_2Cl_2 (20 mL) by following procedure **B** to give compound **4f** (2.18 g, 90%). ^1H NMR (CDCl_3 , 400 MHz): 3.18 (t, $J = 6.8$ Hz, 4H), 3.28 (t, $J = 4.8$ Hz, 4H), 6.98 (d, $J = 8.0$ Hz, 2H), 7.27 (d, $J = 6.4$ Hz, 1H), 7.41 (t, $J = 8.0$ Hz, 2H), 7.52 (d, $J = 8.0$ Hz, 2H), 7.58 (d, $J = 7.2$ Hz, 2H).

Procedure C. 1-(2-(*tert*-Butyldimethylsilyloxy)ethyl)-4-(4'-methoxybiphenyl-4-yl)piperazine (5a). A mixture of compound **4a** (1.5 g, 5.59 mmol), (2-bromo-ethyl)-*tert*-butyldimethylsilane (1.57 g, 6.56 mmol), and K₂CO₃ (2.27 g, 16.44 mmol) in CH₃CN (30 mL) was refluxed for 14 hours. Acetonitrile was evaporated under vacuo and the crude material was purified by silica gel column chromatography (Hexane/EtOAc, 1:4) to give compound **5a** (1.90 g, 80%). ¹H NMR (CDCl₃, 400 MHz): δ 0.09 (s, 6H), 0.92 (s, 9H), 2.61 (t, *J* = 6.0 Hz, 2H), 2.72 (t, *J* = 5.0 Hz, 4H), 3.24 (t, *J* = 4.80 Hz, 4H), 3.80 (t, *J* = 6.4 Hz, 2H), 3.83 (s, 3H), 6.95 (d, *J* = 9.2 Hz, 2H), 6.98(d, *J* = 8.8 Hz, 2H), 7.46 (d, *J* = 8.8 Hz, 2H), 7.48 (d, *J* = 8.4 Hz, 2H).

1-(2-(*tert*-butyldimethylsilyloxy)ethyl)-4-(3'-methoxybiphenyl-4-yl)piperazine

(5b): Compound **4b** (3.20 g, 11.94 mmol), was reacted with (2-bromo-ethyl)-*tert*-butyldimethylsilane (3.42 g, 14.32 mmol), and K₂CO₃ (4.94 g, 35.74 mmol) in CH₃CN (80 mL) by following the procedure **C** to furnish **5b** (4.06 g, 80%). ¹H NMR (CDCl₃, 400 MHz): δ 0.06 (s, 6H), 0.90 (s, 9H), 2.49 (t, *J* = 7.2 Hz, 2H), 2.63 (bs, 4H), 3.26 (t, *J* = 4.8Hz, 4H), 3.68 (t, *J* = 4.0Hz, 2H), 3.83 (s, 3H), 6.84 (dd, *J* = 8.0 Hz, 2.4 Hz, 1H), 6.99 (d, *J* = 8.8 Hz, 2H), 7.09 (t, *J* = 2.4 Hz, 1H), 7.15 (d, *J* = 8.0 Hz, 1H), 7.32 (t, *J* = 8.0 Hz, 1H), 7.51 (d, *J* = 8.0 Hz, 2H).

1-(2-(*tert*-butyldimethylsilyloxy)ethyl)-4-(2'-methoxybiphenyl-4-yl)piperazine

(5c): Compound **4c** (2.20 g, 8.20 mmol) was reacted with (2-bromo-ethyl)-*tert*-butyldimethylsilane (2.34 g, 9.84 mmol), and K₂CO₃ (3.39 g, 24.60 mmol) in CH₃CN (30 mL) by following procedure **C** to afford compound **5c** (2.70 g, 80%). ¹H NMR (CDCl₃, 400 MHz): 0.06 (s, 6H), 0.90 (s, 9H), 2.58 (t, *J* = 5.6 Hz, 2H), 2.69 (bs, 4H), 3.24 (bs, 4H), 3.78 (t, *J* = 4.8Hz, 2H), 3.83 (s, 3H), 6.95-7.06 (m, 4H), 7.24-7.27 (m, 2H), 7.44-7.46 (m, 2H).

1-(2-(tert-butyldimethylsilyloxy)ethyl)-4-(2',5'-dimethoxybiphenyl-4-

yl)piperazine (5d): Compound **4d** (3.0 g, 10.06 mmol) was reacted with (2-bromoethyl)-*tert*-butyldimethylsilane (2.88 g, 12.07 mmol), and K₂CO₃ (4.17 g, 30.18 mmol) in CH₃CN (60 mL) using procedure **C** to afford compound **5d** (3.90 g, 85%). ¹H NMR (CDCl₃, 400 MHz): δ 0.06 (s, 6H), 0.87 (s, 9H), 2.61 (t, *J* = 6.8 Hz, 2H), 2.74 (bs, 4H), 3.16 (bs, 4H), 3.74 (s, 3H), 3.80 (t, *J* = 6.4 Hz, 2H), 3.85 (s, 3H), 6.83 (dd, *J* = 2.4 Hz, 8.0 Hz, 1H), 6.98 (d, *J* = 8.0 Hz, 2H), 7.09 (t, *J* = 2.4 Hz, 1H), 7.14 (d, *J* = 7.2 Hz, 1H), 7.31 (t, *J* = 7.2 Hz, 1H), 7.50 (d, *J* = 8.0 Hz, 2H).

1-(2-((tert-Butyldimethylsilyl)oxy)ethyl)-4-(3',4'-dimethoxy-[1,1'-biphenyl]-4-

yl)piperazine (5e). A mixture of compound **4e** (2.37 g, 7.95 mmol), (2-bromo-ethyl)-*tert*-butyldimethylsilane (2.28 g, 9.56 mmol), and K₂CO₃ (3.17 g, 22.9 mmol) in CH₃CN (30 mL) using procedure **C** to afford compound **5e** (3.41 g, 94%). ¹H NMR (CDCl₃, 400 MHz): δ 0.09 (s, 6H), 0.92 (s, 9H), 2.64 (t, *J* = 6.4 Hz, 2H), 2.75 (t, *J* = 4.8 Hz, 4H), 3.27 (t, *J* = 4.8 Hz, 4H), 3.83 (t, *J* = 6.4 Hz, 2H), 3.92 (s, 3H), 3.95 (s, 3H), 6.93 (d, *J* = 8 Hz, 1H), 6.99 (d, *J* = 8.8 Hz, 2H), 7.04-7.14 (m, 2H), 7.47 (d, *J* = 8.4 Hz, 2H).

1-([1,1'-biphenyl]-4-yl)-4-(2-((tert-butyldimethylsilyl)oxy)ethyl)piperazine(5f):

Compound **4f** (2.1 g, 8.81 mmol) was reacted with (2-bromo-ethyl)-*tert*-butyldimethylsilane (2.52 g, 10.58 mmol), and K₂CO₃ (3.65 g, 26.43 mmol) in CH₃CN (30 mL) by following procedure **C** to afford compound **5f** (2.79 g, 80%). ¹H NMR (CDCl₃, 400 MHz): δ 0.09 (s, 6H), 0.92 (s, 9H), 2.69 (t, *J* = 5.6 Hz, 2H), 3.18 (t, *J* = 6.8 Hz, 4H), 3.30 (t, *J* = 4.8 Hz, 2H), 3.72 (t, *J* = 5.6 Hz, 4H), 6.98 (d, *J* = 8.0 Hz, 2H), 7.25-7.30 (m, 1H), 7.40 (t, *J* = 8.0 Hz, 2H), 7.51-7.56 (m, 4H).

1-(4-((tert-butyldimethylsilyl)oxy)butyl)-4-(3'-methoxy-[1,1'-biphenyl]-4-

yl)piperazine (5g): Compound **4b** (2.0 g, 7.45 mmol) was reacted with (4-bromobutoxy)(tert-butyl)dimethylsilane (2.38 g, 8.94 mmol), and K₂CO₃ (3.08 g, 22.35 mmol) in CH₃CN (40 mL) by following procedure **C** to afford compound **5g** (2.80 g, 85%). ¹H NMR (CDCl₃, 400 MHz): δ 0.09 (s, 6H), 0.92 (s, 9H), 1.62 (t, *J* = 8.0 Hz, 4H), 2.41 (t, *J* = 7.2 Hz, 2H), 2.62 (t, *J* = 7.6 Hz, 4H), 3.27 (t, *J* = 6.8 Hz, 4H), 3.64 (t, *J* = 7.2 Hz, 2H), 3.85 (s, 3H), 6.85 (dd, *J* = 1.6 Hz, 8.0 Hz, 1H), 6.99 (d, *J* = 8.8 Hz, 2H), 7.09 (bs, 1H), 7.15 (d, *J* = 8.0 Hz, 1H), 7.32 (t, *J* = 8.0 Hz, 1H), 7.51 (d, *J* = 8.0 Hz, 2H).

Procedure D. 2-(4-(4'-methoxybiphenyl-4-yl)piperazin-1-yl)ethanol (6a). Into a stirring solution of compound **5a** (1.5 g, 3.52 mmol) in anhydrous THF (30 mL), *n*-tetrabutylammonium fluoride (0.92 g, 3.52 mmol, 1.0 M solution in THF) was added at 0 °C. The reaction mixture was then stirred at room temperature for 1.5 hour. THF was evaporated in vacuo, the residue was diluted with CH₂Cl₂ (50 mL) and washed with water. The water layer was extracted with CH₂Cl₂ (3 x 75 mL). The combined organic layer was washed with brine, dried over Na₂SO₄, and evaporated in vacuo. The crude product was purified by silica gel column chromatography (EtOAc) to yield compound **6a** (1.04 g, 95%). ¹H NMR (CDCl₃, 400 MHz): δ 2.62 (t, *J* = 5.2 Hz, 2H), 2.70 (t, *J* = 4.8 Hz, 4H), 3.25 (t, *J* = 4.8 Hz, 4H), 3.67 (t, *J* = 5.4 Hz, 2H), 3.83 (s, 3H), 6.95 (d, *J* = 9.2 Hz, 2H), 6.98 (d, *J* = 8.0 Hz, 2H), 7.46 (d, *J* = 8.0 Hz, 2H), 7.48 (d, *J* = 9.2 Hz, 2H).

2-(4-(3'-methoxybiphenyl-4-yl)piperazin-1-yl)ethanol (6b): Compound **5b** (4.0 g, 9.39 mmol) was reacted with *n*-tetrabutylammonium fluoride (2.44 g, 9.39 mmol, 1.0 M solution in THF) in anhydrous THF (100 mL) by following procedure **D** to yield compound **6b** (2.62 g, 90%). ¹H NMR (CDCl₃, 400 MHz): δ 2.61 (t, *J* = 5.2 Hz, 2H),

2.69 (t, $J = 4.0$ Hz, 4H), 3.25 (t, $J = 4.8$ Hz, 4H), 3.67 (t, $J = 6.0$ Hz, 2H), 3.83 (s, 3H), 6.83 (dd, $J = 8.0$ Hz, 2.4 Hz, 1H), 6.99 (d, $J = 8.0$ Hz, 2H), 7.09 (bs, 1H), 7.15 (d, $J = 7.2$ Hz, 1H), 7.31 (t, $J = 8.2$ Hz, 1H), 7.51 (d, $J = 8.0$ Hz, 2H).

2-(4-(2'-methoxybiphenyl-4-yl)piperazin-1-yl)ethanol (6c): Compound **5c** (2.5 g, 5.87 mmol) was reacted with *n*-tetrabutylammonium fluoride (1.53 g, 5.87 mmol, 1.0 M solution in THF) in anhydrous THF (50 mL) by following procedure **D** to yield compound **6c** (1.57 g, 86%). ^1H NMR (CDCl_3 , 400 MHz): δ 2.66 (t, $J = 5.4$ Hz, 2H), 2.74 (t, $J = 4.0$ Hz, 4H), 3.29 (t, $J = 5.0$ Hz, 4H), 3.70 (t, $J = 5.6$ Hz, 2H), 3.83 (s, 3H), 6.95-7.02 (m, 4H), 7.27-7.31 (m, 2H), 7.46 (d, $J = 8.8$ Hz, 2H).

2-(4-(2',5'-dimethoxybiphenyl-4-yl)piperazin-1-yl)ethanol (6d): Compound **5d** (3.8 g, 8.93 mmol) was reacted with *n*-tetrabutylammonium fluoride (2.33 g, 8.93 mmol, 1.0 M solution in THF) in THF (80 mL) using procedure **D** to yield compound **6d** (2.27 g, 80%). ^1H NMR (CDCl_3 , 400 MHz): δ 2.62 (t, $J = 5.0$ Hz, 2H), 2.69 (t, $J = 4.4$ Hz, 4H), 3.26 (t, $J = 4.8$ Hz, 4H), 3.67 (t, $J = 5.0$ Hz, 2H), 3.74 (s, 3H), 3.84 (s, 3H), 6.80 (dd, $J = 9.2$ Hz, 3.6 Hz, 1H), 6.89-6.95 (m, 2H), 6.96 (d, $J = 8.8$ Hz, 2H), 7.46 (d, $J = 8.4$ Hz, 2H).

2-(4-(3',4'-dimethoxy-[1,1'-biphenyl]-4-yl)piperazin-1-yl)ethanol (6e). Into a stirring solution of compound **5e** (3.4 g, 7.46 mmol) in anhydrous THF (30 mL), *n*-tetrabutylammonium fluoride (1.95 g, 7.46 mmol, 1.0 M solution in THF) was added at 0 °C using procedure **D** to yield compound **6e** (2.30 g, 90%). ^1H NMR (CDCl_3 , 400 MHz): δ 2.63 (t, $J = 5.2$ Hz, 2H), 2.70 (t, $J = 4.0$ Hz, 4H), 3.25 (t, $J = 4.0$ Hz, 4H), 3.68 (t, $J = 5.2$ Hz, 2H), 3.91 (s, 3H), 3.94 (s, 3H), 6.92 (d, $J = 8.4$ Hz, 1H), 6.98 (d, $J = 8.4$ Hz, 2H), 7.02-7.16 (m, 2H), 7.47 (d, $J = 8.4$ Hz, 2H).

2-(4-([1,1'-biphenyl]-4-yl)piperazin-1-yl)ethanol (6f): Compound **5f** (2.5 g, 6.30 mmol) was reacted with *n*-tetrabutylammonium fluoride (1.65 g, 6.30 mmol, 1.0 M solution in THF) in THF (50 mL) by following procedure **D** to yield compound **6f** (1.50 g, 80%). ¹H NMR (CDCl₃, 400 MHz): δ 2.69 (t, *J* = 8.0 Hz, 4H), 2.78 (t, *J* = 4.0 Hz, 2H), 3.30 (t, *J* = 4.8 Hz, 4H), 3.72 (t, *J* = 5.6 Hz, 2H), 6.97-7.02 (m, 2H), 7.25-7.30 (m, 1H), 7.38-7.42 (m, 2H), 7.51-7.56 (m, 4H).

4-(4-(3'-methoxy-[1,1'-biphenyl]-4-yl)piperazin-1-yl)butan-1-ol (6g): Compound **5g** (2.6 g, 5.72 mmol) was reacted with *n*-tetrabutylammonium fluoride (1.50 g, 5.72 mmol, 1.0 M solution in THF) in THF (40 mL) by following procedure **D** to yield compound **6g** (1.40 g, 72%). ¹H NMR (CDCl₃, 400 MHz): 1.62 (t, *J* = 8.0 Hz, 4H), 2.41 (t, *J* = 7.2 Hz, 2H), 2.62 (t, *J* = 7.6 Hz, 4H), 3.27 (t, *J* = 6.8 Hz, 4H), 3.64 (t, *J* = 7.2 Hz, 2H), 3.85 (s, 3H), 6.85 (dd, *J* = 1.6 Hz, 8.0 Hz, 1H), 6.99 (d, *J* = 8.8 Hz, 2H), 7.09 (bs, 1H), 7.15 (d, *J* = 8.0 Hz, 1H), 7.32 (t, *J* = 8.0 Hz, 1H), 7.51 (d, *J* = 8.0 Hz, 2H).

Procedure E. 2-(4-(4'-methoxybiphenyl-4-yl)piperazin-1-yl)acetaldehyde (7a). Into a stirred solution of oxalyl chloride (0.324 mL, 2.56 mmol) in CH₂Cl₂ (40 mL) at -78 °C, DMSO (0.40 mL, 5.12 mmol) was added. The reaction mixture was stirred for 10 minutes followed by addition of compound **6a** (400 mg, 1.28 mmol, dissolved in 5 mL of CH₂Cl₂). The reaction mixture was stirred at the same temperature for 15 minutes. Then Et₃N (0.78 mL, 7.68 mmol) was added next and stirring was continued for another 1 hour and 20 minutes while allowing the reaction mixture to reach at room temperature. The reaction mixture was quenched by addition of water and extracted with CH₂Cl₂ (3 x 25 mL). The combined organic layer was washed with brine and concentrated to yield the compound **7a** (321 mg, 81%), which was used without purification in the next step.

2-(4-(3'-methoxybiphenyl-4-yl)piperazin-1-yl)acetaldehyde (7b): Compound **6b** (2.6 g, 8.32 mmol) was reacted with oxalyl chloride (1.43 mL, 16.65 mmol), DMSO (2.36 mL, 33.28 mmol) and Et₃N (6.91 mL, 49.92 mmol) in dichloromethane (50 mL) by following procedure **E** to yield compound **7b** (2.18 g, 85%).

2-(4-(2'-methoxybiphenyl-4-yl)piperazin-1-yl)acetaldehyde (7c): Compound **6c** (500 mg, 1.60 mmol) was reacted with oxalyl chloride (0.41 mL, 3.20 mmol), DMSO (0.50 mL, 6.40 mmol) and Et₃N (0.97 mL, 9.60 mmol) in dichloromethane (40 mL) by following procedure **E** to yield compound **7c** (372 mg, 75%).

2-(4-(2',5'-dimethoxybiphenyl-4-yl)piperazin-1-yl)acetaldehyde(7d): Compound **6d** (1.2 g, 3.50 mmol) was reacted with oxalyl chloride (0.60 mL, 7.0 mmol), DMSO (1.0 mL, 14.0 mmol) and Et₃N (2.91 mL, 21.0 mmol) in dichloromethane (50 mL) using procedure **E** to yield compound **7d** (850 mg, 72%).

2-(4-(3',4'-dimethoxy-[1,1'-biphenyl]-4-yl)piperazin-1-yl)acetaldehyde(7e):

Compound **6e** (500 mg, 1.46 mmol, solution in 5 mL of CH₂Cl₂) was reacted with oxalyl chloride (0.25 mL, 2.92 mmol), DMSO (0.42 mL, 5.84 mmol) and Et₃N (1.2 mL, 8.77 mmol) in CH₂Cl₂ (40 mL) using procedure **E** to yield compound **7e** (402 mg, 81%). ¹H NMR (CDCl₃, 400 MHz): δ 2.40-2.80 (m, 4H), 2.82-3.50 (m, 6H), 3.92 (s, 3H), 3.95 (s, 3H), 6.93 (d, *J* = 8 Hz, 1H), 6.98 (d, *J* = 7.6 Hz, 2H), 7.03-7.16 (m, 2H), 7.48 (d, *J* = 6.8 Hz, 2H).

2-(4-([1,1'-biphenyl]-4-yl)piperazin-1-yl)acetaldehyde (7f) : Compound **6f** (1.3 g, 4.60 mmol) was reacted with oxalyl chloride (0.79 mL, 9.21 mmol), DMSO (1.30 mL, 18.4 mmol) and Et₃N (3.82 mL, 27.60 mmol) in dichloromethane (40 mL) by following procedure **E** to yield compound **7f** (1.0 g, 78%).

4-(4-(3'-methoxy-[1,1'-biphenyl]-4-yl)piperazin-1-yl)butanal (7g): Compound **6g** (1.2 g, 3.52 mmol) was reacted with oxalyl chloride (0.60 mL, 7.05 mmol), DMSO (1.00 mL, 14.08 mmol) and Et₃N (2.92 mL, 21.12 mmol) in dichloromethane (30mL) by following procedure **E** to yield compound **7g** (0.89 g, 75%).

Procedure F. N6-(2-(4-(4'-methoxybiphenyl-4-yl)piperazin-1-yl)ethyl)-N6-propyl-4,5,6,7-tetrahydrobenzo[d]thiazole-2,6-diamine (±)(8a). Into a stirring solution of compound **7a** (321 mg, 1.03 mmol) in CH₂Cl₂ (10 mL), (±)-pramipexole (219 mg, 1.03 mmol) was added at room temperature. The reaction mixture was stirred for 1 hour and then NaBH(OAc)₃ (393 mg, 1.85 mmol) was added into the reaction mixture. After stirring for 48 hours, saturated solution of NaHCO₃ was added into the reaction mixture and it was extracted with CH₂Cl₂ (3 x 50 mL). The combined organic layer was washed with brine and finally purified by silica gel column chromatography (EtOAc/MeOH, 9:1) to yield compound (±)-**8a** (313 mg, 60%). ¹H NMR (CDCl₃, 400 MHz): δ 0.91 (t, *J* = 7.2 Hz, 3H), 1.52-1.56 (m, 2H), 1.76-1.79 (m, 1H), 2.06 (d, *J* = 8.8 Hz, 1H), 2.59-2.80 (m, 13H), 3.17-3.26 (m, 6H), 3.84 (s, 3H), 6.91-7.01(m, 4H), 7.42-7.49 (m, 4H).The product was converted into corresponding hydrochloride salt, m.p.268 °C. Anal. (C₂₉H₃₉N₅OS · 4.0 HCl · 2.0 H₂O) : C, H, N.

N6-(2-(4-(3'-methoxybiphenyl-4-yl)piperazin-1-yl)ethyl)-N6-propyl-4,5,6,7-tetrahydrobenzo[d]thiazole-2,6-diamine ((±)-8b): Compound **7b** (250 mg, 0.80 mmol) was reacted with (±)-pramipexole (169 mg, 0.80 mmol) and NaBH(OAc)₃ (305.19 mg, 1.44 mmol) in dichloromethane (30 mL) by following procedure **F** to yield compound (±)**8b** (263 mg, 65%). ¹H NMR (CDCl₃, 400 MHz): δ 0.89 (t, *J* = 7.2 Hz, 3H), 1.46-1.51 (m, 2H), 1.63-1.77 (m, 1H), 1.90 (d, *J* = 11.6 Hz, 1H), 2.42-2.73 (m, 13H), 3.06-3.26 (m, 6H), 3.84 (s, 3H), 5.05 (bs, 2H), 6.82 (d, *J* = 8.0 Hz, 1H), 6.96 (d, *J* = 8.4 Hz, 2H), 7.08 (bs, 1H), 7.14 (d, *J* = 7.6 Hz, 1H), 7.31 (t, *J* = 8.0 Hz,

1H), 7.50 (d, $J = 8.4$ Hz, 2H). The product was converted into corresponding hydrochloride salt, m.p. 255 °C. Anal. ($C_{29}H_{39}N_5OS \cdot 4.0$ HCl \cdot 1.0 H_2O): C, H, N.

(S)-N6-(2-(4-(3'-methoxybiphenyl-4-yl)piperazin-1-yl)ethyl)-N6-propyl-4,5,6,7-tetrahydrobenzo[d]thiazole-2,6-diamine ((-)-8b): Compound **7b** (500 mg, 1.61 mmol) was reacted with **(-)-pramipexole** (340.24 mg, 1.61 mmol) and $NaBH(OAc)_3$ (612.50 mg, 2.89 mmol) in dichloromethane (100 mL) by following procedure **F** to yield compound **(-)-8b** (526 mg, 65%). $[\alpha]_D = -34.6$ ($c = 1$, CH_3OH). Spectral data matching with compound **(±)8b**. The product was converted into corresponding hydrochloride salt, m.p. 245 °C. Anal. ($C_{29}H_{39}N_5OS \cdot 4.0$ HCl \cdot 1.0 H_2O): C, H, N.

(R)-N6-(2-(4-(3'-methoxybiphenyl-4-yl)piperazin-1-yl)ethyl)-N6-propyl-4,5,6,7-tetrahydrobenzo[d]thiazole-2,6-diamine ((+)-8b): Compound **7b** (100 mg, 0.322 mmol) was reacted with **(+)-pramipexole** (68.04 mg, 0.322 mmol) and $NaBH(OAc)_3$ (122.84 mg, 0.579 mmol) in dichloromethane (20 mL) by following procedure **F** to yield compound **(+)-8b** (105 mg, 65%). Spectral data matching with compound **(±)8b**.

N6-(2-(4-(2'-methoxybiphenyl-4-yl)piperazin-1-yl)ethyl)-N6-propyl-4,5,6,7-tetrahydrobenzo[d]thiazole-2,6-diamine ((±)-8c): Compound **7c** (372 mg, 1.19 mmol) was reacted with **(±)-pramipexole** (251.48 mg, 1.19 mmol) and $NaBH(OAc)_3$ (453.60 mg, 2.14 mmol) in dichloromethane (40 mL) by following procedure **F** to yield compound **(±)8c** (391 mg, 65%). 1H NMR ($CDCl_3$, 400 MHz): δ 0.89 (t, $J = 7.2$ Hz, 3H), 1.42-1.50 (m, 2H), 1.66-1.77 (m, 1H), 1.99 (d, $J = 10.8$ Hz, 1H), 2.41-2.76 (m, 13H), 3.02-3.27 (m, 6H), 3.79 (s, 3H), 4.83 (bs, 2H), 6.94-6.97 (m, 2H), 6.99 (dd, $J = 1.2$ Hz, $J = 7.6$ Hz, 2H), 7.24-7.31 (m, 2H), 7.43-7.46 (m, 2H). The product was converted into corresponding hydrochloride salt, m.p. 255 °C. Anal.

(C₂₉H₃₉N₅OS · 4.0 HCl · 1.0 CH₃COOCH₂CH₃) : C, H, N. MS(ES⁺): m/z calculated for C₂₉H₃₉N₅OS [M+H⁺]: calculated 505.29; found 506.56.

N⁶-(2-(4-(2',5'-dimethoxybiphenyl-4-yl)piperazin-1-yl)ethyl)-N⁶-propyl-4,5,6,7-tetrahydrobenzo[d]thiazole-2,6-diamine ((±)-8d): Compound **7d** (200 mg, 0.585 mmol) was reacted with (±)-**pramipexole** (123.62 mg, 0.585 mmol) and NaBH(OAc)₃ (223 mg, 1.05 mmol) in dichloromethane (10 mL) using procedure **F** to yield compound (±)**8d** (205 mg, 65%). ¹H NMR (CDCl₃, 400 MHz): δ 0.92 (t, *J* = 7.6 Hz, 3H), 1.52-1.61 (m, 2H), 1.73-1.77 (m, 1H), 2.03 (d, *J* = 4.0 Hz, 2H), 2.41-2.89 (m, 13 H), 3.00 -3.17 (m, 5H), 3.73 (s, 3H), 3.84 (s, 3H), 4.76 (bs, 2H), 6.79 (dd, *J* = 8.8 Hz, 3.2 Hz, 1H), 6.87-6.95 (m, 2H), 6.94 (d, *J* = 8.8 Hz, 2H), 7.44 (d, *J* = 8.8 Hz, 2H).

(S)-N⁶-(2-(4-(2',5'-dimethoxybiphenyl-4-yl)piperazin-1-yl)ethyl)-N⁶-propyl-4,5,6,7-tetrahydrobenzo[d]thiazole-2,6-diamine ((-)-8d): Compound **7d** (435 mg, 1.27 mmol) was reacted with (-)-**pramipexole** (268 mg, 1.27 mmol) and NaBH(OAc)₃ (485 mg, 2.28 mmol) in dichloromethane (50 mL) using procedure **F** to yield compound (-)**8d** (424 mg, 60%). Spectral data matching with compound (±)**8b**.

(R)-N⁶-(2-(4-(2',5'-dimethoxy-[1,1'-biphenyl]-4-yl)piperazin-1-yl)ethyl)-N⁶-propyl-4,5,6,7-tetrahydrobenzo[d]thiazole-2,6-diamine ((+)-8d): Compound **7d** (200 mg, 0.585 mmol) was reacted with (+)-**pramipexole** (123.62 mg, 0.585 mmol) and NaBH(OAc)₃ (223 mg, 1.05 mmol) in dichloromethane (10 mL) using procedure **F** to yield compound (+)**8d** (203 mg, 65%). Spectral data matching with compound (±)**8b**.

N⁶-(2-(4-(3',4'-dimethoxy-[1,1'-biphenyl]-4-yl)piperazin-1-yl)ethyl)-N⁶-propyl-4,5,6,7-tetrahydrobenzo[d]thiazole-2,6-diamine ((±)-8e): Compound **7e** (402 mg, 1.18 mmol) was reacted with (±)-**pramipexole** (275 mg, 1.30 mmol) and

NaBH(OAc)₃ (451 mg, 2.13 mmol) in dichloromethane (10 mL) using procedure **F** to yield compound (443 mg, 70%) of compound (±)-**8e**. ¹H NMR (CDCl₃, 400 MHz): δ 0.89 (t, *J* = 7.6 Hz, 3H); 1.38-1.60 (m, 2H); 1.62-1.82 (m, 1H); 1.86-2.10 (m, 2H), 2.35-2.84 (m, 12 H), 2.94-3.62 (m, 5H); 3.90 (s, 3H), 3.93 (s, 3H), 6.91 (d, *J* = 8 Hz, 1H); 6.90 (d, *J* = 8.4 Hz, 2H), 7.04-7.14 (m, 2H), 7.46 (d, *J* = 8.8 Hz, 2H).

(S)-N6-(2-(4-(3',4'-dimethoxybiphenyl-4-yl)piperazin-1-yl)ethyl)-N6-propyl-4,5,6,7-tetrahydrobenzo[d]thiazole-2,6-diamine ((-)-8e): Compound **7e** (200 mg, 0.587 mmol) was reacted with (-)-pramipexole (124 mg, 0.587 mmol) and NaBH(OAc)₃ (225 mg, 1.06 mmol) in dichloromethane (30 mL) using procedure **F** to yield compound (-)-**8e** (218 mg, 70%). ¹H NMR (CDCl₃, 400 MHz): δ 0.89 (t, *J* = 7.6 Hz, 3H); 1.38-1.60 (m, 2H); 1.62-1.82 (m, 1H); 1.86-2.10 (m, 2H), 2.35-2.84 (m, 13H), 2.94-3.62 (m, 5H); 3.90 (s, 3H), 3.93 (s, 3H), 6.91 (d, *J* = 8 Hz, 1H); 6.96 (d, *J* = 8.4 Hz, 2H), 7.04-7.14 (m, 2H), 7.46 (d, *J* = 8.8 Hz, 2H).

(R)-N6-(2-(4-(3',4'-dimethoxybiphenyl-4-yl)piperazin-1-yl)ethyl)-N6-propyl-4,5,6,7-tetrahydrobenzo[d]thiazole-2,6-diamine ((+)-8e): Compound **7e** (100 mg, 0.293 mmol) was reacted with (+)-pramipexole (51 mg, 0.293 mmol) and NaBH(OAc)₃ (112 mg, 0.53 mmol) in dichloromethane (20 mL) using procedure **F** to yield compound (+)-**8e** (100 mg, 64%). Spectral data matching with compound (-) **8e**.

N6-(4-(4-(3'-methoxy-[1,1'-biphenyl]-4-yl)piperazin-1-yl)butyl)-N6-propyl-4,5,6,7-tetrahydrobenzo[d]thiazole-2,6-diamine ((±)-8f): Compound **7g** (600 mg, 1.77 mmol) was reacted with (±)-pramipexole (375mg, 1.77mmol) and NaBH(OAc)₃ (675mg, 3.18 mmol) in dichloromethane (25 mL) by following procedure **F** to yield compound (±)**8f** (586 mg, 62%). ¹H NMR (CDCl₃, 400 MHz): δ 0.89 (t, *J* = 7.2 Hz, 3H), 1.39-1.74 (m, 6H), 2.01-2.21 (m, 1H), 2.44-2.68 (m, 13H), 3.11-3.26 (m, 6H),

3.46 (s, 1H), 3.84 (s, 3H), 4.91 (bs, 2H), 6.82 (dd, $J = 2.4$ Hz, 8.0 Hz, 1H), 6.97 (d, $J = 8.8$ Hz, 2H), 7.08 (bs, 1H), 7.14 (d, $J = 8.0$ Hz, 1H), 7.31 (t, $J = 7.6$ Hz, 1H), 7.50 (d, $J = 8.8$ Hz, 2H).

Procedure G. 4'-(4-(2-((2-amino-4,5,6,7-tetrahydrobenzo[d]thiazol-6-yl)(propyl)amino)ethyl)piperazin-1-yl)-[1,1'-biphenyl]-4-ol ((±)-9a): Into a stirring solution of compound (±)-8a (60 mg, 0.11 mmol) in anhydrous CH₂Cl₂ (10 mL) at -78° C, boron tribromide (1.1 mL, 1.1 mmol, 1M solution in CH₂Cl₂) was added. The reaction mixture was allowed to come to room temperature and was stirred for 48 hrs. The reaction was quenched by addition of saturated NaHCO₃ solution, and the mixture was extracted with CH₂Cl₂. The combined organic layer was dried over Na₂SO₄ and evaporated under vacuum, and the crude product was purified by flash chromatography (CH₂Cl₂/MeOH = 9:1) to afford compound (±)-9a (0.029 g, 50%). ¹H NMR (CDCl₃, 400 MHz): δ 0.96 (t, $J = 7.2$ Hz, 3H), 1.60-1.64 (m, 2H), 1.81-1.85 (m, 1H), 2.08 (d, $J = 7.2$ Hz, 1H), 2.52-3.04 (m, 13H), 3.11-3.24 (m, 6H), 6.81(d, $J = 8.4$ Hz, 2H), 7.00 (d, $J = 8.8$ Hz, 2H), 7.38 (d, $J = 8.4$ Hz, 2H), 7.43 (d, $J = 8.8$ Hz, 2H). The product was converted into corresponding hydrochloride salt, m.p.272 °C. Anal. (C₂₈H₃₇N₅OS · 4.0 HCl · 1.0 H₂O) : C, H, N.

4'-(4-(2-((2-amino-4,5,6,7-tetrahydrobenzo[d]thiazol-6-yl)(propyl)amino)ethyl)piperazin-1-yl)-[1,1'-biphenyl]-3-ol ((±)-9b): A mixture of compound (±)-8b (70 mg, 0.13 mmol) in anhydrous CH₂Cl₂ (10 mL) at -78° C, boron tribromide (1.04 mL, 1.04 mmol, 1M solution in CH₂Cl₂) was added as followed by procedure G to yield (±)-9b (40 mg, 60%). The product was converted into corresponding hydrochloride salt, m.p.265 °C. ¹H NMR of HCl salt (CDCl₃, 400 MHz): δ 1.07 (t, $J = 7.2$ Hz, 3H), 1.89-1.95 (m, 2H), 2.13-2.21 (m, 1H), 2.49 (d, $J = 12.0$ Hz, 1H) 2.80 (m, 2H), 2.96-3.32 (m, 4H), 3.38-3.99 (m, 13H), 6.71 (dd, $J = 8.0$

Hz, 1.6 Hz, 1H), 6.98 (bs, 1H), 7.03 (d, $J = 7.2$ Hz, 1H), 7.13-7.24 (m, 3H), 7.55 (d, $J = 8.8$ Hz, 2H). **Anal.** ($C_{28}H_{37}N_5OS \cdot 4.0$ HCl $\cdot 1.0$ H₂O): **C, H, N.** MS(ES⁺): m/z calculated for $C_{28}H_{37}N_5OS$ [$M+H^+$]: calculated 491.27; found 492.52.

Procedure H: (S)-4'-(4-(2-((2-amino-4,5,6,7-tetrahydrobenzo[d]thiazol-6-yl)(propyl)amino)ethyl)piperazin-1-yl)biphenyl-3-ol ((-)-9b): Compound (-)-8b (200 mg, 0.98 mmol) and 48% aqueous HBr (15 ml) was refluxed for 12 hours. The reaction mixture was then evaporated to dryness in vacuo. The crude mixture was then washed with diethylether and finally recrystallized from ethanol to afford compound (-)-9b (246 mg, 70%, recrystallized from ethanol). ¹H NMR of HBr salt (CD₃OD, 400 MHz): δ 1.08 (t, $J = 7.2$ Hz, 3H), 1.94-2.06 (m, 2H), 2.22-2.27 (m, 1H), 2.55 (d, $J = 10.4$ Hz, 1H) 2.83 (m, 2H), 2.99-3.39 (m, 4H), 3.52-4.20 (m, 13H), 6.73 (dd, $J = 8.0$ Hz, 1.6 Hz, 1H), 7.00 (bs, 1H), 7.04 (d, $J = 7.6$ Hz, 1H), 7.20-7.24 (m, 3H), 7.57 (d, $J = 8.8$ Hz, 2H). $[\alpha]_d = -21.0$ (c=0.5, CH₃OH). Hydrobromide salt, m.p.270 °C. **Anal.** ($C_{28}H_{37}N_5OS \cdot 5.0$ HBr) : **C, H, N.**

(R)-4'-(4-(2-((2-amino-4,5,6,7-tetrahydrobenzo[d]thiazol-6-yl)(propyl)amino)ethyl)piperazin-1-yl)biphenyl-3-ol ((+)-9b): Compound (+)-8b (100 mg, 0.20 mmol) and 48% aqueous HBr (10 ml) was refluxed for 12 hours by following procedure H to afford compound (+)-9b (105 mg, 60%, recrystallized from ethanol). Spectral data matching with compound (-)-9b. $[\alpha]_d = +16.0$ (c =0.5, CH₃OH). Hydrobromide salt, m.p.270 °C. **Anal.** ($C_{28}H_{37}N_5OS \cdot 5.0$ HBr $\cdot 1.0$ H₂O) : **C, H, N.**

4'-(4-(2-((2-amino-4,5,6,7-tetrahydrobenzo[d]thiazol-6-yl)(propyl)amino)ethyl)-piperazin-1-yl)biphenyl-2-ol ((±)-9c): Into the mixture of Compound (±)-8c (100 mg, 0.197 mmol) in anhydrous CH₂Cl₂ (10 mL) at -78° C, boron tribromide (1.38 mL,

1.38 mmol, 1M solution in CH₂Cl₂) was added as followed by procedure **G** to yield (**±**)-**9c** (53 mg, 55%). ¹H NMR (CDCl₃, 400 MHz): δ 0.90 (t, *J* = 7.2 Hz, 3H), 1.45-1.51 (m, 2H), 1.66-1.77 (m, 1H), 1.93-2.02 (m, 1H), 2.62-3.12 (m, 13H), 3.16-3.66 (m, 6H), 6.84-6.89 (m, 2H), 7.01 (d, *J* = 8.8 Hz, 2H), 7.07-7.11 (m, 1H), 7.20 (dd, *J* = 1.2 Hz, *J* = 7.6 Hz, 1H), 7.47(d, *J* = 8.4 Hz, 2H). The product was neutralized and converted into corresponding hydrochloride salt, m.p.270 °C. Anal. (C₂₈H₃₇N₅OS · 4.0 HCl · 2.0 H₂O) : C, H, N.

4'-(4-(2-((2-amino-4,5,6,7-tetrahydrobenzo[d]thiazol-6-

yl)(propyl)amino)ethyl)piperazin-1-yl)biphenyl-2,5-diol ((±**)-**9d**):** Compound (**±**)-**8d** (200 mg, 0.37 mmol) and 48% aqueous HBr (10 ml) was refluxed for 12 hours using procedure **H** to afford compound (**±**)-**9d** (243 mg, 71%, recrystallized from ethanol). ¹H NMR of HBr salt (CD₃OD, 400 MHz): δ 1.07 (t, *J* = 7.6 Hz, 3H), 1.91-1.97 (m, 2H), 2.12-2.30 (m, 1H), 2.50 (d, *J* = 8.0 Hz, 1H) 2.81 (m, 2H), 3.0-3.12 (m, 4H), 3.54-4.08 (m, 13H), 6.58 (dd, *J* = 8.8 Hz, 3.2 Hz, 1H), 6.68-6.72 (m, 2H), 7.20-7.28 (m, 2H), 7.56 (d, *J* = 8.0 Hz, 2H). Hydrobromide salt, m.p.265 °C. Anal. (C₂₈H₃₇N₅O₂S · 4.5 HBr · 0.55 C₂H₅OC₂H₅) : C, H, N.

(S)-4'-(4-(2-((2-amino-4,5,6,7-tetrahydrobenzo[d]thiazol-6-yl)(propyl)amino)ethyl)piperazin-1-yl)biphenyl-2,5-diol ((-)-9d**):** Compound (-)-**8d** (400 mg, 0.75 mmol) and 48% aqueous HBr (25 ml) was refluxed for 12 hours using procedure **H** to afford compound (-)-**9d** (439 mg, 65%, recrystallized from ethanol). Spectral data matching with compound (**±**)-**9d**. [α]_D = -18.0 (c = 0.1, CH₃OH). Hydrobromide salt, m.p.265 °C. Anal. (C₂₈H₃₇N₅O₂S · 5.0 HBr · 0· 7H₂O) : C, H, N.

(R)-4'-(4-(2-((2-amino-4,5,6,7-tetrahydrobenzo[d]thiazol-6-

yl)(propyl)amino)ethyl)piperazin-1-yl)-[1,1'-biphenyl]-2,5-diol ((+)-9d**):** Compound (+)-**8d** (150 mg, 0.280 mmol) and 48% aqueous HBr (5 ml) was refluxed

for 12 hours using procedure **H** to afford compound **(+)-9d** (180 mg, 70%, recrystallized from ethanol). Spectral data matching with compound **(±)-9d**. $[\alpha]_d = +15.0$ ($c = 0.1$, CH₃OH). Hydrobromide salt, m.p. 265 °C. Anal. (C₂₈H₃₇N₅O₂S · 5.0 HBr · 0.6 C₂H₅O C₂H₅) : C, H, N.

4'-(4-{2-[(2-Amino-4,5,6,7-tetrahydro-benzothiazol-6-yl)-propyl-amino]-ethyl}-piperazin-1-yl)-biphenyl-3,4-diol ((±)-9e). A mixture of compound **8e** (200 mg, 0.37 mmol) and 48% aqueous HBr (10 ml) was refluxed for 6 hours using procedure **H** to afford compound **(±)-9e** (145 mg, 65%). Mp 209-214 °C. ¹H NMR (CD₃OD, 400 MHz): δ 1.07 (t, $J = 7.2$ Hz, 3H), 1.88-2.06 (m, 2H), 2.12-2.30 (m, 1H), 2.55 (d, $J = 10$ Hz, 1H) 2.74-2.90 (m, 2H), 2.95-3.46 (m, 4H), 3.52-4.20 (m, 13H), 6.82 (d, $J = 8.0$ Hz, 1H), 6.93 (dd, $J = 8.4$ Hz, 1.6 Hz, 1H), 7.03 (d, $J = 1.6$ Hz, 1H), 7.27 (d, $J = 8.4$ Hz, 2H), 7.54 (d, $J = 8.8$ Hz, 2H). ¹³C NMR (CD₃OD, 100 MHz): δ 11.3, 19.0, 19.7, 22.9, 23.5, 24.4, 47.0, 50.0, 51.7, 53.0, 55.0, 61.2, 113.1, 114.7, 116.8, 119.2, 119.6. Anal. calculated for C₂₈H_{45.8}Br₅N₅O_{3.9}S: C, H, N.

(S)-4'-(4-(2-((2-amino-4,5,6,7-tetrahydrobenzo[d]thiazol-6-yl)(propyl)amino)ethyl)piperazin-1-yl)biphenyl-3,4-diol ((-)-9e): Compound **(-)-8e** (200 mg, 0.37 mmol) and 48% aqueous HBr (10 ml) was refluxed for 12 hours using procedure **H** to afford compound **(-)-9e** (219 mg, 65%, recrystallized from ether and ethanol mixture). ¹H NMR (CD₃OD, 400 MHz): δ 1.07 (t, $J = 7.2$ Hz, 3H), 1.88-2.06 (m, 2H), 2.12-2.30 (m, 1H), 2.55 (d, $J = 10$ Hz, 1H) 2.74-2.90 (m, 2H), 2.95-3.46 (m, 4H), 3.52-4.20 (m, 13H), 6.82 (d, $J = 8.0$ Hz, 1H), 6.93 (dd, $J = 8.4$ Hz, 1.6 Hz, 1H), 7.03 (d, $J = 1.6$ Hz, 1H), 7.27 (d, $J = 8.4$ Hz, 2H), 7.54 (d, $J = 8.8$ Hz, 2H). $[\alpha]_d = -18.56$ ($c = 0.6$, CH₃OH). Hydrobromide salt, m.p. 260 °C. Anal. (C₂₈H₃₇N₅ O₂S · 4.5 HBr · 0.7C₂H₅O C₂H₅) : C, H, N.

(R)-4'-(4-(2-((2-amino-4,5,6,7-tetrahydrobenzo[d]thiazol-6-**yl)(propyl)amino)ethyl)piperazin-1-yl)biphenyl-3,4-diol ((+)-9e):** Compound **(+)-****8e** (100 mg, 0.19 mmol) and 48% aqueous HBr (10 ml) was refluxed for 12 hours using procedure **H** to afford compound **(+)-9e** (119 mg, 70%, recrystallized from ethanol). Spectral data matching with compound **(-)-9e**. $[\alpha]_D^{25} = +20.69$ (c = 0.6, CH₃OH).. Hydrobromide salt, m.p. 260 °C. Anal. (C₂₈H₃₇N₅ O₂S · 4.5 HBr · 0.6C₂H₅OC₂H₅) : C, H, N.**4'-(4-(4-((2-amino-4,5,6,7-tetrahydrobenzo[d]thiazol-6-yl)(propyl)amino)-****butyl)piperazin-1-yl)-[1,1'-biphenyl]-3-ol ((±)-9f):** Compound **(±)8f** (200 mg, 0.38mmol) and 48% aqueous HBr (5 ml) was refluxed for 12 hours using procedure **H** to afford compound **(±)-9f** (248 mg, 72%, recrystallized from ethanol). ¹H NMR of HBr salt (CD₃OD, 400 MHz): δ 1.05 (t, *J* = 7.2 Hz, 3H), 1.86-2.16 (m, 6H), 2.45 (bs, 1H), 2.79 (bs, 2H), 2.96-3.94 (m, 18H), 6.73 (dd, *J* = 2.4 Hz, 8.0 Hz, 1H), 7.00 (bs, 1H), 7.04 (d, *J* = 8.0 Hz, 1H), 7.20-7.24 (m, 3H), 7.57 (t, *J* = 7.2 Hz, 2H). m.p. 245 °C. Anal. (C₃₀H₄₁N₅OS · 5.0 HBr · 2.0 H₂O · 1.0 C₂H₅OC₂H₅) : C, H, N. MS(ES⁺): *m/z* calculated for C₃₀H₄₁N₅OS [M+H⁺]: calculated 519.30; found 520.59.**2-(4-(4-(2-((2-amino-4,5,6,7-tetrahydrobenzo[d]thiazol-6-****yl)(propyl)amino)ethyl)piperazin-1-yl)phenyl)cyclohexa-2,5-diene-1,4-dione (±)-****10):** Into the solution of free base of the compound **(±)-9d** (200 mg, 0.396 mmol) in dichloromethane (10 mL), was reacted with MnO₂ (140 mg, 1.58 mmol) for 1 hr. at r.t. The reaction mixture was filtered through celite. The crude compound thus obtained was further purified through silica gel column chromatography (CH₂Cl₂/MeOH, 9:2) to afford compound **(±)-10** (129 mg, 65%). NMR (CDCl₃, 400 MHz): δ 0.88 (t, *J* = 7.2 Hz, 3H), 1.47-1.53 (m, 2H), 1.71-1.75 (m, 1H), 2.01 (d, *J* = 10.0 Hz, 1H), 2.54-2.73 (m, 14H), 3.10-3.30 (m, 5H), 4.85 (bs, 2H), 6.77-6.81 (m,

3H), 6.90 (d, $J = 9.2$ Hz, 2H). 7.46 (d, $J = 8.8$ Hz, 2H). The product was converted into corresponding hydrochloride salt, m.p. 270 °C. Anal. ($C_{28}H_{35}N_5 O_2S \cdot 5.0 HCl \cdot 2.6 H_2O \cdot 0.7 C_2H_5OC_2H_5$): C, H, N.

Procedure I: 1-(2-methoxyphenyl)piperazine (12a): A stirring solution of 2-methoxyaniline **11a** (31.60 g, 256.91 mmol) and *bis*(2-chloroethyl)amine (45.85 g, 256.91 mmol) was heated at 150 °C in diethylene glycol monomethyl ether (100 mL) for 6 hours. After being cooled to room temperature, the mixture was dissolved in MeOH (4 mL) followed by addition of Et₂O (300 mL). The precipitate was filtered off and washed with Et₂O to provide HCl salt. The HCl salt was further converted to free amine by treatment with Na₂CO₃ solution and extracted with EtOAc (2 × 100 mL). The combined organic layers were dried over Na₂SO₄, and concentrated in vacuo to provide the pure free amine product **12a** (34.34 g, 70%). ¹H NMR (CDCl₃, 400 MHz): δ 3.12 (t, $J = 7.6$ Hz, 4H), 3.37 (t, $J = 6.4$ Hz, 4H), 3.79 (s, 3H), 6.86 (t, $J = 7.6$ Hz, 1.6 Hz, 1H), 6.93 (t, $J = 4.8$ Hz, 2H), 6.94-7.07 (m, 1H).

1-(2,5-dimethoxyphenyl)piperazine (12b): Commercially available, 2,5-dimethoxyaniline **11b** (10.0 g, 65.32 mmol) and *bis*(2-chloroethyl)amine (11.65 g, 65.32 mmol) was heated at 150 °C in diethylene glycol monomethyl ether (100 mL) following the procedure I to yield compound **12b** (9.28 gm, 65 % yield). ¹H NMR (CDCl₃, 400 MHz): δ 3.07 (d, $J = 5.2$ Hz, 8H), 3.75 (s, 3H), 3.81 (s, 3H), 6.46-6.54 (m, 2H), 6.76 (d, $J = 8.4$ Hz, 1H).

Procedure J: 1-(4-bromo-2-methoxyphenyl)piperazine (13a): Amine **12a** (15.0 g, 78.07 mmol) was dissolved in CH₂Cl₂ (200 ml) and cooled to 0 °C. Bromine (4.02 ml, 78.07 mmol) was added dropwise into the above solution. After 2 hrs, reaction mixture was washed with 1N sodium hydroxide and the organic layer was separated,

dried over Na_2SO_4 , and concentrated in vacuo to yield **13a** (16.86 gm, 80 % yield). The crude product **13a** thus obtained was converted into its Boc derivative without further purification.

1-(4-iodo-2,5-dimethoxyphenyl)piperazine (13b): Amine **12b** (8.0 g, 36.0 mmol) was reacted with ICl (5.84 g, 36.0 mmol) in acetic acid/water (3:1, 100 ml) at 55 °C. The reaction was stirred at 55 °C for 1 h and then at room temperature for another 1 h. The solution was poured into 400 mL of crushed ice and the pH was adjusted to 13 with 4 N NaOH. The product was then extracted with dichloromethane (3 x 100 mL). The combined organic layer was dried over Na_2SO_4 , filtered and evaporated in vacuo to provide the free amine of compound. The crude product **13b** (9.98 g, 80%) thus obtained was converted into its Boc derivative without further purification.

Procedure K: tert-butyl 4-(4-bromo-2-methoxyphenyl)piperazine-1-carboxylate (14a): Into a stirring solution of amine **13a** (14.0 g, 51.84 mmol) in dichloromethane (40 mL), $(\text{Boc})_2\text{O}$ (11.31 g, 51.84 mmol) and Et_3N (21.55 mL, 155.52 mmol) were added at room temperature. The reaction mixture was stirred at the same temperature for 12 hours and was extracted with CH_2Cl_2 (3 x 100 mL), washed with water, dried over Na_2SO_4 , filtered, and concentrated. The crude material was purified by column chromatography over silica gel (Hexane/EtOAc, 8:2) to give compound **14a** (16.30 g, 85%). ^1H NMR (CDCl_3 , 400 MHz): δ 1.49 (s, 9H), 2.95 (t, J = 4.4 Hz, 4H), 3.58 (t, J = 5.2 Hz, 4H), 3.86 (s, 3H), 6.75 (d, J = 8.4 Hz, 1H), 6.97 (d, J = 2.0 Hz, 1H), 7.58 (dd, J = 8.4 Hz, 2.0 Hz, 1H).

tert-butyl 4-(4-iodo-2,5-dimethoxyphenyl)piperazine-1-carboxylate (14b). Amine, **13b**, (9.0 g, 25.85 mmol) in dichloromethane (100 mL), $(\text{Boc})_2\text{O}$ (5.64 g, 25.85 mmol) and Et_3N (10.75 mL, 77.57 mmol) were reacted followed by procedure

K to give compound **14b** (11.0 g, 95%). ^1H NMR (CDCl_3 , 400 MHz): δ 1.49 (s, 9H), 2.98 (bs, 4H), 3.61 (t, $J=4.0$, 4H), 3.81 (s, 3H), 3.83 (s, 3H), 6.52 (s, 1H), 7.01 (s, 1H).

tert-butyl 4-(3-methoxybiphenyl-4-yl)piperazine-1-carboxylate (15a):

Commercially available, phenylboronic acid (2.63 g, 21.61 mmol) was reacted with bromo compound **14a** (8.0 g, 21.61 mmol), Na_2CO_3 (4.58 g, 43.22 mmol, 2 M solution in water) and $\text{Pd}(\text{PPh}_3)_4$ (1.24 g, 0.75 mmol) in dimethoxy ethane/ethanol (30 mL:30 mL) by following procedure **A** to yield compound **15a** (5.17g, 65% yield). ^1H NMR (CDCl_3 , 400 MHz): δ 1.49 (s, 9H), 3.04 (t, $J = 4.4$ Hz, 4H), 3.63 (t, $J = 4.8$ Hz, 4H), 3.92 (s, 3H), 6.96 (d, $J = 8.0$ Hz, 1H), 7.08 (d, $J = 2.0$ Hz, 1H), 7.15 (dd, $J = 8.4$ Hz, 2.0 Hz, 1H), 7.29-7.32 (m, 1H), 7.41 (t, $J = 7.6$ Hz, 2H), 7.56 (d, $J = 7.20$ Hz, 2H).

tert-butyl 4-(2,5-dimethoxybiphenyl-4-yl)piperazine-1-carboxylate (15b):

Commercially available benzene boronic acid (2.72 g, 22.31 mmol) was reacted with iodo compound **14b** (10.0 g, 22.31 mmol), $\text{Pd}(\text{PPh}_3)_4$ (1.28 g, 1.11 mmol) and Na_2CO_3 (4.72 g, 44.62 mmol) in a mixture of solvent dimethoxy ethane and ethanol (40 mL : 40 mL) followed by procedure **A** to afford compound **15b** (6.16 g, 70%). ^1H NMR (CDCl_3 , 400 MHz): δ 1.49 (s, 9H), 3.07 (t, $J = 4.4$ Hz, 4H), 3.62 (t, $J = 5.2$ Hz, 4H), 3.75 (s, 3H), 3.87 (s, 3H), 6.60 (s, 1H), 6.85 (s, 1H), 7.23-7.31 (m, 1H), 7.39 (t, $J=8.0$,2H),7.53 (d, $J=7.2$, 2H).

1-(3-methoxy-[1,1'-biphenyl]-4-yl)piperazine (16a). Compound **15a** (6.2 g, 16.83 mmol) was reacted with TFA (20 mL) in CH_2Cl_2 (20 mL) by following procedure **B** to give compound **15a** (4.0 g, 90%). ^1H NMR (CDCl_3 , 400 MHz): δ 2.77 (bs, 1H), 3.08 (t, $J = 4.8$ Hz, 4H), 3.18 (t, $J = 5.6$ Hz, 4H), 3.92 (s, 3H), 6.84 (dd, $J = , 2.4$ Hz, 8.0

Hz 1H), 6.94 (d, $J = 8.0$ Hz, 1H), 6.98 (t, $J = 4.8$ Hz, 1H), 7.29-7.34 (m, 1H), 7.44 (t, $J = 7.2$ Hz, 2H), 7.56 (d, $J = 7.6$ Hz, 2H).

1-(2,5-dimethoxy-[1,1'-biphenyl]-4-yl)piperazine (16b): Compound **15b** (6.0 g, 15.06 mmol) was reacted with TFA (20 mL) in CHCl_3 (20 mL) using procedure **B** to give compound **16b** (3.6 g, 80%). ^1H NMR (CDCl_3 , 400 MHz): δ 3.20 (bs, 8H), 3.75 (s, 3H), 3.85 (s, 3H), 6.62 (s, 1H), 6.85 (s, 1H), 7.30 (t, $J = 7.2$ Hz, 1H), 7.40 (t, $J = 8.4$ Hz, 2H), 7.52 (t, $J = 8.0$ Hz, 2H).

1-(2-((tert-butyldimethylsilyl)oxy)ethyl)-4-(3-methoxy-[1,1'-biphenyl]-4-yl)piperazine (17a): Compound **16a** (3.5 g, 13.05 mmol) was reacted with (2-bromo-ethyl)-*tert*-butyldimethylsilane (3.74 g, 15.66 mmol), and K_2CO_3 (4.14 g, 39.15 mmol) in CH_3CN (50 mL) by following procedure **C**. The crude residue was purified by column chromatography (ethylacetate/hexane, 2:3) to afford compound **17a** (5.0 g, 90%). ^1H NMR (CDCl_3 , 400 MHz): δ 0.08 (s, 6H), 0.90 (s, 9H), 2.53 (t, $J = 6.4$ Hz, 2H), 3.08 (t, $J = 4.8$ Hz, 4H), 3.18 (t, $J = 5.6$ Hz, 4H), 3.26 (t, $J = 4.8$ Hz, 2H), 3.92 (s, 3H), 6.84 (dd, $J = 8.0$ Hz, 2.4 Hz, 1H), 6.94 (d, $J = 8.0$ Hz, 1H), 6.98 (t, $J = 4.8$ Hz, 1H), 7.29-7.34 (m, 1H), 7.44 (t, $J = 7.2$ Hz, 2H), 7.56 (d, $J = 7.6$ Hz, 2H).

1-(2-(tert-butyldimethylsilyloxy)ethyl)-4-(2,5-dimethoxybiphenyl-4-yl)piperazine (17b). Compound **16b** (3.0 g, 10.06 mmol) was reacted with (2-bromo-ethyl)-*tert*-butyldimethylsilane (2.88 g, 12.07 mmol), and K_2CO_3 (3.20 g, 30.18 mmol) in CH_3CN (50 mL) using procedure **C**. The crude residue was purified by column chromatography (ethylacetate/hexane, 2:3) to afford compound **17b** (3.90g, 82%). δ 0.09 (s, 6H), 0.92 (s, 9H), 2.61 (t, $J = 6.8$ Hz, 2H), 2.75 (bs, 4H), 3.16 (bs, 4H), 3.74 (s, 3H), 3.78 (t, $J = 6.8$ Hz, 2H), 3.84 (s, 3H), 6.34 (s, 1H), 6.84 (s, 1H), 7.25-7.31 (m, 1H), 7.39 (t, $J = 7.6$ Hz, 2H), 7.53 (d, $J = 6.8$ Hz, 2H).

2-(4-(3-methoxybiphenyl-4-yl)piperazin-1-yl)ethanol (18a). Compound **17a** (4.5 g, 11.72 mmol) was reacted with *n*-tetrabutylammonium fluoride (3.06 g, 11.72 mmol, 1.0 M solution in THF) in THF (30 mL) by following procedure **D**. The crude product was purified by silica gel column chromatography (EtOAc/MeOH, 9:1) to yield compound **18a** (2.25 g, 76%). ¹H NMR (CDCl₃, 400 MHz): ¹H NMR (CDCl₃, 400 MHz): 2.65 (t, *J* = 5.6 Hz, 2H), 2.76 (bs, 4H), 3.15 (bs, 4H), 3.67 (t, *J* = 5.6 Hz, 2H), 3.93 (s, 3H), 6.84 (d, *J* = 2.6 Hz, 1H), 7.08 (d, *J* = 2.4 Hz, 1H), 7.14 (dd, *J* = 8 Hz, 2.4 Hz, 1H), 7.31 (t, 7.2 Hz, 1H), 7.42 (t, *J* = 7.2 Hz, 2H), 7.56 (d, *J* = 7.6 Hz, 2H).

2-(4-(2,5-dimethoxybiphenyl-4-yl)piperazin-1-yl)ethanol (18b). Compound **17b** (3.8 g, 8.32 mmol) was reacted with *n*-tetrabutylammonium fluoride (2.17 g, 8.32 mmol, 1.0 M solution in THF) in THF (30 mL) using procedure **D**. The crude product was purified by silica gel column chromatography (EtOAc/MeOH, 9:1) to yield compound **18b** (2.21 g, 86%). ¹H NMR (CDCl₃, 400 MHz): δ 2.62 (t, *J* = 5.6 Hz, 2H), 2.73 (bs, 4H), 3.16 (bs, 4H), 3.65 (t, *J* = 5.6 Hz, 2H), 3.74 (s, 3H), 3.84 (s, 3H), 6.62 (s, 1H), 6.83 (s, 1H), 7.28-7.30 (m, 1H), 7.38 (t, *J* = 8.0 Hz, 2H), 7.51 (d, *J* = 6.4 Hz, 2H).

2-(4-(3-methoxybiphenyl-4-yl)piperazin-1-yl)acetaldehyde (19a). Compound **18a** (500 mg, 1.60 mmol) was reacted with oxalyl chloride (0.28 mL, 3.20 mmol), DMSO (0.45 mL, 6.40 mmol) and Et₃N (1.33 mL, 9.6 mmol) in dry dichloromethane (30 mL) by following procedure **E**. The crude product was purified by silica gel column chromatography (EtOAc/MeOH, 9.5:0.5) to yield compound **19a** (397 mg, 80%).

2-(4-(2,5-dimethoxybiphenyl-4-yl)piperazin-1-yl)acetaldehyde (19b). Compound **18b** (1.2 g, 3.50 mmol) was reacted with oxalyl chloride (0.60 mL, 7.01 mmol), DMSO (1.0 mL, 14.0 mmol) and Et₃N (2.91 mL, 21.0 mmol) in dichloromethane (30

mL) using procedure **F**. The crude product was purified by silica gel column chromatography (EtOAc/MeOH, 9.5:0.5) to yield compound **19b** (834 mg, 70%).

N6-(2-(4-(3-methoxybiphenyl-4-yl)piperazin-1-yl)ethyl)-N6-propyl-4,5,6,7-

tetrahydrobenzo[d]thiazole-2,6-diamine (\pm)(20a) : Compound **19a** (350 mg, 1.12 mmol) reacted with (\pm)-pramipexole (238 mg, 1.12 mmol) and NaBH(OAc)₃ (427 mg, 2.01 mmol) in dichloromethane (10 mL) by following procedure **F**. The crude product was purified by silica gel column chromatography (EtOAc/MeOH, 9:1) to yield compound (\pm)**20a** (370 mg, 65%). ¹H NMR (CDCl₃, 400 MHz): δ 0.89 (t, J = 7.2 Hz, 3H), 1.45-1.59 (m, 2H), 1.70-1.75 (m, 2H), 1.98-2.04 (m, 1H), 2.49-3.15 (m, 18H), 3.93 (s, 3H), 4.70 (s, 2H), 6.9 (d, J = 8.4 Hz, 1H), 7.07 (bs, 1H), 7.13-7.17 (m, 1H), 7.28-7.33 (m, 1H), 7.42 (t, J = 7.2 Hz, 2H), 7.56 (d, J = 8.0 Hz, 2H).

N6-(2-(4-(2,5-dimethoxybiphenyl-4-yl)piperazin-1-yl)ethyl)-N6-propyl-4,5,6,7-

tetrahydrobenzo[d]thiazole-2,6-diamine (\pm)(20b): Compound (\pm)-**19b** (300mg, 0.88 mmol) was reacted with (\pm)-pramipexole (185 mg, 0.88 mmol) and NaBH(OAc)₃ (334 mg, 1.58 mmol) in dichloromethane (10 mL) using procedure **F**. The crude product was purified by silica gel column chromatography (EtOAc/MeOH, 9:1) to yield compound (\pm) **20b** (456 mg, 65%). ¹H NMR (CDCl₃, 400 MHz): δ 0.89 (t, J = 7.2 Hz, 3H), 1.45-1.48 (m, 2H), 1.70 (d, J = 6.8 Hz, 1H), 1.97-2.02 (m, 1H), 2.48-3.35 (m, 19H), 3.72 (s, 3H), 3.85 (s, 3H), 5.22 (bs, 2H), 6.62 (s, 1H), 6.83 (s, 1H), 7.26 (t, J = 6.8 Hz, 1H), 7.37 (t, J = 7.6 Hz, 2H), 7.51 (d, J = 7.2 Hz, 2H).

(S)-N6-(2-(4-(2,5-dimethoxybiphenyl-4-yl)piperazin-1-yl)ethyl)-N6-propyl-4,5,6,7-

tetrahydrobenzo[d]thiazole-2,6-diamine (-)(20b): Compound **19b** (500 mg, 1.46 mmol) was reacted with (-)-pramipexole (310 mg, 1.46 mmol) and NaBH(OAc)₃ (556 mg, 2.62 mmol) in dichloromethane (10 mL) using procedure **F**. The crude

product was purified by silica gel column chromatography (EtOAc/MeOH, 9:1) to yield compound **(-)-20b** (511 mg, 65%). Spectral data matching with compound **(±)-20b**.

4-(4-(2-((2-amino-4,5,6,7-tetrahydrobenzo[d]thiazol-6-yl)(propyl)amino)ethyl)piperazin-1-yl)-[1,1'-biphenyl]-3-ol (±)-21a : A mixture of compound **(±)-20a** (200 mg, 0.395 mmol) and 48% aqueous HBr (10 ml) was refluxed for 12 h by following procedure **H** to afford compound **(±)-21a** (281 mg, 80%). ¹H NMR of free base (CDCl₃, 400 MHz): δ 0.90 (t, *J* = 7.2 Hz, 3H), 1.45-1.59 (m, 2H), 1.68-1.75 (m, 2H), 2.0 (d, *J* = 10.0 Hz, 1H), 2.48-3.05 (m, 18H), 4.75 (bs, 2H), 7.10 (d, *J* = 8.0 Hz, 1H), 7.16-7.23 (m, 2H), 7.31-7.34 (m, 1H), 7.42 (t, *J* = 8.0 Hz, 2H), 7.55 (d, *J* = 8.0 Hz, 2H). The product was converted into corresponding hydrochloride salt, m.p. 270 °C. Anal. (C₂₈H₃₇N₅OS · 4.0 HCl · 2.0 H₂O) : C, H, N.

4-(4-(2-((2-amino-4,5,6,7-tetrahydrobenzo[d]thiazol-6-yl)(propyl)amino)ethyl)piperazin-1-yl)-[1,1'-biphenyl]-2,5-diol (±)-21b: A mixture of compound **(±)-20b** (300 mg, 0.560 mmol) and 48% aqueous HBr (10 ml) was refluxed for 12 hours followed by procedure **H** to afford compound **(±)-21b** (380 mg, 75%). ¹H NMR (CD₃OD, 400 MHz): δ 1.07 (t, *J* = 7.2 Hz, 3H), 1.90-1.99 (m, 2H), 2.16-2.23 (m, 1H), 2.48-2.56 (m, 1H), 2.81 (bs, 2H), 2.98-3.25 (m, 4H), 3.54-4.08 (m, 13H), 6.70 (s, 1H), 6.89-6.9 (m, 1H), 7.17-7.55 (m, 5H). Hydrobromide salt, m.p. 265 °C. Anal. (C₂₈H₃₇N₅OS · 5.0 HBr · 0.4 C₂H₅OC₂H₅) : C, H, N.

(S)-4-(4-(2-((2-amino-4,5,6,7-tetrahydrobenzo[d]thiazol-6-yl)(propyl)amino)ethyl)piperazin-1-yl)-[1,1'-biphenyl]-2,5-diol (-)-21b: A mixture of compound **(-)-20b** (400 mg, 0.746 mmol) and 48% aqueous HBr (10 ml) was refluxed for 12 hours followed by procedure **H** to afford compound **(-)-21b** (474 mg,

70%). $[\alpha]_d = -22.18$ ($c = 0.55$, CH_3OH). Spectral data matching with compound **(±)(21b)**. Hydrobromide salt, m.p. 260 °C. Anal. ($\text{C}_{28}\text{H}_{37}\text{N}_5 \cdot \text{O}_2\text{S} \cdot 5.0 \text{ HBr} \cdot 0.4 \text{ C}_2\text{H}_5\text{OC}_2\text{H}_5 \cdot 0.2 \text{ H}_2\text{O}$) : C, H, N.

2-(4-(2-((2-amino-4,5,6,7-tetrahydrobenzo[d]thiazol-6-yl)(propyl)amino)ethyl)piperazin-1-yl)-5-phenylcyclohexa-2,5-diene-1,4-

dione(±)(22): Into the solution of free base of the compound **(±)-21b** (100 mg, 0.20 mmol) in dichloromethane (10 mL), was reacted with MnO_2 (140 mg, 0.8 mmol) for 1 hr. at r.t. followed by procedure similar to compound **(±)-10** to yield compound **(±)-22** (59 mg, 60%). NMR (CDCl_3 , 400 MHz): δ 0.89 (t, $J = 6.4$ Hz, 3H), 1.52-2.03 (m, 4H), 2.54-2.73 (m, 15H), 3.47 (bs, 4H), 4.85 (bs, 2H), 5.84 (s, 1H), 6.64 (s, 1H), 7.30-7.46 (m, 5H). The product was converted into corresponding hydrochloride salt, m.p. 240 °C. Anal. ($\text{C}_{28}\text{H}_{35}\text{N}_5\text{O}_2\text{S} \cdot 5.0 \text{ HCl} \cdot 1.8 \text{ C}_2\text{H}_5\text{OC}_2\text{H}_5 \cdot 0.8 \text{ H}_2\text{O}$) : C, H, N.

(S)-5-methoxy-N-(2-(4-(3'-methoxybiphenyl-4-yl)piperazin-1-yl)ethyl)-N-propyl-1,2,3,4-tetrahydronaphthalen-2-amine (-)(23a): Compound **7b** (350 mg, 1.13 mmol) was reacted with (S)-(5-methoxy-1,2,3,4-tetrahydro-naphthalen-2-yl)-propylamine (247.83 mg, 1.13 mmol) and $\text{NaBH}(\text{OAc})_3$ (430.23 mg, 2.03 mmol) in dichloromethane (60 mL) by following procedure **F**. The crude product was purified by silica gel column chromatography (EtOAc/Hexane, 3:2) to yield compound **(-)-23a** (347 mg, 60%). ^1H NMR (400 MHz, CDCl_3): δ 0.90 (t, $J = 7.2$ Hz, 3H), 1.46-1.64 (m, 3H), 2.04-2.25 (m, 1H); 2.51-3.28 (m, 19H), 3.74 (s, 3H); 3.81 (s, 3H), 6.65 (d, $J = 8.0$ Hz, 1H); 6.71 (d, $J = 7.6$ Hz, 1H); 6.82-6.86 (m, 1H), 7.0 (d, $J = 8.4$ Hz, 2H); 7.07-7.15 (m, 3H), 7.31 (t, $J = 8.0$ Hz, 1H); 7.50 (d, $J = 8.4$ Hz, 2H).

(S)-N-(2-(4-(3',4'-dimethoxybiphenyl-4-yl)piperazin-1-yl)ethyl)-5-methoxy-N-propyl-1,2,3,4-tetrahydronaphthalen-2-amine (-)(23b): Compound **7e** (200 mg,

0.59 mmol) was reacted with (S)-(5-methoxy-1,2,3,4-tetrahydro-naphthalen-2-yl)-propyl-amine (130 mg, 0.59 mmol) and NaBH(OAc)₃ (225 mg, 1.06 mmol) in dichloromethane (50 mL) using procedure **F**. The crude product was purified by silica gel column chromatography (EtOAc/Hexane, 4:1) to yield compound **(-)-23b** (174 mg, 55%). ¹H NMR (400 MHz, CDCl₃): δ 0.92 (t, J = 7.2 Hz, 3H); 1.40-1.68 (m, 3H); 2.01-2.18 (m, 1H); 2.36-3.28 (m, 19H); 3.81 (s, 3H); 3.91 (s, 3H), 3.93 (s, 3H); 6.65 (d, J = 8.0 Hz, 1H); 6.71 (d, J = 7.6 Hz, 1H); 6.91(d, J = 8.0 Hz, 1H), 6.97(d, J = 8.8 Hz, 1H), 7.06-7.11(m, 3H); 7.46 (d, J = 8.8 Hz, 2H).

(S)-6-((2-(4-(3'-hydroxybiphenyl-4-yl)piperazin-1-yl)ethyl)(propyl)amino)-5,6,7,8-tetrahydronaphthalen-1-ol (-)(24a): Compound **(-)-23a** (300 mg, 0.58 mmol) and 48% aqueous HBr (15 ml) was refluxed for 10 hours by following procedure **G** to afford compound **(-)-23a** (296 mg, 70%, recrystallized from ethanol). ¹H NMR of HBr salt (400 MHz, CD₃OD): δ 1.04 (t, J = 7.2 Hz, 3H), 1.73-1.93 (m, 3H), 2.30-2.69 (m, 2H), 3.07-3.83 (m, 18 H), 6.60 (d, J = 5.2 Hz, 1H), 6.69 (d, J = 6.4 Hz, 1H), 6.73 (d, J = 7.6 Hz, 1H), 6.96-7.04 (m, 3H), 7.19-7.23 (m, 3H), 7.56 (d, J = 7.2 Hz, 2H). [α]_d = -41.0 (c = 1.0, CH₃OH). Hydrobromide salt, m.p.290 °C. Anal. (C₃₁H₃₉N₃O₂S · 3.0 HBr · 2.0 H₂O) : C, H, N.

(S)-4'-(4-(2-((5-hydroxy-1,2,3,4-tetrahydronaphthalen-2-yl)(propyl)amino)ethyl)piperazin-1-yl)biphenyl-3,4-diol (-)(24b): Compound **(-)-23b** (100 mg, 0.183 mmol) and 48% aqueous HBr (5 ml) was refluxed for 12 hours using procedure **G** to afford compound **(-)-24b** (95 mg, 70%, recrystallized from ether and ethanol mixture). ¹H NMR of HBr Salt (400 MHz, CD₃OD): δ 1.08 (t, J = 7.8 Hz, 3H), 1.80-2.04 (m, 3H), 2.41-2.51 (m, 1H), 2.60-2.80 (m, 1H), 3.09-3.97 (m, 18 H), 6.62 (d, J = 8.4 Hz, 1H), 6.68 (d, J = 8.0 Hz, 1H), 6.80 (d, J = 8.0 Hz, 1H), 6.90-7.01

(m, 3H), 7.18 (d, $J = 8.0$ Hz, 2H), 7.51 (d, $J = 8.8$ Hz, 2H). $[\alpha]_D^{25} = -20.5$ ($c = 1.0$, CH₃OH). Hydrobromide salt, m.p. 255 °C. Anal. (C₃₁H₃₉N₃O₃S · 3.0 HBr · 0.5 H₂O) : C, H, N.

Procedure L : N-(2-(4-([1,1'-biphenyl]-4-yl)piperazin-1-yl)ethyl)-N-propyl-1,4-dioxaspiro[4.5]decan-8-amine (34a) : Into a stirring solution of compound **7f** (750 mg, 2.55 mmol) in ClCH₂CH₂Cl (40 mL), amine **33** (510 mg, 2.55 mmol), NaBH(OAc)₃ (973 mg, 4.59 mmol) and HOAc (153 mg, 2.55 mmol) were added at room temperature. After stirring for 48 hours, saturated solution of NaHCO₃ was added into the reaction mixture and it was extracted with CH₂Cl₂ (3 x 50 mL). The combined organic layer was washed with brine and finally purified by silica gel column chromatography (EtOAc/MeOH, 9:1) to yield (670 mg, 60%) of compound **34a**. ¹H NMR (CDCl₃, 400 MHz): δ 0.90 (t, $J = 6.8$ Hz, 3H), 1.46-1.50 (m, 2H), 1.69-1.79 (m, 2H), 2.04-2.07 (m, 2H), 2.38-2.55 (m, 8H), 2.65-2.70 (m, 6H), 3.01 (t, $J = 7.2$ Hz, 1H), 3.26 (t, $J = 4.4$ Hz, 4H), 3.92 (s, 4H), 6.98 (d, $J = 8.4$ Hz, 2H), 7.27 (d, $J = 7.6$ Hz, 1H), 7.41 (t, $J = 8.0$ Hz, 2H), 7.51 (d, $J = 8.8$ Hz, 2H), 7.55 (d, $J = 8.0$ Hz, 2H).

N-(2-(4-(3'-methoxy-[1,1'-biphenyl]-4-yl)piperazin-1-yl)ethyl)-N-propyl-1,4-dioxaspiro[4.5]decan-8-amine (34b): Into a stirring solution of compound **7b** (700 mg, 2.25 mmol) in ClCH₂CH₂Cl (40 mL), amine **33** (450 mg, 2.25 mmol), NaBH(OAc)₃ (858 mg, 4.05 mmol) and HOAc (135 mg, 2.25 mmol) were added at room temperature using procedure **L** to yield (710mg, 70%) of compound **34b**. ¹H NMR (CDCl₃, 400 MHz): δ 0.89 (t, $J = 7.2$ Hz, 3H), 1.52-1.62 (m, 2H), 1.79-1.82 (m, 4H), 2.59-2.82 (m, 15H), 3.24 (t, $J = 4.8$ Hz, 4H), 3.88 (s, 3H), 3.93 (s, 4H), 6.82 (dd, $J = 1.2$ Hz, 8.4 Hz, 1H), 6.97 (d, $J = 8.8$ Hz, 2H), 7.08 (t, $J = 2.4$ Hz, 1H), 7.13-7.15 (m, 1H), 7.30 (t, $J = 8.0$ Hz, 1H), 7.50 (d, $J = 7.2$ Hz, 2H).

Procedure M :4-((2-(4-([1,1'-biphenyl]-4-yl)piperazin-1-yl)ethyl)(propyl)amino)-cyclohexanone (35a): A solution of ketal **34a** (600 mg, 1.29 mmol) in THF (50 mL) and 1N HCl (10 ml) was stirred at 80°C under N₂ for 2 h. THF was removed under vacuo and saturated NaHCO₃ solution was added slowly. The mixture was extracted with CH₂Cl₂ (4*100 mL) and the combined organic layer was washed with brine, dried over Na₂SO₄, and evaporated to give the crude product, which was purified by silica gel column chromatography (EtOAc/MeOH, 9:2) to yield (490 mg, 90%) of compound **35a**. ¹H NMR (CDCl₃, 400 MHz): δ 0.89 (t, *J* = 7.6 Hz, 3H), 1.46-1.60 (m, 2H), 1.80-1.83 (m, 2H), 2.04-2.37 (m, 2H), 2.39-2.55 (m, 8H), 2.65-2.70 (m, 6H), 3.15 (t, *J* = 7.2 Hz, 1H), 3.25 (t, *J* = 4.4 Hz, 4H), 6.98 (d, *J* = 8.4 Hz, 2H), 7.28 (d, *J* = 7.2 Hz, 1H), 7.40 (t, *J* = 8.0 Hz, 2H), 7.51 (d, *J* = 7.2 Hz, 2H), 7.55 (d, *J* = 8.8 Hz, 2H).

4-((2-(4-(3'-methoxy-[1,1'-biphenyl]-4-yl)piperazin-1-yl)ethyl)(propyl)amino)-cyclohexanone (35b): A solution of ketal **34b** (700 mg, 1.41 mmol) in THF (50 mL) and 1N HCl (10 ml) was stirred at 80°C under N₂ for 2 h followed by procedure **M** to yield (540 mg, 85%) of compound **35b**. ¹H NMR (CDCl₃, 400 MHz): δ 0.89 (t, *J* = 7.2 Hz, 3H), 1.45-1.52 (m, 2H), 1.82-1.91 (m, 2H), 2.04-2.12 (m, 2H), 2.30-2.52 (m, 8H), 2.66-2.70 (m, 6H), 3.15 (t, *J* = 7.2 Hz, 1H), 3.67 (t, *J* = 6.0 Hz, 4H), 3.85 (s, 3H), 6.83 (m, 1H), 6.98 (d, *J* = 8.8 Hz, 2H), 7.14 (bs, 1H), 7.13-7.15 (m, 1H), 7.31 (t, *J* = 8.0 Hz, 1H), 7.50 (d, *J* = 8.4 Hz, 2H).

Procedure N: N6-(2-(4-([1,1'-biphenyl]-4-yl)piperazin-1-yl)ethyl)-N6-propyl-5,6,7,8-tetrahydroquinazoline-2,6-diamine (36a): Into a solution of ketone **35a** (450 mg, 1.07 mmol) in dry toluene (20 mL), tris(dimethylamino)methane (780 mg, 5.36 mmol) was added and the mixture was stirred under nitrogen at 90°C for 4 h. The solvent was removed under vacuo and the residue was dissolved in EtOH (50

mL). Guandine carbonate (460 mg, 2.55 mmol) was added next. The mixture was then refluxed for 17 h. The solvent was evaporated in vacuo and the residue was diluted with CH₂Cl₂ and washed with brine. The organic layer was dried over Na₂SO₄ and evaporated to yield crude product, which was purified by silica gel column chromatography (EtOAc/MeOH, 7:3) to yield (378 mg, 75%) of compound **36a**. ¹H NMR (CDCl₃, 400 MHz): δ 0.87 (t, *J* = 6.4 Hz, 3H), 1.57-1.76 (m, 3H), 2.05-2.13 (m, 1H), 2.64-2.98 (m, 15H), 3.27 (t, *J* = 4.4 Hz, 4H), 4.93 (s, 2H), 6.97 (d, *J* = 8.8 Hz, 2H), 7.28 (d, *J* = 7.6 Hz, 1H), 7.41 (t, *J* = 7.6 Hz, 2H), 7.50 (d, *J* = 8.4 Hz, 2H), 7.54 (d, *J* = 7.2 Hz, 2H), 8.07 (s, 1H). The product was converted into corresponding hydrochloride salt, m.p. 232 °C. Anal. (C₂₉H₃₈N₆ · 4.0 HCl · 1.0 CH₃COOCH₂CH₃) : C, H, N. MS(ES⁺): *m/z* calculated for C₂₉H₃₈N₆ [M+H⁺]: calculated 470.32; found 471.52.

N6-(2-(4-(3'-methoxy-[1,1'-biphenyl]-4-yl)piperazin-1-yl)ethyl)-N6-propyl-5,6,7,8-tetrahydroquinazoline-2,6-diamine (36b): Into a solution of ketone **35b** (500 mg, 1.11 mmol) in dry toluene (30 mL), tris(dimethylamino)methane (807 mg, 5.56 mmol) was added and the mixture was stirred under nitrogen at 90°C for 4 h. The solvent was removed under vacuo and the residue was dissolved in EtOH (50 mL). Guandine carbonate (500 mg, 2.77 mmol) was added next followed by procedure **N** to yield (390 mg, 70%) of compound **36b**. ¹H NMR (CDCl₃, 400 MHz): δ 0.90 (t, *J* = 7.2 Hz, 3H), 1.45-1.51 (m, 2H), 1.67-1.75 (m, 2H), 2.04-2.12 (m, 1H), 2.50-2.93 (m, 14H), 3.24 (t, *J* = 4.8 Hz, 4H), 3.85 (s, 3H), 6.83 (dd, *J* = 2.4 Hz, 7.6 Hz, 1H), 6.97 (d, *J* = 8.8 Hz, 2H), 7.09 (bs, 1H), 7.14 (d, *J* = 8.0 Hz, 2H), 7.31 (t, *J* = 7.6 Hz, 1H), 7.50 (d, *J* = 8.8 Hz, 2H), 8.01 (bs, 2H).

4'-(4-(2-((2-amino-5,6,7,8-tetrahydroquinazolin-6-yl)(propyl)amino)ethyl)piperazin-1-yl)-[1,1'-biphenyl]-3-ol (37) : Compound **36b**

(100 mg, 0.59 mmol) and 48% aqueous HBr (10 ml) was refluxed for 8 hours using procedure **H** to afford compound **37** (118 mg, 65%, recrystallized from ether). ¹H NMR of HBr salt (CD₃OD, 400 MHz): δ 1.08 (t, *J* = 7.2 Hz, 3H), 1.95-2.01 (m, 2H), 2.27-2.29 (m, 1H), 2.58-2.64 (m, 1H), 3.01-3.39 (m, 6 H), 3.48 (bs, 8H), 3.91-4.01 (m, 4H), 4.14 (bs, 1H), 6.71 (d, *J* = 8.0 Hz, 1H), 6.99 (bs, 1H), 7.03 (d, *J* = 7.6 Hz, 2H), 7.19-7.26 (m, 3H), 7.56 (d, *J* = 8.4 Hz, 2H), 8.67 (bs, 1H). Hydrobromide salt, m.p. 255 °C. Anal. (C₂₉H₃₈N₆O · 6.0 HBr · 3.0 H₂O) : C, H, N.

Procedure O: tert-butyl 4-(biphenylcarbonyl)piperazine-1-carboxylate (27) : To a stirring solution of BoC-piperazine, **25** (1.5 g, 8.05 mmol) in THF (25 mL), 4-biphenyl carbonyl chloride, **26** (1.6 g, 7.24 mmol) and diisopropylethylamine (2.53 mL, 14.49 mmol) were added at room temperature. The reaction mixture was stirred at the same temperature for overnight and partitioned between brine and ethylacetate. The organic layer was separated and washed with brine, dried over Na₂SO₄ and concentrated. The crude material was purified by column chromatography over silica gel (Hexane/EtOAc, 8.0:2.0) to give compound **27** (2.16 g, 80%). ¹H (CDCl₃, 400 MHz): δ 1.47 (s, 9 H), 3.47 (bs, 4H), 3.74 (bs, 4H), 7.37 (t, *J* = 7.2 Hz, 1H), 7.43-7.49 (m, 4H), 7.59 (d, *J* = 7.2 Hz, 2H), 7.59 (d, *J* = 7.2 Hz, 2H).

biphenyl-4-yl(piperazin-1-yl)methanone (28): Compound **27** (2.1 g, 5.73 mmol) was reacted with TFA (20 mL) in CH₂Cl₂ (30 mL) by following procedure **B** to give compound **28** (1.44 g, 95%). ¹H (CDCl₃, 400 MHz): 3.47 (bs, 4H), 3.74 (bs, 4H), 7.38 (t, *J* = 7.2 Hz, 1H), 7.44-7.49 (m, 4H), 7.59 (d, *J* = 7.2 Hz, 2H), 7.63 (d, *J* = 8.4 Hz, 2H).

biphenyl-4-yl(4-(2-(tert-butyl)dimethylsilyloxy)ethyl)piperazin-1-yl)methanone (29): A mixture of compound **28** (1.2 g, 4.50 mmol), was reacted with (2-bromo-

ethyl)-*tert*-butyldimethylsilane (1.30 g, 5.41 mmol), and K₂CO₃ (1.86 g, 13.50 mmol) in CH₃CN (50 mL) by following the procedure **C** to furnish **29** (1.30 g, 70%). ¹H NMR (CDCl₃, 400 MHz): δ 0.05 (s, 6H), 0.88 (s, 9H), 2.51-2.62 (m, 6H), 3.47-3.54 (m, 2H), 3.76 (t, *J* = 5.6 Hz, 4H), 7.37 (t, *J* = 7.2 Hz, 1H), 7.43-7.49 (m, 4H), 7.59 (d, *J* = 7.2 Hz, 2H), 7.62 (d, *J* = 8.0 Hz, 2H).

biphenyl-4-yl(4-(2-hydroxyethyl)piperazin-1-yl)methanone (30): Compound **29** (1.2 g, 2.82 mmol) was reacted with *n*-tetrabutylammonium fluoride (0.8 g, 2.82 mmol, 1.0 M solution in THF) in anhydrous THF (20 mL) by following procedure **D** to yield compound **30** (790 mg, 90%). ¹H NMR (CDCl₃, 400 MHz): 2.50-2.61 (m, 6H), 3.46-3.54 (m, 2H), 3.65 (t, *J* = 4.8 Hz, 4H), 7.37 (t, *J* = 8.8 Hz, 1H), 7.43-7.49 (m, 4H), 7.58 (d, *J* = 7.2 Hz, 2H), 7.62 (d, *J* = 8.0 Hz, 2H).

2-(4-(biphenylcarbonyl)piperazin-1-yl)acetaldehyde (31): Compound **30** (500 mg, 1.61 mmol) was reacted with oxalyl chloride (0.29 mL, 3.22 mmol), DMSO (0.46 mL, 6.44 mmol) and Et₃N (1.33 mL, 9.66 mmol) in dichloromethane (20 mL) by following procedure **E** to yield compound **31** (420 mg, 85%).

(4-(2-((2-amino-4,5,6,7-tetrahydrobenzo[d]thiazol-6-yl)(propyl)amino)ethyl)-piperazin-1-yl)(biphenyl-4-yl)methanone(±)(32): Compound **31** (400 mg, 1.29 mmol) was reacted with (±)-pramipexole (275 mg, 1.29 mmol) and NaBH(OAc)₃ (492.12 mg, 2.32 mmol) in dichloromethane (20 mL) using procedure **F** to yield compound (±)**32** (420 mg, 70%). ¹H NMR (CDCl₃, 400 MHz): δ 0.86 (t, *J* = 7.2 Hz, 3H), 1.41-1.46 (m, 2H), 1.57-1.70 (m, 1H), 1.95 (d, *J* = 11.6 Hz, 1H), 2.40-2.70 (m, 13H), 3.01-3.06 (m, 1H), 3.48 (bs, 2H), 3.78 (bs, 2H), 4.02-4.12 (m, 1H), 4.96 (bs, 2H), 7.35 (t, *J* = 7.2 Hz, 1H), 7.41-7.47 (m, 4H), 7.56-7.61 (m, 4H). The product was

converted into corresponding hydrochloride salt, m.p.255 °C. Anal. ($C_{29}H_{37}N_5OS \cdot 5.0$ HCl $\cdot 1.0$ $C_2H_5OC_2H_5$) : C, H, N.

(5-bromo-2-methoxyphenoxy)(tert-butyl)dimethylsilane (39) : A mixture of compound **38** (4.5 g, 22.16 mmol), was reacted with tert-butylchlorodimethylsilane (4.08 g, 26.59mmol), and triethylamine (9.21 ml, 66.48 mmol) in CH_3CN (200 mL) by following the procedure **C** to furnish **39** (5.62 g, 80%). 1H NMR ($CDCl_3$, 400 MHz): δ 0.16 (s, 6H), 1.0 (s, 9H), 3.78 (s, 3H), 6.71(d, $J = 8.8$ Hz, 1H), 6.98-7.03 (m, 2H).

tert-butyl4-(3-(tert-butyl)dimethylsilyloxy)-4-methoxyphenyl)piperazine-1-

carboxylate (41): A suspension of (5-bromo-2-methoxyphenoxy)(tert-butyl)dimethylsilane **39** (2.5 g, 7.88 mmol), monoboc piperazine **40** (1.46 g, 7.88 mmol), sodium t-butoxide (1.51 g, 15.76 mmol,) and Dichlorobis(tri-*o*-tolylphosphine) palladium (II) (875 mg, 0.75 mmol) in toluene (100 ml) was refluxed for 12 hours followed by procedure **A**. The crude residue was purified by flash chromatography on silica gel column using solvent system hexane/ ethyl acetate (7:3) to yield compound **41** (1.85g, 55%). 1H NMR ($CDCl_3$, 400 MHz): δ 1.49 (s, 9H), 3.07 (bs, 4H), 3.61 (t, $J = 4.8$ Hz, 4H), 6.96 (d, $J = 8.0$ Hz, 2H), 7.23 (d, $J = 7.2$ Hz, 1H), 7.41 (t, $J = 8.0$ Hz, 2H), 7.49 (d, $J = 8.0$ Hz, 2H), 7.52 (d, $J = 7.2$ Hz, 2H).

2-methoxy-5-(piperazin-1-yl)phenol (42): To a stirring solution of compound **41** (1.5 g, 3.54 mmol) in CH_2Cl_2 (30 mL), TFA (10 mL) was added slowly at room temperature and the reaction mixture was stirred for three hours. Followed by procedure **B** to provide the compound **42** (629 mg, 85%). 1H NMR ($CDCl_3$, 400 MHz): δ 3.25-3.31 (m, 4H), 3.34-3.37 (m, 4H); 3.83 (s, 3H), 6.95 (dd, $J = 8.8$ Hz, 3.2 Hz 1H), 6.67(d, $J = 2.4$ Hz, 1H), 7.72 (d, $J = 8.4$ Hz, 1H).

1-(3-(tert-butyl)dimethylsilyloxy)-4-methoxyphenyl)piperazine (43): A mixture of compound **42** (629 mg, 3.02 mmol), was reacted with tert-butylchlorodimethylsilane (546 mg, 3.62 mmol), and triethylamine (1.25 ml, 9.06 mmol) in CH₃CN (100 mL) by following the procedure **C**. The crude residue was purified by flash chromatography on silica gel column using solvent system dichloromethane: methanol (1: 9) to furnish **43** (730 mg, 75%). ¹H NMR (CDCl₃, 400 MHz): δ 0.14 (s, 6H), 0.98 (s, 9H), 3.26-3.28 (m, 4H), 3.31-3.34 (m, 4H), 3.75 (s, 3H), 6.46-6.49 (m, 2H), 6.76 (d, *J* = 8.8 Hz, 2H).

Procedure P: 1-(4-(3-(tert-butyl)dimethylsilyloxy)-4-methoxyphenyl)piperazin-1-yl)-2-chloroethanone (44): Into the solution of substituted phenyl piperazine **43** (700 mg, 2.17 mmol) and triethylamine (10 ml) in anhydrous dichloromethane (50 ml) was added chloroacetyl chloride (0.26 ml, 3.26 mmol) at -40°C under nitrogen atmosphere. Reaction mixture was stirred for half an hour, diluted with dichloromethane. The organic layer was washed with water, dried over Na₂SO₄ and evaporated in vacuo. The crude residue was purified by flash chromatography on silica gel column using solvent system hexane/ ethyl acetate (4:1) to yield **44** (432 mg, 50%). ¹H NMR (CDCl₃, 400 MHz): δ 0.15 (s, 6H), 0.99 (s, 9H), 3.05 (t, *J* = 5.6 Hz, 2H), 3.10 (t, *J* = 4.8 Hz, 2H), 3.68 (t, *J* = 5.6 Hz, 2H), 3.76 (s, 3H), 3.79 (t, *J* = 4.0 Hz, 2H), 4.10 (s, 2H), 6.49-6.53 (m, 2H), 6.78 (d, *J* = 8.8 Hz, 2H).

Procedure Q: 2-((2-amino-4,5,6,7-tetrahydrobenzo[d]thiazol-6-yl)(propyl)amino)-1-(4-(3-(tert-butyl)dimethylsilyloxy)-4-methoxyphenyl)piperazin-1-yl)ethanone (45): Into a suspension of compound **44** (430 mg, 1.08 mmol), K₂CO₃ (447 mg, 3.24 mmol) and catalytic amount of KI in acetonitrile (50 ml) was added (**±**)-pramipexole (205 mg, 0.97 mmol). Reaction mixture was refluxed for 3 hours. The crude reaction mixture was filtered, washed

with ethyl acetate, evaporated in vacuo and purified by flash chromatography on silica gel column using solvent system ethyl acetate/methanol (95:5) to yield **45** (247 mg, 40%). ^1H NMR (CDCl_3 , 400 MHz): δ 0.15 (s, 6H), δ 0.88 (t, $J = 7.2$ Hz, 3H), 0.99 (s, 9H), 1.44-1.53 (m, 2H), 1.71-1.80 (m, 1H), 2.00-2.04 (m, 1H), 2.48-2.73 (m, 6H), 2.95-3.12 (m, 5H), 3.41-3.51 (m, 2H) 3.67-3.85 (m, 7H), 4.87 (bs, 2H), 6.47 (dd, $J = 8.0$ Hz, 2.4 Hz 1H), 6.51 (d, $J = 2.4$ Hz, 1H), 6.81 (d, $J = 8.0$ Hz, 1H).

Procedure R: 5-(4-(2-((2-amino-4,5,6,7-tetrahydrobenzo[d]thiazol-6-yl)(propyl)amino)ethyl)piperazin-1-yl)-2-methoxyphenol (46) : Into the solution of **45** (140 mg, 0.24 mmol) in dry THF (10 ml) at 0°C was added (2.43 ml, 2.43 mmol) solution of borane-THF complex (1 M solution) with stirring under nitrogen atmosphere. The reaction mixture was stirred at room temperature for 36 hours and quenched with methanol. The solvent was evaporated. The white solid complex was suspended in 6 N HCl in methanol, stirred for 3 hours at room temperature. Methanol was evaporated under vacuo. Reaction mixture was made alkaline using saturated NaHCO_3 Solution. The aqueous layer was extracted with ethyl acetate (3 \times 100 ml), dried over Na_2SO_4 , concentrated under vacuo and purified by flash chromatography on silica gel column using solvent system ethyl acetate/methanol (9:1) to to yield **46** (65 mg, 60%).

^1H NMR (CDCl_3 , 400 MHz): δ 0.94 (t, $J = 7.2$ Hz, 3H), 1.52-1.60 (m, 2H), 1.74-1.85 (m, 1H), 2.05-2.07 (m, 1H), 2.49-2.80 (m, 11H), 2.86-2.93 (m, 2H), 3.07 (t, $J = 4.4$ Hz, 4H), 3.23-3.31 (m, 2H), 3.77 (s, 3H), 4.89 (bs, 2H), 6.41(dd, $J = 8.8$ Hz, 2.4 Hz 1H), 6.98-7.03 (d, $J = 3.2$ Hz, 1H), 6.81 (d, $J = 9.2$ Hz, 1H).

The product was converted into corresponding hydrochloride salt, m.p. 250°C . Anal. ($\text{C}_{23}\text{H}_{44}\text{N}_5\text{O}_4\text{S} \cdot 5.0 \text{ HCl} \cdot 2.0 \text{ H}_2\text{O}$) : C, H, N.

Procedure S: 3-(tert-butyldimethylsilyloxy)-4-methoxyphenylboronic acid (47) :

Into a stirred solution of bromo compound **39** (11.0 g, 34.66 mmol) in dry THF at -78 °C, 1M n-BuLi (20.80 mL, 52.0 mmol) was added. The reaction mixture was stirred for 1 hr minutes followed by addition of triisopropylborate (24.14 mg, 103.98 mmol) and allow to stir for over night. Next day, the reaction mixture was quenched by addition of saturated NH₄Cl and extracted with CH₂Cl₂ (3 x 100 mL). The combined organic layer was washed with brine and concentrated to yield the compound **47** (7.3 g, 75%), which was used without purification in the next step.

tert-butyl 4-(3'-(tert-butyldimethylsilyloxy)-4'-methoxybiphenyl-4-yl)piperazine-

1-carboxylate (48): Substituted boronic acid, **47** (2.5 g, 8.85mmol) was reacted with iodo compound **1** (3.43 g, 8.85 mmol), Na₂CO₃ (1.87 g, 17.7 mmol, 2 M solution in water) and Pd(PPh₃)₄ (442 mg, 0.442 mmol) in dimethoxy ethane/ethanol (50 mL:50 mL) followed by procedure **A**. The crude residue was purified by flash chromatography on silica gel column using solvent system hexane/ ethyl acetate (8:2) to yield of compound **48** (1.60g, 50% yield). ¹H NMR (CDCl₃, 400 MHz): δ 0.18 (s, 6H), 1.01 (s, 9H), δ 1.49 (s, 12H), 3.14-3.20 (m, 4H), 3.54-3.65 (m, 4H), 3.85 (s, 3H), 6.96-7.04 (d, *J* = 8.4 Hz, H), 6.98-7.03 (m, 5H), 7.48 (d, *J* = 9.2 Hz, 2H). 6.82 (dd, *J* = 8.0 Hz, 1.6 Hz, 1H), 6.99 (d, *J* = 8.0 Hz, 2H), 7.09 (bs, 1H), 7.15 (d, *J* = 7.2 Hz, 1H), 7.32 (t, *J* = 7.8Hz, 1H), 7.52 (d, *J* = 8.0 Hz, 2H).

4-methoxy-4'-(piperazin-1-yl)biphenyl-3-ol (49): To a stirring solution of compound **48**(1.5 g, 3.01 mmol) in CH₂Cl₂ (20 mL), TFA (10 mL) was added slowly at room temperature and the reaction mixture was stirred for three hours. Followed by procedure **B** to provide the compound **49** (812 mg, 95%). ¹H NMR (CDCl₃, 400 MHz): 3.04-3.07 (m, 4H), 3.17-3.19 (m, 4H), 3.94 (s, 3H); 6.95 (d, *J* = 8.4 Hz, 2H), 6.98(d, *J* = 8.8 Hz, 2H), 7.47 (d, *J* = 8.0 Hz, 2H), 7.49 (d, *J* = 8.0 Hz, 2H).

1-(3'-(tert-butyldimethylsilyloxy)-4'-methoxybiphenyl-4-yl)piperazine (50): A mixture of compound **49** (800 mg, 2.81 mmol), was reacted with tert-butylchlorodimethylsilane (508 mg, 3.37 mmol), and triethylamine (1.16 ml, 8.43 mmol) in CH₃CN (100 mL) by following the procedure **C**. The crude residue was purified by flash chromatography on silica gel column using solvent system dichloromethane: methanol (2: 8) to furnish **50** (952 mg, 85%). ¹H NMR (CDCl₃, 400 MHz): δ 0.18 (s, 6H), 1.02 (s, 9H), 3.05-3.11 (m, 4H), 3.20-3.22 (m, 4H), 3.82 (s, 3H), 6.88 (d, *J* = 8.4 Hz, 1H), 6.95 (d, *J* = 9.2 Hz, 2H), 7.07 (d, *J* = 2.4 Hz, 1H), 7.10 (dd, *J* = 8.0 Hz, 1.6 Hz, 1H), 7.44 (d, *J* = 8.8 Hz, 2H).

1-(4-(3'-(tert-butyldimethylsilyloxy)-4'-methoxybiphenyl-4-yl)piperazin-1-yl)-2-chloroethanone (51) : Into the solution of substituted biphenylphenyl piperazine **50** (800 mg, 2.01 mmol) and triethylamine (10 ml) in anhydrous dichloromethane (50 ml) was added chloroacetyl chloride (0.24 ml, 3.01 mmol) at -40°C under nitrogen atmosphere followed by procedure **A**. The crude residue was purified by flash chromatography on silica gel column using solvent system hexane/ ethyl acetate (8:2) to yield **51** (480 mg, 50%). ¹H NMR (CDCl₃, 400 MHz): δ 0.18 (s, 6H), 1.01 (s, 9H), 3.21 (t, *J* = 5.6 Hz, 2H), 3.26 (t, *J* = 4.8 Hz, 2H), 3.70 (t, *J* = 5.2 Hz, 2H), 3.79-3.83 (m, 5H), 4.11 (s, 2H), 6.88 (d, *J* = 8.4 Hz, 1H), 6.95 (d, *J* = 9.2 Hz, 2H), 7.07 (d, *J* = 2.4 Hz, 1H), 7.10 (dd, *J* = 8.8 Hz, 2.4 Hz, 1H), 7.46 (d, *J* = 8.8 Hz, 2H).

2-((2-amino-4,5,6,7-tetrahydrobenzo[d]thiazol-6-yl)(propyl)amino)-1-(4-(3'-(tert-butyldimethylsilyloxy)-4'-methoxybiphenyl-4-yl)piperazin-1-yl)ethanone (52): Into a suspension of compound **51** (450 mg, 0.95 mmol), K₂CO₃ (392 mg, 2.85 mmol) and catalytic amount of KI in acetonitrile (50 ml) was added (**±**)-pramipexole (182 mg, 0.86 mmol) and reaction mixture was refluxed for 3 hours followed by procedure **Q**. The crude residue was purified by flash chromatography on silica gel

column using solvent system ethyl acetate/methanol (98:2) to yield **52** (198 mg, 30%). ¹H NMR (CDCl₃, 400 MHz): δ 0.17 (s, 6H), δ 0.89 (t, *J* = 7.2 Hz, 3H), 0.99 (s, 9H), 1.42-1.55 (m, 2H), 1.70-1.80 (m, 1H), 2.00-2.04 (m, 1H), 2.47-2.73 (m, 6H), 3.07-3.22 (m, 5H), 3.40-3.50 (m, 2H) 3.70-3.90 (m, 7H), 4.76 (bs, 2H), 6.88 (d, *J* = 9.2 Hz, 1H), 6.97 (d, *J* = 8.4 Hz, 2H), 7.05 (d, *J* = 2.4 Hz, 1H), 7.10 (dd, *J* = 8.0 Hz, 2.4 Hz, 1H), 7.45 (d, *J* = 8.0 Hz, 2H).

4'-(4-(2-((2-amino-4,5,6,7-tetrahydrobenzo[d]thiazol-6-

yl)(propyl)amino)ethyl)piperazin-1-yl)-4-methoxybiphenyl-3-ol (53): Into the solution of **52** (110 mg, 0.17 mmol) in dry THF (10 ml) at 0°C was added (1.7 ml, 1.7 mmol) solution of borane-THF complex (1 M solution) with stirring under nitrogen atmosphere followed by procedure **R**. Crude residue was purified by flash chromatography on silica gel column using solvent system ethyl acetate/methanol (9:1) to yield **53** (52 mg, 60%). ¹H NMR (CDCl₃, 400 MHz): δ 0.95 (t, *J* = 7.2 Hz, 3H), 1.52-1.63 (m, 2H), 1.76-1.86 (m, 1H), 2.06-2.09 (m, 1H), 2.51-2.74 (m, 11H), 2.86-2.96 (m, 2H), 3.22 (t, *J* = 4.8 Hz, 4H), 3.28-3.31 (m, 2H), 3.86 (s, 3H), 4.87 (bs, 2H), 6.92-7.02 (m, 5H), 7.43 (d, *J* = 9.2 Hz, 2H). The product was converted into corresponding hydrochloride salt, m.p. 248 °C. Anal. (C₂₉H₃₉N₅O₂S · 5.0 HCl · 1.0 C₂H₅COOCH₂CH₃) : C, H, N.

6.2. In vitro binding assay:

All final compounds were tested for their in vitro affinity for human D2L, D3 receptors, expressed in HEK 293 cells. Binding affinities were assessed according to previously published procedure^{65, 153, 165, 166}. In this competitive binding assay, the affinity of the compounds were determined by their ability to compete for [³H]-Spiperone for binding to the D2L or D3 receptors. HEK 293 cells expressing D2L or

D3 receptors were homogenized and used fresh as a source of membrane bound receptors. Approximately 20 (for D2L) or 50 (for D3) μg of protein were incubated with each test compound and [^3H]-spiperone (0.4 nM) for 1 h at 30°C in 50 mM Tris-HCl (pH 7.4) with 0.9% NaCl, and 0.025% ascorbic acid in the absence of GTP, in a total volume of 0.8 ml. (+)-Butaclamol (2 μM) was used to define nonspecific binding. Assays were terminated by addition of ice-cold buffer and filtration through glass fibre filtermats with cold saline as wash buffer in the MACH 3-96 Tomtec harvester (Wallac, Gaithersburg, MD). IC_{50} values were estimated by nonlinear regression analysis with the logistic model in the least squares fitting program ORIGIN, and converted to inhibition constants (K_i) by the Cheng-Prusoff equation¹⁶⁵. In this conversion, the K_d values for [^3H]-spiperone binding were 0.057 nM for D₂ receptors and 0.125 nM for D₃ receptors.

6.3. *In vitro* [^{35}S]-GTP γ S-binding functional assay:

GTP γ S (guanosine 5'-[γ - ^{35}S] thio] triphosphate)-binding functional assay is an *in vitro* assay which is used to measure the agonist efficacy of ligands for G-protein coupled receptors (GPCRs). Agonist efficacy is a measure of how well an agonist can stimulate G-proteins linked to a receptor. This assay is based on direct measurement of guanine nucleotide exchange on G-proteins. A heterotrimeric G-proteins consisting of α , β , γ subunits bound to guanosine diphosphate (GDP) represents resting state which remains coupled to the receptor. Ligand receptor interaction causes conformational change in the receptor that triggers the exchange of guanosine diphosphate (GDP) by guanosine triphosphate (GTP) and subsequent dissociation of α -subunit which then interacts with adenylyl cyclase and initiates cascade of downstream events¹⁶⁷. The normal GTP binding event to the α -subunit of G-proteins in response to the ligand receptor interaction in GPCR is replaced by

the binding of nonhydrolyzable analogue of GTP, [³⁵S]GTPγ[S] to the α-subunit of G-proteins^{167, 168}. GTPγS can not be hydrolyzed by intrinsic GTPase activity of α subunit of heterotrimeric G-proteins. The time course of [³⁵S]GTPγ[S] binding follows a pseudo-first-order reaction with [³⁵S]GTPγ [S] binding reaching equilibrium after approx. 3 h¹⁶⁹. The [³⁵S]GTPγ [S]-binding event is the rate-determining step in the assay. Agonists regulate the maximal level of [³⁵S]GTPγ [S] bound, rather than the rate constant for binding. The [³⁵S]GTPγ[S]-binding assay therefore determines agonist efficacy on the basis of the amount of [³⁵S]GTPγ [S] bound rather than the rate of binding. Therefore, the more efficacious the ligand is in stimulating the receptor, the more radioligand will be bound to the G-proteins as a result of the stimulation. Generally, the parameter E_{max} provides a good estimate of efficacy, based on which a ligand can be full agonist or partial agonist or antagonist. EC₅₀ is the concentration of agonist that produces half maximal response which correlates with the affinity of the agonist for particular receptor under the assay condition.

Cell culture:

Chinese hamster ovary (CHO) cells expressing human D2 receptors were grown in Dulbecco's modified Eagle's medium enriched with 5% bovine calf serum, 1% L-glutamine, 0.5% penicillin/ streptomycin, and 2 μg/mL puromycin. AtT-20 cells expressing human D3 receptors were grown in Gibco F10 medium with 10% horse serum, 5% fetal bovine serum, 1% L-glutamine, 50 ug/mL gentamicin, and 500 ug/mL G418.

Assay procedure:

The general procedures used for measuring [³⁵S]GTPγS binding are modified from protocols described for DA receptors^{167, 170} and other G protein-coupled

receptors^{167, 168}. To make membranes, cells were washed with phosphate-buffered saline (PBS), and then centrifuged in PBS at 1000 *g* for five minutes at 4°C. The supernatant was removed, and cells were resuspended in 50 mM Tris HCl, 1mM EDTA, pH 7.4 (resuspension buffer), by polytron, and then centrifuged at 35,000 *g* for 15 minutes at 4°C twice. The cell mass was resuspended with assay buffer (D2: 20mM HEPES, 3mM MgCl₂, 150mM NaCl, 0.2mM EDTA, 0.001% bovine serum albumin (BSA); D3: 20mM HEPES, 3mM MgCl₂, 100mM NaCl, 0.2mM EGTA, 0.001% BSA). The [³⁵S]GTPγS binding assays were performed in triplicates. The final 1-mL volume was composed of 100 μL of 10% (v/v) dimethylsulfoxide (DMSO) as vehicle, drug dilution (in 10% DMSO), or DA (1 mM for D2 cells, and 100 μM for D3 cells) as indicator of binding plateau; 400 μL [³⁵S]GTPγS dilution (4.3 pmol in 10 mL assay buffer per 24-well filter mat); and 500 μL cell suspension (cells suspended, per 24-well filter, in 12.5 mL assay buffer and 7.5 μL GDP, for final concentration of 3 μM in assay). This solution was incubated at room temperature in a shaking water bath for 60 minutes. Cells were harvested using Brandel GF/B filtermats and a 24-pin Brandel harvester (Biomedical Research & Development Laboratories, Inc., Gaithersburg, MD) with cold resuspension buffer as the washing fluid. A Beckman LS 6500 scintillation counter was used to determine ³⁵S radioactivity at 70% efficiency. Nonspecific binding of [³⁵S]GTPγS measured in the presence of 10 μM GTPγS was a very small fraction (5% or less) of basal binding in the absence of drug (vehicle) and did not impact the EC₅₀ (concentration producing half-maximal stimulation) of the test drug estimated by nonlinear logarithmic fitting (logistics model) with Origin Pro 7.0. The plateau binding (maximal binding stimulation) with test drug was expressed as percent of maximal binding observed with the full agonist DA (% E_{max}).

6.4. Reversal of Reserpine-Induced Hypolocomotion in Rats DA Agonists:

Animals:

In rodent studies, animals were male Sprague-Dawley rats from Harlan (Indianapolis, IN) weighing 220-225 g unless otherwise specified. They were maintained in sawdust-lined cages in a temperature and humidity controlled environment at $22 \pm 1^\circ\text{C}$ and $60 \pm 5\%$ respectively, with a 12-h light/dark cycle, with lights on from 6:00 AM to 6:00 PM. They were group housed with unrestricted access to food and water. All experiment was performed during the light component. All animal use procedures were in compliance with the Wayne State University Animal Investigation Committee consistent with AALAC guidelines.

Administration of reserpine induces catalepsy in rodents primarily by blocking the vesicular monoamine transporter (VMAT) which helps in the internalization of monoamines into vesicles, resulting in metabolism of unprotected monoamines in the cytosol that ultimately causes depletion of monoamines in the synapse of the peripheral sympathetic nerve terminals^{158, 171}. The ability of the compounds to reverse the reserpine induced hypolocomotion was investigated¹⁷². Ropinirole was used as standard reference compound in this study.

6.5. Rotational experiment with 6-Hydroxy dopamine lesioned rats:

This animal model for PD, also known as the Ungerstedt Rat rotation model for PD is an well accepted model to screen drug candidate for the treatment of PD¹⁷³. In this animal model, rats were administered surgically neurotoxic 6-Hydroxy dopamine in the MFB region of the one side of the brain which will selectively and completely degenerate the nigrostriatal dopaminergic system at the lesioned side. The selective

destruction of the pre synaptic dopaminergic neurons will cause development of post synaptic supersensitivity on the lesioned side. DA agonist, when administered systemically will produce contra lateral rotation in the rat that is toward non lesioned side. The result of this experiment will indicate in vivo agonist potency of the compound and its potential utility for the treatment of PD as well as the ability of the compound to cross blood brain barrier.

Assay procedure: - Reversal of Reserpine-Induced Hypolocomotion in Rats:

Administration of reserpine induces catalepsy in rodents primarily by blocking the vesicular monoamine transporter (VMAT) which helps in the internalization of monoamines into vesicles, resulting in metabolism of unprotected monoamines in the cytosol that ultimately causes depletion of monoamines in the synapse of the peripheral sympathetic nerve terminals^{158, 171}. The ability of the DA agonists to reverse the reserpine induced hypolocomotion was investigated¹⁷². Ropinirole was used as standard reference compound in this study. Rats were administered with reserpine (5.0 mg/kg, s.c.) or saline (s.c.) 18 h before the injection of test compounds, Ropinirole (5 µM/Kg s.c.) or vehicle (s.c.). Immediately after administration of the latter drugs, animals were individually placed in versamax animal activity monitor chamber (45X30X20 cm) (AccuScan Instruments, Inc. Columbus, OH) to start measuring locomotor activity. The rats were placed individually in chambers for 30 minutes for acclimatization purpose before the administration of the latter drug. Locomotion was monitored for 6 h. Consecutive interruption of two infrared beams situated 24 cm apart and 4 cm above the cage floor in the monitor chamber recorded movement. The data were presented as horizontal counts (HACTV) and total distance travelled (TOTDIST) at 30 min interval.

The data were collected at every 30 minutes. Data were analyzed by Graph Pad (Version 4, San Diego) program.

Assay procedure: - Rotational experiment with 6-OHDA lesioned rats:

Animals were administered apomorphine, potent dopamine receptor agonist, 14 days post surgery to check for rotational behavior. In the second challenge with apomorphine (0.05 mg/kg) 21 days post lesion, contralateral rotations were recorded for 30 mins; apomorphine produced rotations in all four rats (average rotation > 250) indicating successful unilateral lesion. In these rats, lesion was performed on the left side with the rotations produced upon agonist challenge occurring clockwise. In this study, apomorphine was also used as a reference compound. The number of rotations was measured over 10 hours. For control, vehicle was administered alone. The rotations were measured in a rotational chamber immediately after administration of drugs for a time period of 10 to 12 hours. The data were collected at every 30 minutes. Data were analyzed by Graph Pad (Version 4, San Diego) program.

Statistical analysis:The data were analyzed by one way analysis of variance (ANOVA). If ANOVA was significant, post-hoc comparisons were made using Dannett's method between control and drug treated groups.

6.6. Evaluation of Antioxidant Activity. DPPH Radical Scavenging Assay.

DPPH Assay: The DPPH radical-scavenging effect was measured according to reported method¹⁷⁴. This method measures hydrogen atom or electron donating activity. DPPH (1,1-Diphenyl-2-picrylhydrazyl) is a stable free radical of a purple color which gets reduced to a yellow colored 1,1,-diphenyl-2-picryl hydrazine. Each

tested sample was mixed with DPPH radical in methanol and after 20 min incubation at room temperature (30 °C) in the dark, the absorbance was read at 517 nm.

Assay procedure:

To a 96-well plate, an amount of 100 µL of drug solutions (dissolved in methanol) ranging from 20 to 250 µM was added. To release the free bases from their salts, the stock solutions of the compounds were neutralized using saturated sodium bicarbonate solution. Next 100 µL of 200 µM methanolic solution of DPPH (1,1-diphenyl-2-picrylhydrazyl) was added and the plate was shaken vigorously at 30 °C for 25 min. Control wells received 100 µL of methanol and 100 µL of 200 µM methanolic DPPH solution. Wells containing only 200 µL of methanol served as a background correction. The change in absorbance of all samples and standard (ascorbic acid) was measured at 517 nm. Radical scavenging activity was expressed as inhibition percentage and was calculated using the following formula:

$$\% \text{ scavenging activity} = \frac{(\text{absorbance of control} - \text{absorbance of sample})}{(\text{absorbance of control})} \times 100.$$

6.7. Neuroprotection Studies:

The hybridoma dopaminergic MN9D cells are derived from the somatic infusion of rostral mesencephalic neurons from embryonic C57BL/6J (E14) mice with N18TG2 mouse cells. They were cultured in T-75 flask (Greiner Bio One, Frickenhausen, Germany) coated with 1 mg/ml poly-L-lysine and maintained in DMEM (high glucose with phenol red) supplemented with 10% Fetal Clone III serum, penicillin (50 units/ml) and streptomycin (50 µg/ml) at 37 °C under 5% CO₂ atmosphere. Stock solution of D-264 and D-433 were prepared in DMSO and stored at -20 °C for the period of experiments. MN9D cells were pre-treated with various concentrations of

drugs for 1 h and then, co-treated with 100 μ M MPP⁺ (prepared freshly before addition from a stock solution in DMSO stored at -20 °C) for 24 h. The control cells were treated with the above medium having 0.01% DMSO only.

Assessment of Cell Viability: Assay Procedure:

To evaluate the neuroprotection ability of the test compounds in the presence of the neurotoxins MPP⁺, the quantitative and colorimetric MTT (3-(4,5-dimethylthiazolyl-2)-2,5-diphenyltetrazoliumbromide) tetrazolium salt assay was used to assess cell viability. MN9D cells were seeded into poly-L-lysine coated 96-well plates at 1×10^4 cells/well in 100 μ L medium. After the plate was equilibrated for 40 h, old medium was taken out from each well and 160 μ L of fresh medium (containing 0.01% DMSO) was added to control wells and wells which were to be treated with MPP⁺. A solution of 160 μ L of D-264 or D-433 in the above medium without DMSO in 20, 10, 5, 1, 0.1, 0.01, 0.001 μ M were added to wells which would be co-treated with MPP⁺. The plate was incubated for 1 h at 37 °C under 5% CO₂ atmosphere. At the end of incubation, required amount of MPP⁺ was added to each well (except the control wells) to maintain a final concentration of 100 μ M. The plate was then incubated for 24 h at 37 °C under 5% CO₂ atmosphere. Next, 20 μ L of MTT stock solution (prepared in Dulbecco's phosphate-buffered saline) was added to each well to maintain a final concentration of 0.5 mg/ml and the plate was incubated for another 3 h at 37 °C under 5% CO₂ atmosphere. Next, the plate was centrifuged at 1500 rpm for 10 min and the supernatants were removed carefully. The formazan crystals were dissolved in 100 μ L of a 1:1 mixture of DMSO/Methanol solution by shaking gently at 400 rpm for 30 min at room temperature on a Thermomix R shaker (Eppendorf, Hamburg, Germany). Then, the absorbance was measured at 570 nM and 690 nM using an Epoch microplate reader (BioTek, Winooski, VT, USA).

Background corrected values (570 nM – 690 nM) were used to plot the graph. Data from at least three experiments were analyzed using GraphPad software (Version 4, San Diego, USA).

6.8. ASN Aggregation Studies:

Chemicals: α -synuclein was purchased from rpeptide (Bogart, GA, USA). Dopamine hydrochloride, ammonium iron(II) sulphate hexahydrate, ferric citrate ascorbic acid, rifampicin, sodium thiosulphate, silver nitrate, sodium hydroxide, formalin (36.5-38% formaldehyde in water), and thioflavin-T were purchased from Sigma-Aldrich (St. Louis, MO, USA). Sodium carbonate, methanol. Glacial acetic acid, sodium phosphate, ethanol, and sodium chloride were purchased from Fisher scientific (New Jersey, USA).

Cell-culture and treatments: PC12 Adh (ATCC[®] CRL1721.1[™]) cells, a rat adrenal pheochromocytoma cell line, were purchased from ATCC. RPMI 1640, heat-inactivated horse serum, fetal bovine serum, penicillin-streptomycin, and trypsin were purchased from GIBCO (Grand Island, NY, USA). PC12 cells were cultured in T-75 flask (Sarstedt Inc, Newtown, NC, USA) and maintained in RPMI 1640 medium supplemented with 10% heat-inactivated horse serum, 5% fetal bovine serum, penicillin (100 units/mL), and streptomycin (100ug/mL) at 37°C in 5% CO₂ atmosphere.

Visualization of ASN aggregates by silver-staining

Samples were analyzed on 12% SDS-PAGE (Bio-rad) and visualized with silver staining. Briefly, the gel were fixed in the fixing solution (50% MeOH, 12% HAc, 0.05% formalin) for 2 hrs, followed by three times washing with 35% EtOH for 20

minutes each time point. Then, the gels were exposed to sensitizer for 2 minutes and washed with water for 5 minutes. Subsequently, the gels were stained with silver staining (0.2% AgNO₃, 0.076% formalin) for 20 minutes and washed with water for 5 minutes. Finally, the gels were developed with developer (6% Na₂CO₃, 0.05% formalin, 0.0004% Na₂S₂O₃) and left over in the stop solution (1% HAc). Gel images were taken using Biorad Gel Doc XR+ imaging system.

Confirmation of β -sheet positive protein structure by Thioflavin-T assay

42 μ l of 500 μ M (1.1 mg of ThT in 7 ml of PBS) ThT solution was mixed with 479 μ l PBS to get 40 μ M ThT solution. 10 μ l of protein from each time point was mixed with 10 μ l of 40 μ M ThT into 384 black well plate (solid bottom, corning) and fluorescence was measured using synergy hybrid H1 Fluorescence Microplate Reader (BioTek) at 440 nm and 485 nm with autosensitivity mode. Control well received 10 μ l PBS and 10 μ l of 40 μ M ThT. However, when overflow was observed during the fluorescence reading the sensitivity mode of the reader was changed to 100.

1. Generation of α -synuclein aggregates using cell-free system

For cell-free system experiments, all solutions were prepared in 1X PBS. Shaking experiments were conducted on Thermomix R shaker (Eppendorf, Hamburg, Germany) at 1400 rpm and 37°C. 1mg α -synuclein was dissolved in 576.3 μ l 1X PBS to generate 120 μ M stock solution of protein (protein concentration was also verified by BCA protein assay). 400 μ M dopamine hydrochloride was made by dissolving 2mg dopamine hydrochloride in 26.36mL 1X PBS. 35 μ M ferric citrate was prepared by diluting 350 μ M ferric citrate, which was prepared by dissolving 1.78 mg ferric citrate (III) in 20mL 1X PBS. H₂O₂ concentration was calculated using UV.

Protocol A: Generation of dopamine-induced, SDS-resistant ASN oligomers

alpha-synuclein (1 mg) was dissolved in 2 ml of PBS (without calcium and magnesium), followed by passing the solution through a 0.2 μM filter to ensure removal of preformed aggregates. The concentration of stock was 35 μM , 125 μL of this stock was combined with 125 μL of 400 μM DA, this gave give the final concentration of DA 200 μM and that of α -synuclein 17.5 μM . This mixture was then incubated at 37°C with shaking at 1400 rpm (Thermomixer comfort, Eppendorf) for 72 hrs. Aliquots of the reactions were removed at each time point: 4, 8, 12, 24, 48 and 72 hrs and we collected 10 μL for silver staining and 15 μL for Thioflavin T assay.

Protocol B: Generation of dopamine and hydrogen peroxide induced, SDS-resistant ASN oligomers

First 62.5 μL of 1200 μM H_2O_2 was mixed with 800 μM , 62.5 μL of DA to get total 125 μL of 600 μM H_2O_2 and 400 μM of DA. This solution was mixed with 125 μL of 35 μM α -synuclein. Overall, we got ASN: DA: H_2O_2 : : 17.5: 200:300 μM respectively. Remaining protocol is similar to protocol **A**.

Protocol C: Generation of iron-induced, SDS-sensitive ASN fibrils

110 μL of 35 μM ferric citrate (III) was combined with 110 μL of 35 μM ASN. This gave the final concentration of ferric citrate (III) 17.5 μM and that of ASN was 17.5 μM (based on molecular weight). This mixture was then incubated at 37°C with shaking at 1400 rpm for 6 days. The samples were collected at 0, 0, 24, 48, 72, 96, and 144 hrs. At each time point we collected 10 μL for silver staining and 15 μL for Thioflavin T assay.

2. Assessment of potential lead compounds', and comarision with refrence compounds for their ability to modify ASN aggregation in cell-free system

We evaluated the effects of ascorbic acid (anti-oxidant), rifampicin (known ASN aggregation inhibitor), and our lead compound D-520 on dopamine-induced ASN oligomerization employing cell-free system. All solutions were prepared in 1X PBS. Shaking experiments were conducted on Thermomix R shaker (Eppendorf, Hamburg, Germany) at 1400 rpm and 37°C.

Protocol for ASN+DA: 2 mg of DA hydrochloride was dissolved in 26.36 ml of PBS to get 400 μ M DA. 125 μ L of 400 μ M DA was mixed with 125 μ L of 35 μ M ASN to get 200 μ M DA and 17.5 μ M ASN. This mixture was then incubated at 37°C with shaking at 1400 rpm (Thermomixer comfort, Eppendorf) for 10 days. Aliquots of the reactions were removed at each time point: 0, 2, 4, 6, 8 and 10 days and we collected 10 μ L for silver staining and 15 μ L for Thioflavin T assay.

Protocol for ASN+DA+AA: 2 mg of DA hydrochloride was dissolved in 13.18 ml of PBS to get 800 μ M DA. Similarly, 2.81 mg of ascorbic acid (AA) was dissolved in 10 ml of PBS to get 1600 μ M of AA. Subsequently, 62.5 μ L of 800 μ M DA was mixed with 1600 μ M, 62.5 μ L of AA to get total 125 μ L of 400 μ M DA and 800 μ M of AA. This solution was mixed with 125 μ L of 35 μ M ASN. Overall, we got ASN: AA: DA : 17.5: 200:400 μ M respectively. Remaining protocol is similar to above ASN+DA.

Protocol for ASN+DA+Rifampicin: 1.0 mg of Rifampicin was dissolved in 1.52 ml of 1 x-PBS to get 800 μ M stock solutions. 62.5 μ L of 800 μ M DA was mixed with 70 μ M, 62.5 μ L of ASN to get total 125 μ L of 400 μ M DA and 35 μ M of ASN. This solution was mixed with 125 μ L of 800 μ M Rifa. Overall, we got ASN: DA: Rifa : 17.5: 200:400 μ M respectively. Remaining protocol is similar to above ASN+DA.

Protocol for ASN+DA+D-520: 4.2 mg of D-520 was dissolved in 1% DMSO in 7ml 1 x-PBS to get 800 μ M stock solutions. 62.5 μ L of 800 μ M DA was mixed with 70

μM , 62.5 μL of ASN to get total 125 μL of 400 μM DA and 35 μM of ASN. This solution was mixed with 125 μL of 800 μM D-520. Overall, we got ASN: DA: D-520: 17.5: 200:400 μM respectively. Remaining protocol is similar to above ASN+DA.

3. Generation of α -synuclein aggregates to assess extracellular toxicity in cell-culture models

ASN aggregates were generated with primary goal to evaluate the effect various extracellular ASN species on cellular viability in PC12 cells. In this experiment, ASN aggregates were formed by two different methods, either to yield β -sheet positive fibrillar structure or to yield β -sheet negative dopamine-induced and co-valently modified oligomeric structure of ASN. All samples were prepared in 1X PBS. Shaking experiments were conducted on Thermomix R shaker (Eppendorf, Hamburg, Germany) at 1400 rpm and 37°C. 1mg α -synuclein was dissolved in 576.3 μL 1X PBS to yield 120 μM stock solution. 180 μM dopamine was prepared by dissolving 1mg dopamine hydrochloride in 29.24mL 1X PBS.

Protocol A: Generation of ASN fibrils

250 μL α -synuclein (120 μL) was mixed with 250 μL 1X PBS to yield 60 μM ASN. 70 μL aliquot was taken from the mixture and then the solution was shaken for 10 days. 70 μL aliquots were collected at day 2, day 4, day 6, day 8, and day 10. Aliquots were used to assess cytotoxicity (40 μL), Thioflavin-T assay (10 μL).

Protocol B: Generation of ASN oligomers co-valently modified with dopamine

250 μL α -synuclein (120 μL) was mixed with 250 μL 180 μM dopamine to yield the mixture of 60 μM ASN and 90 μM dopamine. Remaining protocol is similar to above A (60 μM ASN)

4. Evaluation of cytotoxicity of extracellular ASN aggregates (pre-formed) in cell-culture system

Aliquots obtained from experiments mentioned above were used to evaluate the effect of (pre-formed) various species generated from ASN aggregation experiments on PC12 cell viability (extracellular toxicity). The main objective of this experiment was to optimize the time-point and the aggregation environment that would induce desired cytotoxicity (in ideal conditions, ~50% cell death). For cell-culture experiments, 40 μL aliquots (60 μM ASN) from various time-points were diluted with 200 μL PC12 cell media to make the final concentration of ASN 10 μM for cell culture experiments.

Experimental protocol: Cell viability assay to assess extracellular toxicity of various ASN synuclein aggregation species quantitative and colorimetric MTT assay was used to evaluate cytotoxic effects of ASN. PC12 cells were seeded at 17000 cells/well density in 100 μL media in 96 well plate. Cells were allowed to adhere to the surface for 24 hours. Media was removed and the adhered PC12 cells were treated with 55 μL ASN (10 μM) containing media. Control cells were treated with appropriately diluted PC12 media. Treatment with extracellular ASN was conducted for 24 hours. After incubation, 6 μL 5 mg/mL MTT was added to the cells and the plate was further incubated at 37°C in 95% air/5% CO₂ atmosphere for 3 hours to produce dark blue formazan crystals. Afterwards, the plate was centrifuged at 1500 rpm for 10 minutes and the supernatants were carefully removed. The formazan crystals were dissolved by adding 100 μL of DMSO/methanol (50:50) mixture to each well and shaking the plate gently at room temperature at 400rpm for 30 minutes at room temperature using a Thermomix R shaker (Eppendorf, Hamburg, Germany). The absorbance values were measured using Epoch microplate reader (Biotek,

Winooski, VT, USA) at 570 nm with background correction done at 690nm. Data from at least 3 experiments were analyzed using Graphpad software (Version 4, San Diego, USA). Cell viability was defined as a percentage reduction in absorbance compared to untreated controls.

5. Assessment of some lead compounds and standard drug's ability to alter cytotoxicity induced by extracellular α -synuclein

ASN alone (60 μ M) was able to induce around ~ 40% cell death after shaking for 6 days. Therefore, we assessed the ability of some of our lead compound D-520 and a standard drug (rifampicin) to alter cytotoxicity induced by ASN (60 μ M) after shaking for 6 days. All solutions were prepared in 1X PBS. Shaking experiments were conducted on Thermomix R shaker (Eppendorf, Hamburg, Germany) at 1400 rpm and 37°C. 120 μ M ASN was prepared by dissolving 1mg α -synuclein in 576.3 μ L 1X PBS. 240 μ M rifampicin was prepared by dissolving 1mg rifampicin in 4.84mL 1X PBS. 240 μ M D-520 was prepared by dissolving 1mg D-520 in 5.6mL 1X PBS.

Protocol for α -synuclein alone experiments

70 μ L ASN (120 μ M) was mixed with 70 μ L 1X PBS to yield 60 μ M ASN. 50 μ L aliquot was taken from the mixture and the remaining mixture was shaken for 6 days. After 6 days, the mixture was frozen at -20°C until further use. From day 0 aliquot, 40 μ L was used for cell viability assay and 10 μ L was used for ThT assay, whereas, from day 6 aliquot, 40 μ L was used for cell viability assay, 10 μ L was used for ThT assay, and remaining volume was used for electron microscopy.

Protocols for rifampicin, and D520 experiments

70 μ L ASN (120 μ M) was mixed with 70 μ L rifampicin (240 μ M)/70 μ L D-520 (240 μ M) to yield 60 μ M ASN and 120 μ M rifampicin/ D-520. 50 μ L aliquot was taken from the mixture and the remaining mixture was shaken for 6 days. After 6 days, the mixture was frozen at -20°C until further use. From day 0 aliquot, 40 μ L was used for cell viability assay and 10 μ L was used for ThT assay, whereas, from day 6 aliquot, 40 μ L was used for cell viability assay, 10 μ L was used for ThT assay, and remaining volume was used for electron microscopy.

Evaluation of ability of potential lead compounds' and standard's ability to alter cytotoxicity induced by extracellular α -synuclein

The aliquots were diluted with PC12 media to get final concentration of ASN to 10 μ M in PC12 media. MTT assay was carried out as described above in evaluation of cytotoxicity of extracellular ASN aggregates (pre-formed) in cell-culture system.

6.9. Molecular Modeling Studies:

6.9.1. Biological data:

The 3D-QSAR studies were performed on a chemically diverse hybrid D2/D3 agonist molecules belonging to aminothiazole, aminotetraline and conformationally rigid (**table 8**) analogs are reported in our earlier publications.^{141, 143-152} The biological activity had been determined for dopamine D2 and D3 receptors by competitive radioligand binding assays. The same general protocol was used to determine the inhibition constant for displacing [³H]-spiroperidol binding to the cloned D2L and D3 receptors expressed in HEK cells. The IC₅₀ values were converted into Ki with Cheng-Prusoff equation. These compounds covered a wide range of biological activity and spanned over 3.31 and 2.73 log units for D2 and D3 activities,

respectively. The negative logarithm (pK_i) of respective equilibrium constants (K_i) for D2 and D3 receptors binding were used as dependent variable for QSAR studies. For selectivity analysis between D2 and D3 binding, the differences between pK_i for each compound at D2 and D3 were used as dependent variable in the model generation process.^{175, 176}

In order to validate the QSAR models total 45 compounds were divided into a training set of 37 compounds and data set of 8 compounds were used for external prediction. Since the experimental activity varied significantly, different training and test sets were built for three cases. The compounds were rationally divided into training and test sets by considering the fact that test set molecules cover range of biological activity similar to the training set. The basic criterion for selection of test set was binding affinity for D2/D3 as shown in **table 8**. Further, CoMFA based hierarchical clustering using molecular steric and electrostatic field as parameters was also applied for selection of test set molecules. Thus, both the biological activity and structural features were used to validate the generated models. The structures and the respective biological activities of the molecules used in this study at D2/D3 receptors along with their selectivity are shown in **table 8**.

6.9.2. Hardware and Software:

All the molecular modeling studies including CoMFA and CoMSIA reported herein were performed on a Hewlett-Packard xw4300 computer workstation with main memory of 2 GB and Intel® Pentium® 4 CPU of 3.4 GHz under the operating system Linux Red Hat 5. The molecular modeling software packages a) Sybyl 8.0¹⁷⁷ from Tripos Inc.¹⁷⁷ and b) Molecular Operating Environment (MOE) 2011.10 from Chemical Computing Group, Inc.¹⁷⁸ were employed for the present work.

6.9.3. CoMFA analysis:

All the compounds in the present study were built using fragments in the Sybyl's library. Each structure was fully geometry-optimized using Tripos force field with a distance-dependent dielectric function until a root mean square (rms) deviation of 0.001 kcal/mol Å⁻¹ was achieved. Partial atomic charges required for electrostatic interaction were computed by Gasteiger Hu"ckel and MOPAC method. The conformational search for the most active compound at D2/D3 receptors, **4**, was performed using systemic search approach. The rotatable bonds were searched from 0 to 359 ° in 10 ° increments. The conformations within ± 10 kcal/mol from the lowest energy conformation were chosen for further analysis. The minimum energy conformation thus obtained was further used in subsequent analysis. Further, based on the structural diversity the whole database was divided into three subsets: a) molecules containing aminotetraline as the head group (Ar₁= A, B, C, compound **5 and 6**) **table 7** b) aminothiazolidum containing compounds, (Ar₁= D) **table 7**, and c) compounds possessing aminothiazolidum as head group and an amide bond at the piperazine nitrogen atom, distal to the agonist head group (compound **12-14**, and **41-45**) **table 7**. Next, most active compounds from each subset (compounds **33** and **42** from subset b and c respectively) were built on the minimum energy conformation of **4** (most active in whole database) and their geometry was optimized as mentioned above. Thereafter, the generated conformations of compounds **33** and **42** were used as template to construct the remaining molecules of their respective subset, followed by energy minimization, and geometry optimization. For the selectivity analysis compound **42** was used as a template to align the whole database.

6.9.4. Alignment:

Structural alignment is considered as one of the most critical step to successfully build a 3D-QSAR model. However, in contrast to CoMFA, CoMSIA is not much sensitive to changes in orientation of aligned molecules in the lattice. In our present work, the ligand alignments were achieved by two different methods.

1. Atom-based alignment: for atom-base fitting, atoms indicated by asterisk (*) in **table 7** were used for rms fitting onto the corresponding atoms of the template molecule (compound **4**). The most active compound from each subset (compound **33** and **42** from subset b and c) was aligned on the template molecule, **4**, and subsequently, each molecule of particular subset was aligned on this molecule.
2. Flexible fitting alignment: The energy minimized conformations were imported in TriposMol2 (.mol2) format in MOE 2011.10 and stored in a molecular database. This database was used as an input in the Flexible Alignment functionality in MOE. It is an application in MOE for flexibly aligning small molecules by maximizing steric and other features, like shape, refractivity, hydrogen bond donor acceptor, and donor overlap while minimizing internal ligand strain. The most active compound, **4**, was used as a template to align the whole database described above. **Compound 42** was used as template to align the whole database for selectivity analysis (D2/D3). In the present study Flexible Alignment panel was used with following settings: alignment mode flexible, iteration 1000, failure limit 50, energy cutoff 15 and configuration limit 1000. Other parameters values in the Flexible Alignment panel were kept at their default values.

6.9.5. CoMFA studies:

All the superimposed molecules were kept in a 3D grid and CoMFA steric and electrostatic interaction fields were calculated at each lattice interaction points of a regularly spaced grid of 2.0 Å. An sp³ carbon atom with Van der Waals radius of 1.52 Å and +1.0 charge was used as a probe to calculate steric and electrostatic fields. Values of both the fields were truncated at +30 kcal/mol. The electrostatic fields were ignored at the lattice points with maximal steric interactions. In the end, the results from the both steric and electrostatic field sampling along with biological activity (pki) of the molecules were put into a spread sheet, and partial least square (PLS) was applied to get the final results.

Another molecular modeling CoMSIA which is an extension of CoMFA methodology was also applied. CoMSIA is thought to be less affected by changes in molecular alignment and it uses Gaussian-type distance dependence which provides smoother and easily interpretable contour maps. Furthermore, in addition to steric and electrostatic fields, CoMSIA includes hydrophobic and hydrogen bond interaction as well. CoMSIA calculates similarity indices at the intersections of a surrounding lattice.^R The similarity index $A_{(F,K)}$ for a molecule j with atom i at a grid point q was calculated.

6.9.6. Partial Least Square (PLS):

PLS was used to correlate the binding affinity at D2/D3 receptors with CoMFA and CoMSIA descriptors. PLS analyses were performed following standard implementation in SYBYL8.0. The statistical significance of the generated 3D-QSAR models was assessed using leave-one-out (LOO procedure). Optimal numbers of components were determined by selecting the smallest s_{press} value and the last added component was considered if it increases the r^2_{cv} by more than 5% according

to the parsimony principle.²¹ In order to speed up the analysis and reduce noise, minimum standard deviation threshold was set at 2.0 kcal./mol. The r^2_{cv} , S_{press} , r^2_{conv} , SE and F_{ratio} were computed as defined in SYBYL8.0.

6.9.7. Predictive r^2 value

The predictive r^2 was computed for the test set molecules. and was regarded as

$$r^2_{pred.}=(SD-PRESS)/SD$$

where SD is sum of square deviation between biological activities and the mean observed activity of the test set molecules and PRESS is sum of squared deviation between the observed and predicated activates of the test set molecule. Like r^2_{cv} , predictive r^2 can assume a negative value reflecting a complete lack of predictive ability of the training set for the molecules included in the test set. When $Pr^2=0$, it indicates that the results are not by chance and are significant.

CHAPTER 7

CONCLUSION

Parkinson's disease (PD) is a progressive age-related neurodegenerative disorder of the central nervous system that is characterized by gradual loss of dopaminergic neurons in the substantia nigra region of the brain. It is increasingly evident that drugs aiming a single target may be inadequate for the treatment of complex diseases such as PD, which is multifactorial in nature. Thus, it is hypothesized that multifunctional drugs having multiple pharmacological activities addressing multiple pathogenic factors of PD will be effective as disease modifying agent for the treatment of this disease.

Our first objective was to design and develop a series of novel ligands for dopamine receptors that will possess enhanced blood brain barrier crossing ability compared to the first generation hybrid compound **D-264** without compromising its DA receptor binding and neuroprotection properties. Our current structure activity relationship study is focused on introduction of methoxy and hydroxyl group at various positions on the accessory binding biphenyl ring of this hybrid molecule. The introduction of hydroxyl group or combination of hydroxyl/methoxy group at a suitable position could further potentiate its antioxidant and neuroprotection property. The molecules with high affinity and selectivity for binding at the dopamine D3 receptor compared to D2 in *in vitro* binding assay were selected as potential candidate for *in vitro* functional assay to test its agonist potency. The compounds that produced appreciable stimulation of the dopamine receptors in *in vitro* functional assay system compared to **D-264** were tested in *in vivo* assay to evaluate potential antiparkinsonian property. Next, objective was to carry out *in vitro* biochemical assay system to evaluate the antioxidant potency. In line with our multifunctional drug development objective,

one of our important goal was to evaluate *in vitro* neuroprotection ability of the lead compounds.

Among all synthesized compounds in the first series, compound **D-433** and **D-533** exhibited the highest selectivity for the D3 over D2 receptor in both binding and functional assays. Lead compounds **D-433** and **D-533** also exhibited potent free radical quenching property, possibly indicating antioxidant activity. The lead compounds were tested in two PD animal models. Both the compounds exhibited higher blood brain barrier crossing ability compared to parent compounds D-264. Furthermore, in MTT assay lead compounds are able to protect MN9D cells from the exposure to neurotoxin MPP⁺ and 6-OHDA in a dose dependent manner.

A substantial body of literature points to a pivotal role of ASN in producing oxidative stress leading to neurodegeneration. ASN is a component of Lewy bodies, a pathological hall mark of PD. These protein aggregates may be responsible for triggering the degeneration of dopaminergic neurons in the SN region of the brain. ASN forms toxic oligomers or fibrils. Currently, it is not known how the aggregation of ASN triggers cell death. The modulation of its aggregation is emerging as a novel therapeutic target to treat PD. One of the major aspects that might be targeted therapeutically is to inhibit the aggregation of ASN so anti-aggregative compounds or the compounds that can break the preexisting aggregates may be helpful. These ASN modulators have been proven to be neuroprotective in both *in vitro* and *in vivo* animal models of PD. Our final goal was to develop potent *in vivo* active dopamine D2/D3 receptor agonists which should modulate ASN aggregation in a way that will inhibit the toxicity of wild type ASN aggregates in the cell culture system

Compounds **D-519** and **D-520** were selected as lead molecules from the second

series and they exhibited nanomolar to sub nanomolar range affinity at D2/D3 receptors in the receptor binding assay and [³⁵S]GTPγS binding assay. It was concluded from this *in vivo* study that both **D-519** and **D-520** was able to efficiently cross blood brain barrier and exhibited high *in vivo* agonist efficacy. **D-519** and **D-520** can potentially chelate with Fe(III). Furthermore, **D-520** is able to reverse the ASN aggregates induced toxicity at a significant level in PC-12 cells. Finally, three dimensional quantitative structure activity relationship (3DQSAR) studies CoMFA and CoMSIA were performed. Two alignment methods (atom base and flexible) and two charge calculation methods (Gasteinger-Huckel and MOPAC) were used. The presence of carbonyl group attached to piperazine ring and hydrophobic biphenyl ring was found to be one of the most important factors responsible for the D3 selectivity over D2.

REFERENCES

1. Braak, H.; Del Tredici, K.; Rub, U.; de Vos, R. A.; Jansen Steur, E. N.; Braak, E. Staging of brain pathology related to sporadic Parkinson's disease. *Neurobiol Aging* 2003, 24, 197-211.
2. Fink, A. L. The aggregation and fibrillation of alpha-synuclein. *Acc Chem Res* 2006, 39, 628-34.
3. Sherer, T. B.; Betarbet, R.; Greenamyre, J. T. Pathogenesis of Parkinson's disease. *Curr Opin Investig Drugs* 2001, 2, 657-62.
4. Joyce, J. N. Dopamine D3 receptor as a therapeutic target for antipsychotic and antiparkinsonian drugs. *Pharmacol Ther* 2001, 90, 231-59.
5. Foundation, P. D.
6. Dawson, T. M.; Dawson, V. L. Molecular pathways of neurodegeneration in Parkinson's disease. *Science* 2003, 302, 819-22.
7. Bennett, J. P., Jr.; Piercey, M. F. Pramipexole--a new dopamine agonist for the treatment of Parkinson's disease. *J Neurol Sci* 1999, 163, 25-31.
8. Le, W.; Appel, S. H. Mutant genes responsible for Parkinson's disease. *Curr Opin Pharmacol* 2004, 4, 79-84.
9. Chinta, S. J.; Andersen, J. K. Redox imbalance in Parkinson's disease. *Biochim Biophys Acta* 2008, 1780, 1362-7.
10. Kumar, M. J.; Andersen, J. K. Perspectives on MAO-B in aging and neurological disease: where do we go from here? *Mol Neurobiol* 2004, 30, 77-89.
11. Marttila, R. J.; Lorentz, H.; Rinne, U. K. Oxygen toxicity protecting enzymes in Parkinson's disease. Increase of superoxide dismutase-like activity in the substantia nigra and basal nucleus. *J Neurol Sci* 1988, 86, 321-31.
12. Singleton, A. B.; Farrer, M.; Johnson, J.; Singleton, A.; Hague, S.; Kachergus, J.; Hulihan, M.; Peuralinna, T.; Dutra, A.; Nussbaum, R.; Lincoln, S.; Crawley, A.; Hanson, M.; Maraganore, D.;

Adler, C.; Cookson, M. R.; Muenter, M.; Baptista, M.; Miller, D.; Blancato, J.; Hardy, J.; Gwinn-Hardy, K. alpha-Synuclein locus triplication causes Parkinson's disease. *Science* 2003, 302, 841.

13. Kruger, R.; Kuhn, W.; Muller, T.; Woitalla, D.; Graeber, M.; Kosel, S.; Przuntek, H.; Epplen, J. T.; Schols, L.; Riess, O. Ala30Pro mutation in the gene encoding alpha-synuclein in Parkinson's disease. *Nat Genet* 1998, 18, 106-8.

14. Hsu, L. J.; Sagara, Y.; Arroyo, A.; Rockenstein, E.; Sisk, A.; Mallory, M.; Wong, J.; Takenouchi, T.; Hashimoto, M.; Masliah, E. alpha-synuclein promotes mitochondrial deficit and oxidative stress. *Am J Pathol* 2000, 157, 401-10.

15. Feany, M. B.; Bender, W. W. A Drosophila model of Parkinson's disease. *Nature* 2000, 404, 394-8.

16. Maroteaux, L.; Campanelli, J. T.; Scheller, R. H. Synuclein: a neuron-specific protein localized to the nucleus and presynaptic nerve terminal. *J Neurosci* 1988, 8, 2804-15.

17. Paleologou, K. E.; Irvine, G. B.; El-Agnaf, O. M. Alpha-synuclein aggregation in neurodegenerative diseases and its inhibition as a potential therapeutic strategy. *Biochem Soc Trans* 2005, 33, 1106-10.

18. Galvin, J. E.; Uryu, K.; Lee, V. M.; Trojanowski, J. Q. Axon pathology in Parkinson's disease and Lewy body dementia hippocampus contains alpha-, beta-, and gamma-synuclein. *Proc Natl Acad Sci U S A* 1999, 96, 13450-5.

19. Barbour, R.; Kling, K.; Anderson, J. P.; Banducci, K.; Cole, T.; Diep, L.; Fox, M.; Goldstein, J. M.; Soriano, F.; Seubert, P.; Chilcote, T. J. Red blood cells are the major source of alpha-synuclein in blood. *Neurodegener Dis* 2008, 5, 55-9.

20. Stefanis, L. alpha-Synuclein in Parkinson's disease. *Cold Spring Harb Perspect Med* 2012, 2, a009399.

21. Murphy, D. D.; Rueter, S. M.; Trojanowski, J. Q.; Lee, V. M. Synucleins are developmentally expressed, and alpha-synuclein regulates the size of the presynaptic vesicular pool in primary hippocampal neurons. *J Neurosci* 2000, 20, 3214-20.

22. Recchia, A.; Debetto, P.; Negro, A.; Guidolin, D.; Skaper, S. D.; Giusti, P. Alpha-synuclein and Parkinson's disease. *FASEB J* 2004, 18, 617-26.
23. Jellinger, K. A. Synuclein deposition and non-motor symptoms in Parkinson disease. *J Neurol Sci* 2011, 310, 107-11.
24. Lee, S. J.; Lim, H. S.; Masliah, E.; Lee, H. J. Protein aggregate spreading in neurodegenerative diseases: problems and perspectives. *Neurosci Res* 2011, 70, 339-48.
25. Steiner, J. A.; Angot, E.; Brundin, P. A deadly spread: cellular mechanisms of alpha-synuclein transfer. *Cell Death Differ* 2011, 18, 1425-33.
26. Nemani, V. M.; Lu, W.; Berge, V.; Nakamura, K.; Onoa, B.; Lee, M. K.; Chaudhry, F. A.; Nicoll, R. A.; Edwards, R. H. Increased expression of alpha-synuclein reduces neurotransmitter release by inhibiting synaptic vesicle recluster after endocytosis. *Neuron* 2010, 65, 66-79.
27. Garcia-Reitböck, P.; Anichtchik, O.; Bellucci, A.; Iovino, M.; Ballini, C.; Fineberg, E.; Ghetti, B.; Della Corte, L.; Spano, P.; Tofaris, G. K.; Goedert, M.; Spillantini, M. G. SNARE protein redistribution and synaptic failure in a transgenic mouse model of Parkinson's disease. *Brain* 2010, 133, 2032-44.
28. Mosharov, E. V.; Larsen, K. E.; Kanter, E.; Phillips, K. A.; Wilson, K.; Schmitz, Y.; Krantz, D. E.; Kobayashi, K.; Edwards, R. H.; Sulzer, D. Interplay between cytosolic dopamine, calcium, and alpha-synuclein causes selective death of substantia nigra neurons. *Neuron* 2009, 62, 218-29.
29. Volles, M. J.; Lansbury, P. T., Jr. Vesicle permeabilization by protofibrillar alpha-synuclein is sensitive to Parkinson's disease-linked mutations and occurs by a pore-like mechanism. *Biochemistry* 2002, 41, 4595-602.
30. Mosharov, E. V.; Staal, R. G.; Bove, J.; Prou, D.; Hananiya, A.; Markov, D.; Poulsen, N.; Larsen, K. E.; Moore, C. M.; Troyer, M. D.; Edwards, R. H.; Przedborski, S.; Sulzer, D. Alpha-synuclein overexpression increases cytosolic catecholamine concentration. *J Neurosci* 2006, 26, 9304-11.

31. Alim, M. A.; Hossain, M. S.; Arima, K.; Takeda, K.; Izumiyama, Y.; Nakamura, M.; Kaji, H.; Shinoda, T.; Hisanaga, S.; Ueda, K. Tubulin seeds alpha-synuclein fibril formation. *J Biol Chem* 2002, 277, 2112-7.
32. Bartels, T.; Choi, J. G.; Selkoe, D. J. alpha-Synuclein occurs physiologically as a helically folded tetramer that resists aggregation. *Nature* 2011, 477, 107-10.
33. Fauvet, B.; Mbefo, M. K.; Fares, M. B.; Desobry, C.; Michael, S.; Ardah, M. T.; Tsika, E.; Coune, P.; Prudent, M.; Lion, N.; Eliezer, D.; Moore, D. J.; Schneider, B.; Aebischer, P.; El-Agnaf, O. M.; Masliah, E.; Lashuel, H. A. alpha-Synuclein in central nervous system and from erythrocytes, mammalian cells, and Escherichia coli exists predominantly as disordered monomer. *J Biol Chem* 2012, 287, 15345-64.
34. Conway, K. A.; Harper, J. D.; Lansbury, P. T., Jr. Fibrils formed in vitro from alpha-synuclein and two mutant forms linked to Parkinson's disease are typical amyloid. *Biochemistry* 2000, 39, 2552-63.
35. Xu, J.; Kao, S. Y.; Lee, F. J.; Song, W.; Jin, L. W.; Yankner, B. A. Dopamine-dependent neurotoxicity of alpha-synuclein: a mechanism for selective neurodegeneration in Parkinson disease. *Nat Med* 2002, 8, 600-6.
36. Cole, N. B. Metal catalyzed oxidation of alpha-synuclein--a role for oligomerization in pathology? *Curr Alzheimer Res* 2008, 5, 599-606.
37. Wang, C.; Liu, L.; Zhang, L.; Peng, Y.; Zhou, F. Redox reactions of the alpha-synuclein-Cu(2+) complex and their effects on neuronal cell viability. *Biochemistry* 2010, 49, 8134-42.
38. Pfefferbaum, A.; Adalsteinsson, E.; Rohlfing, T.; Sullivan, E. V. MRI estimates of brain iron concentration in normal aging: Comparison of field-dependent (FDRI) and phase (SWI) methods. *NeuroImage* 2009, 47, 493-500.
39. Graham, D. G. Oxidative pathways for catecholamines in the genesis of neuromelanin and cytotoxic quinones. *Mol Pharmacol* 1978, 14, 633-43.

40. Hokfelt, T.; Ungerstedt, U. Specificity of 6-hydroxydopamine induced degeneration of central monoamine neurones: an electron and fluorescence microscopic study with special reference to intracerebral injection on the nigro-striatal dopamine system. *Brain Res* 1973, 60, 269-97.
41. Zecca, L.; Youdim, M. B.; Riederer, P.; Connor, J. R.; Crichton, R. R. Iron, brain ageing and neurodegenerative disorders. *Nat Rev Neurosci* 2004, 5, 863-73.
42. Mandel, S.; Grunblatt, E.; Riederer, P.; Gerlach, M.; Levites, Y.; Youdim, M. B. Neuroprotective strategies in Parkinson's disease : an update on progress. *CNS Drugs* 2003, 17, 729-62.
43. Koeppen, A. H. The history of iron in the brain. *J Neurol Sci* 1995, 134 Suppl, 1-9.
44. Koeppen, A. H.; Dickson, A. C.; McEvoy, J. A. The cellular reactions to experimental intracerebral hemorrhage. *J Neurol Sci* 1995, 134 Suppl, 102-112.
45. Jellinger, K.; Kienzl, E.; Rumpelmair, G.; Riederer, P.; Stachelberger, H.; Ben-Shachar, D.; Youdim, M. B. Iron-melanin complex in substantia nigra of parkinsonian brains: an x-ray microanalysis. *J Neurochem* 1992, 59, 1168-71.
46. Youdim, M. B.; Stephenson, G.; Ben Shachar, D. Ironing iron out in Parkinson's disease and other neurodegenerative diseases with iron chelators: a lesson from 6-hydroxydopamine and iron chelators, desferal and VK-28. *Ann N Y Acad Sci* 2004, 1012, 306-25.
47. Temlett, J. A.; Landsberg, J. P.; Watt, F.; Grime, G. W. Increased iron in the substantia nigra compacta of the MPTP-lesioned hemiparkinsonian African green monkey: evidence from proton microprobe elemental microanalysis. *J Neurochem* 1994, 62, 134-46.
48. Marras, C.; Lang, A. E. Measuring motor complications in clinical trials for early Parkinson's disease. *J Neurol Neurosurg Psychiatry* 2003, 74, 143-6.
49. Olanow, C. W.; Jankovic, J. Neuroprotective therapy in Parkinson's disease and motor complications: a search for a pathogenesis-targeted, disease-modifying strategy. *Mov Disord* 2005, 20 Suppl 11, S3-10.

50. Schapira, A. H.; Olanow, C. W. Neuroprotection in Parkinson disease: mysteries, myths, and misconceptions. *JAMA* 2004, 291, 358-64.
51. Birkmayer, W.; Hornykiewicz, O. The effect of L-3,4-dihydroxyphenylalanine (= DOPA) on akinesia in parkinsonism. 1961. *Wien Klin Wochenschr* 2001, 113, 851-4.
52. Fahn, S. Does levodopa slow or hasten the rate of progression of Parkinson's disease? *J Neurol* 2005, 252 Suppl 4, IV37-IV42.
53. Carter, A. J.; Muller, R. E. Pramipexole, a dopamine D2 autoreceptor agonist, decreases the extracellular concentration of dopamine in vivo. *Eur J Pharmacol* 1991, 200, 65-72.
54. Olanow, C. W.; Jenner, P.; Brooks, D. Dopamine agonists and neuroprotection in Parkinson's disease. *Ann Neurol* 1998, 44, S167-74.
55. Sokoloff, P.; Giros, B.; Martres, M. P.; Andrieux, M.; Besancon, R.; Pilon, C.; Bouthenet, M. L.; Souil, E.; Schwartz, J. C. Localization and function of the D3 dopamine receptor. *Arzneimittelforschung* 1992, 42, 224-30.
56. Hall, D. A.; Strange, P. G. Comparison of the ability of dopamine receptor agonists to inhibit forskolin-stimulated adenosine 3'5'-cyclic monophosphate (cAMP) accumulation via D2L (long isoform) and D3 receptors expressed in Chinese hamster ovary (CHO) cells. *Biochem Pharmacol* 1999, 58, 285-9.
57. Dal Toso, R.; Sommer, B.; Ewert, M.; Herb, A.; Pritchett, D. B.; Bach, A.; Shivers, B. D.; Seeburg, P. H. The dopamine D2 receptor: two molecular forms generated by alternative splicing. *EMBO J* 1989, 8, 4025-34.
58. Seeman, P.; Nam, D.; Ulpian, C.; Liu, I. S.; Talerico, T. New dopamine receptor, D2(Longer), with unique TG splice site, in human brain. *Brain Res Mol Brain Res* 2000, 76, 132-41.
59. Fishburn, C. S.; Belleli, D.; David, C.; Carmon, S.; Fuchs, S. A novel short isoform of the D3 dopamine receptor generated by alternative splicing in the third cytoplasmic loop. *J Biol Chem* 1993, 268, 5872-8.

60. Fu, D.; Skryabin, B. V.; Brosius, J.; Robakis, N. K. Molecular cloning and characterization of the mouse dopamine D3 receptor gene: an additional intron and an mRNA variant. *DNA Cell Biol* 1995, 14, 485-92.
61. Boeckler, F.; Gmeiner, P. The structural evolution of dopamine D3 receptor ligands: structure-activity relationships and selected neuropharmacological aspects. *Pharmacol Ther* 2006, 112, 281-333.
62. Asghari, V.; Sanyal, S.; Buchwaldt, S.; Paterson, A.; Jovanovic, V.; Van Tol, H. H. Modulation of intracellular cyclic AMP levels by different human dopamine D4 receptor variants. *J Neurochem* 1995, 65, 1157-65.
63. Chio, C. L.; Lajiness, M. E.; Huff, R. M. Activation of heterologously expressed D3 dopamine receptors: comparison with D2 dopamine receptors. *Mol Pharmacol* 1994, 45, 51-60.
64. MacKenzie, R. G.; VanLeeuwen, D.; Pugsley, T. A.; Shih, Y. H.; Demattos, S.; Tang, L.; Todd, R. D.; O'Malley, K. L. Characterization of the human dopamine D3 receptor expressed in transfected cell lines. *Eur J Pharmacol* 1994, 266, 79-85.
65. Watts, V. J.; Neve, K. A. Sensitization of endogenous and recombinant adenylate cyclase by activation of D2 dopamine receptors. *Mol Pharmacol* 1996, 50, 966-76.
66. Landwehrmeyer, B.; Mengod, G.; Palacios, J. M. Differential visualization of dopamine D2 and D3 receptor sites in rat brain. A comparative study using in situ hybridization histochemistry and ligand binding autoradiography. *Eur J Neurosci* 1993, 5, 145-53.
67. Joyce, J. N.; Millan, M. J. Dopamine D3 receptor agonists for protection and repair in Parkinson's disease. *Curr Opin Pharmacol* 2007, 7, 100-5.
68. Carvey, P. M.; Pieri, S.; Ling, Z. D. Attenuation of levodopa-induced toxicity in mesencephalic cultures by pramipexole. *J Neural Transm* 1997, 104, 209-28.
69. Kitamura, Y.; Kosaka, T.; Kakimura, J. I.; Matsuoka, Y.; Kohno, Y.; Nomura, Y.; Taniguchi, T. Protective effects of the antiparkinsonian drugs talipexole and pramipexole against 1-methyl-4-

phenylpyridinium-induced apoptotic death in human neuroblastoma SH-SY5Y cells. *Mol Pharmacol* 1998, 54, 1046-54.

70. Ferrari-Toninelli, G.; Maccarinelli, G.; Uberti, D.; Buerger, E.; Memo, M. Mitochondria-targeted antioxidant effects of S(-) and R(+) pramipexole. *BMC Pharmacol* 2010, 10, 2.

71. Iida, M.; Miyazaki, I.; Tanaka, K.; Kabuto, H.; Iwata-Ichikawa, E.; Ogawa, N. Dopamine D2 receptor-mediated antioxidant and neuroprotective effects of ropinirole, a dopamine agonist. *Brain Res* 1999, 838, 51-9.

72. Schapira, A. H.; Olanow, C. W. Rationale for the use of dopamine agonists as neuroprotective agents in Parkinson's disease. *Ann Neurol* 2003, 53 Suppl 3, S149-57; discussion S157-9.

73. Presgraves, S. P.; Borwege, S.; Millan, M. J.; Joyce, J. N. Involvement of dopamine D(2)/D(3) receptors and BDNF in the neuroprotective effects of S32504 and pramipexole against 1-methyl-4-phenylpyridinium in terminally differentiated SH-SY5Y cells. *Exp Neurol* 2004, 190, 157-70.

74. Li, C.; Biswas, S.; Li, X.; Dutta, A. K.; Le, W. Novel D3 dopamine receptor-preferring agonist D-264: Evidence of neuroprotective property in Parkinson's disease animal models induced by 1-methyl-4-phenyl-1,2,3,6-tetrahydropyridine and lactacystin. *J Neurosci Res* 2010, 88, 2513-23.

75. Effects of tocopherol and deprenyl on the progression of disability in early Parkinson's disease. The Parkinson Study Group. *N Engl J Med* 1993, 328, 176-83.

76. Montine, T. J.; Neely, M. D.; Quinn, J. F.; Beal, M. F.; Markesbery, W. R.; Roberts, L. J.; Morrow, J. D. Lipid peroxidation in aging brain and Alzheimer's disease. *Free Radic Biol Med* 2002, 33, 620-6.

77. Levites, Y.; Weinreb, O.; Maor, G.; Youdim, M. B.; Mandel, S. Green tea polyphenol (-)-epigallocatechin-3-gallate prevents N-methyl-4-phenyl-1,2,3,6-tetrahydropyridine-induced dopaminergic neurodegeneration. *J Neurochem* 2001, 78, 1073-82.

78. LeVine, H., 3rd. Quantification of beta-sheet amyloid fibril structures with thioflavin T. *Methods Enzymol* 1999, 309, 274-84.
79. Prabhudesai, S.; Sinha, S.; Attar, A.; Kotagiri, A.; Fitzmaurice, A. G.; Lakshmanan, R.; Ivanova, M. I.; Loo, J. A.; Klarner, F. G.; Schrader, T.; Stahl, M.; Bitan, G.; Bronstein, J. M. A novel "molecular tweezer" inhibitor of alpha-synuclein neurotoxicity in vitro and in vivo. *Neurotherapeutics* 2012, 9, 464-76.
80. Bodner, R. A.; Outeiro, T. F.; Altmann, S.; Maxwell, M. M.; Cho, S. H.; Hyman, B. T.; McLean, P. J.; Young, A. B.; Housman, D. E.; Kazantsev, A. G. Pharmacological promotion of inclusion formation: a therapeutic approach for Huntington's and Parkinson's diseases. *Proc Natl Acad Sci U S A* 2006, 103, 4246-51.
81. Putcha, P.; Danzer, K. M.; Kranich, L. R.; Scott, A.; Silinski, M.; Mabbett, S.; Hicks, C. D.; Veal, J. M.; Steed, P. M.; Hyman, B. T.; McLean, P. J. Brain-permeable small-molecule inhibitors of Hsp90 prevent alpha-synuclein oligomer formation and rescue alpha-synuclein-induced toxicity. *J Pharmacol Exp Ther* 2010, 332, 849-57.
82. El-Agnaf, O. M.; Paleologou, K. E.; Greer, B.; Abogrein, A. M.; King, J. E.; Salem, S. A.; Fullwood, N. J.; Benson, F. E.; Hewitt, R.; Ford, K. J.; Martin, F. L.; Harriott, P.; Cookson, M. R.; Allsop, D. A strategy for designing inhibitors of alpha-synuclein aggregation and toxicity as a novel treatment for Parkinson's disease and related disorders. *FASEB J* 2004, 18, 1315-7.
83. Vekrellis, K.; Stefanis, L. Targeting intracellular and extracellular alpha-synuclein as a therapeutic strategy in Parkinson's disease and other synucleinopathies. *Expert Opin Ther Targets* 2012, 16, 421-32.
84. Masliah, E.; Rockenstein, E.; Adame, A.; Alford, M.; Crews, L.; Hashimoto, M.; Seubert, P.; Lee, M.; Goldstein, J.; Chilcote, T.; Games, D.; Schenk, D. Effects of alpha-synuclein immunization in a mouse model of Parkinson's disease. *Neuron* 2005, 46, 857-68.

85. Cavalli, A.; Bolognesi, M. L.; Minarini, A.; Rosini, M.; Tumiatti, V.; Recanatini, M.; Melchiorre, C. Multi-target-directed ligands to combat neurodegenerative diseases. *J Med Chem* 2008, 51, 347-72.
86. Park, B. H.; Fishburn, C. S.; Carmon, S.; Accili, D.; Fuchs, S. Structural organization of the murine D3 dopamine receptor gene. *J Neurochem* 1995, 64, 482-6.
87. Missale, C.; Nash, S. R.; Robinson, S. W.; Jaber, M.; Caron, M. G. Dopamine receptors: from structure to function. *Physiol Rev* 1998, 78, 189-225.
88. Banala, A. K.; Levy, B. A.; Khatri, S. S.; Furman, C. A.; Roof, R. A.; Mishra, Y.; Griffin, S. A.; Sibley, D. R.; Luedtke, R. R.; Newman, A. H. N-(3-fluoro-4-(4-(2-methoxy or 2,3-dichlorophenyl)piperazine-1-yl)butyl)arylcarboxamides as selective dopamine D3 receptor ligands: critical role of the carboxamide linker for D3 receptor selectivity. *J Med Chem* 2011, 54, 3581-94.
89. Boeckler, F.; Ohnmacht, U.; Lehmann, T.; Utz, W.; Hubner, H.; Gmeiner, P. CoMFA and CoMSIA investigations revealing novel insights into the binding modes of dopamine D3 receptor agonists. *J Med Chem* 2005, 48, 2493-508.
90. Ehrlich, K.; Gotz, A.; Bollinger, S.; Tschammer, N.; Bettinetti, L.; Harterich, S.; Hubner, H.; Lanig, H.; Gmeiner, P. Dopamine D2, D3, and D4 selective phenylpiperazines as molecular probes to explore the origins of subtype specific receptor binding. *J Med Chem* 2009, 52, 4923-35.
91. Elsner, J.; Boeckler, F.; Heinemann, F. W.; Hubner, H.; Gmeiner, P. Pharmacophore-guided drug discovery investigations leading to bioactive 5-aminotetrahydropyrazolopyridines. Implications for the binding mode of heterocyclic dopamine D3 receptor agonists. *J Med Chem* 2005, 48, 5771-9.
92. Gil-Mast, S.; Kortagere, S.; Kota, K.; Kuzhikandathil, E. V. An Amino Acid Residue in the Second Extracellular Loop Determines the Agonist-Dependent Tolerance Property of the Human D3 Dopamine Receptor. *ACS Chem Neurosci* 2013.
93. Grundt, P.; Carlson, E. E.; Cao, J.; Bennett, C. J.; McElveen, E.; Taylor, M.; Luedtke, R. R.; Newman, A. H. Novel heterocyclic trans olefin analogues of N-{4-[4-(2,3-dichlorophenyl)piperazin-

1-yl]butyl}arylcarboxamides as selective probes with high affinity for the dopamine D3 receptor. *J Med Chem* 2005, 48, 839-48.

94. Varady, J.; Wu, X.; Fang, X.; Min, J.; Hu, Z.; Levant, B.; Wang, S. Molecular modeling of the three-dimensional structure of dopamine 3 (D3) subtype receptor: discovery of novel and potent D3 ligands through a hybrid pharmacophore- and structure-based database searching approach. *J Med Chem* 2003, 46, 4377-92.

95. Newman, A. H.; Beuming, T.; Banala, A. K.; Donthamsetti, P.; Pongetti, K.; LaBounty, A.; Levy, B.; Cao, J.; Michino, M.; Luedtke, R. R.; Javitch, J. A.; Shi, L. Molecular determinants of selectivity and efficacy at the dopamine D3 receptor. *J Med Chem* 2012, 55, 6689-99.

96. Zhao, Y.; Lu, X.; Yang, C. Y.; Huang, Z.; Fu, W.; Hou, T.; Zhang, J. Computational modeling toward understanding agonist binding on dopamine 3. *J Chem Inf Model* 2010, 50, 1633-43.

97. van Vliet, L. A.; Tepper, P. G.; Dijkstra, D.; Damsma, G.; Wikstrom, H.; Pugsley, T. A.; Akunne, H. C.; Heffner, T. G.; Glase, S. A.; Wise, L. D. Affinity for dopamine D2, D3, and D4 receptors of 2-aminotetralins. Relevance of D2 agonist binding for determination of receptor subtype selectivity. *J Med Chem* 1996, 39, 4233-7.

98. Damsma, G.; Bottema, T.; Westerink, B. H.; Tepper, P. G.; Dijkstra, D.; Pugsley, T. A.; MacKenzie, R. G.; Heffner, T. G.; Wikstrom, H. Pharmacological aspects of R-(+)-7-OH-DPAT, a putative dopamine D3 receptor ligand. *Eur J Pharmacol* 1993, 249, R9-10.

99. Horn, A. S.; Grol, C. J.; Dijkstra, D.; Mulder, A. H. Facile syntheses of potent dopaminergic agonists and their effect on neurotransmitter release. *J Med Chem* 1978, 21, 825-8.

100. DeWald, H. A.; Heffner, T. G.; Jaen, J. C.; Lustgarten, D. M.; McPhail, A. T.; Meltzer, L. T.; Pugsley, T. A.; Wise, L. D. Synthesis and dopamine agonist properties of (+)-trans-3,4,4a,10b-tetrahydro-4-propyl-2H,5H-[1]benzopyrano [4,3-b]-1,4-oxazin-9-ol and its enantiomers. *J Med Chem* 1990, 33, 445-50.

101. Martin, G. E.; Williams, M.; Haubrich, D. R. A pharmacological comparison of 6,7-dihydroxy-2-dimethylaminotetralin (TL-99) and N-n-propyl-3-(3-hydroxyphenyl)piperidine with (3-PPP) selected dopamine agonists. *J Pharmacol Exp Ther* 1982, 223, 298-304.
102. Tang, L.; Todd, R. D.; Heller, A.; O'Malley, K. L. Pharmacological and functional characterization of D2, D3 and D4 dopamine receptors in fibroblast and dopaminergic cell lines. *J Pharmacol Exp Ther* 1994, 268, 495-502.
103. Gmeiner, P.; Mierau, J.; Hofner, G. Enantiomerically pure aminoindolizines: bicyclic ergoline analogues with dopamine autoreceptor activity. *Arch Pharm (Weinheim)* 1992, 325, 57-60.
104. Perachon, S.; Schwartz, J. C.; Sokoloff, P. Functional potencies of new antiparkinsonian drugs at recombinant human dopamine D1, D2 and D3 receptors. *Eur J Pharmacol* 1999, 366, 293-300.
105. Newman-Tancredi, A.; Cussac, D.; Brocco, M.; Rivet, J. M.; Chaput, C.; Touzard, M.; Pasteau, V.; Millan, M. J. Dopamine D2 receptor-mediated G-protein activation in rat striatum: functional autoradiography and influence of unilateral 6-hydroxydopamine lesions of the substantia nigra. *Brain Res* 2001, 920, 41-54.
106. Hacksell, U.; Svensson, U.; Nilsson, J. L.; Hjorth, S.; Carlsson, A.; Wikstrom, H.; Lindenberg, P.; Sanchez, D. N-Alkylated 2-aminotetralins: central dopamine-receptor stimulating activity. *J Med Chem* 1979, 22, 1469-75.
107. Ohmori, J.; Maeno, K.; Hidaka, K.; Nakato, K.; Matsumoto, M.; Tada, S.; Hattori, H.; Sakamoto, S.; Tsukamoto, S.; Usuda, S.; Mase, T. Dopamine D3 and D4 receptor antagonists: synthesis and structure--activity relationships of (S)-(+)-N-(1-Benzyl-3-pyrrolidiny)-5-chloro-4-[(cyclopropylcarbonyl) amino]-2-methoxybenzamide (YM-43611) and related compounds. *J Med Chem* 1996, 39, 2764-72.
108. John Murray, P.; Harrison, L. A.; Johnson, M. R.; Robertson, G. M.; Scopes, D. I. C.; Bull, D. R.; Graham, E. A.; Hayes, A. G.; Kilpatrick, G. J.; Daas, I. D.; Large, C.; Sheehan, M. J.; Stubbs, C. M.;

Turpin, M. P. A novel series of arylpiperazines with high affinity and selectivity for the dopamine D3 receptor. *Bioorganic & Medicinal Chemistry Letters* 1995, 5, 219-222.

109. Boyfield, I.; Coldwell, M. C.; Hadley, M. S.; Johnson, C. N.; Riley, G. J.; Scott, E. E.; Stacey, R.; Stemp, G.; Thewlis, K. M. A novel series of 2-aminotetralins with high affinity and selectivity for the dopamine D3 receptor. *Bioorganic & Medicinal Chemistry Letters* 1997, 7, 1995-1998.

110. Avenell, K. Y.; Boyfield, I.; Hadley, M. S.; Johnson, C. N.; Nash, D. J.; Riley, G. J.; Stemp, G. Heterocyclic analogues of 2-aminotetralins with high affinity and selectivity for the dopamine D3 receptor. *Bioorg Med Chem Lett* 1999, 9, 2715-20.

111. Geldenhuys, W. J.; Youdim, M. B.; Carroll, R. T.; Van der Schyf, C. J. The emergence of designed multiple ligands for neurodegenerative disorders. *Prog Neurobiol* 2011, 94, 347-59.

112. Fernandez, H. H.; Chen, J. J. Monamine oxidase inhibitors: current and emerging agents for Parkinson disease. *Clin Neuropharmacol* 2007, 30, 150-68.

113. Schrag, A. Entacapone in the treatment of Parkinson's disease. *Lancet Neurol* 2005, 4, 366-70.

114. Singh, N.; Pillay, V.; Choonara, Y. E. Advances in the treatment of Parkinson's disease. *Prog Neurobiol* 2007, 81, 29-44.

115. Youdim, M. B.; Amit, T.; Falach-Yogev, M.; Bar Am, O.; Maruyama, W.; Naoi, M. The essentiality of Bcl-2, PKC and proteasome-ubiquitin complex activations in the neuroprotective-antiapoptotic action of the anti-Parkinson drug, rasagiline. *Biochem Pharmacol* 2003, 66, 1635-41.

116. Maruyama, W.; Akao, Y.; Youdim, M. B.; Naoi, M. Neurotoxins induce apoptosis in dopamine neurons: protection by N-propargylamine-1(R)- and (S)-aminoindan, rasagiline and TV1022. *J Neural Transm Suppl* 2000, 171-86.

117. Yogev-Falach, M.; Amit, T.; Bar-Am, O.; Youdim, M. B. The importance of propargylamine moiety in the anti-Parkinson drug rasagiline and its derivatives in MAPK-dependent amyloid precursor protein processing. *FASEB J* 2003, 17, 2325-7.

118. Zheng, H.; Gal, S.; Weiner, L. M.; Bar-Am, O.; Warshawsky, A.; Fridkin, M.; Youdim, M. B. Novel multifunctional neuroprotective iron chelator-monoamine oxidase inhibitor drugs for neurodegenerative diseases: in vitro studies on antioxidant activity, prevention of lipid peroxide formation and monoamine oxidase inhibition. *J Neurochem* 2005, 95, 68-78.
119. Kalir, A.; Sabbagh, A.; Youdim, M. B. Selective acetylenic 'suicide' and reversible inhibitors of monoamine oxidase types A and B. *Br J Pharmacol* 1981, 73, 55-64.
120. Ascherio, A.; Zhang, S. M.; Hernan, M. A.; Kawachi, I.; Colditz, G. A.; Speizer, F. E.; Willett, W. C. Prospective study of caffeine consumption and risk of Parkinson's disease in men and women. *Ann Neurol* 2001, 50, 56-63.
121. Ross, G. W.; Abbott, R. D.; Petrovitch, H.; Morens, D. M.; Grandinetti, A.; Tung, K. H.; Tanner, C. M.; Masaki, K. H.; Blanchette, P. L.; Curb, J. D.; Popper, J. S.; White, L. R. Association of coffee and caffeine intake with the risk of Parkinson disease. *JAMA* 2000, 283, 2674-9.
122. Xu, K.; Bastia, E.; Schwarzschild, M. Therapeutic potential of adenosine A(2A) receptor antagonists in Parkinson's disease. *Pharmacol Ther* 2005, 105, 267-310.
123. Bara-Jimenez, W.; Sherzai, A.; Dimitrova, T.; Favit, A.; Bibbiani, F.; Gillespie, M.; Morris, M. J.; Mouradian, M. M.; Chase, T. N. Adenosine A(2A) receptor antagonist treatment of Parkinson's disease. *Neurology* 2003, 61, 293-6.
124. Chen, J. F.; Xu, K.; Petzer, J. P.; Staal, R.; Xu, Y. H.; Beilstein, M.; Sonsalla, P. K.; Castagnoli, K.; Castagnoli, N., Jr.; Schwarzschild, M. A. Neuroprotection by caffeine and A(2A) adenosine receptor inactivation in a model of Parkinson's disease. *J Neurosci* 2001, 21, RC143.
125. Ikeda, K.; Kurokawa, M.; Aoyama, S.; Kuwana, Y. Neuroprotection by adenosine A2A receptor blockade in experimental models of Parkinson's disease. *J Neurochem* 2002, 80, 262-70.
126. Jacobson, K. A.; Nikodijevic, O.; Padgett, W. L.; Gallo-Rodriguez, C.; Maillard, M.; Daly, J. W. 8-(3-Chlorostyryl)caffeine (CSC) is a selective A2-adenosine antagonist in vitro and in vivo. *FEBS Lett* 1993, 323, 141-4.

127. Gerlach, M.; Riederer, P. Animal models of Parkinson's disease: an empirical comparison with the phenomenology of the disease in man. *J Neural Transm* 1996, 103, 987-1041.
128. Chen, J. F.; Steyn, S.; Staal, R.; Petzer, J. P.; Xu, K.; Van Der Schyf, C. J.; Castagnoli, K.; Sonsalla, P. K.; Castagnoli, N., Jr.; Schwarzschild, M. A. 8-(3-Chlorostyryl)caffeine may attenuate MPTP neurotoxicity through dual actions of monoamine oxidase inhibition and A2A receptor antagonism. *J Biol Chem* 2002, 277, 36040-4.
129. Bolognesi, M. L.; Chiriano, G.; Bartolini, M.; Mancini, F.; Bottegoni, G.; Maestri, V.; Czvitkovich, S.; Windisch, M.; Cavalli, A.; Minarini, A.; Rosini, M.; Tumiatti, V.; Andrisano, V.; Melchiorre, C. Synthesis of monomeric derivatives to probe memoquin's bivalent interactions. *J Med Chem* 2011, 54, 8299-304.
130. Wang, M. S.; Boddapati, S.; Emadi, S.; Sierks, M. R. Curcumin reduces alpha-synuclein induced cytotoxicity in Parkinson's disease cell model. *BMC Neurosci* 2010, 11, 57.
131. Li, J.; Zhu, M.; Rajamani, S.; Uversky, V. N.; Fink, A. L. Rifampicin inhibits alpha-synuclein fibrillation and disaggregates fibrils. *Chem Biol* 2004, 11, 1513-21.
132. Lu, J. H.; Ardah, M. T.; Durairajan, S. S.; Liu, L. F.; Xie, L. X.; Fong, W. F.; Hasan, M. Y.; Huang, J. D.; El-Agnaf, O. M.; Li, M. Baicalein inhibits formation of alpha-synuclein oligomers within living cells and prevents Abeta peptide fibrillation and oligomerisation. *Chembiochem* 2011, 12, 615-24.
133. Cappai, R.; Leck, S. L.; Tew, D. J.; Williamson, N. A.; Smith, D. P.; Galatis, D.; Sharples, R. A.; Curtain, C. C.; Ali, F. E.; Cherny, R. A.; Culvenor, J. G.; Bottomley, S. P.; Masters, C. L.; Barnham, K. J.; Hill, A. F. Dopamine promotes alpha-synuclein aggregation into SDS-resistant soluble oligomers via a distinct folding pathway. *FASEB J* 2005, 19, 1377-9.
134. Li, H. T.; Lin, D. H.; Luo, X. Y.; Zhang, F.; Ji, L. N.; Du, H. N.; Song, G. Q.; Hu, J.; Zhou, J. W.; Hu, H. Y. Inhibition of alpha-synuclein fibrillization by dopamine analogs via reaction with the amino groups of alpha-synuclein. Implication for dopaminergic neurodegeneration. *FEBS J* 2005, 272, 3661-72.

135. Culman, J.; Zhao, Y.; Gohlke, P.; Herdegen, T. PPAR-gamma: therapeutic target for ischemic stroke. *Trends Pharmacol Sci* 2007, 28, 244-9.
136. Combs, C. K.; Johnson, D. E.; Karlo, J. C.; Cannady, S. B.; Landreth, G. E. Inflammatory mechanisms in Alzheimer's disease: inhibition of beta-amyloid-stimulated proinflammatory responses and neurotoxicity by PPARgamma agonists. *J Neurosci* 2000, 20, 558-67.
137. Quinn, L. P.; Crook, B.; Hows, M. E.; Vidgeon-Hart, M.; Chapman, H.; Upton, N.; Medhurst, A. D.; Virley, D. J. The PPARgamma agonist pioglitazone is effective in the MPTP mouse model of Parkinson's disease through inhibition of monoamine oxidase B. *Br J Pharmacol* 2008, 154, 226-33.
138. Di Stefano, A.; Sozio, P.; Cocco, A.; Iannitelli, A.; Santucci, E.; Costa, M.; Pecci, L.; Nasuti, C.; Cantalamessa, F.; Pinnen, F. L-dopa- and dopamine-(R)-alpha-lipoic acid conjugates as multifunctional codrugs with antioxidant properties. *J Med Chem* 2006, 49, 1486-93.
139. Packer, L.; Tritschler, H. J.; Wessel, K. Neuroprotection by the metabolic antioxidant alpha-lipoic acid. *Free Radic Biol Med* 1997, 22, 359-78.
140. Suh, J. H.; Zhu, B. Z.; deSzoeko, E.; Frei, B.; Hagen, T. M. Dihydrolipoic acid lowers the redox activity of transition metal ions but does not remove them from the active site of enzymes. *Redox Rep* 2004, 9, 57-61.
141. Johnson, M.; Antonio, T.; Reith, M. E.; Dutta, A. K. Structure-activity relationship study of N(6)-(2-(4-(1H-Indol-5-yl)piperazin-1-yl)ethyl)-N(6)-propyl-4,5,6,7-tetrahydrobenzo[d]thiazole-2,6-diamine analogues: development of highly selective D3 dopamine receptor agonists along with a highly potent D2/D3 agonist and their pharmacological characterization. *J Med Chem* 2012, 55, 5826-40.
142. Gogoi, S.; Biswas, S.; Modi, G.; Antonio, T.; Reith, M. E. A.; Dutta, A. K. Novel Bivalent Ligands for D2/D3 Dopamine Receptors: Significant Cooperative Gain in D2 Affinity and Potency. *ACS Medicinal Chemistry Letters* 2012, 3, 991-996.
143. Gogoi, S.; Antonio, T.; Rajagopalan, S.; Reith, M.; Andersen, J.; Dutta, A. K. Dopamine D(2)/D(3) agonists with potent iron chelation, antioxidant and neuroprotective properties:

potential implication in symptomatic and neuroprotective treatment of Parkinson's disease. *ChemMedChem* 2011, 6, 991-5.

144. Kortagere, S.; Cheng, S. Y.; Antonio, T.; Zhen, J.; Reith, M. E.; Dutta, A. K. Interaction of novel hybrid compounds with the D3 dopamine receptor: Site-directed mutagenesis and homology modeling studies. *Biochem Pharmacol* 2011, 81, 157-63.

145. Ghosh, B.; Antonio, T.; Reith, M. E.; Dutta, A. K. Discovery of 4-(4-(2-((5-Hydroxy-1,2,3,4-tetrahydronaphthalen-2-yl)(propyl)amino)ethyl)piperazin-1-yl)quinolin-8-ol and its analogues as highly potent dopamine D2/D3 agonists and as iron chelator: in vivo activity indicates potential application in symptomatic and neuroprotective therapy for Parkinson's disease. *J Med Chem* 2010, 53, 2114-25.

146. Ghosh, B.; Antonio, T.; Zhen, J.; Kharkar, P.; Reith, M. E.; Dutta, A. K. Development of (S)-N6-(2-(4-(isoquinolin-1-yl)piperazin-1-yl)ethyl)-N6-propyl-4,5,6,7-tetrahydro benzo[d]-thiazole-2,6-diamine and its analogue as a D3 receptor preferring agonist: potent in vivo activity in Parkinson's disease animal models. *J Med Chem* 2010, 53, 1023-37.

147. Ghosh, B.; Antonio, T.; Gopishetty, B.; Reith, M.; Dutta, A. Further delineation of hydrophobic binding sites in dopamine D(2)/D(3) receptors for N-4 substituents on the piperazine ring of the hybrid template 5/7-[[2-(4-aryl-piperazin-1-yl)-ethyl]-propyl-amino]-5,6,7,8-tetrahydronaphthalen-2-ol. *Bioorg Med Chem* 2010, 18, 5661-74.

148. Brown, D. A.; Mishra, M.; Zhang, S.; Biswas, S.; Parrington, I.; Antonio, T.; Reith, M. E.; Dutta, A. K. Investigation of various N-heterocyclic substituted piperazine versions of 5/7-[[2-(4-aryl-piperazin-1-yl)-ethyl]-propyl-amino]-5,6,7,8-tetrahydronaphthalen-2-ol: effect on affinity and selectivity for dopamine D3 receptor. *Bioorg Med Chem* 2009, 17, 3923-33.

149. Biswas, S.; Hazeldine, S.; Ghosh, B.; Parrington, I.; Kuzhikandathil, E.; Reith, M. E.; Dutta, A. K. Bioisosteric heterocyclic versions of 7-[[2-(4-phenyl-piperazin-1-yl)ethyl]propylamino]-5,6,7,8-tetrahydronaphthalen-2-ol: identification of highly potent and selective agonists for dopamine D3 receptor with potent in vivo activity. *J Med Chem* 2008, 51, 3005-19.

150. Biswas, S.; Zhang, S.; Fernandez, F.; Ghosh, B.; Zhen, J.; Kuzhikandathil, E.; Reith, M. E.; Dutta, A. K. Further structure-activity relationships study of hybrid 7-[[2-(4-phenylpiperazin-1-yl)ethyl]propylamino]-5,6,7,8-tetrahydronaphthalen-2-ol analogues: identification of a high-affinity D3-preferring agonist with potent in vivo activity with long duration of action. *J Med Chem* 2008, 51, 101-17.
151. Brown, D. A.; Kharkar, P. S.; Parrington, I.; Reith, M. E.; Dutta, A. K. Structurally constrained hybrid derivatives containing octahydrobenzo[g or f]quinoline moieties for dopamine D2 and D3 receptors: binding characterization at D2/D3 receptors and elucidation of a pharmacophore model. *J Med Chem* 2008, 51, 7806-19.
152. Dutta, A. K.; Venkataraman, S. K.; Fei, X. S.; Kolhatkar, R.; Zhang, S.; Reith, M. E. Synthesis and biological characterization of novel hybrid 7-[[2-(4-phenyl-piperazin-1-yl)-ethyl]-propyl-amino]-5,6,7,8-tetrahydro-naphthalen-2-ol and their heterocyclic bioisosteric analogues for dopamine D2 and D3 receptors. *Bioorg Med Chem* 2004, 12, 4361-73.
153. Dutta, A. K.; Venkataraman, S. K.; Fei, X.-S.; Kolhatkar, R.; Zhang, S.; Reith, M. E. A. Synthesis and biological characterization of novel hybrid 7-[[2-(4-phenyl-piperazin-1-yl)-ethyl]-propyl-amino]-5,6,7,8-tetrahydro-naphthalen-2-ol and their heterocyclic bioisosteric analogues for dopamine D2 and D3 receptors. *Bioorganic & Medicinal Chemistry* 2004, 12, 4361-4373.
154. Ghosh, B.; Antonio, T.; Zhen, J.; Kharkar, P.; Reith, M. E.; Dutta, A. K. Development of (S)-N6-(2-(4-(isoquinolin-1-yl)piperazin-1-yl)ethyl)-N6-propyl-4,5,6,7-tetrahydrobenzo[d]-thiazole-2,6-diamine and its analogue as a D3 receptor preferring agonist: Potent in vivo activity in Parkinson's disease animal models. *Submitted to J. Med. Chem.*
155. Jensen, M. S.; Hoerrner, R. S.; Li, W.; Nelson, D. P.; Javadi, G. J.; Dormer, P. G.; Cai, D.; Larsen, R. D. Efficient synthesis of a GABA A α 2,3-selective allosteric modulator via a sequential Pd-catalyzed cross-coupling approach. *J Org Chem* 2005, 70, 6034-9.

156. Li, W.; Nelson, D. P.; Jensen, M. S.; Hoerrner, R. S.; Cai, D.; Larsen, R. D.; Reider, P. J. An improved protocol for the preparation of 3-pyridyl- and some arylboronic acids. *J Org Chem* 2002, 67, 5394-7.
157. Liu, K. G.; Robichaud, A. J. A general and convenient synthesis of N-aryl piperazines. *Tetrahedron Letters* 2005, 46, 7921-7922.
158. Carlsson, A.; Lindqvist, M.; Magnusson, T. 3,4-Dihydroxyphenylalanine and 5-hydroxytryptophan as reserpine antagonists. *Nature* 1957, 180, 1200.
159. Skalisz, L. L.; Beijamini, V.; Joca, S. L.; Vital, M. A.; Da Cunha, C.; Andreatini, R. Evaluation of the face validity of reserpine administration as an animal model of depression--Parkinson's disease association. *Prog Neuropsychopharmacol Biol Psychiatry* 2002, 26, 879-83.
160. Ungerstedt, U.; Arbuthnott, G. W. Quantitative recording of rotational behavior in rats after 6-hydroxy-dopamine lesions of the nigrostriatal dopamine system. *Brain Res* 1970, 24, 485-93.
161. Jayaprakasha, G. K.; Girenavar, B.; Patil, B. S. Radical scavenging activities of Rio Red grapefruits and Sour orange fruit extracts in different in vitro model systems. *Bioresour Technol* 2008, 99, 4484-94.
162. Ungerstedt, U. 6-Hydroxy-dopamine induced degeneration of central monoamine neurons. *Eur J Pharmacol* 1968, 5, 107-10.
163. Meng, X.; Munishkina, L. A.; Fink, A. L.; Uversky, V. N. Effects of Various Flavonoids on the alpha-Synuclein Fibrillation Process. *Parkinsons Dis* 2010, 2010, 650794.
164. Dixit, A.; Kashaw, S. K.; Gaur, S.; Saxena, A. K. Development of CoMFA, advance CoMFA and CoMSIA models in pyrroloquinazolines as thrombin receptor antagonist. *Bioorg Med Chem* 2004, 12, 3591-8.
165. Cheng, Y.; Prusoff, W. H. Relationship between the inhibition constant (K₁) and the concentration of inhibitor which causes 50 per cent inhibition (I₅₀) of an enzymatic reaction. *Biochem Pharmacol* 1973, 22, 3099-108.

166. Watts, V. J.; Lawler, C. P.; Knoerzer, T.; Mayleben, M. A.; Neve, K. A.; Nichols, D. E.; Mailman, R. B. Hexahydrobenzo[a]phenanthridines: novel dopamine D3 receptor ligands. *Eur J Pharmacol* 1993, 239, 271-3.
167. Lazareno, S. Measurement of agonist-stimulated [³⁵S]GTP gamma S binding to cell membranes. *Methods Mol Biol* 1997, 83, 107-16.
168. Bidlack, J. M.; Parkhill, A. L. Assay of G protein-coupled receptor activation of G proteins in native cell membranes using [³⁵S]GTP gamma S binding. *Methods Mol Biol* 2004, 237, 135-43.
169. Strange, P. G. Mechanisms underlying agonist efficacy. *Biochem Soc Trans* 2007, 35, 733-6.
170. Newman-Tancredi, A.; Cussac, D.; Audinot, V.; Millan, M. J. Actions of roxindole at recombinant human dopamine D2, D3 and D4 and serotonin 5-HT1A, 5-HT1B and 5-HT1D receptors. *Naunyn Schmiedebergs Arch Pharmacol* 1999, 359, 447-53.
171. Millan, M. J.; Di Cara, B.; Hill, M.; Jackson, M.; Joyce, J. N.; Brotchie, J.; McGuire, S.; Crossman, A.; Smith, L.; Jenner, P.; Gobert, A.; Peglion, J. L.; Brocco, M. S32504, a novel naphthoxazine agonist at dopamine D3/D2 receptors: II. Actions in rodent, primate, and cellular models of antiparkinsonian activity in comparison to ropinirole. *J Pharmacol Exp Ther* 2004, 309, 921-35.
172. McCall, R. B.; Lookingland, K. J.; Bedard, P. J.; Huff, R. M. Sumanrole, a highly dopamine D2-selective receptor agonist: in vitro and in vivo pharmacological characterization and efficacy in animal models of Parkinson's disease. *J Pharmacol Exp Ther* 2005, 314, 1248-56.
173. Ungerstedt, U. Postsynaptic supersensitivity after 6-hydroxy-dopamine induced degeneration of the nigro-striatal dopamine system. *Acta Physiol Scand Suppl* 1971, 367, 69-93.
174. Kang, H. M.; Saltveit, M. E. Antioxidant enzymes and DPPH-radical scavenging activity in chilled and heat-shocked rice (*Oryza sativa* L.) seedlings radicles. *J Agric Food Chem* 2002, 50, 513-8.
175. Bohm, M.; St rzebecher, J.; Klebe, G. Three-dimensional quantitative structure-activity relationship analyses using comparative molecular field analysis and comparative molecular

similarity indices analysis to elucidate selectivity differences of inhibitors binding to trypsin, thrombin, and factor Xa. *J Med Chem* 1999, 42, 458-77.

176. Wong, G.; Koehler, K. F.; Skolnick, P.; Gu, Z. Q.; Ananthan, S.; Schonholzer, P.; Hunkeler, W.; Zhang, W.; Cook, J. M. Synthetic and computer-assisted analysis of the structural requirements for selective, high-affinity ligand binding to diazepam-insensitive benzodiazepine receptors. *J Med Chem* 1993, 36, 1820-30.

177. Inc, T. *Sybyl Molecular Modeling System 8.0*.

178. Chemical Computing Group, I. *Molecular Operating Environment (MOE) 2009.10*.

ABSTRACT**DESIGN, SYNTHESIS, BIOLOGICAL EVALUATION AND MOLECULAR MODELING STUDIES OF NOVEL MULTIFUNCTIONAL NEUROPROTECTIVE DRUGS FOR THE TREATMENT OF PARKINSON'S DISEASE: AN EFFORT TOWARDS THE IMPROVEMENT OF *IN VIVO* EFFICACY AND MODULATION OF ALPHA SYNUCLEIN AGGREGATION PROPERTY OF THE NEUROPROTECTIVE PARENT MOLECULE (D-264)**

by

GYAN PRAKASH MODI

May 2014

Advisor: Dr. Alope K. Dutta**Major:** Pharmaceutical Sciences**Degree:** Doctor of Philosophy

Parkinson's disease (PD) is a progressive age-related neurodegenerative disorder of the central nervous system that is characterized by gradual loss of dopaminergic neurons in the substantia nigra region of the brain. The research from the past two decades in PD area has provided more insights into the basic pathogenetic factors of PD such as roles of oxidative stress, aggregation of α -synuclein (ASN) proteins in the form soluble toxic aggregates and fibrils, increased concentration of iron in the PD brain. Levodopa (L-DOPA) became available in 1960 for the treatment of PD and is still being considered as one of the main stream therapy. However, prolog use of L-DOPA gives rise to "on" and "off" episode along with motor fluctuations and eventual oxidation of dopamine (DA) derived from L-DOPA further facilitates neurodegeneration. It is increasingly evident that drugs aiming a single target may be inadequate for the treatment of complex diseases

such as PD, which is multifactorial in nature. Thus, it is hypothesized that multifunctional drugs having multiple pharmacological activities addressing multiple pathogenic factors of PD will be effective as disease modifying agent for the treatment of this disease. Our aim in the first study was to enhance brain penetration of one of our lead molecule D-264. Our current structure activity relationship study is focused on introduction of methoxy and hydroxyl group at various positions on the accessory binding biphenyl ring of this hybrid molecule. The introduction of hydroxyl group or combination of hydroxyl/methoxy group at a suitable position could further potentiate its antioxidant and neuroprotection property. Among all synthesized compounds in the first series, compound **D-433** and **D-533** exhibited the highest selectivity for the D3 over D2 receptor in both binding and functional assays. Lead compounds **D-433** and **D-533** also exhibited potent free radical quenching property, possibly indicating antioxidant activity. The lead compounds were tested in two PD animal models. Both the compounds exhibited higher blood brain barrier crossing ability compared to parent compounds D-264. Furthermore, in MTT assay lead compounds are able to protect MN9D cells from the exposure to neurotoxin MPP+ and 6-OHDA in a dose dependent manner. Compounds **D-519** and **D-520** were selected as lead molecules from the second series and they exhibited nanomolar to sub nanomolar range affinity at D2/D3 receptors in the receptor binding assay and [³⁵S]GTPγS binding assay. It was concluded from this *in vivo* study that both **D-519** and **D-520** was able to efficiently cross blood brain barrier and exhibited high *in vivo* agonist efficacy. **D-519** and **D-520** can potentially chelate with Fe(III). Furthermore, **D-520** is able to reverse the ASN aggregates induced toxicity at a significant level in PC-12 cells. Finally, three dimensional quantitative structure activity relationship (3DQSAR) studies CoMFA and CoMSIA were performed. Two alignment methods

(atom base and flexible) and two charge calculation methods (Gasteinger-Huckel and MOPAC) were used. The presence of carbonyl group attached to piperazine ring and hydrophobic biphenyl ring was found to be one of the most important factors responsible for the D3 selectivity over D2.

AUTOBIOGRAPHICAL STATEMENT
Gyan Prakash Modi

MS (Pharmaceutical chemistry) 2007

Department of Pharmaceutics, Institute of Technology-Banaras Hindu University, India.

BS (Pharmaceutical Sciences) 2004

Sanjiveeni College of pharmaceutical Sciences, University of Rajasthan, India.

POSITIONS

- January'2009 -August'2009, Teaching Faculty, RCP, Pharmacy College, India India.
- August'2007-June2008, Teaching Faculty, SVCP, Pharmacy College, India.

Awards

- **Frank O. Taylor pharmacy graduate student award 2013**, awarded by the department of Pharmaceutical sciences, Wayne State University for the outstanding performance in research and graduate studies.
- **Travel Award 2013**, awarded by the department of Pharmaceutical sciences, Wayne State University.
- Graduate Research Assistantship, Wayne State University (2005-till date).
- Junior Research Fellowship, University Grants Commissions, New Delhi, India for MS studies (2005-2007).
- Best Outgoing Student Award, Sanjiveeni College of pharmaceutical Sciences.

Publications in Peer reviewed journals

1. Further Structure Activity Relationship Studies on 4-(((3S,6S)- 6-Benzhydryltetrahydro-2H-pyran-3- yl)amino)methyl)phenol: Identification of Compounds with Triple Uptake Inhibitory Activity as Potential Antidepressant Agents. Bhaskar Gopishetty, Stuart Hazeldine, Soumava Santra, Mark Johnson, **Gyan Modi**, Solav Ali, Juan Zhen, Maarten Reith, and Alope Dutta. ***J. Med. Chem.*, 2011, 54, 2924–2932.**
2. Novel bivalent ligands for D2/D3 dopamine receptors: Significant co-operative gain in D2 affinity and potency. Sanjib Gogoi, Swati Biswas, **Gyan Modi**, Tamara Antonio, Maarten Reith, Alope K. Dutta. ***Medicinal Chemistry Letter*, 2012, 3(12), 991-996.**